UNIVERSITY OF
LIVERPOOL

Regulation of the diurnal rhythmicity of intestinal absorption

Thesis submitted in accordance with the requirements of the University of Liverpool for the degree of Doctor in Philosophy by

Anita Balakrishnan

March 2011

DECLARATION

This thesis is the result of my own work, unless otherwise stated, and is based upon results from experiments performed as a PhD student between March 2008 and March 2010 at the Department of Clinical Sciences in the University of Liverpool.

Neither this thesis nor any part of it has been submitted in support of an application of another degree or qualification of this or any other University or other institute of learning. However, some parts of the material contained herein have been previously published.

Anita Balakrishnan

March 2011

To my parents for their unfailing belief in me
and to my husband Sanjeev for his unwavering support.

ACKNOWLEDGEMENTS

The author wishes to acknowledge the following people:

Dr John Jenkins, Professor Mark Pritchard and Professor Alastair Watson for their advice and supervision of the work that forms this thesis

Professor Stanley W Ashley, Dr A Tavakkolizadeh and Dr D Rhoads at the Brigham and Women's Hospital and Harvard Medical School for supervising my experiments and their constant advice and support

Jan Rounds at the Brigham and Women's Hospital for her invaluable managerial and administrative assistance Adam Stearns for the endless entertainment and cookies on our many, many overnight harvests

Fellow researchers Kamran Abolmaali, Michael Abramson, Amarsanaa Jazag and Lin Chi Iou for their tireless support and encouragement.

ABSTRACT

Background: Short bowel syndrome remains a condition with high morbidity and mortality. The intestine exhibits pronounced diurnal rhythms in glucose absorption, mediated by rhythmicity in expression of the sodium glucose co-transporter SGLT1 and facilitated by rhythms in enterocyte proliferation. Understanding the mechanisms driving these rhythms may facilitate the development of new treatments for short bowel syndrome.

Aims: The work in this thesis aims to decipher the molecular pathways behind the rhythms in intestinal glucose absorption by examining the role of clock genes, implicated in the regulation of other diurnal intestinal transporters, in the regulation of SGLT1 rhythmicity and exploring the role of microRNAs, known to regulate proliferation in other experimental models, in the regulation of rhythmicity in intestinal proliferation.

Methods: Rhythmicity of *Sglt1* and clock gene expression was investigated in the jejunum of *ad libitum* and restricted-fed rats. *SGLT1* and clock gene expression was measured in Caco-2 enterocytes bearing knockdown vectors for PER1. The effects of PER1 and E-box sequences on the *SGLT1* promoter were determined in CHO cells. Rhythmicity of microRNA expression in diurnally harvested rat jejunum was analyzed by microarrays and validated by qPCR. Temporal expression of the diurnally rhythmic microRNA *mir-16* was further quantified in intestinal crypts, villi and smooth muscle using laser capture microdissection and qPCR. Morphological rhythms in rat jejunum were assessed by histology and proliferation by immunostaining for bromodeoxyuridine. In IEC-6 cells stably overexpressing *mir-16*, proliferation was assessed by cell counting and MTS assay, cell cycle progression and apoptosis by flow cytometry and cell cycle gene expression by qPCR and immunoblotting.

Results: 24-hour periodicity was noted in the expressions of clock genes and *Sglt1* in ad libitum fed rats. The *Sglt1* rhythm phase shifted in parallel with *Per1* upon light-restricted feeding. PER1 suppressed *SGLT1* in vitro via E-box independent sites on the *SGLT1* promoter. Diurnal rhythmicity was noted for *mir-16*, *mir-20a* and *mir-141* in rat jejunum. Diurnal changes in *mir-16* were restricted to the crypt fraction and peaked in antiphase to crypt depth and villus height. Overexpression of *mir-16* suppressed specific G1/S regulators and produced G1 arrest. Protein expression of these genes exhibited diurnal rhythmicity in rat jejunum, peaking in antiphase to *mir-16*.

Conclusions: These findings highlight luminal nutrients as a key Zeitgeber in the intestine, capable of simultaneously shifting the phases of transporter and clock gene expression and suggest a role for clock genes, specifically PER1, in regulating *Sglt1* and therefore glucose uptake. These data further identify diurnal rhythmicity of specific microRNAs in rat jejunum; highlighting *mir-16* as an important regulator of rhythmicity of proliferation in jejunal crypts. Together these findings suggest that rhythmicity in intestinal absorption may be mediated by at least two molecular pathways, circadian clock genes and microRNAs, thereby matching proliferation and absorptive capacity with nutrient availability. These new insights may allow the development of new therapies for short bowel syndrome.

LIST OF ABBREVIATIONS

ABC	ATP-binding cassette
AchRβ	acetylcholine receptor β
Adcy6	adenylate cyclase 6
AL	ad libitum
α-MDG	α-methyl-d-glycopyranoside
AR	androgen receptor
AVP	arginine vasopressin
BBM	brush border membrane
BCRP	breast cancer resistance protein
bHLH	basic helix-loop-helix
Bmal1	brain muscle arnt-like 1
bp	basepair
BrdU	5-bromo-2-deoxyuridine
CCG	clock-controlled gene
Ccnd	cyclin D
Ccne	cyclin E
CDK	cyclin-dependent kinase
CDX2	caudal-type homeobox protein 2
CHO	Chinese Hamster Ovary
CLK	clock
CMV	cytomegalovirus
CREB	cAMP response element-binding protein
Cry	cryptochrome

CYC	cycle
DBP	albumin D-element-binding protein
DEPC	diethylpyrocarbonate
DF	dark-fed
DMEM	Dulbecco's Modified Eagle Media
DMSO	dimethylsulfoxide
DNA	deoxyribonucleic acid
DTT	dithiothreitol
ECL	enhanced chemiluminescence
EDTA	ethylenediaminetetraacetic acid
EMSA	electrophoretic mobility shift assay
E4BP4	E4 promoter binding protein-4
FAS	fatty acid synthase
FBS	foetal bovine serum
G	gap phase
GEO	Gene Expression Omnibus
GI	gastrointestinal
GTP	guanosine tripphosphate
HALO	hours after lights on
HLF	hepatic leukemia factor
HNF1	hepatocyte nuclear factor 1
Hsp70	heat shock protein 70
IEC	Intestinal Enterocyte Cells
IFABP	intestinal fatty acid binding protein
Kb	kilobase

kDa	kiloDalton
LB	Luria broth
LCM	laser capture microdissection
LDS	lithium dodecyl sulphate
LF	light-fed
LH	luteinizing hormone
M	mitosis phase
MCT1	monocarboxylate transporter 1
Mdr1	multidrug resistance 1
MITF	microphthalmia-associated transcription factor
mRNA	messenger ribonucleic acid
MRP2	multidrug resistance protein 2
NHE3	Na^+/H^+ exchanger
NPC1L1	Niemann-Pick C1 like 1
nt	nucleotide
OCT	optimal cutting temperature
PARP	poly-ADP-ribose-polymerase
PAS	Per-Arnt-Sim
PBS	phosphate-buffered saline
PCNA	proliferating cell nuclear antigen
Per	period
PPAR-α	peroxisome-proliferator-activated-receptor alpha
PVDF	polyvinyldifluoride
qPCR	quantitative polymerase chain reaction

RHT	retinohypothalamic tract
RIPA	radioimmunoprecipitation assay
RISC	RNA-induced silencing complex
RNA	ribonucleic acid
ROR	retinoic acid-receptor-related orphan receptor
RORE	retinoic acid receptor-related orphan receptor responsive element
RS1	regulatory subunit 1
RT	reverse transcription
S	synthesis phase
SCN	suprachiasmatic nucleus
SGLT1	sodium glucose cotransporter 1
shRNA	short hairpin ribonucleic acid
siRNA	small-interfering RNA
SLC5	solute carrier family 5
SMA	smooth muscle actin
snoRNA	small nucleolar ribonucleic acid
TAE	tris-acetate ethylenediaminetetraacetic acid
TF	transcription factor
TGF-β	transforming growth factor β
Tim	timeless
TPN	total parenteral nutrition
USF	upstream stimulatory factor
UTR	untranslated region
UV	ultraviolet

CONTENTS

ABSTRACT I

LIST OF ABBREVIATIONS II

TABLE OF CONTENTS VI

LIST OF FIGURES XI

LIST OF TABLES XIII

CHAPTER 1 1

1.1 Overview of short bowel syndrome 1
1.2 The role of the intestine in absorption 2
1.2.1 Anatomy and physiology of the human intestinal tract 2
1.2.2 Intestinal absorption of nutrients 5
1.3 Intestinal glucose transport 7
1.3.1 Background 7
1.3.2 SGLT1 7
1.3.2.1 SGLT1-mediated glucose transport 7
1.3.2.2 Regulation of SGLT1 9
1.3.2.3 Mutations of SGLT1 cause glucose-galactose malabsorption 10
1.3.2.4 History of cloning and characterization of SGLT1 10
1.3.3 Other intestinal glucose transporters 11
1.3.4 Transport of other nutrients 11
1.4 Circadian rhythmicity in intestinal absorption 13
1.4.1 Overview of circadian rhythmicity 13
1.4.2 Circadian rhythmicity in feeding across species 14
1.4.3 Rhythmicity of intestinal absorption 15
1.4.3.1 Overview of the rhythmicity of intestinal absorption 15
1.4.3.2 Rhythmicity in absorption of individual nutrients 16
1.4.3.2.1 Rhythmicity in SGLT1-mediated glucose uptake 16
1.4.3.2.2 Rhythmicity of other transporters 16
1.4.4 Tissue-specific circadian rhythmicity 17
1.4.5 The rationale for using rats in diurnal rhythm experiments 18
1.4.6 Cues regulating feeding rhythms 18
1.4.6.1 Nutrient availability and light cycle 18
1.4.6.2 Effects of food deprivation and intravenous nutrition 19

1.4.7 Physiological mediators of rhythmicity 20
1.4.7.1 Circadian hormones 20
1.4.7.2 Neural mediation of circadian rhythmicity 21
1.5 Circadian rhythmicity of intestinal proliferation 23
1.5.1 Apoptosis and proliferation in the intestine 23
1.5.2 Overview of rhythmicity in intestinal proliferation and apoptosis 24
1.5.3 The role of nutrients in the regulation of rhythmicity in intestinal proliferation and apoptosis 25
1.5.4 Molecular pathways regulating circadian rhythmicity in intestinal proliferation 26
1.6 Clock genes 29
1.6.1 Overview of clock genes 29
1.6.2 Description of the discovery of clock genes 29
1.6.3 Clock genes in Drosophila 30
1.6.3.1 Circadian rhythmicity in Drosophila 30
1.6.3.2 Clock genes and feedback loops in Drosophila 31
1.6.4 The molecular feedback loops of clock genes in mammals 32
1.6.5 Peripheral circadian oscillators 35
1.6.6 Clock genes as rhythmic transcriptional regulators 38
1.7 microRNAs 40
1.7.1 Overview of microRNAs 40
1.7.2 Functions of microRNAs 41
1.7.3 Background of microRNA discovery 42
1.7.4 Biogenesis of microRNAs 43
1.7.5 Mechanism of action of microRNAs 44
1.7.5.1 Transcriptional regulation 44
1.7.5.2 Post-transcriptional regulation 45
1.7.6 Rhythmicity of microRNA expression 46
1.7.7 Distinction between microRNAs and siRNAs 47
1.8 Short bowel syndrome 49
1.8.1 Aetiology 49
1.8.2 Morphologic and physiologic adaptation to short bowel syndrome 49
1.8.3 Management of short bowel syndrome 50
1.9 Previous work from our group 51
1.10 Purpose of the proposed studies 52

CHAPTER 2 53

2.1. Animal studies 53
2.1.1. Feeding patterns 54

2.1.1.1. Ad libitum and restricted feeding regimens 54
2.1.1.2. Diurnal ad libitum feeding regimens 56
2.1.2. Harvest protocols 56
2.1.2.1. Anaesthesia 56
2.1.2.2. Tissue harvest and preparation 57
2.2. RNA 60
2.2.1. RNA extraction 60
2.2.2. Reverse transcription 60
2.2.3. Real-time quantitative PCR 61
2.3. microRNA profiling 65
2.3.1. In situ hybridization on microRNA microarrays 65
2.3.2. Validation by qPCR 65
2.4. Laser capture microdissection (LCM) 67
2.4.1. Laser capture of crypts, villi and smooth muscle 67
2.4.2. Real-time PCR of laser captured samples 67
2.5. Protein 69
2.5.1. Protein extraction and quantification 69
2.5.1.1. Protein extraction from cultured cells 69
2.5.1.2. Protein extraction from tissue 70
2.5.2. Quantification of extracted protein (BCA assay) 70
2.5.3. Gel electrophoresis 71
2.5.4. Western blotting 71
2.5.4.1. Incubation with antibodies 72
2.5.4.2. Detection and quantification of the protein 74
2.6. Routine cell maintenance 75
2.6.1. CHO cells 75
2.6.2. Caco-2 cells 75
2.6.3. IEC-6 cells 76
2.6.4. HEK293 cells 76
2.7. Cell transfection 77
2.7.1. CHO transfection 77
2.7.2. Caco-2 cell transfection 77
2.7.3. IEC-6 transfection 78
2.7.4. HEK293 transfection 79
2.8. DNA plasmids and site-directed mutagenesis 80
2.8.1. PCR amplification of PER1 80
2.8.2. Gel electrophoresis 81
2.8.3. Digestion of PCR products and vectors 81
2.8.4. Ligation of insert and vector and amplification 82
2.8.5. Plasmid preparation 82
2.8.6. Knockdown vectors and sequences 84

2.8.7.Creation of the *mir-16* overexpression vector 86
2.8.7.1. Identification of the necessary *mir-16* sequence 86
2.8.7.2. Cloning the *mir-16* sequence 87
2.9. SGLT1 promoter constructs (wild-type and mutants) 89
2.10. SGLT1 promoter reporter assays 92
2.11. Quantification of apoptosis 93
2.12. Measurement of cell proliferation 94
2.12.1. In vitro proliferation 94
2.12.2. Cell growth rate (counting method) 94
2.13. Measurement of cell cycle changes 95
2.14. Statistical analysis 95

CHAPTER 3 96

3.1. Introduction 96
3.2. Clock genes and *Sglt1* display diurnal rhythmicity in the jejunum of ad libitum fed rats 99
3.3. Nutrient consumption and body weight normalize within 7 days of lights-on restricted feeding 106
3.4. Restricted feeding induces a similar phase shift in clock genes and *Sglt1* in rat jejunum 110
3.5. PER1 rhythmicity in rat jejunum occurs in antiphase to the temporal profile of *Sglt1* 117
3.6. Discussion 121

CHAPTER 4 132

4.1. Introduction 132
4.2. Testing the knockdown efficiency of acquired shPER1 sequences 134
4.3. Downregulation of PER1 increases *SGLT1* expression in Caco-2 cells 138
4.4. Downregulation of PER1 does not significantly alter expression of other clock genes 143
4.5. Analysis of the *SGLT1* promoter 148
4.6. Creation and validation of the *SGLT1* promoter construct 150
4.7. Creation and validation of the *PER1* overexpression construct 153
4.8. PER1 represses *SGLT1* promoter activity in vitro 157
4.9. E-boxes are negative elements in the *SGLT1* promoter 160
4.10. Repression of SGLT1 promoter activity by PER1 is independent of E-boxes 167
4.11. Discussion 174

CHAPTER 5 ..... **184**

5.1. Introduction **184**
5.2. microRNAs exhibit diurnal rhythmicity in rat intestine **186**
5.2.1. *mir-16*, *mir-141* and *mir-20a* demonstrate diurnal rhythmicity on qPCR 188
5.2.2. *mir-16* rhythmicity is restricted to the crypt fraction of the intestine 194
5.3. *mir-16* suppresses cell proliferation in enterocytes **196**
5.4. *mir-16* induces cell cycle arrest in enterocytes **200**
5.5. *mir-16* suppresses key G1/S regulators in enterocytes **204**
5.6. G1/S regulatory proteins targeted by *mir-16* peak in antiphase to *mir-16* expression in jejunum **212**
5.7. Diurnal rhythmicity in DNA synthesis and morphology in rat jejunum .. **219**
5.8. Discussion **223**

CHAPTER 6 ..... **237**

REFERENCES **250**

ABSTRACTS ARISING FROM THIS WORK **272**

PUBLICATIONS ARISING FROM THIS WORK **273**

LIST OF FIGURES

Figure 1.1: A schematic showing the anatomy of the human gastrointestinal tract with the small intestine magnified..... 3
Figure 1.2: Diagram of the small intestinal crypt-villus axis and differentiated cell types..... 4
Figure 1.3: Schematic showing the distribution of the glucose transporters on enterocytes..... 8
Figure 1.4: Schematic showing the molecular feedback loops of circadian clock genes..... 33
Figure 1.5: Schematic showing the outline of the biogenesis of microRNAs..... 44
Figure 2.1: Schematic showing light cycle, time of food availability and harvest times..... 55
Figure 2.2: Schematic of the harvest of rat jejunum for subsequent extraction of RNA, protein and morphologic analysis..... 59
Figure 3.1: Expression of *Per1* and *β-actin* at HALO 0..... 100
Figure 3.2: Clock gene expression in AL rats..... 102
Figure 3.3: *Sglt1* mRNA expression in AL rats..... 105
Figure 3.4: Daily food intake in rats fed during only the lights-on period..... 108
Figure 3.5: Increase in weight in DF and LF rats..... 109
Figure 3.6: Clock gene expression in DF and LF rats..... 111
Figure 3.7: *Sglt1* expression in DF and LF rats..... 112
Figure 3.8: PER1 and SGLT1 protein expression in rat jejunum..... 118
Figure 4.1: Knockdown efficiency of shPER1 vectors in HEK293 cells..... 136
Figure 4.2: *PER1* mRNA and protein expression in Caco-2 cells following *PER1* knockdown..... 139
Figure 4.3: *SGLT1* mRNA expression following *PER1* knockdown in Caco-2 cells..... 140
Figure 4.4: *PER2* mRNA expression following *PER1* knockdown in Caco-2 cells..... 144
Figure 4.5: mRNA expression of *BMAL1*, *CLOCK*, *REVERBA*, *REVERBB*, *CRY1* and *CRY2* following *PER1* knockdown in Caco-2 cells..... 146
Figure 4.6: The *SGLT1* promoter sequence..... 149
Figure 4.7: Activation of the *SGLT1* promoter by *HNF1α* in CHO cells..... 152
Figure 4.8: PER1 overexpression in CHO cells..... 155
Figure 4.9: Effect of PER1 overexpression and knockdown on *SGLT1* promoter activity..... 158
Figure 4.10: Effect of E-box mutations on *SGLT1* promoter activity in CHO cells. 162
Figure 4.11: Effect of PER1 on the *SGLT1* promoter bearing E-box mutations in CHO cells..... 168

Figure 4.12: Effect of PER1 vs pcDNA on the *SGLT1* promoter bearing E-box mutations in CHO cells..... 173
Figure 5.1: *mir-16* and *snoRNA* expression at HALO 0..... 189
Figure 5.2: Temporal pattern of microRNAs showing a 24-hour periodicity in rat jejunum..... 191
Figure 5.3: *mir-16* expression in intestinal fractions..... 195
Figure 5.4: Overexpression of *mir-16* in IEC-6 cells..... 197
Figure 5.5: Effect of *mir-16* on IEC-6 proliferation..... 199
Figure 5.6: Effect of *mir-16* on G1 of the cell cycle in IEC6 cells..... 201
Figure 5.7: Effect of *mir-16* on apoptosis in IEC-6 cells..... 203
Figure 5.8: Effect of mir-16 on protein expression of G1/S regulators in IEC-6 cells..... 206
Figure 5.9: Effect of *mir-16* on mRNA expression of G1/S regulators in IEC-6 cells..... 209
Figure 5.10: Rhythmicity of protein expression in rat jejunum..... 214
Figure 5.11: Rhythmicity of mRNA expression in rat jejunum..... 217
Figure 5.12: Temporal changes in intestinal DNA synthesis and morphologic parameters..... 221
Figure 6.1: Interaction of clock genes and *SGLT1*..... 240
Figure 6.2: Effects of *mir-16* on intestinal proliferation..... 242
Figure 6.3: Schematic showing the proposed regulatory mechanisms contributing to the rhythmicity in intestinal absorption..... 243

LIST OF TABLES

Table 2.1: Rat qPCR primers for G1/S regulators as used in Chapter 5..... 62
Table 2.2: Rat qPCR primers for clock genes, the sodium glucose co-transporter *Sglt1* and *β-actin* as used in Chapter 3..... 63
Table 2.3: Human qPCR primers for clock genes, *Sglt1* and *β-actin* as used in Chapter 4..... 64
Table 2.4: Catalog numbers of microRNAs validated by reverse transcription and qPCR..... 66
Table 2.5: List of antibodies, manufacturers and concentrations used for Western blotting in Chapters 3, 4 and 5..... 73
Table 2.6: Primers for amplification of PER1 for creation of the PER1 overexpression plasmid..... 80
Table 2.7: Sequencing primers for PER1 overexpression plasmid..... 83
Table 2.8: shRNA vectors used for knockdown of PER1..... 85
Table 2.9: Primers used for amplification of *mir-16* for creation of the *mir-16* overexpression vector in Chapter 5..... 86
Table 2.10: Primers used for sequencing the *mir-16* overexpression plasmid in Chapter 5..... 88
Table 2.11: Primers for the amplification of the wild-type human SGLT1 promoter and the introduction of mutations within the promoter..... 90
Table 2.12: Sequencing primers used to confirm the introduction of the wild-type SGLT1 promoter and mutations (Chapter 4)..... 91
Table 3.1: Circadian rhythmicity of clock genes and *Sglt1*..... 101
Table 3.2: Effect and interaction of feeding times and harvest times on clock gene and *Sglt1* expression in DF and LF rats..... 113
Table 3.3: Expression of PER1 and SGLT1 in DF and LF rats..... 119
Table 4.1: Residual expression of *PER1* following knockdown in HEK293 cells..... 137
Table 4.2: *PER1* mRNA and protein expression and *SGLT1* mRNA expression following knockdown of *PER1* in Caco-2 cells..... 141
Table 4.3: Relative expression of clock gene mRNA expression following knockdown of *PER1* in Caco-2 cells..... 145
Table 4.4: Overexpression of *PER1* in CHO cells..... 156
Table 4.5: Effect of PER1 overexpression and knockdown on *SGLT1* promoter activity..... 159
Table 4.6: Effect of single E-box mutations on *SGLT1* promoter activity in CHO cells..... 163
Table 4.7: Effect of combinatorial E-box mutations on *SGLT1* promoter activity in CHO cells..... 164

Table 4.8: Effect of PER1 on single E-box mutations in the *SGLT1* promoter in CHO cells..... 169
Table 4.9: Effect of PER1 on the *SGLT1* promoter bearing combinatorial E-box mutations in CHO cells..... 170
Table 5.1: 24-hour periodicity of microRNAs validated by qPCR..... 192
Table 5.2: Effect of *mir-16* overexpression on G1/S regulator protein expression in IEC-6 cells..... 207
Table 5.3: Effect of *mir-16* overexpression on G1/S regulator mRNA expression in IEC-6 cells..... 210
Table 5.4: Rhythms in G1/S regulator protein expression in diurnally harvested rat jejunum..... 215
Table 5.5: Rhythms in G1/S regulator mRNA expression in diurnally harvested rat jejunum..... 218
Table 5.6: Rhythmicity in morphological parameters in diurnally harvested rat jejunum..... 222

Chapter 1: Introduction

1.1. Overview of short bowel syndrome

The major role of the intestine is the absorption of nutrients from the luminal surface into the bloodstream[1] and intestinal physiology and anatomy have evolved to meet this function. Intestinal absorption of nutrients, fluid and electrolytes is proportional to intestinal length[1]. Loss of intestinal length, most often caused by massive small bowel resection, significantly compromises intestinal function and results in failure of the intestine to meet nutritional needs, a phenomenon known as short bowel syndrome[2]. The lack of a suitable therapeutic option for the management of short bowel syndrome merits the search for new alternatives. Current management options are limited and bear many associated side-effects[2]. The identification of new treatments requires a greater understanding of intestinal absorption and may be realised by improved insights into the physiological regulation of intestinal absorption.

1.2. The role of the intestine in absorption

1.2.1. Anatomy and physiology of the human intestinal tract

The intra-abdominal digestive tract begins at the stomach, which receives food boluses travelling down from the oesophagus[1]. The stomach acts as a reservoir which controls the rate of entry of nutrients into the first part of the small intestine known as the duodenum[1]. The duodenum measures 25 cm, becoming the jejunum at the Ligament of Treitz, a band-like ligament which attaches the duodenal-jejunal flexure to the posterior abdominal wall[3] (Figure 1.1). The jejunum and ileum are the predominant sites of absorption in the intestine, particularly the jejunum and together measure between 4 to 6 m in length[1, 3] (Figure 1.1). The ileocaecal valve, at the end of the ileum, is the site of connection between the small intestine and the colon, specifically the region of the colon known as the caecum with the attached appendix[1] (Figure 1.1).

The intestinal epithelium proliferates rapidly via the division of progenitor or stem cells residing in the intestinal Crypts of Lieberkuhn and is countered by cell shedding at the tips of the villi[4]. Cells hence migrate upwards from the crypt towards the tip of a villus, differentiating from progenitor cells to one of 3 cell types in the process – enterocytes (responsible for intestinal absorption), enteroendocrine cells (which secrete hormones such as glucagon-like peptide 1 and cholecystokinin) and goblet cells (which secrete mucous)[4, 5] (Figure 1.2). Progenitor cells may also remain in the crypt and differentiate into Paneth cells[4, 5] (Figure 1.2).

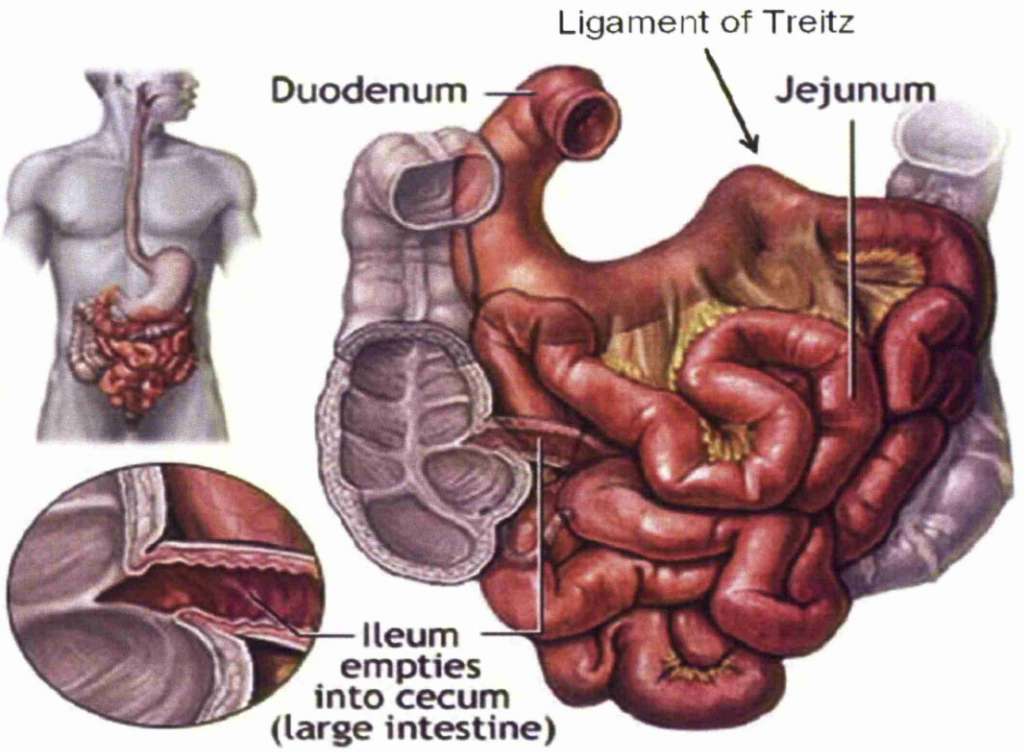

Figure 1.1: A schematic showing the anatomy of the human gastrointestinal tract, with the small intestine magnified. Modified from Medline Plus, freely accessible at www.nlm.nih.gov.

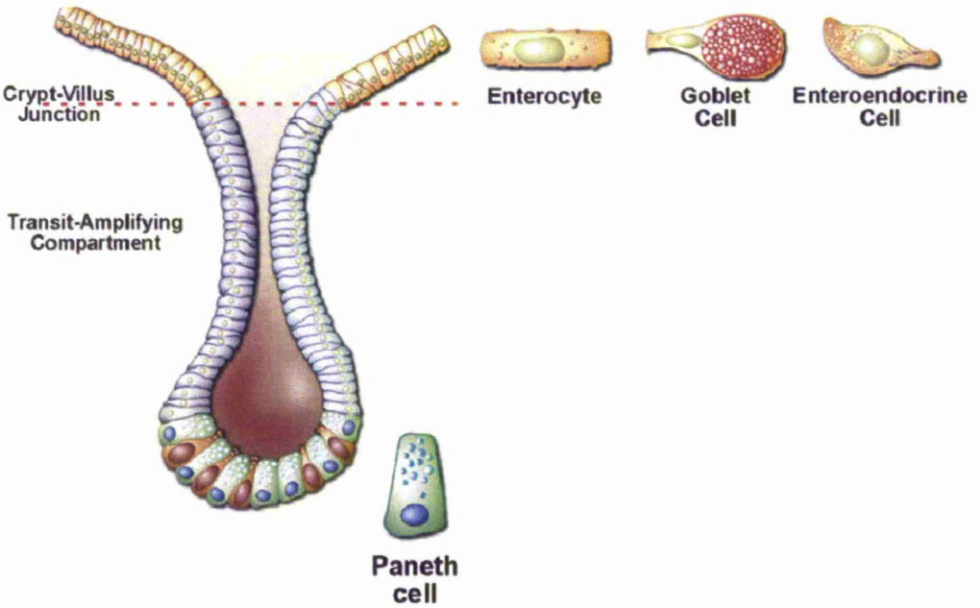

Figure 1.2: Diagram of the small intestinal crypt-villus axis and differentiated cell types. Adapted and modified from Barker et al, Genes Dev 2008 Jul 15;22(14):1856-64.

1.2.2. Intestinal absorption of nutrients

The absorptive function of the intestine has been the subject of much research dating back to the late 1800s, when it was discovered that the absorption of substrates from the intestine was not dependent on the hydrostatic pressure within the lumen, or the osmotic pressure of the luminal contents[6-8]. Indeed it was further demonstrated that two solutions of similar osmotic pressure might be absorbed at varying rates, leading the researchers of the time to conclude that the intestine "is a membrane of varying permeability depending on the nature of the substances presented to it"[6-8]. Although these early reports preceded the discovery of specific nutrient and non-nutrient transporters in the intestine, it was already noted in these studies that the absorption of

hexose sugars from the intestine could not be explained by mere diffusion or osmosis and that sodium appeared to play a role in the regulation of absorption of glucose from the intestine[9], heralding the subsequent discovery of active transport mechanisms in the intestine.

Understanding the regulation of intestinal absorption is likely to be a key factor in developing new treatments for short bowel syndrome. Glucose is one of the most important absorbed nutrients and adequate glucose absorption is essential in meeting the nutritional demands of the individual[2, 3]. The sodium glucose co-transporter SGLT1 is responsible for all active glucose uptake in the intestine; subsequent movement of glucose across the basolateral membrane occurs down a diffusion gradient[10, 11]. Absorption of glucose by SGLT1 is therefore the most important component of intestinal glucose absorption and SGLT1 is hence the main transporter of interest in understanding the regulation of glucose absorption in the intestine.

Subsequent studies have identified the existence of rhythmicity in intestinal glucose absorption in rats, with peak absorption occurring at the time of maximal nutrient delivery[12, 13]. The mechanisms underlying this have yet to be fully characterized. Circadian clock genes have been shown to regulate rhythms of other intestinal transporters[14-16], however their role in the regulation of the rhythmicity of glucose absorption has yet to be identified. microRNAs are a class of non-coding ribonucleic acids (RNAs) that have been found to regulate rhythmicity in hepatic gene expression[17] and are known to regulate proliferation in other tissues[18-24], however their expression in the intestine has yet to be profiled and their role in rhythmicity of

intestinal absorption remains unknown. These molecular pathways may be responsible for regulating the rhythmicity of intestinal absorption and understanding the regulatory networks behind this phenomenon may allow the development of new therapies for short bowel syndrome.

1.3. Intestinal glucose transport

1.3.1. Background

The first insights into the physiology of glucose absorption by the intestine were published in 1955[25], when Fisher showed that no water absorption occurred in the intestine of rats in the absence of luminal glucose and that the absorption of water and glucose was entirely an active process. Newey et al[26] subsequently demonstrated the ability of the flavonoid phloridzin to inhibit the mucosal absorption of glucose, leading to the discovery of specific glucose transporters sensitive to phloridzin. The first description of active sodium glucose co-transport was initiated by Crane et al[10], who demonstrated, using the Na^+K^+ ATPase inhibitor ouabain in hamster intestine, that a sodium gradient was required for glucose transport.

1.3.2. SGLT1

1.3.2.1. SGLT1-mediated glucose transport

SGLT1 is a 73kDa protein which reacts with 2 Na^+ molecules for every glucose molecule[27]. SGLT1-mediated glucose uptake from the intestine is a form of active transport, inhibited by phloridzin and facilitated by the Na^+K^+ATPase on the basolateral membrane[28] which maintains the sodium gradient (Figure 1.3). During active glucose transport, two Na^+ ions bind to SGLT1 on the luminal side of the brush border membrane (BBM), producing a conformational change that permits sugar binding[27]. This is followed by a further conformational change which allows the substrates (either glucose or galactose) to enter the enterocyte[27]. The low affinity of the cytosolic sites

for sugar and Na^+, as well as the low intracellular concentration of Na^+, results in dissociation of these molecules from SGLT1[27]. The ability of SGLT1 to transport water as well as glucose (249 water molecules are transported with every glucose molecule)[29] facilitated the development of oral rehydration therapy and saved millions of lives by treatment of diarrhoeal dehydration in the developing world[29, 30].

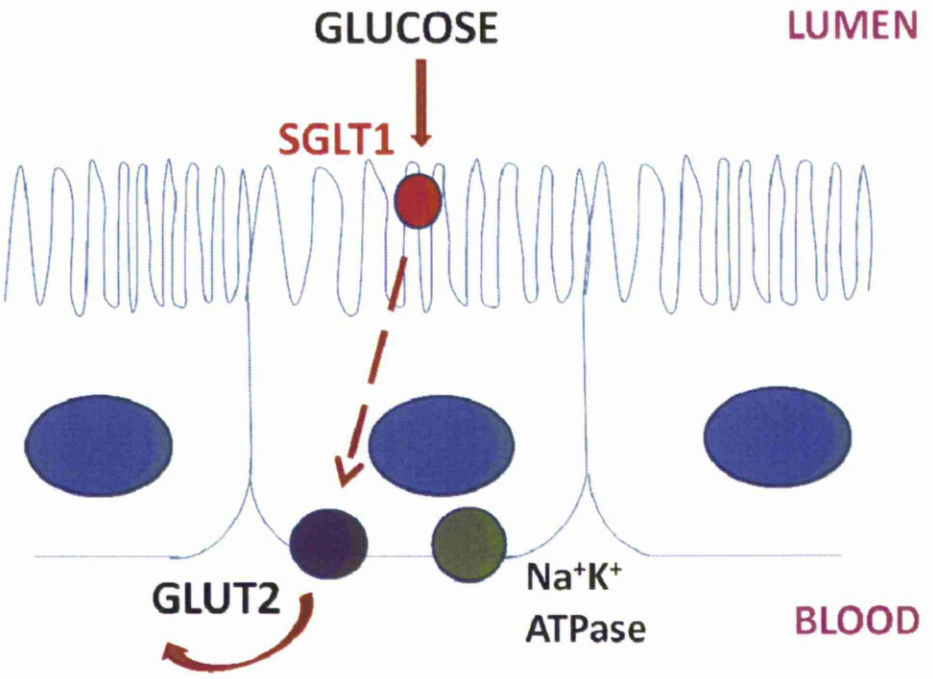

Figure 1.3: Schematic showing the distribution of the glucose transporters on enterocytes. SGLT1 (red circle) is situated on the apical border of the enterocyte while GLUT2 (purple circle) is on the basolateral membrane. The Na^+K^+ ATPase (green circle) facilitates active transport by SGLT1 and is also situated on the basolateral membrane.

1.3.2.2. Regulation of SGLT1

SGLT1 has been shown to be regulated at a transcriptional level by intestinal transcription factors such as hepatocyte nuclear factor 1 (HNF1) and Sp1[31], which are also known to regulate transcription of other intestinal genes such as sucrase-isomaltase[32] and lactase[33]. These transcription factors are able to bind to GC elements on the *SGLT1* promoter and synergistically activate *Sglt1* transcription[31]. Despite this however, no symptoms of glucose-galactose malabsorption were noted in HNF1α or β knockout mice[34, 35]. This is corroborated by the fact that humans with deficiencies of either HNF1α or β do not exhibit diarrhoea or glucose malabsorption, suggesting that HNF1 may not be essential for maintaining basal expression of SGLT1[36]. SGLT1 activity can be modified by the expression levels of an intracellular regulatory protein, regulatory subunit 1 (RS1), via modulation of dynamin-dependent SGLT1 trafficking[37]. RS1-/- mice developed obesity associated with post-transcriptional increased intestinal expression of SGLT1 and upregulated glucose transport[38]. Transforming growth factor β (TGF-β) is another protein that has also been shown to increase glucose uptake, but through as yet undefined mechanisms, possibly approximating hsp70 (heat shock protein 70, a member of the heat shock protein family), thereby stabilising membrane SGLT1[39]. Apical localization of SGLT1 is a feature essential for SGLT1 function: mice deficient in the small guanosine triphosphate (GTP) -binding protein Rab8, which is essential for the apical localization of SGLT1, showed reduced levels of α-methyl-d-glycopyranoside (α-MDG) absorption compared to their wild-type counterparts[40].

1.3.2.3. Mutations of SGLT1 cause glucose-galactose malabsorption

Glucose-galactose malabsorption is a rare autosomal recessive disorder causing a failure of SGLT1 protein trafficking to the BBM[41], resulting in severe life-threatening diarrhoea which begins at birth and continues until glucose, galactose and lactose are all removed from the diet[41, 42]. Over 300 cases have been diagnosed worldwide, the majority in females and often as a product of consanguineous relationships[41]. The varied and unique mutations in each case of glucose-galactose malabsorption make prenatal diagnosis by genetic screening difficult. This condition is diagnosed by the lack of response to an oral glucose challenge and treated by abstinence from all glucose, galactose and lactose in the diet[11].

1.3.2.4. History of cloning and characterization of SGLT1

These studies laid the groundwork for further research into active intestinal glucose transport, however it was not until the 1980s[43] that the first eukaryotic transporter was characterized and cloned. This was the sodium glucose co-transporter SGLT1[11, 43], found to reside on the brush border membrane of enterocytes. SGLT1 was found to belong to the solute carrier family 5 (SLC5) group of proteins, containing over 200 eukaryotic and prokaryotic members and contains 14 transmembrane α-helices, an extracellular N and C terminus, a glycosylation site and two phosphorylation sites[43]. SGLT1 (also known as SLC5A1) is expressed in the brush border of enterocytes as well as in small quantities in renal proximal tubular cells and the heart and is able to transport both glucose and galactose[42, 43].

1.3.3. Other intestinal glucose transporters

Two other intestinal transporters cooperate with SGLT1 in the intestinal absorption of glucose – GLUT2 and GLUT5[44-46]. While SGLT1 transports glucose from the lumen into the cytoplasm of the enterocyte, the high-capacity low-affinity transporter GLUT2 resides on the basolateral membrane of enterocytes and transports glucose, fructose, galactose and mannose out of the cell[44, 45]. The facilitated glucose transporter GLUT5 is responsible for the uptake of fructose at the brush border membrane of the intestine[46]. Fructose is then transported out of the enterocyte by GLUT2 at the basolateral membrane[46].

1.3.4. Transport of other nutrients

The transporter PEPT1 is the only oligopeptide transporter at the intestinal brush-border, responsible for the transport of 400 dipeptides and 8000 tripeptides as well as a wide range of peptide-like drugs, such as β-lactam antibiotics and angiotensin-converting enzyme inhibitors[47]. PEPT1 is a H^+-peptide cotransporter that relies on a proton gradient for the uphill transport of peptides, which are subsequently transported across the basolateral membrane by the facilitative basolateral peptide transporter[48]. Targeted disruption of PEPT1 in mice significantly reduced uptake of dipeptides from the intestine, suggesting an essential role for PEPT1 in intestinal peptide absorption[49]. Lipids are digested in the intestine into free fatty acids and glycerol[50]. Fatty acids are absorbed by FAT/CD36 and FATP4[50]. Cholesterol influx into enterocytes is regulated by Niemann-Pick C1 like 1(NPC1L1) and efflux regulated by ATP-binding cassette (ABC)

proteins ABCG5 and ABCG8[50]. The route of glycerol absorption on the other hand is still a topic of much research; paracellular passive diffusion has been assumed to be the main route of glycerol absorption, however more recent studies suggest a potential carrier-mediated route of absorption[51].

1.4. Circadian rhythmicity in intestinal absorption

1.4.1. Overview of circadian rhythmicity

Circadian rhythmicity reflects the innate ability of all organisms to detect and adapt to external stimuli, evidenced by the adaptation to the 24-hour cyclic pattern of light and the daily and seasonal patterns of food availability and temperature[52]. The phenomenon of circadian rhythmicity has been discovered in unicellular organisms to complex organisms such as plants and humans[52]. One of the earliest forms of circadian behavior was the tendency for early metazoans to migrate to deep ocean waters during the daylight for protection from ultraviolet (UV) radiation[52]. The first descriptions of circadian rhythmicity were written centuries ago; one of the most famous descriptions of this was by Christoph Wilhelm Hufeland, who wrote in 1797 the text "Die Kunst das menschliche Leben zu verlangern" "Due to the regular rotation of our planet there is a 24-hour period transmitted to all inhabitants on earth. . .and in all kinds of diseases this regular period can be found again and this 24-hour period determines the wonderful timing of all our bodily functions. This period can be called the unit of the chronology of nature"[53, 54]. Physiological and pathological examples of circadian rhythms in visceral function include circadian rhythms in heart rate[55], blood pressure[56], nocturnal worsening of asthma [57] and gout[54, 58]. Circadian rhythms share similar characteristics common to many species, including flies, mice and humans; synchronization by environmental stimuli (zeitgebers – "time-givers")[59], the most important of which is light, as almost all rhythms synchronize to the day:night cycle and

persistence in the absence of cycling zeitgebers, i.e. under constant conditions, such as constant darkness[60].

1.4.2. Circadian rhythmicity in feeding across species

Humans and rodents exhibit similarities in their patterns of food consumption. Both species engage in specific bouts of eating (meals), which occur across the day at differing time intervals[61, 62]. In both cases the longest interval between meals is often the inactive rest period, such as during the night in humans and during the day in the nocturnal rodent[61, 62]. The existence of these specific feeding patterns may allow animals to adapt to their unique environmental conditions, e.g. the availability of food and may therefore act as a survival advantage on an evolutionary level[61]. As mentioned above, rats in the wild are nocturnal feeders that feed at intervals spaced across the dark period and rest during the day. Despite many generations of inbreeding, laboratory rats continue to maintain similar feeding patterns[61]. Although mice are also nocturnal animals, they have not been observed to exhibit such clear feeding patterns as rats and tend to graze during the day (personal communication from David B Rhoads). The rhythmicity observed in SGLT1 expression in rats has also been documented in non-human primates[63], with a 12 hour difference in the time of peak expression consistent with the nocturnal rat versus the diurnal Rhesus monkey. This highlights the relevance of circadian rhythmicity across species and suggests that the circadian rhythmicity noted in the rat can be extrapolated to primates.

1.4.3. Rhythmicity of intestinal absorption

1.4.3.1. Overview of the rhythmicity of intestinal absorption

Furuya and Yugari first demonstrated in 1974 that intestinal absorption exhibits a diurnal rhythm in nocturnal feeding rat, with a peak in histidine absorption during the nocturnal feeding period[64, 65]. This work was further developed by Fisher and Gardner in 1976, who confirmed peak absorption of glucose during the nocturnal period, but also demonstrated that this rhythm in absorption was related to nutrients, as restricting the feeding period to the daytime only resulted in peak levels of absorption during the day[12]. These findings preceded the discovery and characterization of specific glucose transporters, hence these experiments measured total glucose uptake using isolated segments of intestine at diurnal timepoints. The authors hypothesized that these rhythms were likely to be mediated at least in part by the known rhythmicity in intestinal proliferation[66].

Other groups have also demonstrated rhythmicity in intestinal function besides rhythms in absorption. Saito demonstrated diurnal rhythms in the activities of maltase and leucylnaphthylamidase, with peak activity occurring during feeding periods[67]. Subsequently circadian rhythmicity in intestinal absorption was confirmed and further developed in a series of experiments by Stevenson et al, who demonstrated circadian rhythmicity in the activity of sucrase, lactase, trehalase, γ-glutamyltransferase and as previously shown, maltase and leucylnaphthylamidase[68].

1.4.3.2. Rhythmicity in absorption of individual nutrients

1.4.3.2.1. Rhythmicity in SGLT1-mediated glucose uptake

The initial findings of diurnal rhythmicity in intestinal glucose absorption preceded the characterization of specific intestinal transporters. As described previously, the sodium glucose co-transporter SGLT1 was the first transporter to be characterized[43]. *Sglt1* was found to exhibit diurnal rhythmicity with peak mRNA expression in the afternoon and evening, in anticipation of and during the time of peak nutrient uptake[13, 63, 69]. These studies used phloridzin as an SGLT1-specific inhibitor and identified complete loss of rhythmicity following SGLT1 inhibition, indicating that SGLT1-mediated glucose uptake was entirely responsible for the diurnal rhythmicity of glucose absorption[13, 69].

1.4.3.2.2. Rhythmicity of other transporters

Circadian rhythmicity has also been noted for a number of other intestinal transporters[70, 71]. The H^+-coupled peptide transporter is responsible for active uptake of peptides at the brush border of the intestine[47]. Peptide absorption has been shown to display diurnal rhythmicity with peak in absorption of L-histidine occurring during the dark phase in nocturnal animals[64], coincident with higher levels of PEPT1 protein expression during the dark phase than the light phase[70].

Recent studies have shown that certain drug transporters also exhibit rhythmicity of expression in the intestine[71]. These transporters act as efflux proteins in the intestine to facilitate the excretion of the metabolic products of many drugs including digoxin[72] and methotrexate[73]. Five drug transporters (*Mdr1*, *Mct1*, *Mrp2*, *Bcrp* and the peptide transporter *Pept1*, which also transports β-lactam drugs[74]) are diurnally rhythmic in the intestine at a transcriptional level[71]. A 2-5 fold change in expression was observed between peak and trough times and peak expression varied from morning to late afternoon[71].

1.4.4. Tissue-specific circadian rhythmicity

It is of interest to note that the same transporters that exhibit circadian rhythmicity in the intestine do not necessarily show a similar rhythmicity in other organ systems. SGLT1 and PEPT1 are two such examples, displaying profound rhythmicity in the intestine, but lacking diurnal rhythmicity in either mRNA or protein expression in the kidney[70]. This has implications for the regulatory mechanisms driving this rhythmicity and suggests that tissue-specific regulatory factors may be responsible for this differential pattern of expression across tissues.

1.4.5. The rationale for using rats in diurnal rhythm experiments

The vast majority of experimental research on circadian rhythms in feeding has been performed in rats. Although mice may be better suited for genetic manipulation to decipher the molecular pathways regulating circadian anticipatory rhythms, mice are not as adaptable to restricted patterns of food availability[75]. Rats are nocturnal opportunistic feeders, which adapt well to "stuff-and-starve" schedules based on food availability, making them an ideal species for investigation of the regulatory pathways behind circadian rhythmicity[75]. While non-human primates may ideally represent the closest genetic species to humans, the use of this species as an animal model is limited by cost and the need for dedicated primate research facilities.

1.4.6. Cues regulating feeding rhythms

1.4.6.1. Nutrient availability and light cycle

The majority of research performed on circadian rhythmicity in nutrient absorption has been performed in rats. The association of nutrient consumption with the dark phase in the rat[13] has necessitated further experiments to isolate the period of nutrient availability from light cycle. The first experiments on this were performed by Fisher and Gardner[12], who demonstrated that restricting feeding to only a few hours during the daytime resulted in an initial reduction in food consumption and weight loss, but this

normalized within one week. Rates of absorption were similar toward the end of the feeding period regardless of whether animals were fed during the lights on or lights off period[12]. Pan et al[76] corroborated the findings of Fisher et al[12] by showing that peak SGLT1 mRNA and protein expression was shifted forwards by 8 hours in rats fed for a few hours during the day compared to those fed at night[76], suggesting that the effect of restricted feeding on shifting glucose absorption may be mediated by a phase shift in SGLT1 expression.

1.4.6.2. Effects of food deprivation and intravenous nutrition

The necessity for luminal nutrient exposure for the maintenance of diurnal rhythmicity has been investigated in animals subjected to food deprivation followed by a period of refeeding[76]. Food deprivation decreased overall levels of SGLT1 mRNA and protein at all timepoints compared to fed rats[76]. In addition rhythmicity in SGLT1 protein expression was abolished after as little as two days of food deprivation despite persistent rhythmicity in expression of *Sglt1*, suggesting that nutrient exposure may regulate rhythmicity at a post-transcriptional level, but was not essential for transcriptional rhythmicity[76].

Circadian rhythmicity in glucose absorption was lost after 9 days of continuous intravenous feeding[77] however rats administered discontinuous periods of

intravenous infusion showed persistent rhythmicity with discontinuous intravenous infusion, suggesting that the episodic nature of nutrient availability is a more important cue than local nutrient exposure.

1.4.7. Physiological mediators of rhythmicity

1.4.7.1. Circadian hormones

Several hormones are known to exhibit circadian rhythmicity and also have a role in regulating baseline glucose absorption[78-80]. These hormones may therefore represent candidate mediators of the rhythmicity in glucose absorption; however at present few studies have investigated this. Glucocorticoids are secreted by the adrenal gland[1] with a circadian rhythm[81], reaching a peak around or just before the onset of activity in both diurnal and nocturnal mammals and have been implicated in the regulation of circadian function as the rhythmicity in their expression is able to rapidly adapt to alterations in activity or feeding schedule[82]. Administration of glucocorticoids was able to synchronize asynchronous fibroblasts in vitro to a common circadian phase[83, 84] and transiently induce the expression of *mPer1* in the mouse liver in vivo[85]. The effects of glucocorticoids are dependent on a functional glucocorticoid receptor, which is absent in the suprachiasmatic nucleus (SCN)[85, 86], hence glucocorticoid administration was unable to shift SCN clock gene expression. Glucocorticoids are also known to affect glucose absorption in rats by stimulating transcription of glucose transporters[78]. The effects of glucocorticoids on peripheral

tissues will be described further later in this chapter. The specific role of glucocorticoids in the regulation of the circadian rhythm of intestinal glucose absorption has not been studied.

Leptin is another circadian hormone released by adipose tissues, with levels reaching a peak after a meal and declining until the next meal[79]. Leptin has also been shown to inhibit glucose absorption via SGLT1 and has therefore been implicated in the circadian regulation of glucose absorption[80]. Other circadian hormones such as ghrelin have been implicated in regulation of nutrient intake, but are as yet not known to have a direct role in nutrient absorption[87].

1.4.7.2. Neural mediation of circadian rhythmicity

The nerve supply of the small intestine consists of the afferent and efferent limbs of the vagus and the intrinsic enteric nervous plexuses[1]. Rhythmicity of SGLT1 protein expression was lost following total vagotomy (ablation of both the afferent and efferent vagal limbs) despite persistence of transcriptional rhythmicity[88]. These findings were reproduced with selective ablation of only the afferent limb of the vagus[89], suggesting a role for the afferent limb of the vagus in post-transcriptional regulation of SGLT1 rhythmicity.

Less is known on the exact role of the intrinsic or intramural neural network in regulation of intestinal function. A recent study examining the effects of disruption of the intrinsic nervous system by transection and reanastomosis of the intestine revealed no effect on basal levels of hexose transporter expression or glucose uptake[90], suggesting that baseline or non-diurnal intestinal absorptive function is independent of the intrinsic neural network. This does not exclude a role for the intrinsic nervous system in the diurnal regulation of intestinal absorption, which has yet to be studied.

1.5. Circadian rhythmicity of intestinal proliferation

1.5.1. Apoptosis and proliferation in the intestine

The proliferative capacity of the intestine is uniquely tailored to meet the absorptive needs of the organism. Intestinal proliferation is confined to the crypt fraction[91], and driven by the division of intestinal stem cells situated at position +4 relative to the crypt bottom[92]. Cell division in the crypt is mediated by the transcription factor c-myc[93] and facilitated by cell cycle proteins which mediate the progression of cells through the successive stages of the cell cycle[94] which are detailed further in section 1.5.4. Crypt cells are able to differentiate into secretory cells, namely Paneth cells, goblet cells, and enteroendocrine cells or absorptive enterocytes, as described in section 1.2.1 and shown in Figure 1.2. Lineage specification in the intestine is mediated by the Wnt[95] and Notch[96] signaling pathways, which direct differentiation into the secretory and absorptive lineages respectively .

Proliferation in the intestine is countered by a low rate of apoptosis, which serves to regulate the number of crypt cells entering the crypt villus axis and is also thought to occur as part of the cell shedding process on the villus tip[97]. The tumour suppressor p53 has been shown to play a vital role in mediating the induction of apoptosis in many tissues[98]. Nuclear p53 binds to Mdm2 [99]; cellular stress induces translocation of p53 into the cytoplasm, allowing sequestration of p53 by anti-apoptotic Bcl-2 family members such as Bcl-XL and Bcl2[100]. The interaction of p53 with anti-apoptotic proteins is disrupted by one of its targets, PUMA, which liberates p53 to associate with

pro-apoptotic proteins such as Bax or Bak[101, 102]. This is turn activates caspases, cysteine proteases which cleave target proteins to bring about the characteristic nuclear changes of apoptosis[103-105].

Studies using transgenic mice have attempted to better characterize the proteins mediating apoptosis in the small intestine. In particulary these experiments have shown an insignificant role for p53[106, 107] Bax[108, 109] and Bcl2[110, 111] in small intestinal apoptosis – mice deficient in either of these proteins have similar rates of apoptosis to their wildtype counterparts. These findings indicate that the specific proteins and perhaps also the regulatory cues mediating the apoptotic process in the small intestine are distinct from that in other tissues.

1.5.2. Overview of rhythmicity in intestinal proliferation and apoptosis

The first description of circadian rhythmicity in proliferation in the intestine was by Sigdestad et al, in 1969[66], who identified a circadian rhythm in both the mitotic index as well as deoxyribonucleic acid (DNA) synthesis in mouse duodenum. This was subsequently corroborated by Scheving et al in 1972[112], who showed that although the amplitude of change in DNA synthesis was low, varying from 30 to 60% depending on the site, there was nonetheless a consistent rhythm across circadian timepoints. In animals acclimatized to a 12:12 light dark cycle, DNA synthesis peaked at the transition from dark to light and reached a trough at the transition from light to dark[66]. In addition, although the amplitude of the rhythms of proliferation varied significantly depending on the site within the gastrointestinal (GI) tract (rhythms exhibited greatest

amplitude in the mouth and anus, the most proximal and distal ends of the gastrointestinal tract respectively), the time of peak DNA synthesis was relatively consistent along the length of the GI tract. For example, DNA synthesis in mouse jejunum demonstrated peak ^{3}H-thymidine uptake during daylight hours, with rhythms of amplitude between 40 to 51%, a similar peak to that demonstrated in the oesophagus, duodenum and colon [112].

Circadian rhythmicity of intestinal apoptosis has similarly been studied, however the assessment of circadian rhythmicity of spontaneous apoptosis in the small intestine is difficult due to the low levels of spontaneous apoptosis[113]. Radiation-induced apoptosis has proved a well-characterized model, facilitating the measurement of circadian rhythms in apoptosis. Using this model several groups have identified higher rates of apoptosis in mouse duodenum and colon during the fasting lights-on period compared to the nocturnal feeding period[114-116].

1.5.3. The role of nutrients in the regulation of rhythmicity in intestinal proliferation and apoptosis

DNA synthesis in the rodent gastrointestinal tract begins to increase following the light-dark transition, in phase with feeding behaviour and motor activity, reaching a peak at or after the dark-light transition[112]. Rhythmicity of cell proliferation in the intestine is synchronized to the light cycle in animals fed ad libitum, however restricted feeding shifts the peak in DNA synthesis – suggesting a role for nutrients in the regulation of the rhythm in intestinal proliferation[112]. Circadian rhythmicity in proliferation persisted

for up to 34 hours in the stomach, foregut and hindgut of animals fasted for a period of 8 hours[117]. Other studies have shown rhythmicity of tongue epithelium to persist for even longer periods of fasting of up to 72 hours[118].

Ablation of the SCN did not abolish rhythmicity in the digestive tract, but instead caused a phase advance in the rhythms of proliferation in the tongue, esophagus, stomach and colon and had a variable effect on the amplitude of rhythmicity depending on the site along the GI tract[112]. Overall these findings suggested that the SCN was not essential for maintenance of rhythmicity in GI proliferation, which might instead have a greater reliance on molecular pathways triggered by food availability.

Nutrient exposure is also likely to play a role in the regulation of circadian rhythmicity of apoptosis. In contrast to the nocturnal feeding mice, the diurnal Mongolian gerbil did not demonstrate circadian rhythmicity in intestinal apoptosis[119]. Fasting increased the rates of apoptosis in the intestine of these gerbils, while refeeding decreased the rate of apoptosis. A similar increase in the rate of apoptosis was demonstrated in fasted rats compared to fed rats[120]. Together these findings highlight a role for luminal nutrient exposure in the regulation of circadian rhythms in apoptosis.

1.5.4. Molecular pathways regulating circadian rhythmicity in intestinal proliferation

To date the molecular pathways underlying circadian rhythmicity in cellular proliferation in the intestine remain unclear. A recent microarray-based study on circadian gene

expression in mouse colon revealed that a large percentage of rhythmically-expressed genes (26%) were involved in cell proliferation, cell cycle and DNA replication[121]. Of greater interest, not all oscillating transcripts in this study displayed corroboratory rhythms in protein expression, highlighting the importance of both transcriptional and translational regulation in maintenance of cell proliferation rhythms in the GI tract[121]. Despite this, only one study to date has attempted to identify specific proteins that may regulate this rhythmicity in enterocyte proliferation[122]. Cell cycle proteins are known regulators of cell division and facilitate the transition between quiescence, DNA replication and mitosis[123-125]. Cyclin D/ CDK4/6 and cyclin E/CDK2 complexes, largely restricted to the crypts, facilitate the G1/S transition of crypt cells, promoting enterocyte proliferation[94]. These cell cycle proteins have been shown to exhibit diurnal rhythmicity in expression in human intestinal tissue - colonic biopsies taken at 6 hourly intervals over a diurnal period revealed rhythmicity in the expression of G1/S regulators cyclins D1 and E, with peak expression in the evening at 18:00 and the trough in expression at 00:00[122]. Conversely in the same study p16 and p21, proteins which inhibit the activity of cyclin-dependent kinases, exhibited circadian rhythmicity in antiphase to cyclins D1 and E, with lowest expression at 12:00 and 18:00. The rhythmicity in cell cycle proteins and CDK inhibitors corroborates the hypothesis of a potential role for these proteins in the circadian regulation of enterocyte proliferation.

Rhythmicity in indices of intestinal cellular proliferation has also been described; human rectal mucosa exhibits circadian rhythmicity in DNA synthesis (S-phase) in both fasting and fed conditions as measured with ^{3}H-thymidine incorporation, with a peak at 07:00[126, 127]. This is in keeping with rodent data, although the timing of peak DNA

synthesis is in antiphase in rats[112] versus humans[126, 127] (early activity in humans vs. late activity in rodents), consistent with the nocturnal feeding behaviour of rats versus diurnal humans.

1.6. Clock genes

1.6.1. Overview of clock genes

The circadian clockwork is regulated by a set of genes, referred to as clock genes, involved in the regulation of circadian rhythms such as hormone secretion and autonomic functions including body temperature and blood pressure[128, 129]. Clock genes have been shown to regulate other intestinal transporters[14-16] and are hence a potential candidate for mediating transcriptional rhythmicity in the main intestinal glucose transporter, SGLT1. In mammals, the master clock resides in the SCN and maintains a 24-h periodicity entrained by light[130] and regulated via opposing positive and negative molecular feedback loops. Rhythmicity of the SCN is cell autonomous , as rhythms can persist in cultured conditions for weeks in the absence of external entraining stimuli[131].

1.6.2. Description of the discovery of clock genes

The molecular pathways and genes regulating circadian rhythms were first investigated in the suprachiasmatic nuclei (SCN), considered the master circadian clock and responsible for generating circadian rhythms[132-134]. The SCN are small paired structures situated in the anterior hypothalamus, just above the optic chiasm and strategically positioned for receiving visual input for light-dark entrainment via the

retina[135]. Although the first and most complete description of the molecular control of the circadian clock was accomplished in the fruit fly, *Drosophila melanogaster*; the core clock mechanisms of *Drosophila* and mammals are highly similar, in both cases consisting of interlocking positive and negative transcriptional-/translational-feedback loops[134]. Minor differences exist in the clock control pathways between the two species and will be discussed further later in this chapter. For a thorough review of the clock gene molecular feedback loops in *Drosophila*, readers are recommended to consult the following articles[136-138].

1.6.3. Clock genes in Drosophila

1.6.3.1. Circadian rhythmicity in Drosophila

Initial studies on circadian rhythmicity in *Drosophila* used two major rhythmic behavioral outputs—eclosion and locomotor activity[139, 140]. Eclosion - the hatching of adult flies from their pupal cases, occurs predominantly at dawn and was used to examine the role of clock genes in the circadian rhythm of metamorphosis[139]. This evolved from the original habitat of fruit flies in sub-Saharan Africa, when the morning hours were optimal for pumping of haemolymph into their wings to allow them to fly (hence the name Drosophila – "dew-lover" in Greek)[136]. Locomotor activity also shows circadian rhythmicity in *Drosophila*, with a bimodal distribution of activity confined largely to daylight hours when kept under light:dark cycles[140]. The circadian

nature of this activity is confirmed by the observation that under free-running conditions such as constant darkness, the bimodal peak in activity usually disappears and activity occurs throughout the subjective day[137]. More recently circadian rhythmicity has been noted in other processes such as olfactory responses, visual pigment and sensitivity and egg-laying [141-143].

1.6.3.2. Clock genes and feedback loops in *Drosophila*

The clock molecular pathways and the feedback loops mediating circadian rhythmicity in *Drosophila* are well-characterized[136, 144, 145]. Clock proteins CLK (clock) and CYC (cycle, the homologue of mammalian BMAL1) dimerize and activate transcriptional induction of *period (per)* and *timeless (tim,* the analogue of mammalian *Cry)* at ~ZT12 via E-box elements[146]. As *per* and *tim* RNA levels rise, phosphorylation by DBT (double-time*)* prevents PER from accumulating and renders it unstable in the absence of TIM[147-149]. TIM is a light-labile protein, hence at nightfall levels of TIM rise, protecting PER from degradation and allowing stable TIM:PER heterodimers to form and translocate into the nucleus[150-152]. PER binds to dCLK via a small conserved dCLK binding domain (CBD) thereby inhibiting the transactivation potential of dCLK-CYC[153]. TIM in turn stabilises PER in the cytoplasm by attenuating the degradation of PER by DOUBLETIME (DBT, the *Drosophila* homologue of CK1ε/δ. Although TIM has no repressional activity of its own[146, 154, 155], it is able to act as a scaffold to bridge the association of PER and CLK, thereby mediating the transcriptional repression of

PER[153]. The onset of daylight destabilises TIM and with reducing TIM levels, PER is no longer protected from degradation[150, 151]. Levels of PER and TIM are therefore sufficiently low by next dawn to disinhibit CLK:CYC activity, stimulating the next cycle of transcription of *per* and *tim* and a new round of synthesis[138]. Readers are recommended the following references for a thorough review of clock genes in *Drosophila*[136, 144, 145].

1.6.4. The molecular feedback loops of clock genes in mammals

The molecular clockwork within the SCN consists of interacting positive and negative feedback loops[134, 135]. The negative-feedback loop involves the rhythmic induction of three *Period* genes (designated *Per1–3*) and two *Cryptochrome* genes (*Cry1* and *Cry2*) by heterodimerization of the transcription factors CLOCK and BMAL1 (Figure 1.4)[156-159]. CLOCK and BMAL1 contain the functionally important basic helix-loop-helix (bHLH)–PER-ARNT-SIM (PAS) protein dimerization domain[160, 161], which binds to and activates E-boxes (sequences of CAnnTG) on the promoters of the *Per* and *Cry* genes[161, 162]. PER and CRY subsequently form multimers that translocate to the nucleus, where they directly interact with CLOCK and/or BMAL1 to inhibit transcription[156, 158]. This is turn induces rhythmicity in the transcription of *Bmal1*, with a phase opposite that of *Per* or *Cry*, resulting in a positive-feedback loop[158, 163].

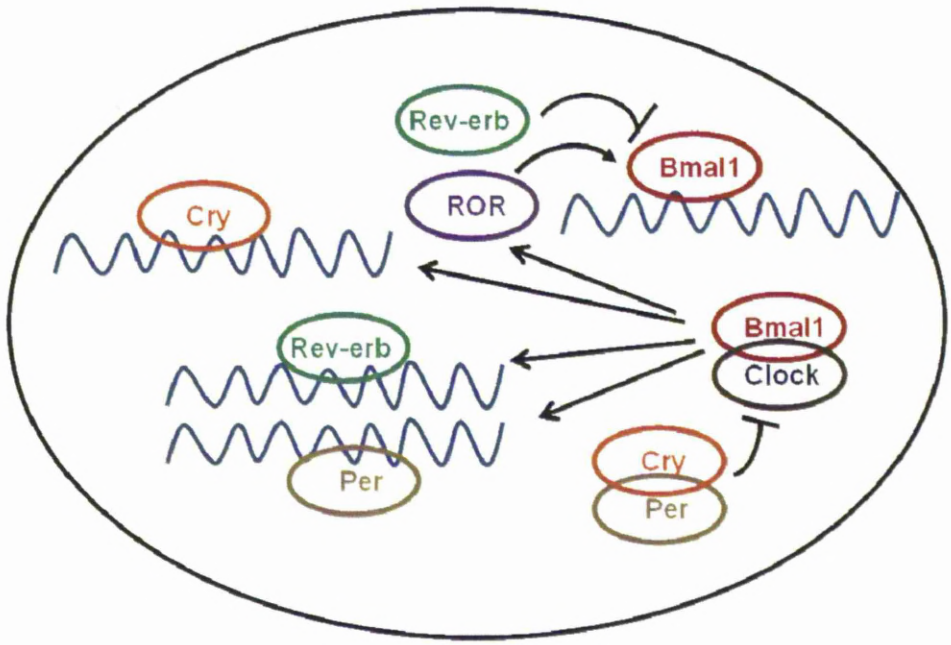

Figure 1.4: Schematic showing the molecular feedback loops of circadian clock genes. Black pointed arrows indicate stimulation of one clock gene component by another, while the truncated arrows indicate repression.

More recently three further genes have been identified – Retinoic acid-receptor-related orphan receptor (*ROR) -α* and *Rev-erbA* and *Rev-erbB*[164]. These orphan nuclear receptors have been identified as key regulators linking the positive and negative limbs of the circadian oscillator, with *Reverb* and *ROR-α* transcription driven by BMAL1/CLOCK and in turn suppressing and activating *Bmal1* expression respectively, acting as an accessory loop to improve the amplitude and stability of the core clock regulatory loops[164, 165].

Clock genes subsequently regulate downstream events via rhythmically expressed clock-controlled genes (CCGs) that are regulated (directly or indirectly) by the core feedback loops[166, 167]. Examples of CCGs directly regulated via CLOCK:BMAL1 heterodimers acting on E-box enhancers include arginine vasopressin (AVP)[166] and albumin D-element-binding protein (DBP)[166, 167]. Both these genes express robust rhythmicity in the SCN which is blunted in *Clock* mutant mice[135].

Clock gene expression in the SCN is cued by the detection of light by the retina, which is transmitted to the SCN by several convergent pathways, the most important of which is the retinohypothalamic tract (RHT)[168-170] which arises from the retinal ganglion cells and transmits the light signal to the SCN using the neurotransmitter glutamate[171]. Indirect pathways such as the geniculohypothalamic tract also play a role, as do neurohumoral signals such as the pineal hormone melatonin[135]. Previous studies suggest that *Per1* is the most likely candidate clock gene for resetting the circadian clock via photic stimulation[172, 173]. *mPer1* was the only gene altered by exposure to light at night in mice; this was blunted by the introduction of antisense oligonucleotides to *mPer1*[172, 173]. *mPer1* is directly stimulated by phosphorylation of cAMP response element-binding protein (CREB) acting via a cAMP response element (CRE) in the 5′-flanking region of the *mPer1* gene[174]. mPER1 in turn stabilizes mCRY1, extending the duration of negative feedback on the clock[172].

1.6.5. Peripheral circadian oscillators

Circadian rhythmicity exists in many tissues besides the SCN[175-179] and may be mediated by rhythmically expressed clock genes in these tissues. These peripheral oscillators may exist to provide increased flexibility to allow the organism to adapt to a greater variety of stimuli. Although cued by the SCN, the ability of peripheral oscillators to be entrained by other external stimuli such as nutrients[180-182] allows the organism to optimally adapt to match environmental challenges, for example to alter liver function to match the timing of delivery of nutrients and metabolites[180, 181].

Circadian rhythmicity had been noted in other tissues outside the SCN long before the cloning of clock genes[175-179]. The retinae of hamsters was found to exhibit circadian rhythmicity of melatonin production in vitro, entrainable by light[175]. Subsequent cloning of clock genes revealed that this rhythmicity in function corresponded with rhythmicity of *mPer1-3* in the mouse eye, with a 3-6h delay relative to the SCN[183]. Peripheral oscillators now been characterized in a number of other tissues, including the heart, lung, kidney, peripheral blood cells and liver, with a 3-9h phase delay in oscillatory rhythms relative to the SCN [176-179].

A number of observations suggest that the molecular machinery driving rhythmicity of the circadian clock in peripheral tissues may bear a number of significant differences to

that in the SCN. Firstly, rhythms of clock genes exhibit a phase delay in peripheral tissues relative to that in the SCN[180, 181]. Secondly *Bmal1* levels are elevated in the peripheral tissues of *Clock-/-* mutants, but blunted and expressed at reduced levels in the SCN of these mice[184], suggesting that negative autoregulation by CLOCK/BMAL1 heterodimers affects *Bmal1* transcription in the periphery but not in the SCN. Thirdly, unlike in vitro cultures of SCN cells, which maintain their rhythms indefinitely[131], cultures derived from peripheral tissues exhibit circadian rhythms which dampen after 2-7 cycles[185]. These findings suggest that peripheral oscillators may involve a population of asynchronous cells requiring intermittent synchronizing stimuli, either from the SCN or external entraining cues as occurs in vivo. This is further corroborated by the ability of a serum shock consisting of 50% serum to induce rhythmicity in clock gene transcription in cell lines including fibroblast derived cell lines *in vitro*[84].

Peripheral clocks are primarily cued by the SCN master clock - destruction of the SCN flattens oscillatory rhythms in peripheral tissues such as the liver[186]. Circadian transcripts continued to oscillate following liver-specific deletion of *Clock* in mice in the presence of an intact SCN clock[187, 188], possibly as a result of persistent rhythmicity in feeding behaviour.

Although light (which is the predominant Zeitgeber ("time-giver" or circadian cue) for the SCN) may indirectly initiate rhythmicity of peripheral tissues, a number of other stimuli are able to regulate peripheral oscillators and dissociate rhythms of the peripheral clock from that of the SCN[85, 180, 181, 186, 189-191]. These include

adrenergic stimulation[186], glucocorticoid exposure[85, 189-191] and one of the strongest cues – nutrient availability[180, 181]. Nutrient availability in contrast is a powerful Zeitgeber - restricted feeding was able to reinstate circadian rhythmicity of hundreds of genes which had been blunted in *Cry1-/-Cry2-/-* mice and in otherwise arrhythmic SCN-lesioned mice[192]. Restricted feeding also reset the peripheral clocks in the liver, kidney, heart and pancreas within one week with no change in the phase of the SCN clock[180, 181, 193]. Glucocorticoid signalling has been postulated as a potential regulator of peripheral clocks, specifically as mediators of the effects of nutrient-induced phase shifts in clock gene expression[85, 189-191]. However recent studies have demonstrated that the phase shifts in rat liver seen in restricted feeding could not be induced by daily corticosterone injections to simulate the endogenous peak of these hormones in animals subjected to restricted feeding[180]. Le Minh et al developed these findings further by showing that rather than facilitating phase shift, glucocorticoids act to inhibit phase shifts of peripheral oscillators to daytime feeding and may in fact exist to prevent a rapid uncoupling of peripheral oscillators from the SCN[82].

Other studies have identified a role for intracellular kinases such as protein kinase A, protein kinase C and mitrogen-activaged protein kinase (MAPK) in the synchronization of the peripheral clock acting through cAMP response elements (CRE sequences) of *Per* genes[194-197]. The oscillation of clock genes in vascular smooth muscle can be initiated by angiotensin II and reset by retinoic acid[198, 199], while in the pituitary gland rhythmicity of Per expression is maintained by an interaction between melatonin

secretion and adenosine[200]. Together these studies suggest that the synchronization of peripheral clocks may be regulated by a number of endorine and paracrine cues in a tissue-specific manner[201].

Light cycle alone is not a strong cue for clock genes in peripheral tissues; mice held in constant darkness continued to exhibit rhythmic feeding and examination of liver transcripts in these mice revealed that 15% of transcripts continued to exhibit circadian rhythmicity despite a 24-hour dark-dark cycle[202].

1.6.6. Clock genes as rhythmic transcriptional regulators

Clock genes are clearly important transcriptional regulators[14-16]. Several intestinal proteins have been found to be regulated by clock and clock-controlled genes; for instance CLOCK/BMAL1 heterodimers bind directly to the promoter of the Na^+/H^+ exchanger *Nhe3* in the kidney to induce circadian rhythmicity of *Nhe3* mRNA in the rat[14]. The clock-controlled output gene, DBP has been noted to bind to and activate the promoter of the oligopeptide transporter *Pept1* [16], while similarly clock-controlled output genes hepatic leukemia factor (HLF) and E4 promoter binding protein-4 (E4BP4) regulated transcription of the multidrug resistance 1 (*Mdr1a*) gene via a reciprocating mechanism involving competition for the same *Mdr1a* promoter DNA binding site[15].

To date no studies have examined the role of clock genes in the regulation of SGLT1 rhythmicity and thereby the rhythmicity of glucose uptake in the intestine.

While clock genes may be candidates for the regulation of individual genes involved in intestinal absorption such as SGLT1, a newly discovered class of molecules known as microRNAs has been shown to regulate cellular properties such as proliferation[18-24] and circadian rhythmicity[17, 203] in non-intestinal tissues, making these genes potential regulators of the rhythmicity of intestinal proliferation.

1.7. microRNAs

1.7.1. Overview of microRNAs

microRNAs are a class of endogenous gene silencers, capable of simultaneously regulating multiple genes and implicated in the control of many cellular processes including proliferation[18-24]. Recent studies have suggested that microRNAs are able to regulate the phenotype of tissues [204, 205] facilitated by the ability of a single microRNA to simultaneously silence the expression of multiple genes[20, 206-209], thereby targeting many proteins within the molecular pathway[207-209]. By this method, microRNAs might exert a greater degree of control over each cellular process than by controlling individual genes; as the degree of control over individual genes identified in most studies is often modest[207-209]. One example of this is the ability of *miR-16*, to not only downregulate the anti-apoptotic gene Bcl2-like 2[18], but to also independently causes cell cycle arrest by downregulation of cell cycle components cyclin D1, cyclin D3, cyclin E1 and CDK6 in hepatocytes[20], simultaneously inducing an accumulation of cells in G0/G1 as well as an increase in apoptosis.

Other studies have demonstrated the importance of "clusters" of microRNAs. Analysis of tumour samples compared to normal samples has revealed the presence of a microRNA "signature" – a group of similarly overexpressed or underexpressed microRNAs associated with a particular type of malignancy[210-213]. These expression profiles correlated with lineage and stage of differentiation of tumours better than

transcriptional profiling using mRNAs[214]. Overexpression of clusters of microRNAs, often genomically adjacent, results in phenotypic changes in vivo such as increased proliferation and an undifferentiated phenotype[215].

1.7.2. Functions of microRNAs

microRNAs have been shown to exhibit varied functions in a number of tissues[210, 211, 214, 216-220]. microRNAs are able to regulate development and differentiation at a global level or at a tissue-specific level[221-224]. Knockout of Dicer, a key enzyme in microRNA biogenesis, produced embryonic lethality and morphological abnormalities in mice[221]. Dicer-null mouse embryonic stem cells similarly exhibited severe defects in growth and differentiation and exhibited prolonged G0 and G1 and failed to express key differentiation markers[222, 223]. microRNAs also play a role in adult stem cells; for instance *miR-221*, *miR-222* and *miR-223* regulate terminal haematopoietic differentiation pathways[224].

The ability of microRNAs to simultaneously regulate multiple genes has made this class of molecules a particular topic of interest in cancer research. Several studies have identified differences in the profile of microRNAs in cancerous and non-cancerous tissues[210, 211, 214, 218]. microRNAs have also been shown to mediate changes in visceral function, such as cardiac failure[216, 217], diabetic nephropathy[219] and

hypertension[220]. For a review of the role of microRNAs in differentiation, cancer and visceral function, readers are recommended the following review articles[225-228].

microRNAs are already known to exhibit circadian rhythmicity in the SCN[229] as well as some peripheral tissues[17, 203] and hence rhythmicity in microRNA expression in the intestine may represent a potential mechanism governing the rhythmicity in intestinal function.

1.7.3. Background of microRNA discovery

microRNAs were first discovered when Ambros and colleagues, in 1993, found that *lin-4*, a gene known to regulate *C.elegans* larval development, was not translated into a protein, but instead was transcribed into a 22nt RNA[230]. Ruvkun et al subsequently identified translational repression of LIN-14 by *lin-4* following binding of lin-4 to 3'UTR binding sites in the *lin-14* gene[230, 231]. *lin-4* is now recognized as the first member of a new class of regulatory RNAs now termed microRNAs[232-234]. Further work since this discovery has further characterized the biogenesis and function of microRNAs. These single stranded RNA molecules are able to suppress protein translation of multiple targets, thereby simultaneously regulating the expression of hundreds of genes[232-234].

1.7.4. Biogenesis of microRNAs

microRNAs are transcribed via the action of pol II RNA polymerases, often from regions within introns of protein-coding genes (Figure 1.5), to yield the primary microRNA transcript, known as the pri-miRNA[235]. Nuclear cleavage by the microprocessor protein complex (containing DROSHA, an Rnase III endonuclease and DiGeorge syndrome critical region gene 8 (DGCR8 or PASHA)) at the base of the pri-miRNA releases a 60-70nt stem-loop microRNA precursor, or pre-miRNA[235, 236]. The pre-miRNA is transported into the cytoplasm via Ran-GTP and the export receptor Exportin-5 [237, 238], where the RNase III endonuclease, DICER, removes the terminal base pairs and loop of the pre-miRNA leaving an imperfect duplex with a 5' phosphate and 2 nt 3' overhang[239, 240]. This duplex is unwound to release 2 strands of RNA, the mature microRNA sequence and the microRNA* sequence. The mature microRNA is incorporated as a single-stranded RNA molecule into the RNA-induced silencing complex, or the RISC complex, which also mediates siRNA activity on its target sequence [241-243]. The microRNA* sequence is typically found in much lower concentrations in the cell than the miR sequences [233, 244]. microRNA processing has been shown to exhibit strand bias and the strand that is less tightly paired at the 5' end is preferentially loaded into the RISC complex[245, 246].

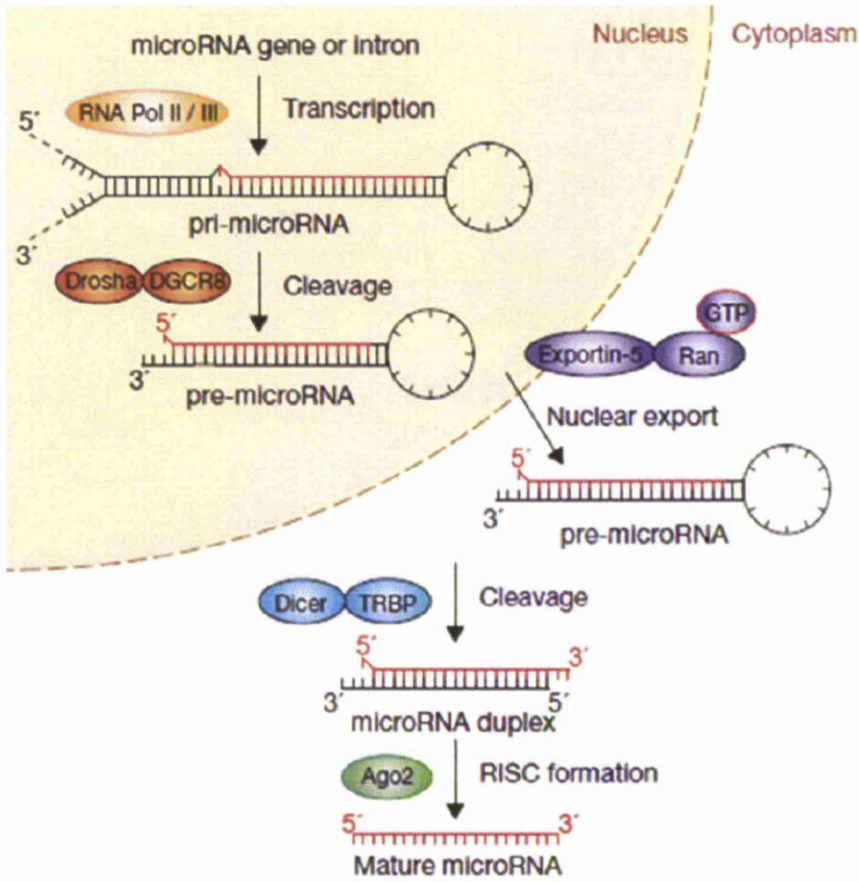

Figure 1.5: Schematic showing the outline of the biogenesis of microRNAs. Adapted from Winter, J et al, Nature Cell Biology 11, 228 - 234 (2009).

1.7.5. Mechanism of action of microRNAs

1.7.5.1. Transcriptional regulation

One method of microRNA-mediated target suppression is by RISC-mediated cleavage of the target sequence, facilitated by high sequence complementarity between the

microRNA and the target mRNA[242, 247]. The most important microRNA-mRNA pairing is that at the 2-8nt "seed region" of the microRNA[248]. microRNA-mediated cleavage occurs between nucleotides pairing at residues 10-11 of the microRNA, identical to cleavage mediated by siRNAs[242, 249]. Similar to siRNAs, microRNAs are themselves left intact following cleavage and able to cleave other targets.

1.7.5.2. Post-transcriptional regulation

The exact mechanism behind microRNA-mediated post-transcriptional suppression of target gene expression remains unclear; and several methods have been proposed[250-257]. Repression at the adenylation stage may occur by progressive shortening of the polyA tail following binding of the RISC complex to mRNA 3' UTR, resulting in decay of target mRNAs[250, 251]. Alternatively, miRNPs can repress translation initiation at either the cap-recognition stage, by inhibiting eukaryotic initiation factor EIF4e/cap and polyA tail function, or by preventing the 60S ribosomal subunit joining the 40s initiation complex [252-254]. microRNAs may also effect translational repression at post-initiation phases either by slowing elongation or ribosome 'drop-off' [255-257]. Another hypothesis is that repression may occur through proteolytic cleavage of nascent polypeptides by an as yet unidentified protease[256]. microRNAs have been postulated to each suppress multiple gene targets, both from bioinformatic as well as experimental studies[20, 206-209]. Several recent studies have demonstrated suppression of hundreds of proteins to a modest degree by a single microRNA[207-209]. It has

therefore been suggested that microRNAs may exist as a fine-tuning mechanism, designed to modulate the expression of many targets but only to a relatively small degree[207].

1.7.6. Rhythmicity of microRNA expression

Circadian rhythmicity has been described in 5-10% of gene transcripts[165, 193, 258, 259]. Of greater interest, an even greater fraction of proteins demonstrate circadian rhythmicity, for instance almost half of the proteins demonstrating circadian rhythmicity in the mouse liver lack a corresponding cycling transcript[260]. Regulation of this rhythmicity at both the transcriptional and post-transcriptional level suggests a role for microRNAs in this process.

MicroRNAs have been found to demonstrate circadian rhythmicity in a number of tissues[17, 203, 229]. Cheng et al found circadian rhythmicity in the expressions of *miR-132* and *miR-219* in murine brain, with up to a 3-fold difference in microRNA levels between subjective day and night[203, 229]. A subsequent study demonstrated rhythmicity of 12 microRNAs in the retina[203]. Two of these microRNAs– *miR-96* and *miR-182* – were shown to mediate rhythmic expression of the adenylate cyclase 6 (*Adcy6)* gene[203]. microRNAs were also found to exhibit circadian rhythmicity in Drosophila; two miRNAs (*dme-miR-263a* and *-263b*) demonstrated circadian rhythmicity

in Drosophila head which persisted in complete darkness, further supporting the circadian nature of this rhythmicity[261]. Another recent study identified circadian rhythmicity of *miR-122* precursors in the liver[17]. To date there have been no studies examining the temporal expression profile of microRNAs in the intestine.

1.7.7. Distinction between microRNAs and siRNAs

Although microRNAs can function very similarly to siRNAs, particularly when causing mRNA cleavage, a number of clear distinctions between these two classes of regulatory RNAs were described by Bartel[262]. First, miRNAs derive from genomic loci separate from other known genes while siRNAs often derive from mRNAs, transposons, viruses, or heterochromatic DNA. Second, miRNAs are processed from transcripts which form RNA short hairpin structures, while siRNAs result from long bimolecular RNA duplexes or extended hairpins. Third, each miRNA hairpin precursor molecule only produces two RNA sequences which pair as a single miRNA:miRNA* duplex. In contrast, each siRNA precursor molecule produces a multitude of siRNA duplexes resulting in many different siRNAs accumulating from both strands of this extended hairpin. Fourth, miRNA sequences often demonstrate evolutionary conservation, while endogenous siRNA sequences are rarely conserved. Fifth, microRNAs specify hetero-silencing, as they silence genes distinct from the gene of origin. In contrast, siRNAs specify auto-silencing, as they silence loci similar to that from which they originate.

1.8. Short bowel syndrome

1.8.1. Aetiology

Current estimates suggest the prevalence of short bowel syndrome in Europe to be approximately 2 patients per million[2]. Short bowel syndrome is defined as a remnant length of <200cm of small intestine, resulting in compromised absorption which may lead to intestinal failure, defined by the requirement for specialised nutritional support to maintain adequate nutritional status[2]. Short bowel syndrome may rarely be of congenital origin as a result of jejunal or ileal atresia[2]. In the majority of cases however, short bowel syndrome occurs as a result of surgical resection of small intestine. This may occur in the form of multiple resections for relapsing and remitting inflammatory conditions such as Crohn's disease, or as a result of massive small bowel resection for conditions of irretrievable vascular infarction and mesenteric ischaemia[2]. Sparing the colon in these patients improves absorptive capacity as the colon is able to absorb water, sodium and some amino acids, thereby allowing patients to tolerate greater loss of small intestinal length and avoiding supplemental nutrition[263].

1.8.2. Morphologic and physiologic adaptation to short bowel syndrome

Loss of a significant length of intestine is associated with adaptive changes, first described in by Dowling and Booth in 1967 using the model of massive small bowel resection in the rat[264]. This adaptive response includes increases in intestinal length as well as villus height and diameter to increase absorptive surface area[265, 266]. The decreased absorptive surface area in short bowel syndrome may also be compensated

for by increased food consumption (hyperphagia). The adaptive response to short bowel syndrome in rats is also associated with upregulation of SGLT1[267]. The diurnal rhythms of glucose absorption and proliferation have not been studied in the experimental model of massive small bowel resection and represent interesting studies for the future, however any data from these experiments should be interpreted with caution as altered food intake rhythms are likely to be a confounding factor in these animals.

1.8.3. Management of short bowel syndrome

Intestinal transplantation remains an important therapeutic option for short bowel syndrome, however graft rejection rates (one year graft and patient survival of 20%) remain high[268]. Post-operative infection[269] and the complications of immunosuppressive therapy[270] further limit the applicability of this option in the management of short bowel syndrome. Other recently developed intestinal reconstructive options such as the Bianchi procedure[271] and serial transverse enteroplasty[272] have a relatively high rate of complications and limited long-term outcomes data.

Nutrient delivery remains the one of the biggest challenges in short bowel syndrome. Parenteral nutrition, the delivery of nutrients via long-term intravenous access, is frequently necessary, but associated with significant side-effects, in particular the risk of line sepsis and the risk of cholestasis-associated liver dysfunction[273]. The morbidity and complications from total parenteral nutrition (TPN) contribute to an overall 5-year

survival of 60% in patients requiring home parenteral nutrition[274]. For a thorough review of the aetiology and management of short bowel syndrome readers are recommended the review articles by Wales et al[270] and Buchman[2].

1.9. Previous work from our group

Previous studies from our laboratory have confirmed the presence of diurnal rhythms in intestinal absorption. SGLT1 was found to exhibit a diurnal rhythm of expression at both the mRNA and protein level in the intestine, with peak mRNA and protein expression occurring at 1600h (just before the arrival of nutrients at 1900h) and during peak feeding time at 2200h[13, 63]. These studies suggested that rhythmicity of SGLT1 may mediate the known rhythms in intestinal glucose absorption and implicated the existence of rhythmic molecular pathways that increased SGLT1 expression in anticipation of nutrient arrival. Rhythmicity in SGLT1 was also confirmed at the mRNA level in duodenal biopsies from Rhesus monkeys[63], with peak expression of *Sglt1* occurring during the morning feeding period, confirming that this phenomenon also existed in non-human primates[63]. Subsequent studies used the SGLT1-specific inhibitor phloridzin to specifically examine the contribution of SGLT1-mediated glucose uptake to diurnal rhythmicity of glucose absorption[13, 69]. Patterns of rhythmicity in glucose uptake corresponded with rhythms in SGLT1 protein expression, which in turn was preceded by a peak in *Sglt1* mRNA expression[69]. These studies highlighted the need for further studies to identify the molecular pathways behind these rhythms. The intestine is known to exhibit rhythms in cellular proliferation, allowing peak absorptive capacity during the period of maximal nutrient availability, which are likely to contribute to the rhythmicity in glucose absorption. The mechanisms behind this remain poorly characterized.

1.10. Purpose of the proposed studies

The work in this thesis aims to investigate the molecular pathways behind the rhythmicity in intestinal glucose absorption. To decipher the molecular mechanisms behind this, this thesis will use two approaches - first, to identify the role of clock genes, implicated in the regulation of other diurnally expressed intestinal transporters, in the regulation of SGLT1 rhythmicity. Secondly, this thesis aims to identify the role of microRNAs, known to regulate proliferation in other experimental models, in the regulation of rhythmicity in intestinal proliferation.

AIMS:

- To correlate rhythms in *Sglt1* expression with rhythms in clock gene expression and identify clock genes that may be potential transcriptional regulators of *Sglt1* using in vitro studies.

- To identify microRNAs exhibiting diurnal rhythmicity in expression in the intestine and determine the effects of these microRNAs on enterocyte proliferation in vitro and to correlate rhythmicity in this microRNA with rhythms in morphology and proliferation in vivo

Chapter 2: Methods

2.1. Animal studies

All animal study protocols were prospectively approved by the Harvard Medical Area Standing Committee on Animals. Animals were maintained in a dedicated small animal facility in Thorn Building in Brigham & Women's Hospital, Boston. This animal facility is regulated by the Harvard Medical School ARCM and is fully accredited under the Association for Assessment and Accreditation of Laboratory Animal Care International (AAALAC) guidelines. Standard temperature (22°C) and humidity (70%) was maintained. An automated timer was used to control the light cycle; lights were switched-on at 7AM Eastern Standard Time and switched-off 12-hours later at 7PM. All time points used in the following experiments are expressed as Zeitgeber Time (ZT), where 7AM is ZT0.

All rats used were Sprague-Dawleys, an outbred albino rat species, purchased at 7 weeks of age from Harlan World (Indianapolis, IN) and housed in the Thorn Building Animal Research Facility at the Brigham and Women's Hospital, Boston, MA. Rats were caged in pairs in Perspex cages with wood chipping bedding. All animals had unrestricted access to water. All rats were fed Picolab Rodent Diet 20, Catalog no. 5053, LabDiet, Brentwood, MO, containing 21% protein, 9.9% fat, 4.4% fiber and a caloric value of 3.42kcal/gm.

2.1.1. Feeding patterns

2.1.1.1. Ad libitum and restricted feeding regimens

For examination of the temporal profiles of clock genes and SGLT1 in ad libitum and restricted fed rats in Chapter 3, 100 male Sprague-Dawley rats were acclimatized to a 12: 12-h light: dark photoperiod for 5 days with *ad libitum* access to food and water. In the control arm (n=50, designated "AL"), rats were culled at 3-hourly intervals after the 5 day acclimatization period, beginning at ZT 0 (n=6-7 per time, Figure 2.1(A)). A second group of rats (n=50) were randomly assigned after the 5 day acclimatization period to be fed for 7 days either during only the dark phase (designated "DF", ZT 12-24, Figure 2.1(B)), or light phase (ZT 0-12, designated "LF", Figure 2.1(C)). DF rats were pair-fed to LF rats to ensure equal food intake. Rats were housed in pairs in cages. LF animals were given 100g of food per cage at 0700. The remaining food at 1900 was weighed and subtracted from 100g to calculate the amount consumed per pair of rats (it was assumed that both rats consumed equal amounts of food). The mean daily consumption of LF animals was calculated, multiplied by 2 and provided to each pair of DF animals at 1900. No food remained in the cages of DF animals at 0700 the next day. To minimize disruption during restricted feeding, rats were weighed only 3 times (days 0, 4 and 8). On day 8, rats (n=6-7) were culled at 6-hourly intervals beginning at ZT 3.

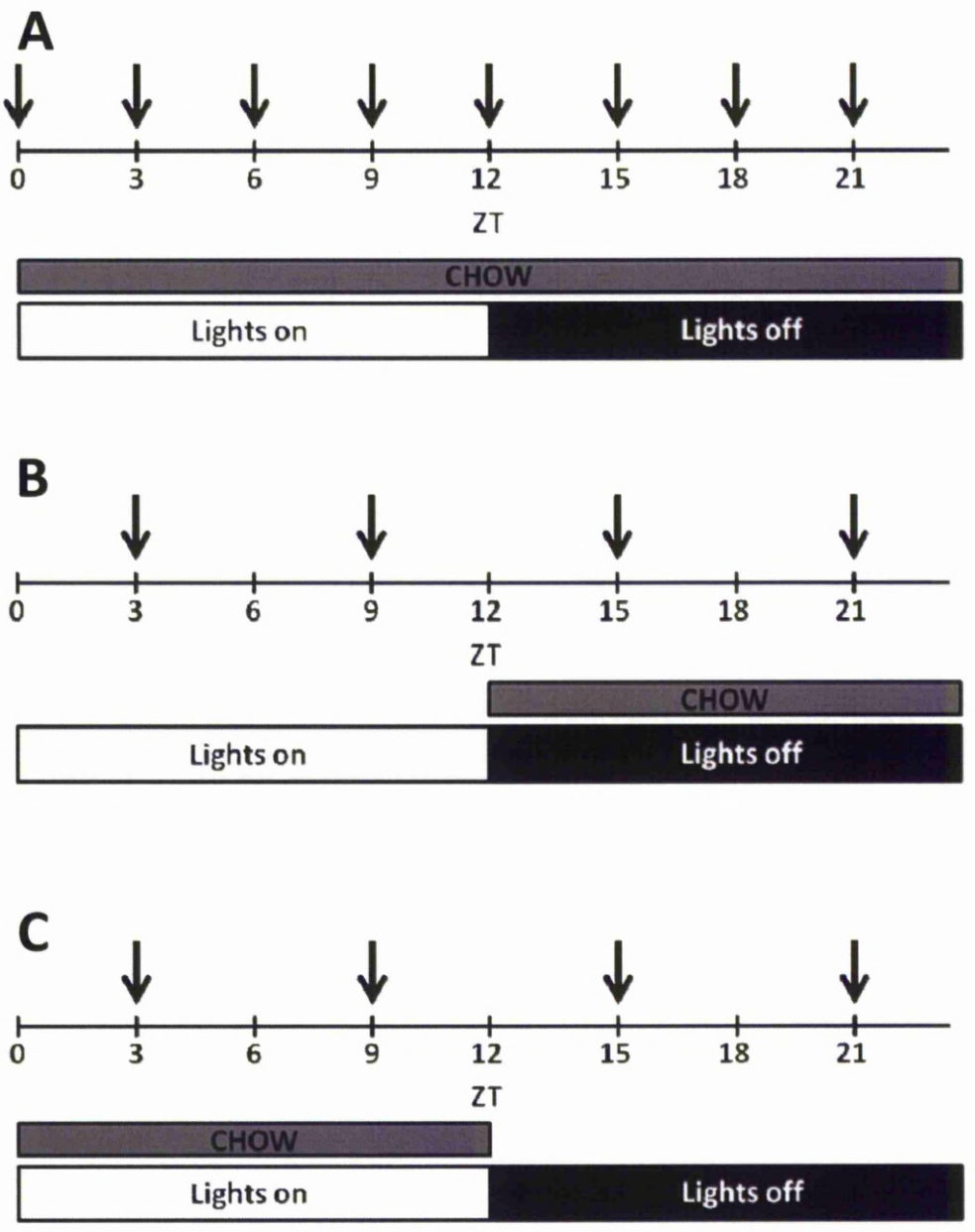

Figure 2.1: Schematic showing light cycle, time of food availability and harvest times. Harvest times are indicated in black arrows in AL (A), DF (B) and LF (C) rats, n=6-7 per time for all groups.

2.1.1.2. Diurnal ad libitum feeding regimens

For the microRNA and proliferation experiments in Chapter 5, 50 male Sprague-Dawley rats were acclimatized to a 12: 12-h light: dark photoperiod for 5 days with *ad libitum* access to food and water. Rats were injected with BrdU (5-bromo-2-deoxyuridine, 50mg/kg; Catalog no. B5002, Sigma, St Louis, MO) 1 hour before harvest to label DNA as an index of S-phase. Rats were culled at 3-h intervals over 24 hours (n=6-7 per time) and jejunum harvested for microRNA microarrays, RNA and protein determination and morphological analysis.

2.1.2. Harvest protocols

2.1.2.1. Anaesthesia

Rats were harvested in groups of 6-7 animals per time at the times described above. Tissue collection was performed while animals were still alive but anaesthetized to ensure the intestine remained perfused to ensure integrity of RNA, protein and morphology during harvest. Rats were anaesthetized by intraperitoneal injection with sodium pentobarbital (50mg/kg, Ovation Pharmaceuticals, Deerfield, IL). Adequate depth of anaesthesia was ensured by monitoring respiratory rate, response to paw or tail pinch and loss of corneal blink reflex. At the end of tissue harvest, animals were euthanised by thoracotomy and exsanguination by transecting the heart.

2.1.2.2. Tissue harvest and preservation

A midline laparotomy was performed and the ligament of Treitz identified, demarcating the duodenojejunal flexure and the beginning of the jejunum. The small intestine was cut at the ligament of Treitz and flushed with ice cold Ringer's lactate using a blunt needle on a 20ml syringe while still on the mesenteric pedicle to remove luminal contents. The entire length of small intestine was stripped off the mesentery, measured along the length of a ruler and sections of jejunum divided with a scalpel as follows (Figure 2.2): the first 2 cm distal to the ligament of Treitz was discarded. The following 10cm of intestine was divided along the mesenteric border and the mucosa scraped off the muscular layers over glass plates on ice, then divided into 3 equal aliquots. Two of these aliquots were snap-frozen in liquid nitrogen for subsequent analysis of RNA and total protein expression. Snap-frozen mucosa was stored at -80°C until further analysis. The remaining aliquot was added to 1ml of ice-cold Nxtract lysis buffer (CellLytic Nuclear Extraction Kit, Catalog no NXTRACT, Sigma, St Louis, MO), then processed to obtain nuclear protein extracts as per manufacturer's instructions[275]. Nuclear protein extracts were stored at -80°C until further analysis.

For the microRNA and proliferation experiments in Chapter 5, tissue harvest was performed as above, but in addition a further 2cm of intact jejunum was removed, immersed in 10% formalin (Catalog no. 23-245-684, Fisher Scientific, Pittsburgh, PA) and

fixed overnight at 4°C (Figure 2.2). An additional 2cm of intact jejunum was cut in transverse "doughnut"-shaped sections, embedded in a mould containing OCT (optimal cutting temperature) compound (Catalog no. 4583, Sakura FineTek, Torrance, CA) and frozen slowly over dry ice immersed in isopentane (Catalog no. O3551-4, Fisher Scientific, Figure 2.2). The formalin fixed sections were sent to the Brigham and Women's Histopathology Core Facility for processing the following day, while the fresh frozen sections were stored at -80°C until further analysis.

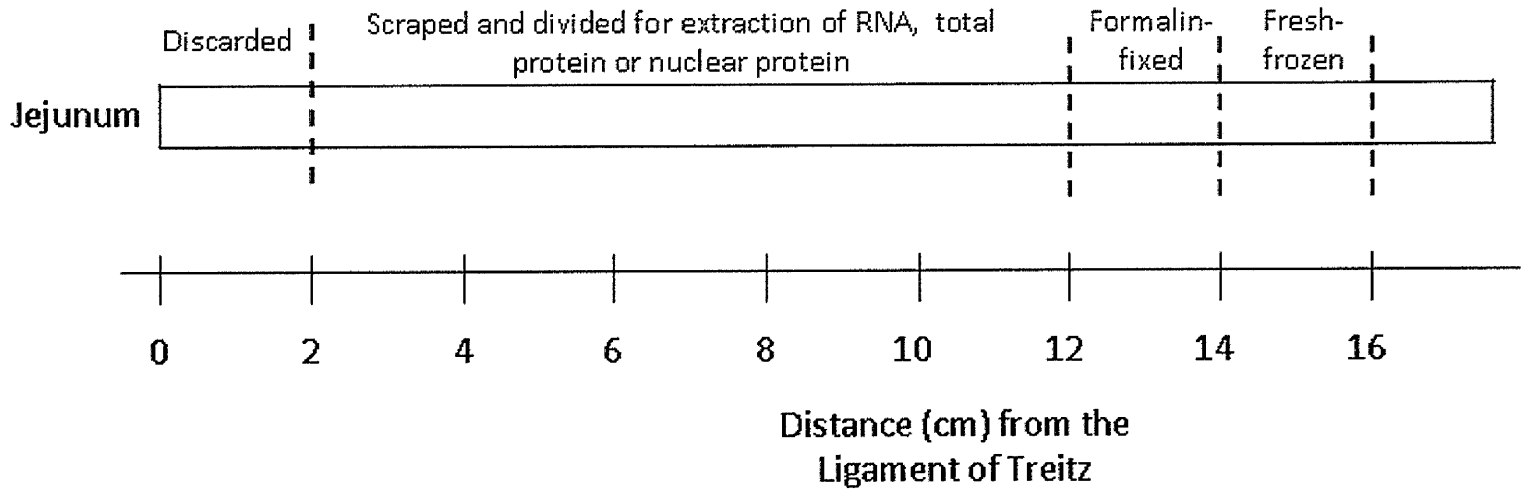

Figure 2.2: Schematic of the harvest of rat jejunum for subsequent extraction of RNA, protein and morphologic analysis. The scale bar indicates the distance form the Ligament of Treitz. The length of the intestine was measured with a ruler and the appropriate lengths of jejunum cut with a scalpel.

2.2. RNA

2.2.1. RNA extraction

Total RNA was extracted from snap-frozen scrapings of rat jejunum or rat IEC-6 cells using the mirVana kit as per manufacturer's instructions (Catalog no. AM1560, Ambion; Austin, TX)[276]. Extracted RNA was quantified using a 1:50 dilution (in diethypyrocarbonate (DEPC)-treated water) by measurement of absorbance at 260nm (A_{260}) in a final volume of 100µl on a Spectramax M5 microplate reader (Catalog no. M5, Molecular Devices, Sunnyvale, CA). RNA purity was assessed using the A_{260} to A_{280} ratio, with levels over 1.8 taken as sufficient purity. RNA concentration was abstracted from calculations performed by the Spectramax M5 software. Extracted RNA was stored at -80°C until further use.

2.2.2. Reverse transcription

1.6µg of each RNA sample was reverse transcribed using the Superscript III kit according to manufacturer's instructions (Cat no: 18080-051, Invitrogen, Carslbad, CA)[277]. A no template control and a no reverse transcriptase control were included in each reverse transcription (RT) to exclude contamination. All samples in any individual experiment were reverse transcribed simultaneously to minimise variability.

2.2.3. Real-time quantitative PCR

The resulting cDNA was diluted 1:50 to 1:100 with DEPC-treated water. Primers were designed using the PRIMER3 software available online[278], using mRNA sequences available from UCSC Genome Browser[279]. Primer sequences (with the exception of rat Ccnd1, rat Per2, human SGLT1 and human Per1) were custom-ordered from Invitrogen; primer sequences are available in Table 2.1 to 2.3. A mastermix consisting of the commercially available SYBR Green PCR Mastermix (Catalog no. 4309155, Applied Biosystems, Foster City, CA) diluted cDNA and specific forward and reverse primers (12.5pmol of each primer) was created and real-time PCR cycling performed as per manufacturer's instructions[280]. The final ratio of SYBR green in the mastermix was 1:1. Rat Ccnd1, rat Per2, human SGLT1 and human Per1 were quantified using primers commercially available from Applied Biosystems (Catalog nos Rn00432359_m1, Rn01427704_m1, Hs00165793_m1, Hs00242988_m1 respectively) as the custom designed primers for these genes resulted in multiple non-specific products. PCR was carried out as part of the Taqman primer-probe system with Taqman mastermix according to manufacturer's instructions (Cat no 4324018, Applied Biosystems)[281]. Thermal cycler conditions used were 2 min 50°C; 10 min 95°C; followed by 40 cycles of 15 sec at 95°C and 1 min 60°C. Dissociation curves were obtained to ensure a single amplicon and to exclude non-specific amplification and primer-dimerization. All samples were run in triplicate. Use of 384-well plates allowed simultaneous analysis of all samples being compared. Expression of the gene of interest was normalised against β-actin as the loading control.

Gene	Primer sequence
Ccnd2	5'- TTACCTGGACCGTTTCTTGG
	3'- CCTCACGACTTCATTGAGCA
Ccnd3	5'- TGGTCAAAAAGCATGCTCAG
	3'- TCACAGGCACTGAAGTGGAC
Ccne1	5'- GTGAAAAGCGAGGATAGCAG
	3'- CGTTACATGGCATCACAACA
Cdk4	5'- AAGCGGCCTAGATTTCCTTC
	3'- TGTTGGCTGTATCTTCGCAG
Cdk6	5'- TGTTTCAGCTTCTCCGAGGT
	3'- GAAGTCCTGCTCCAGTCCAG
β-actin	5' GGATCAGCAAGCAGGAGTACGA 3'
	3' AACGCAGCTCAGTAACAGTCCG 5'

Table 2.1: Rat qPCR primers for G1/S regulators as used in Chapter 5. Thermal cycler conditions used were 2 min 50°C; 10 min 95°C; followed by 40 cycles of 15 s at 95°C and 1 min 60°C. Dissociation curves were obtained to ensure a single amplicon.

Gene	Primer sequence
Per1	5′ CGCACTTCGGGAGCTCAAACTTC 3′
	3′ GTCCATGGCACAGGGCTCACC 5′
Bmall	5′ TCCGATGACGAACTGAAACAC 3′
	3′ CTCGGTCACATCCTACGACAA 5′
Clock	5′ TTCGATCACAGCCCAACTCC 3′
	3′ ACCTCCGCTGTGTCATCTTCTC 5′
Reverb A	5′ TAGGCACCTCACCTGGCAACT 3′
	3′ GCACTGTGGAGTGGTAGCCG 5′
Reverb B	5′ TTTTGAGGTTTTAATGGTGCG 3′
	3′ GTGACAGTCCGCTCCTTTGC 5′
Cry1	5′ GGGAAGCGCCCAAGTCAGGAAG 3′
	3′ CCTCCCGCATGCTTTCATATC 5′
Cry2	5′ TTCAGAAGGCCGCTAATTGC 3′
	3′ AGATCTGCTTCATCCGCTCAA 5′
Sglt1	5′ CCAAGCCCATCCCAGACGTACACC 3′
	5′ _CTTCCTTAGTCATCTTCGGTCCTT 3′
β-actin	5′ GGATCAGCAAGCAGGAGTACGA 3′
	3′ AACGCAGCTCAGTAACAGTCCG 5′

Table 2.2: Rat qPCR primers for clock genes, the sodium glucose co-transporter *Sglt1* and *β-actin* as used in Chapter 3. Thermal cycler conditions used were 2 min 50˚C; 10 min 95˚C; followed by 40 cycles of 15 s at 95˚C and 1 min 60˚C. Dissociation curves were obtained to ensure a single amplicon.

Gene	Primer sequence
PER2	5′ GACCCGTGATGAACCCTCAGAC 3′
	3′ GCCGGAGGATTTGGAGGACG 5′
BMALI	5′ GTTTGTCGTAGGATGTGACCG 3′
	3′ TGTCGGTCTTACTAGACTAACCA 5′
CLOCK	5′ GCCGTCTCAGACCCTTCCTC 3′
	3′ GCCTATGCTCGTGAGGTGGG 5′
REVERB A	5′ GCCACCAGTCCAACAGCAAC 3′
	3′ GCACATACGTCGGGGTCTTC 5′
REVERB B	5′ CGATGAGCTTCACTCCAGCAG 3′
	3′ GCATAAGGACCCAAGTCTCTA 5′
CRY1	5′ GTGAGGCAATTCTCTTGGAAGC 3′
	3′ GCCTCGGAGGAAGGAACTTAAA 5′
CRY2	5′ AAGGAATGGGGAGTGACCCG 3′
	3′ TTCTTGCCCTACGTCGGTAG 5′
β-ACTIN	5′ AGCAGGAGTATGACGAGTCCG 3′
	3′ ACGAAGATCCGCCTGATACTGA 5′

Table 2.3: Human qPCR primers for clock genes, and *β-ACTIN* as used in Chapter 4. Thermal cycler conditions used were 2 min 50°C; 10 min 95°C; followed by 40 cycles of 15 s at 95°C and 1 min 60°C. Dissociation curves were obtained to ensure a single amplicon.

2.3. microRNA profiling

2.3.1. In situ hybridization on microRNA microarrays

microRNA in situ hybridization was performed by the Harvard Partners Centre for Genetics and Genomics, Cambridge, Massachusetts on total RNA extracted from rats harvested at diurnal timepoints as above. Samples were hybridized against a reference sample consisting of RNA pooled from ZT0 rats. 3 arrays were used per timepoint. RNA from 2 animals was used per timepoint and one sample per timepoint was run with the dye swapped to act as a biological replicate and control for any dye bias. 21 arrays were used in total.

2.3.2. Validation by qPCR

Conserved microRNAs exhibiting a two-fold or greater change in expression between timepoints were validated by qPCR. Total RNA extracted from rats harvested at 3-hourly intervals (n=6 to 7 per timepoint) as described above was subjected to reverse transcription using the Taqman microRNA reverse transcription kit (Catalog no. 4366596, Applied Biosystems) according to manufacturer's instructions[282]. microRNA-specific reverse transcription and PCR primers were obtained from Applied Biosystems (the list of microRNAs validated and catalog numbers of RT and PCR primer pairs are given in Table 2.4).

	Catalog numbers	
microRNA	**Part number**	**Assay ID**
mir-16	4427975	000391
mir-141	4427975	000463
mir-20a	4427975	000580
mir-142	4427975	000464
mir-21	4427975	000397
mir-503	4427975	001048
mir-17	4427975	002308
mir-26a	4427975	000405

Table 2.4: Catalog numbers of microRNAs validated by reverse transcription and qPCR. microRNA RT-PCR primer probe pairs were purchased from Applied Biosystems and RT-PCR performed as per manufacturer's protocols.

snoRNA, a small nucleolar RNA, was used as a housekeeping gene to normalize for RNA loading in microRNA quantification experiments (Catalog no 4386738, Applied Biosystems). 200ng of RNA was used in each reverse transcription reaction. The resulting cDNA was subjected to real-time PCR analysis using Taqman mastermix and thermal cycling conditions as per manufacturer's instructions as described above[281].

2.4. Laser capture microdissection (LCM)

2.4.1. Laser capture of crypts, villi and smooth muscle

Sections of jejunum were fresh-frozen in OCT as previously described. Sections from ZT 6 and ZT 18 were chosen for LCM as the respective peak and trough in expression of the rhythmic microRNA of interest, *mir-16*. These sections were cut at 9μm thickness after equilibration in the cryostat (Thermo Shandon SME, Thermo Scientific, Waltham, MA) just prior to laser capture. Sections were prepared and stained for laser capture microdissection using the Histogene LCM Frozen Section Staining Kit (Catalog no. KIT0401, Molecular Devices, Sunnyvale CA) according to manufacturer's instructions[283]. Crypts (lower half), villi (top half), or smooth muscle were isolated by laser capture microdissection (Veritas Microdissection System, Molecular Devices). An approximate 5000 cells were obtained from each fraction of each sample. Purity of isolation was confirmed by measuring PCNA (proliferating cell nuclear antigen, denoting isolation of the crypt fraction), SMA (smooth muscle actin, denoting isolation of the smooth muscle fraction) and IFABP (intestinal fatty acid binding protein, denoting isolation of the differentiated cells of the villi).

2.4.2. Real-time PCR of laser captured samples

Total RNA was extracted from each section (RNAqueous micro RNA extraction kit, Catalog no: AM 1931, Ambion, Austin, TX) according to manufacturer's instructions[284]. The extracted total RNA was subjected to microRNA reverse

transcription using the mir-16 specific RT/PCR primer pair (Catalog no 000391, Applied Biosystems) and the Taqman microRNA reverse transcription kit and subsequently underwent real-time PCR using the Taqman PCR mastermix according to manufacturer's instructions as described above[281, 282].

2.5. Protein

2.5.1. Protein extraction and quantification

2.5.1.1. Protein extraction from cultured cells

Cells were grown in 10cm cell culture dishes as previously described and at the time of harvest, washed once with 10ml sterile phosphate-buffered saline (PBS, Catalog no. P5638, Sigma, autoclaved at 140°C for 75 minutes then stored at 4°C). The PBS was aspirated off the cells and 200µl of radioimmunoprecipitation assay (RIPA) buffer (Catalog no. BP115, Boston Bioproducts) containing an added 2ul of protease inhibitor cocktail (Catalog no. P8340, Sigma) added to each dish. Cells were scraped off into the RIPA buffer mixture using a disposable cell lifter (Catalog no. 3008, Corning, Lowell, MA) and the lysed cell mixture pipetted into 1.5ml microcentrifuge tubes for storage (Catalog no. 05-408-129, Fisher Scientific, Pittsburgh, PA). Cells were snap-frozen in liquid nitrogen and stored at -80°C until further analysis.

For protein extraction, snap-frozen cells were thawed on ice, then sonicated for 30 seconds, before incubating for 30 minutes on ice. Cells were centrifuged 10,000rpm for 15 minutes and the supernatant transferred into another microcentrifuge tube and stored at -80°C until further analysis. For chapter 4, nuclear protein was extracted from cultured cells using the QProteome Nuclear Protein Kit (Catalog no. 37582, Qiagen). Cells were grown in 10cm tissue-culture treated dishes under routine conditions and

nuclear protein extracted according to manufacturer's instructions[285] and stored at -80°C until further analysis.

2.5.1.2. Protein extraction from tissue

Snap-frozen jejunal mucosal scrapings were transferred into chilled Falcon tubes (15ml capacity) on ice, each tube containing 750µl Triton lysis buffer (Catalog no. BP-117, Boston Bioproducts, Wocester, MA) and 7.5µl protease inhibitor cocktail (Catalog no. P8340, Sigma). Samples were incubated for 20 min on ice, then each sample was homogenized using a polytron on ice for 30 seconds until the sample appeared uniform in consistency. Following homogenization, samples were sonicated on ice for 1 min, then centrifuged at 4°C at 11,000g for 15mins. The resulting supernatant was transferred into another microcentrifuge tube and stored at -80°C until further analysis.

2.5.2. Quantification of extracted protein (BCA assay)

The extracted total and nuclear protein from each sample was quantified using the bicinchoninic acid assay (BCA, Catalog no. BCA1, Sigma) by measurement of absorbance at 562nm of each sample relative to a standard curve according to manufacturer's instructions[286]. Measurements were performed in 96-well clear-bottom plates (Catalog no. 351172, BD Falcon, BD Biosciences, San Jose, CA) each well containing a single sample, in a Spectramax M5.

2.5.3. Gel electrophoresis

75µg or 15µg of protein (from tissues or cells respectively) was added to 1µmol dithiothreitol (DTT, 154µg), sterile water and 4x lithium dodecyl sulphate (LDS) buffer (Catalog no. LP0007, Invitrogen) to achieve a final volume of 14µl of prepared protein sample under denaturing reducing conditions. Prepared protein samples were linearized at 95°C for 6 minutes. A 15-well NuPAGE Novex 10% Bis-Tris gel (Catalog no. NP0303BOX, Invitrogen, Carlsbad, CA) was assembled into an XCell SureLock Mini-Cell (Catalog no. EI0001, Invitrogen) and the assembly filled with NuPAGE Running Buffer (Catalog no. NP0002, Invitrogen) according to manufacturer's instructions[287]. Each 14µl prepared protein sample was loaded into a single well of the 15-well gel. The first well of each well was filled with 10µl of a protein ladder (Novex Sharp Pre-stained Protein Standard, Catalog no. LC5800, Invitrogen). Gel electrophoresis was performed at room temperature at 150V for 45 minutes.

2.5.4. Western blotting

Transfer buffer was prepared by adding 40ml of Novex Tris-Glycine Transfer Buffer (Catalog no. LC3675, Invitrogen) to 200ml of 100% methanol (Catalog no. A456-500, Fisher) and 760ml of distilled water and the polyvinyldifluoride (PVDF) membrane (Catalog no. LC2002, Invitrogen) removed from between the two pieces of pre-cut filter paper and "wet" by brief immersion in 100% methanol. After gel electrophoresis was complete, the gel was sandwiched between two pieces of filter paper and the PVDF membrane placed on top of the gel. This assembly was placed between 5 pieces of

sponge above and below and the transfer carried out at 4°C overnight (approximately 16 hours) at 22V within the transfer blot module (XCell II Blot Module, Catalog no. EI9051, Invitrogen) according to manufacturer's instructions[288].

2.5.4.1. Incubation with antibodies

Following transfer, the membrane was washed with PBS with Tween 20 (PBST, Catalog no. P3563, Sigma, diluted in 1L distilled water) then blocked with 10ml 2.5% w/v non-fat dry milk for 1 hour at room temperature. The membrane was then washed three times for five minutes each with PBST, then incubated with 10ml of a 1:200 dilution of primary antibody in PBST for 2 hours at room temperature or overnight at 4°C, depending on the instructions of the antibody manufacturer.

The primary antibody solution was drained off and the membrane washed five times for 10 minutes each with PBST. The membrane was then incubated with 10ml of a 1:5000 dilution in PBST of secondary antibody to the appropriate species for 1 hour at room temperature, then washed 5 times for 10 minutes each with PBST. All secondary antibodies used were from Vector Labs, Burlingame, CA. The catalog number, species and concentrations for all antibodies used are detailed in Table 2.5.

Protein	Primary antibody			Secondary antibody		
	Cat no	Manufacturer	Concentration	Species	Cat no	Concentration
PER1	sc-25362	SCBT	1:200	Rabbit	PI-1000	1:5000
SGLT1	07-1417	Chemicon International	1:4000	Rabbit	PI-1000	1:5000
CCND1	H-295	SCBT	1:200	Rabbit	PI-1000	1:5000
CCND2	H-289	SCBT	1:200	Rabbit	PI-1000	1:5000
CCND3	H-292	SCBT	1:200	Rabbit	PI-1000	1:5000
CCNE1	M-20	SCBT	1:200	Rabbit	PI-1000	1:5000
CDK4	C-22	SCBT	1:200	Rabbit	PI-1000	1:5000
CDK6	H-230	SCBT	1:200	Rabbit	PI-1000	1:5000
β-ACTIN	MS-1295-PCL	Labvision	1:1000	Mouse	PI-2000	1:5000

Table 2.5: List of antibodies, manufacturers and concentrations used for Western blotting in Chapters 3, 4 and 5. Western blotting was carried out as described in Section 2.5, and incubation with antibodies carried out as per antibody manufacturer's protocol.

2.5.4.2. Detection and quantification of the protein

The membrane was covered with 4ml of enhanced chemiluminescence solution (ECL, Catalog no. RPN2106, GE Healthcare, Piscataway, NJ) and exposed to according to manufacturer's instructions[289]. The membrane was exposed to autoradiography film (Kodak Biomax XAR ready film pack, Catalog No. 1651579001EA, Kodak) for varying durations depending on the antibody used. β-ACTIN was used as the housekeeping gene to control for protein loading. Membranes probed for the protein of interest were stripped after exposure using the Western Blot Recycling Kit (Catalog no. 90100-T, Alpha Diagnostic International, San Antonio, TX) according to manufacturer's instructions to remove the first primary antibody then blocked using 10ml 2.5% w/v non-fat dry milk for 1 hour at room temperature. After blocking, membranes were washed 3 times with PBST for five minutes each, then incubated for 1 hour with a 1:1000 concentration of β-ACTIN antibody. Membranes were then washed, probed with secondary antibody and exposed as described above.

The film was scanned using a Canoscan 4200F plate scanner (Canon, Lake Success, NY) and ArcSoft Photostudio V5.5 software (ArcSoft, Fremont, CA). For semi-quantitative densitometry, images were imported into Image J (National Institutes of Health, Bethseda, MD) and band densities calculated. The expression of the protein of interest was expressed relative to β-ACTIN.

2.6. Routine cell maintenance

2.6.1. CHO cells

Chinese Hamster Ovary (CHO) cells were purchased from the American Type Culture Collection (ATCC, Catalog no. CCL-61, Manassas, VI). The aliquot of purchased cells was thawed and centrifuged at 220g for 5 minutes to remove the cryopreservative DMSO (dimethylsulfoxide), the cell pellet resuspended in 10ml of F12K medium (Catalog no. 21127022, Invitrogen) containing 10% foetal bovine serum (FBS, Catalog no. 10091-148, Invitrogen) and 1% penicillin-streptomycin (Catalog no. 15140163, Invitrogen) and the resuspended cells added to a 10cm tissue-culture treated cell culture dish (Catalog no. 430167, Corning). Cells were maintained in an incubator at 37°C at 95% humidity and 5% CO_2. CHO cells were subcultivated at a ratio of 1:5 every 5 days by washing with sterile PBS, then detached with 3ml of trypsin per 10cm dish and centrifuged at 220g for 5 minutes. Cell pellets were resuspended in 5ml of F-12K with FBS and penicillin-streptomycin and divided into 5 equal aliquots which were each plated into a 10cm dish with an additional 9ml of media.

2.6.2. Caco-2 cells

Caco-2 cells, human colonic carcinoma-derived cells, were purchased from the ATCC (Catalog no. HTB-37). Thawing, propagation and subculturing were performed as for CHO cells described above, except that Caco-2 cells were grown in Dulbecco's Modified

Eagle Media (DMEM, Catalog no. 11965-092) containing 10% FBS and 1% penicillin-streptomycin.

2.6.3. IEC-6 cells

IEC-6 cells, rat intestinal crypt-derived cells, were purchased from the ATCC (Catalog no. CRL-1592). Thawing, propagation and subculturing were performed as for CHO cells described above, except that IEC-6 cells were grown in Dulbecco's Modified Eagle Media (DMEM, Catalog no. 11965-092) containing 10% FBS and 1% penicillin-streptomycin, as well as 0.001% bovine insulin (Catalog no. I0516, Sigma).

2.6.4. HEK293 cells

HEK293 cells, an embryonic kidney derived cell line, were purchased from the ATCC (Catalog no. CRL-1573). Thawing, propagation and subculturing were performed as for CHO cells described above, except that HEK293 cells were grown in Dulbecco's Modified Eagle Media (DMEM, Catalog no. 11965-092) containing 10% FBS and 1% penicillin-streptomycin.

2.7. Cell transfection

2.7.1. CHO transfection

All transfections of CHO cells were carried out using the transfection reagent Effectene (Catalog no. 301425, Qiagen) according to manufacturer's instructions[290]. The effect of PER1 overexpression on the *SGLT1* promoter was assessed in CHO cells passages 10-12 transfected at 80% confluence with combinations of reporter vector (pGL3-Basic, wild-type *SGLT1* pGL3/WT-*SGLT1*luc, or mutated *SGLT1* promoter constructs) and expression vector (pcDNA3.1(+) with or without PER1 cDNA). Conversely, the effect of *PER1* knockdown on *SGLT1* promoter activity was assessed by co-transfection of shRNA vectors in place of expression vectors. Renilla luciferase (Catalog no. E2241, pRL-TK; Promega) was cotransfected into all wells in all experiments to normalize for transfection efficiency. After 24 hours, the media was aspirated from each well and replaced with fresh media (F12K containing 10% FBS and 1% penicillin-streptomycin) and cells returned to the incubator. Each sequence of transient transfection to measurement of luminescence was performed three times and each well in triplicate.

2.7.2. Caco-2 cell transfection

Caco-2 cells at passages 10-12 were transfected at 40% confluence with knockdown vectors for PER1 using Effectene according to manufacturer's instructions[291]. At 24 hours post-transfection the media was aspirated and replaced with fresh DMEM containing 10% FBS and 1% penicillin-streptomycin and cells returned to the incubator.

At 48 hours, the transfected cells were trypsinized and re-plated at 40% confluence in DMEM containing 10% FBS, 1% penicillin-streptomycin but this time also containing 4μg/ml puromycin (Catalog no. ant-pr-1, Invivogen, San Diego, CA) to allow stable selection of transfected cells. This concentration of puromycin was determined by a previously performed kill-dose curve using normal untransfected Caco-2 cells plated at 40% confluence in media containing antibiotic concentrations ranging from 1ug/ml to 10μg/ml. Cells were returned to the incubator and maintained under routine cell culture conditions, with the media changed every 3 days. Cells were monitored for the onset of confluence and harvested for RNA analysis at 7-days post-confluence.

2.7.3. IEC-6 transfection

IEC-6 cells at passages 6-8 were transfected at 90% confluence with the transfection reagent Lipofectamine 2000 (Catalog no. 11668-019, Invitrogen) according to manufacturer's instructions[292]. At 24 hours post-transfection the media was aspirated and replaced with fresh DMEM containing 10% FBS, 1% penicillin-streptomycin and 0.001% insulin and cells returned to the incubator. At 48 hours post-transfection, the transfected cells were trypsinized and re-plated at 40% confluence in DMEM containing 10% FBS, 1% penicillin-streptomycin and 0.001% insulin, but this time to allow stable selection of transfected cells, the media also contained 2μg/ml puromycin (Catalog no. ant-pr-1, Invivogen, San Diego, CA). This concentration of puromycin was determined by a previously performed kill-dose curve using normal untransfected IEC-6 cells plated at 40% confluence in media containing antibiotic concentrations ranging from 1μg/ml to 10μg/ml. Cells were returned to the incubator and maintained under routine cell culture

conditions, with the media changed every 3 days. *mir-16* expression was induced by addition of 2μg/ml doxycycline (Clontech, Mountain View, CA) to the cell culture media 72 h prior to plating for each assay.

2.7.4. HEK293 transfection

HEK293 cells at passages 10-12 were transiently transfected with knockdown sequences for PER1 or the control scrambled shRNA in 10cm tissue culture dishes at 70% confluence using the transfection reagent Effectene (Catalog no. 301425, Qiagen) according to manufacturer's instructions[290]. After 24 hours, the media was aspirated from each well and replaced with fresh media (DMEM containing 10% FBS and 1% penicillin-streptomycin) and cells returned to the incubator. Cells were harvested after 48 hours for determination of PER1 mRNA expression.

2.8. DNA plasmids and site-directed mutagenesis

All sequencing to confirm accurate insertion of DNA was carried out by technicians at the Brigham and Women's Hospital DNA Sequencing Core facility.

2.8.1. PCR amplification of PER1

The PER1 expression vector was generated by amplifying human PER1 cDNA obtained from reverse transcription of Caco2 cell mRNA using the Platinum Taq High-Fidelity DNA polymerase (Catalog no. 11304-011, Invitrogen) using primer-encoded NheI and NotI restriction sites (cloning primers listed in Table 2.6). The following thermal cycling conditions were used: 1 cycle at 94°C for 1 minute then 35 cycles of 94°C for 30 sec, 55°C for 30 sec and 68°C for 4 min.

Cloning primer	Sequence
Per1	5' GGCC**GCTAGC**GCGACCAGGTACTGGCTGTGATCGAA 3'
	3' GGCC**GCGGCCGC**CAACTTTGTCCAGGGGAGGGAAGGATTC 5'

Table 2.6: Primers for amplification of PER1 for creation of the PER1 overexpression plasmid. Thermal cycler conditions used were 1 cycle at 94°C for 1 minute then 35 cycles of 94°C for 30 sec, 55°C for 30 sec and 68°C for 4 min.

2.8.2. Gel electrophoresis

To identify successful amplification of the target region, 2µl of the PCR product (total 50ul volume) was added to 2µl of DNA loading buffer (created by addition of 25mg of xylene cyanol to 4g of sucrose and making the solution up to 10ml with distilled water) and 8µl of DEPC-treated water and run alongside 2µl of a DNA ladder added to 2µl of DNA loading buffer and 8µl of DEPC-treated water on a 1% agarose gel. Gels were prepared by adding 1g of agarose gel powder (Catalog no. 16500-100, Invitrogen) to 100ml of distilled water, microwaving until all agarose fragments had dissolved (approximately 2 minutes), then pouring the molten agarose while still hot into gel casting trays fitted with combs. Once cooled, gels were transferred to the electrophoresis module and TAE (Tris-Acetate EDTA buffer, Catalog no. T4038, Sigma) added into the module to completely immerse the gel. The prepared PCR product and DNA ladder were slowly pipetted into one well each. Gels were run at 50V for 20mins, then removed from the module and transferred into a deep pipette tray containing 100ml of water and 20µg of ethidium bromide. Gels were incubated in this for 5 minutes, then visualised on an UV transilluminator. A 4kb PCR fragment was identified on UV transillumination, corresponding to the expected weight of PER1 cDNA, confirming successful amplification.

2.8.3. Digestion of PCR products and vectors

Once amplification was confirmed, the remaining 48µl of PCR product was digested using restriction enzymes NotI (10U, Catalog no. R3189, NEB) and NheI (10U, Catalog no.

R3131, NEB) according to manufacturer's recommendations. The pcDNA3.1(+) vector (Catalog no. V790-20, Invitrogen) was digested under similar conditions, gel electrophoresis performed as described in section 2.8.2 above and DNA extracted from the band of 5.4kb and quantified.

2.8.4. Ligation of insert and vector and amplification

The ligation was performed with 50ng of insert, 50ng of vector and 1µl each of T4 reaction buffer and T4 DNA ligase (Catalog no. M0202S, NEB) according to manufacturer's recommendations. A no-insert control ligation was also performed to assess the rate of self-circularization of any single cut vector fragments, omitting the insert from the reaction. After ligation, the plasmids were amplified by transforming *E.coli* (One-Shot Top10 Chemically Competent E.coli, Catalog no.C4040-10, Invitrogen) with 4µl of the ligation reaction (~50ng) according to manufacturer's instructions[293].

2.8.5. Plasmid preparation

5 colonies were picked using a sterile toothpick and each colony added to a 50ml microcentrifuge tube containing 5ml LB (prepared as described above). These miniprep cultures were incubated overnight at 37°C (~16 hours) with shaking, then plasmids extracted using the Qiaprep Spin Miniprep Kit (Catalog no. 27104, Qiagen) according to manufacturer's instructions[294] and the DNA quantified as described above. Accurate cDNA insertion was confirmed by sequencing (primers are listed in Table 2.7).

Sequencing primer	Sequence
1P1Seq	5' GTCAAGCAGGTGCAGGCCAACCAGGAATACTACCAGCA 3'
2P1Seq	5' GGGGAGTATGTCACCATGGACACCAGCTGGGCTGGCTTTGT 3'
3P1Seq	5' ACCCCACGGAAGGAGCCAGTGGTGGGAGGCACCCTGAGCC 3'
4P1Seq	5' TCCAGCTATCCTTATGGGGCACTCCAGACCCCTGCTGAAG 3'
5P1Seq	5' CTGCTCATGGCCAATGCTGACCAGCGCGTCATGATGACC 3'

Table 2.7: Sequencing primers for PER1 overexpression plasmid. Sequencing was carried out by technicians at the Brigham and Women's Hospital DNA Sequencing Core Facility.

2.8.6. Knockdown vectors and sequences

Knockdown vectors containing short-hairpin RNA sequences against *PER1* (pLKO.1-puro) were purchased from Sigma (Catalog no. SHCLNG-NM_002616), consisting of 5 shRNA sequences designed against the *PER1* RefSeq sequence NM_002616 (sequences listed in Table 2.8). BLAST searches were conducted for each shRNA sequence against human GenBank and RefSeq databases (http://www.ncbi.nlm.nih.gov.ezp-prod1.hul.harvard.edu/BLAST/, accessed on 11th November 2008) to exclude homology of the *PER1* shRNA to other genes. The pLKO.1-puro vector containing a scrambled oligonucleotide sequence (Catalog no. SHC001, Sigma) was used as a negative control. Knockdown efficiency of each sequence was determined by measuring PER1 mRNA expression after transient transfection of HEK293 cells with either knockdown sequences for PER1 or the control scrambled shRNA sequence. The two constructs with the highest knockdown efficiency were chosen for stable knockdown of PER1 in Caco2 cells and promoter assays (co-transfected with the SGLT1 promoter) in CHO cells.

Catalog No.	Sequence
TRCN0000074183	CCGGCCCAATTCTCAGAACTCAGATCTCGAGATCTGAGTTCTGAGAATTGGGTTTTTG
TRCN0000074184	CCGGCCAGCACCACTAAGCGTAAATCTCGAGATTTACGCTTAGTGGTGCTGGTTTTTG
TRCN0000074185	CCGGCAGCCACACAAGCAAATACTTCTCGAGAAGTATTTGCTTGTGTGGCTGTTTTTG
TRCN0000074186	CCGGCCATGGACATGTCCACCTATACTCGAGTATAGGTGGACATGTCCATGGTTTTTG
TRCN0000074187	CCGGGCACAAACTCTCAGAGCCCATCTCGAGATGGGCTCTGAGAGTTTGTGCTTTTTG

Table 2.8: shRNA vectors used for knockdown of PER1. Plasmids were purchased from Sigma.

2.8.7. Creation of the *mir-16* overexpression vector

2.8.7.1. Identification of the necessary *mir-16* sequence

The sequence and coordinates of *mir-16* were identified using the microRNA database miRBase[295] and Genome Browser at University of California Santa Cruz[279]. In accordance with previous reports, primer sequences were designed to include the proximal and distal 200bp flanking sequences in the *mir-16* overexpression insert. Primers were designed using Primer 3 software as described above and are listed in Table 2.9.

Cloning primers	Sequence
mir-16	5' GCGC***ACGCGT***TGTTTTATCCCAAGTAAAAATCTGAA 3'
	3' ATGC***ATCGAT***TTCTTTAGGCGCGAATGTG 5'

Table 2.9: Primers used for amplification of *mir-16* for creation of the *mir-16* overexpression vector in Chapter 5. Primers used for cloning *mir-16* from human genomic DNA. Restriction sites are highlighted in bold and italicized. Thermal cycling conditions were as follows: initial denaturation of 94°C for 30 sec, then 35 cycles of denaturation at 94°C for 30 seconds, 61°C for 30 seconds and 68°C for 1 minute.

2.8.7.2. Cloning the *mir-16* sequence

The *mir-16* insert was amplified from human genomic DNA acquired from Promega (Catalog no. G3041, Promega, Madison, WI) using the forward and reverse primers designed above and the Elongase Amplification System (Catalog no. 10480010, Invitrogen) according to manufacturer's instructions[296]. The following thermal cycling conditions were used: 1 cycle at 94°C for 30 sec then 35 cycles of 94°C for 30 sec, 61°C for 30 sec and 68°C for 1 min. Products were identified by agarose gel electorphoresis as described in section 2.8.2.

The vector chosen for expression of the *mir-16* insert was the pTRIPZ vector (Catalog no. RHS4750, Open Biosystems, Huntsville, AL). The vector was amplified as per manufacturer's instructions in Dam-/- E.coli (Catalog no. C2925I, New England Biolabs, Ipswich, MA)[297]. Plasmids were prepared from the amplified *E.coli* using the GenElute HP Plasmid Maxiprep Kit (Catalog no. NA0310, Sigma) as per manufacturer's instructions[298]. Prepared DNA was quantified using the protocol employed for RNA quantification as described above, with calculations performed by Spectramax M5 software using specific concentration constants for DNA rather than RNA. The amplified vector was stored at -20°C until further use.

2µg of the pTRIPZ vector and the amplified PCR product were individually digested using 5µl of the restriction enzyme MluI (Catalog no. R0198S, NEB) and 2.5µl of the restriction enzyme ClaI (Catalog no. R0197, NEB) according to manufacturer's instructions. The cut vector and PCR products were identified by gel electrophoresis and extracted using the

QIAquick Gel Extraction Kit (Catalog no. 28704, Qiagen, Valencia, CA) according to manufacturer's instructions[299]. The ligation was performed with a ratio of 6:1 insert:vector and the resulting plasmids amplified by transforming *E.coli* as previously described in section 2.8.4.

10 colonies were amplified in miniprep cultures. Plasmids were prepared as described in section 2.8.5 and were sent for sequencing. The primers used for sequencing are provided in Table 2.10.

Sequencing primer	Sequence
pTRseq	5' GGAAAGAATCAAGGAGG 3'

Table 2.10: Primers used for sequencing the *mir-16* overexpression plasmid in Chapter 5. Sequencing was carried out by technicians at the Brigham and Women's Hospital DNA Sequencing Core Facility.

2.9. SGLT1 promoter constructs (wild-type and mutants)

For promoter assays used in Chapter 4, the previously characterized human *SGLT1* promoter (−1968/+14, designated WT *SGLT1*-Luc) [31] was cloned by PCR from human genomic DNA (Promega) using the Elongase DNA polymerase (Invitrogen) and PCR conditions as described in section 2.8.1 above. Primers used encoded MluI and BglII restriction sites at the 5' and 3' ends respectively (listed in Table 2.11). Successful amplification was confirmed using gel electrophoresis of 2µl of the PCR product, which revealed the expected 2kb band on UV transillumination.

The remaining 48µl of PCR product and the pGL3 basic empty vector (Catalog no. E1751, Promega), were individually digested using restriction enzymes MluI(10U, Catalog no. R0198, NEB) and BglII(10U, Catalog no. R0144, NEB) according to manufacturer's instructions. The cut vector and PCR product were identified by gel electrophoresis and DNA extracted and quantified.

The ligation was performed with a ratio of 2:1 insert:vector and plasmids amplified by transforming E.coli as previously described in section 2.8.4. Seven colonies were amplified in miniprep cultures. Plasmids were prepared as described in section 2.8.5 and were sent for sequencing. The primers used for sequencing are provided in Table 2.12.

Construct	Primer	Template
WT *SGLT1*-Luc	5' GCGC***ACGCGT***TGTCTCATCTTTGATGCTGATCT 3' 3' GCGC***AGATCT***GGGCCGCTAGCTCCTTATAC 5'	Human genomic DNA
SGLT1-Luc mutEB1	5' CCAGCTCTGGCAAGGG***GCTAGC***TGGTGGCGCTGCTGGT3' 3' AGTGGCTCCATTGAGGGAACAGGCCACCTGGGGC 5'	Human genomic DNA
SGLT1-Luc mutEB2	5' CTAGGCTCCTAGCCC***GCTAGC***GCCTGTTCCCTCAA 3' 3' AGGCTTCAGATCACCTGCCACCCATCCTTGGACTAGTCCC5'	Human genomic DNA
SGLT1-Luc mutEB3	5' TTAGACATGTGTTTC***GCTAGC***GGTGAGCTGAGTCCCCA 3' 3' ACAGCAAGCCAGGGCTCAGAACAGAGATGACCA 5'	Human genomic DNA
SGLT1-Luc mutEB4	5' TGGCTTGCTGTTTAGA***GCTAGC***TTTCCAGATGGGTGAG 3' 3' GGGCTCAGAACAGAGATGACCAAGAGAGGAG 5'	Human genomic DNA
SGLT1-Luc mutEB1+2	5' CTAGGCTCCTAGCCC***GCTAGC***GCCTGTTCCCTCAA 3' 3' AGGCTTCAGATCACCTGCCACCCATCCTTGGACTAGTCCC 5'	*SGLT1*-Luc mutEB1
SGLT1-Luc mutEB1+3	5' TTAGACATGTGTTTC***GCTAGC***GGTGAGCTGAGTCCCCA 3' 3' ACAGCAAGCCAGGGCTCAGAACAGAGATGACCA 5'	*SGLT1*-Luc mutEB1
SGLT1-Luc mutEB1+2+3	5' TTAGACATGTGTTTC***GCTAGC***GGTGAGCTGAGTCCCCA 3' 3' ACAGCAAGCCAGGGCTCAGAACAGAGATGACCA 5'	*SGLT1*-Luc mutEB1+2

Table 2.11: Primers for the amplification of the wild-type human SGLT1 promoter and the introduction of mutations within the promoter. Restriction sites for the WT *SGLT1*-Luc construct and the introduced mutations for the mutant constructs have been highlighted in bold and italicized. Thermal cycler conditions used were 1 cycle at 94°C for 1 minute then 35 cycles of 94°C for 30 sec, 55°C for 30 sec and 68°C for 4 min.

Sequencing primers	Sequence
RVprimer3	5' CTAGCAAAATAGGCTGTCCC 3'
GLprimer2	5' CTTTATGTTTTTGGCGTCTTCCA 3'

Table 2.12: Sequencing primers used to confirm the introduction of the wild-type SGLT1 promoter and mutations (Chapter 4). Sequencing was carried out by technicians at the Brigham and Women's Hospital DNA Sequencing Core Facility.

The E-box sites within the SGLT1 promoter were mutated by conversion to NheI restriction sites (GCTAGC) and designated *SGLT1*-Luc mutEB1, mutEB2, mutEB3 and mutEB4. Site-directed mutagenesis was performed on the pGL3-SGLT1 vector created above using the Phusion Site-directed Mutagenesis kit (Catalog no. F-541, NEB). Primers were designed according to instructions for the Phusion kit[300]. Forward primers for the site-directed mutagenesis were designed to incorporate the NheI restriction site in place of the E-box sequence and including 15-20bp of the proximal and distal flanking sequences; while reverse primers did not incorporate any mutations. All primers for site-directed mutagenesis were acquired from Invitrogen. Primers were designed to incorporate single E-box mutations as well as combinations of E-box mutations (designated mutEB1+2, 1+3 and 1+2+3), by adding a further mutation onto a mutated promoter, to assess synergistic interactions. All constructs were sequenced to confirm successful mutation. Mutagenesis primers are listed in Table 2.11 and sequencing primers listed in Table 2.12.

2.10. SGLT1 promoter reporter assays

For reporter assays carried out in Chapter 4, CHO cells were transfected as described in section 2.7.1 above. The effect of PER1 overexpression on the *SGLT1* promoter was assessed in CHO cells passages 10-12 transfected at 80% confluence with combinations of reporter vector (pGL3-Basic, wild-type *SGLT1* pGL3/WT-*SGLT1*luc, or mutated *SGLT1* promoter constructs) and expression vector (pcDNA3.1(+) with or without PER1 cDNA). Conversely, the effect of *PER1* knockdown on *SGLT1* promoter activity was assessed by co-transfection of shRNA vectors in place of expression vectors. Renilla luciferase (Catalog no. E2241, pRL-TK; Promega) was co-transfected into all wells in all experiments to normalize for transfection efficiency.

After 48 hours, cells were washed once with PBS, then reporter expression measured using the Promega Dual Luciferase Reporter Assay System (Catalog no. E1960, Promega, Madison, WI) according to manufacturer's instructions[301]. Luminescence was measured on an M5 Spectramax using the provided software.

2.11. Quantification of apoptosis

Apoptosis in IEC-6 cells in Chapter 5 was quantified using the FITC-Annexin-V Apoptosis Detection Kit I (BD), Cells were counter-stained with the nucleic acid stain Sytox Blue (Catalog no. S34857, Invitrogen) to specifically identify dead or necrotic cells which also stain Annexin-V positive. IEC-6 cells stably overexpressing either mir-16 or the scrambled negative control were grown in 10cm tissue-culture treated dishes in the presence of 2μg/ml puromycin and 2μg/ml of doxycycline to induce mir-16 or control expression. After 48 hours, cells were trypsinized and counted and stained with Annexin V-FITC and Sytox Blue according to manufacturer's recommendations[302, 303]. Stained cells were analyzed at 10,000 events per sample by Miss Ashley Lansing, a technician at the Dana Farber Cancer Institute Flow Cytometry Core Facility on an LSRII flow cytometer (BD). The percentage of cells in each of the four quadrants (live, early apoptosis, late apoptosis and necrosis) was determined by Ashley Lansing using the software Diva (BD) and the results provided to me for further analysis.

2.12. Measurement of cell proliferation

2.12.1. In vitro proliferation

Cell proliferation was measured using the CellTiter96 Aqueous One Solution Cell Proliferation Assay (MTS assay, Catalog no. G3582, Promega, Madison, WI) according to manufacturer's instructions[304].

2.12.2. Cell growth rate (counting method)

Cell growth rates were confirmed by manual cell counting. IEC-6 cells were trypsinized, stained with trypan blue and counted at 10x magnification. 5 high-powered fields were counted per sample.

2.13. Measurement of cell cycle changes

Cell cycle analysis was performed using propidium iodide. Cells were trypsinized and counted and each sample resuspended at 5000 cells/µl PBS. Resuspended cells were added dropwise into ice-cold 70% ethanol in a 50ml conical centrifuge tube while vortexing (250,000cells/ml of ethanol); and incubated overnight at -20°C. The next day cells were centrifuged at 1,200rpm for 10 minutes at 4°C, the ethanol aspirated off and the cell pellet resuspended in propidium iodide containing RNAse (Catalog no. 550825, BD) at a final density of 0.5 x 10^6 cells/ml. Resuspended cells were incubated for 30mins at 37°C in darkness and analyzed at 10,000 events per sample by Ashley Lansing at the Dana Farber Cancer Institute Flow Cytometry Core Facility on a BD FACScan flow cytometer (BD). The percentage of cells in each of the cell cycle stages (G1, S, G2 and M) was determined by Ashley Lansing using the software ModFit (Verity, Topsham, ME) and the results provided to me for further analysis.

2.14. Statistical analysis

All experiments were performed a total of three times. Data are presented as means ± SE. Graphical analysis was performed using Graphpad Prism (San Diego, CA). Unless mentioned otherwise all statistical analysis was performed using Microsoft Excel 2007 (Microsoft, Redmond, WA). For all experiments the probability of $p < 0.05$ was taken as significant.

Chapter 3: Restricted feeding phase shifts circadian rhythmicity in clock gene and sodium glucose co-transporter expression in rat jejunum

3.1. Introduction

The mammalian intestine is known to exhibit diurnal rhythmicity in a number of physiologic functions, including absorption[12, 13, 69, 70], enzyme activity[305], motility[306] and proliferation[307]. Glucose absorption in particular is known to exhibit a robust diurnal rhythmicity in the jejunum, mediated entirely by rhythmicity in the expression of the intestinal sodium glucose co-transporter SGLT1[12, 13, 69]. The mechanisms governing rhythmicity in SGLT1 expression remain unclear. Clock genes exhibit diurnal rhythmicity in the intestine and have been implicated in the regulation of intestinal proteins such as *Pept1* [16] and *Mdr1* [15], however no studies have examined the role of clock genes in the regulation of SGLT1 rhythmicity in the intestine and thereby the rhythmicity of intestinal glucose uptake.

Clock genes were first characterized in the SCN, the master circadian clock[158]. These genes interact to create positive and negative molecular feedback loops, resulting in a circadian pattern of gene expression with 24 hour periodicity[158]. The negative-feedback loop involves the rhythmic induction of three *Period* genes (designated *Per1–3*) and two *Cryptochrome* genes (*Cry1* and *Cry2*) by the binding of CLOCK and BMAL1 to E-boxes (sequences of CAnnTG) on *Per* and *Cry* promoters [158]. PER and CRY subsequently inhibit transcription of *Clock* and *Bmal1*[156], inducing rhythmicity of *Bmal1* expression with a phase opposite to that of *Per* or *Cry,* resulting in a positive-

feedback loop[134]. An accessory loop involving the orphan nuclear receptors *Rora* and *Rev-erbA* and *B* links the positive and negative limbs of the circadian oscillator[308]. *ReverbA* and *B* and *Rora* transcription is driven by BMAL1/CLOCK[309]. *Reverbs* and *Rora* in turn suppress and activate *Bmal1* expression respectively[309].

More recently clock genes have been shown to form peripheral circadian oscillators in tissues outside the SCN, including the retina[177, 310], heart[177, 179], lung[177], kidney[177], peripheral blood cells[176, 178] and liver[178], with rhythms exhibiting a 3-9 hour phase delay compared to the SCN. As yet, clock gene expression in the intestine has not been completely profiled. A few clock genes (*Bmal1*, *Clock*, *Per1-2* and *Cry1*) have been shown to exhibit rhythmicity in rodent jejunum[16, 311], however further work is required to fully characterize the expression of clock genes in the small intestine.

While circadian clock rhythmicity in the SCN is known to be entrained to light[130, 134] clock gene expression in certain peripheral tissues[180, 182] is entrained by nutrients – restricted feeding regimens have been shown to shift the oscillatory rhythms of clock genes in the colon[182] and liver[180] but not in the light-entrained SCN[180, 182]. Nutrient availability may therefore have a similar effect on the entrainment of clock genes in the intestine, another organ exposed to wide fluctuations in nutrient exposure.

I hypothesized that members of the clock gene family exhibit circadian rhythmicity in the intestine and that this rhythmicity in clock gene expression mediates the rhythmicity

in expression of the sodium glucose co-transporter SGLT1. The cues entraining rhythmicity in clock gene expression in the intestine have not been identified and I proposed that nutrient availability is likely to act as a strong cue for entrainment of rhythmicity in the intestine. In particular I aimed to determine whether restricting food availability to the light phase, which would disrupt the normal nocturnal feeding pattern of rats, would shift the pattern of rhythmicity of clock genes and/or *Sglt1*. Altering the timing of nutrient availability would impose a new feeding pattern on the rats, thereby altering the period of nutrient exposure in the jejunum and resulting in a shift in the pattern of rhythmicity of clock genes and *Sglt1* expression. By simultaneously examining the temporal profiles of clock gene expression and *Sglt1* expression under conditions of ad libitum and restricted feeding, I hoped to identify the clock gene(s) that shifted in phase (to the same degree) as *Sglt1* and thereby identify potential clock genes capable of regulating the transcriptional rhythmicity of *Sglt1*.

3.2. Clock genes and *Sglt1* display diurnal rhythmicity in the jejunum of ad libitum fed rats

Rats were maintained in a 12-hourly light dark cycle (lights turned on at ZT 0 or 7am and turned off at ZT 12 or 7pm), fed ad libitum over the 24 hour period with free access to water, then after 5 days killed at 3 hourly intervals (n=6-7 per time point) beginning at ZT 0 (7am). To facilitate comparison to subsequent restricted-fed rats, these ad libitum fed rats will be designated "AL" rats.

Total RNA was extracted from jejunal mucosal scrapings from these rats and subjected to reverse transcription and qPCR as described in section 2.2. The rat *β-actin* gene was used as a housekeeping gene to normalize for RNA loading. The means and spread of *Per1* expression (taken as a representative clock gene) and of *β-actin* expression for ZT 0 (taken as a representative timepoint) are similar, as shown in Figure 3.1.

The data (expression of each gene relative to *β-actin* for each rat) were loaded into the Cosinor program (freely available at www.circadian.org). Cosinor analysis uses the least squares method to fit a sine wave to time series data assuming a 24-h period [312]. Clock genes were considered to display diurnal rhythmicity in ad libitum fed animals if a significant fit to a 24-hour period (as indicated by the p-value) was determined by the cosinor analysis performed by the program. For clock genes that were shown to display diurnal rhythmicity, the acrophase (time of peak expression) was determined by the program. The significance of fit to a 24-hour period, mesor (rhythm-adjusted mean),

amplitude of rhythmicity and the acrophase for each clock gene are expressed in Table 3.1. Amplitudes (abstracted from the cosinor program) have been expressed as percentages of the mesor to allow for comparisons to be made across genes. Cosinor analysis can often be inaccurate in small sample sizes and with a limited number of diurnal harvest timepoints, hence ANOVA with post-hoc Tukey analysis was also used to identify a significant difference ($p<0.05$) between timepoints.

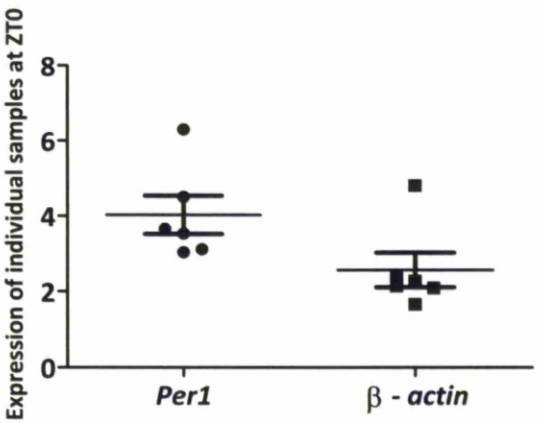

Figure 3.1: Expression of *Per1* and *β-actin* at ZT 0. RNA from the jejunum of rats (n=6) killed at ZT 0 (7am) was extracted, reverse transcribed and subjected to qPCR. PCR was performed twice for each gene and each sample was plated in triplicate for each PCR. The mean expression of each gene for each sample at ZT 0 is shown as a circle (*Per1*) or a square (the housekeeping gene *β-actin*) and the mean expression and standard error of the mean for each gene per timepoint indicated.

To allow ease of visual comparisons of rhythmicity and amplitude to be made, the mean expression for each gene at each timepoint for the AL rats has been expressed as a ratio to the mean expression of the same gene at ZT3, chosen as the reference timepoint as it was common to AL, DF and LF rats. These values are displayed graphically in Figure 3.2A-H (clock genes) and Figure 3.3 (*Sglt1*).

Gene	p-value	Acrophase (ZT, hh:mm)	Mesor	Amplitude(%)	p value on ANOVA
Per1	0.0014	09:28	1.29	48	0.0249
Per2	0.0008	15:59	3.02	57	<0.0001
Bmal1	<0.0001	23:04	0.71	100	<0.0001
Clock	0.0008	21:23	0.80	38	0.0151
ReverbA	<0.0001	06:21	0.57	76	<0.0001
ReverbB	0.0003	08:34	0.81	41	<0.0001
Cry1	0.0015	20:08	1.41	17	<0.0001
Cry2	0.0097	18:41	1.47	36	0.0029
Sglt1	<0.0001	10:44	1.60	51	<0.0001

Table 3.1: Circadian rhythmicity of clock genes and *Sglt1*. The expression of each gene was normalized to the expression of the housekeeping gene *β-actin* for the same sample. The data were arranged as if a single animal was harvested at 3-hourly intervals over 6 days and cross-sectional pattern analysis was performed with the cosinor procedure, freely available at www.circadian.org. This software was used to determine the significance of fit of the temporal expression of the data to a cosinor pattern with a 24-hour period. The p-values indicate the significance of fit of the data to a cosinor pattern with 24-hour periodicity as determined by the cosinor program, with a p value of 0.05 indicating a 5% probability that the observed 24-hour periodicity occurred by chance alone. The acrophase, abstracted from the cosinor program, is expressed as hours after light onset (ZT, lights on is at 0700 hence ZT 0 is 0700). The mesor is the rhythm adjusted mean, also abstracted from the cosinor program. The amplitude has been expressed as a percentage of the mean to facilitate comparison across genes.

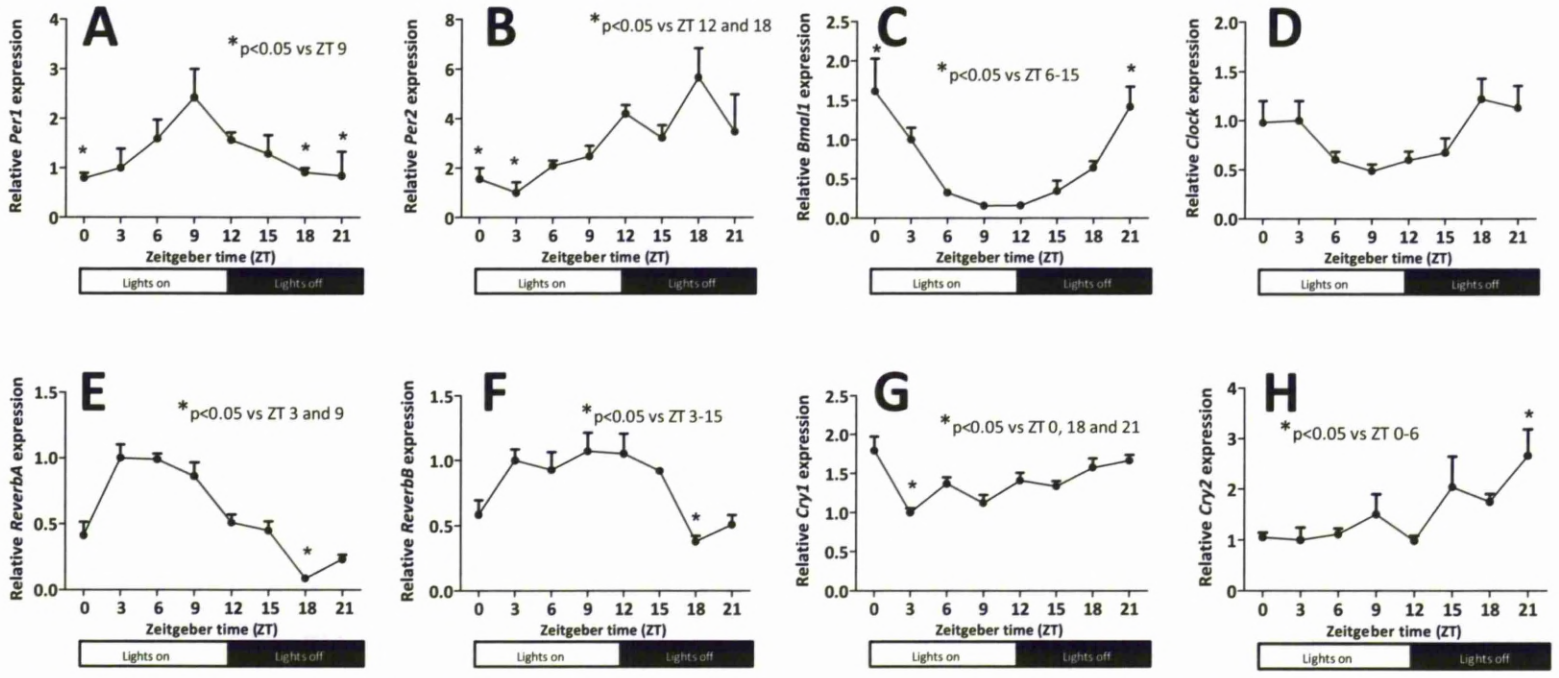

Figure 3.2: Clock gene expression in AL rats. Rats fed ad libitum ("AL") were culled at 3 hourly intervals (6-7 rats per timepoint) beginning at ZT 0 (7am). mRNA was extracted from jejunal mucosal scrapings and subjected to reverse transcription and qPCR to determine the expression of clock genes *Per1*(**A**), *Per2* (**B**), *Bmal1* (**C**), *Clock* (**D**), *ReverbA*(**E**), *ReverbB* (**F**), *Cry1* (**G**) and *Cry2* (**H**). Each well was plated in triplicate and the qPCR reaction performed twice for each experiment. mRNA expression for each gene was expressed as a ratio to the expression of the housekeeping gene *β-actin* for the same sample. The graphs show the mean and standard error for each gene at each timepoint. To facilitate comparisons of rhythmicity and amplitude, mean expression at each timepoint has been expressed as a ratio to the mean expression at ZT3. ANOVA with post-hoc Tukey test was used to identify significant differences between timepoints.

All clock genes exhibited diurnal rhythmicity with a 24 hour periodicity in the jejunal mucosa of ad libitum fed rats on cosinor analysis (Table 3.1, Figure 3.2A-H), however significant differences between individual timepoints could not be demonstrated for *Clock*. The time of peak expression varied across genes. Both *Per1* and *Per2* were rhythmic in the jejunum, however had opposite patterns of rhythmicity. *Per1* peaked during the lights-on phase at ZT 9 ($F^{7,42}$=2.666, p=0.0249, Figure 3.2A), while *Per2* peaked at ZT12-18 ($F^{7,42}$=6.704, p<0001, Figure 3.2B). Such a marked difference in peak expression was not noted for the other clock gene homologue pairs such as *ReverbA* and *B* and *Cry1* and *2* (Figure 3.2E-H). *ReverbA* peaked at ZT 3-9 ($F^{7,42}$=6.370, p<0.0001, Figure 3.2E), while *ReverbB* had a more sustained peak from ZT3-15 ($F^{7,42}$=6.424, p<0.0001, Figure 3.2F). Similarly *Cry1* peaked at ZT 18-0 ($F^{7,42}$=6.370, p<0.0001, Figure 3.2G), while its homologue *Cry2* peaked at ZT 21 ($F^{7,42}$=3.881, p=0.0029, Figure 3.2H).

Bmal1 and *Clock*, two clock genes known to dimerize to act as transcriptional regulators[161, 162], peaked at similar timepoints as would be expected (Figures 3.2C and D). *Bmal1* peaked at ZT 21-0 ($F^{7,42}$=9.609, p<0.0001, Figure 3.2C) while *Clock* did not demonstrate a statistically significant peak on post-hoc Tukey test but displayed higher expression at the end of the dark phase ($F^{7,42}$=2.899, p=0.0151, Figure 3.2D, Table 3.1). The pattern of expression of *Bmal1* and *Clock* showed that these genes, which activate transcription of *Per1* and *Per2*[161, 162], peaked in antiphase to *Per1* (out of phase by almost 12 hours, Figures 3.2A, C and D, Table 3.1) but were only 6 hours out of phase with *Per2* (Figures 3.2B-D, Table 3.1). The expression of *Cry1* and *Cry2*, known to suppress *Bmal1* and *Clock*[156, 158], was similarly only ~3 hours out of phase with *Bmal1* and *Clock* (Figures 3.2C, D, G and H, Table 3.1). *ReverbA* and *ReverbB* are known

to be stimulated by *Bmal1* and *Clock*[164, 309] and correspondingly peaked between 6-15 hours after the peak in *Bmal1* and *Clock* expression (Figures 3.2C-F, Table 3.1).

The amplitude of change also varied dramatically across the clock genes examined. The mesor of each gene (the rhythm-adjusted mean) was abstracted from the cosinor program. The amplitude of each gene (calculated as the absolute difference in value between the peak level and the mesor) was also abstracted from the cosinor program, then expressed as a ratio to the mesor to allow comparisons of amplitude to be made across genes.

The greatest amplitude was displayed by *Bmal1*, which showed a 100% increase in expression between the mesor and the peak (Figure 3.2C, Table 3.1). *ReverbA* also showed high amplitude of rhythmicity across timepoints (76%, Figure 3.2E, Table 3.1) and to a lesser degree *ReverbB* (41%, Figure 3.2F, Table 3.1). Although widely dissimilar in the time of peak expression, paralogues *Per1* and *Per2* showed similar amplitudes of change, at 48% and 47% respectively (Figure 3.2A and B, Table 3.1). The smallest amplitudes were displayed by *Clock* and *Cry1* (38% and 17% respectively, Figure 3.2D and G, Table 3.1). In contrast to *Per1* and *Per2*, *Cry1* and *Cry2* peaked at around the same timepoint but displayed a more profound difference in the amplitude; *Cry2* had a higher amplitude of rhythmicity than *Cry1* at 36% (Figure 3.2H and G, Table 3.1).

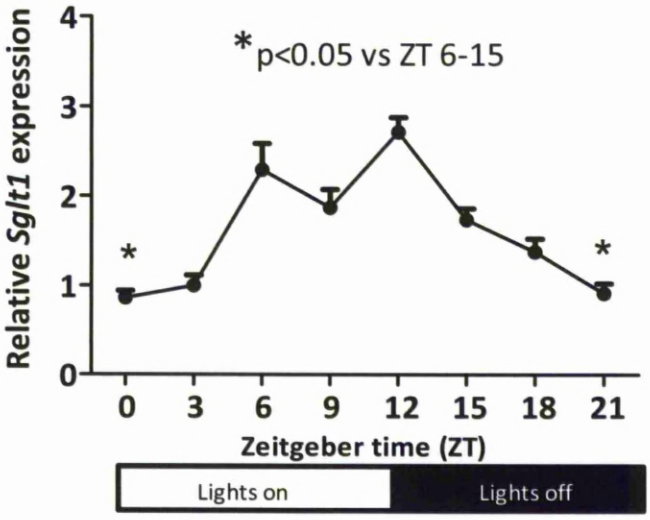

Figure 3.3: *Sglt1* mRNA expression in AL rats. Rats fed ad libitum ("AL") were culled at 3 hourly intervals (6-7 rats per timepoint) beginning at ZT 0 (7am). mRNA was extracted from jejunal mucosal scrapings and subjected to reverse transcription and qPCR to determine the expression of *Sglt1*. Each well was plated in triplicate and the qPCR reaction performed twice for each experiment. mRNA expression of *Sglt1* was expressed as a ratio to the expression of the housekeeping gene *β-actin* for the same sample. The graphs show the mean and standard error at each timepoint. To facilitate comparisons of rhythmicity and amplitude, mean expression at each timepoint has been expressed as a ratio to the mean expression at ZT 3. ANOVA with post-hoc Tukey test was used to identify significant differences between timepoints.

Like clock genes, *Sglt1* mRNA also exhibited robust 24 h rhythmicity ($F^{7,42}$=17.22, p<0.0001, Figure 3.3), with peak expression between ZT 6-15 (Table 3.1), overlapping that for *Per1* (ZT 9, Figure 3.2A, Table 3.1) as well as *ReverbB* (ZT 3-15, Figure 3.2F, Table 3.1). The amplitude of rhythmicity of *Sglt1* (51%, Figure 3.3) was similar to the amplitudes of *Per1* (48%, Figure 3.2) and *Per2* (57%, Figure 3.2B, Table 3.1).

As described above, AL rats displayed rhythmicity in all examined clock genes as well as *Sglt1* (Figures 3.2 A-H, 3.3 and Table 3.1). While light is the dominant entraining cue for the master clock in the SCN[130, 134], nutrient availability has been shown to be the dominant zeitgeber in the liver[180]. I therefore next investigated the entraining effect of food on the rhythmicity of clock genes and *Sglt1* in the jejunum.

3.3. Nutrient consumption and body weight normalize within 7 days of lights-on restricted feeding

To determine the effect of nutrient availability on clock gene and *Sglt1* expression, rats (n=50) were fed for 7 days either during only the dark phase (designated "DF", ZT 12-24), or light phase (ZT 0-12, designated "LF"). DF rats were pair-fed to LF rats to ensure equal food intake. Rats were housed in pairs in cages. LF animals were given 100g of food per cage at 0700. The remaining food at 1900 was weighed and subtracted from 100g to calculate the amount consumed per pair of rats (it was assumed that both rats consumed equal amounts of food). The mean daily consumption of LF animals was calculated and provided to each pair of DF animals at 1900. No food remained in the cages of DF animals at 0700 the next day. Food consumption by LF rats over the 7 day study period is displayed graphically in Figure 3.4.Food consumption by LF rats on day 1 averaged 16g (Figure 3.4), about 4g less than the 20g/day consumed by rats of similar weight fed ad libitum[89] but had normalised by day 3.

To confirm acclimatization to the feeding pattern, body weights for each group were measured over the 7 day study duration and are shown graphically in Figure 3.5. A restricted feeding regimen of sufficient duration to allow acclimatization of LF rats to the new feeding schedule would be expected to result in equal weights between the groups at the end of the study period. To minimize disruption to the rats' circadian behaviour during restricted feeding, rats were weighed only 3 times during the study period - days 0 (the beginning of the study period), 4 and 8 (prior to harvest). A two-way ANOVA was performed to identify the effects of feeding pattern and duration of feeding (0, 4 or 8 days) on the weights of rats in the two groups and to identify any interaction between the two factors. Feeding time was a significant factor in the difference in weights in LF vs DF rats at day 4 (244g $\pm$1.4g vs 251g +1.5g respectively, $F^{1,96}$=4.14, $p<0.05$, Figure 3.5) but not at days 0 or 8. The weights of both groups of rats increased significantly across day 0 to day 8 ($F^{2,96}$=481, $p<0.0001$, Figure 3.5). No significant interaction was observed between duration of feeding and feeding time ($F^{2,96}$=2.02 $p=0.139$).

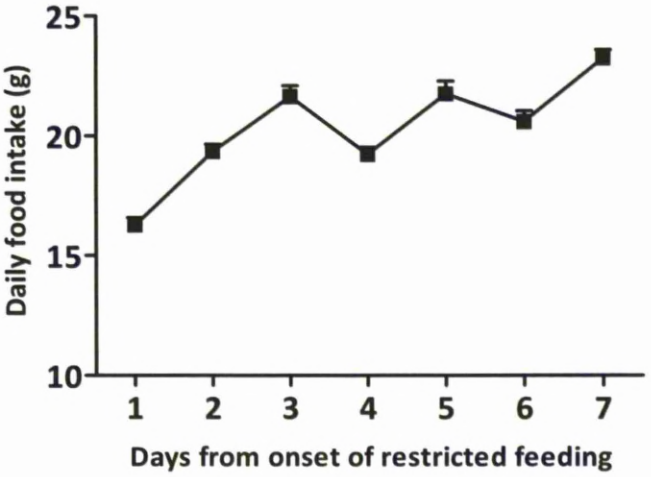

Figure 3.4: Daily food intake in rats fed during only the lights-on period. Rats (n=25) were maintained in a 12-hourly light-dark cycle (lights turned on at ZT 0 or 7am and turned off at ZT 12 or 7pm) and fed for 7 days during only the lights-on phase (ZT 0-12, 7am to 7pm). Rats were given a fixed excess of food each day (100g) at ZT 0; remaining food was removed at ZT 12 and weighed. DF rats were given the exact amount of food consumed by LF rats and fed between ZT 12 and ZT 24. Values are expressed as means and standard error of the mean.

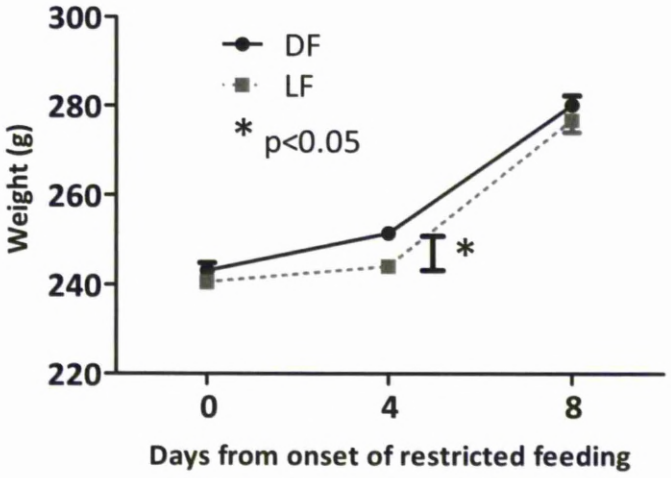

Figure 3.5: Increase in weight in DF and LF rats. Rats (n=50) were maintained in a 12-hourly light-dark cycle and fed during either the lights-off period (DF rats, n=25, indicated by black circles) or lights-on period (LF rats, n=25, indicated by grey squares) for 7 days. Rats were weighed at days 0 (at the beginning of the study period), 4 and 8 (before harvest). Weights are expressed as means and standard error of the mean. A two-way ANOVA was used to identify the effects of feeding time and duration of feeding on weight as well as any interaction between the two factors.

3.4. Restricted feeding induces a similar phase shift in clock genes and *Sglt1* in rat jejunum

DF and LF rats were maintained on the feeding regimens shown above for 7 days and on day 8 were killed (n=6-7 per time point per group) at 6-hourly intervals beginning at ZT 3 (10am). Total RNA was extracted from jejunal mucosal scrapings from these rats and subjected to reverse transcription and qPCR as described in section 2.2. The rat *β-actin* gene was used as a housekeeping gene to normalize for RNA loading. The level of each gene was expressed as a ratio to the level of *β-actin* in the same sample. The temporal profiles of all genes examined are displayed graphically in Figure 3.6A-H and Figure 3.7.

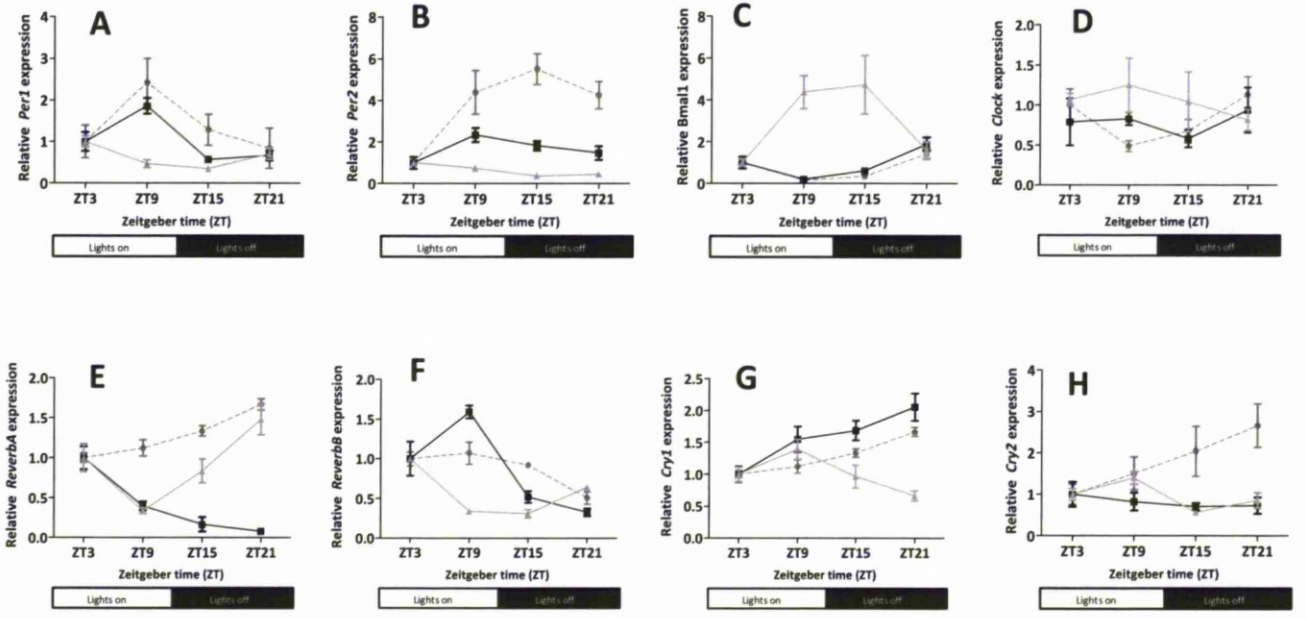

Figure 3.6: Clock gene expression in AL, DF and LF rats. Rats fed during either the lights-off period ("DF", dark grey circles) or lights on period ("LF", light grey triangles) were culled at 6 hourly intervals (6-7 rats per timepoint) beginning at ZT 3 (10am). mRNA was extracted from jejunal mucosal scrapings and subjected to reverse transcription and qPCR to determine the expression of clock genes *Per1*(**A**), *Per2* (**B**), *Bmal1* (**C**), *Clock* (**D**), *ReverbA*(**E**), *ReverbB* (**F**), *Cry1* (**G**) and *Cry2* (**H**). Each well was plated in triplicate and the qPCR reaction performed twice for each experiment. mRNA expression was expressed as a ratio to *β-actin* for the same sample. Gene expression at the same timepoints in rats fed libitum ("AL") as described in the previous section have been co-plotted for comparison (black squares). Graphs show mean and standard error for each gene at each timepoint. To facilitate comparisons of rhythmicity and amplitude, mean expression for each group at each timepoint has been expressed as a ratio to the mean expression of the same group at ZT 3.

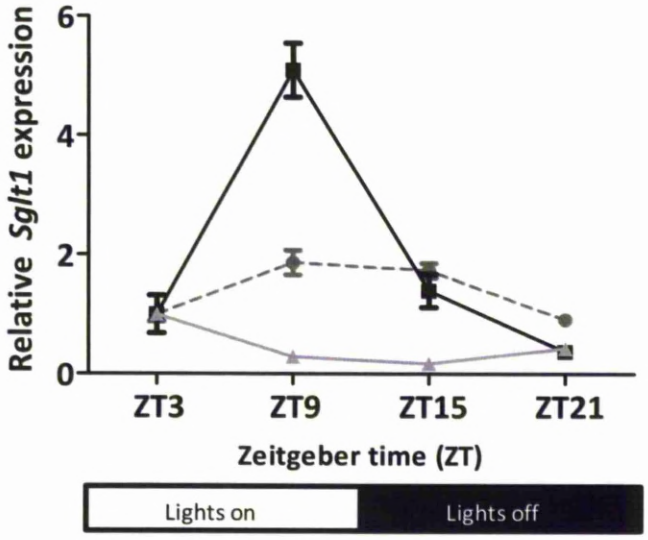

Figure 3.7: *Sglt1* expression in AL, DF and LF rats. Rats fed during either the lights-off period ("DF") or lights on period ("LF") were culled at 6 hourly intervals (6-7 rats per timepoint) beginning at ZT 3 (10am). mRNA was extracted from jejunal mucosal scrapings and subjected to reverse transcription and qPCR to determine the expression of *Sglt1*. Each well was plated in triplicate and the qPCR reaction performed twice for each experiment. mRNA expression of *Sglt1* was expressed as a ratio to the expression of the housekeeping gene *β-actin* for the same sample. The graphs show the mean and standard error at each timepoint. DF rats are shown in dark grey circles and LF rats in light grey triangles. *Sglt1* expression at the same timepoints in rats fed libitum ("AL") as described in the previous section have been co-plotted for comparison (black squares). To facilitate comparisons of rhythmicity and amplitude, mean expression for each group at each timepoint has been expressed as a ratio to the mean expression of the same group at ZT 3.

Gene	Effect of feeding time (p value)	Effect of harvest time (p value)	Interaction (p value)	Significant differences in gene expression at specific timepoints		
				AL vs DF	AL vs LF	DF vs LF
Per1	0.0006	0.0005	0.0067	None	ZT9 and ZT15	ZT9
Per2	<0.0001	<0.0001	<0.0001	ZT9, ZT 15 and ZT21	ZT9, ZT15 and ZT21	ZT 9 and ZT15
Bmal1	<0.0001	0.2041	<0.0001	None	ZT9 and ZT15	ZT 9 and ZT15
Clock	0.2233	0.6724	0.3344	None	None	None
ReverbA	<0.0001	<0.0001	<0.0001	ZT9, ZT15 and ZT21	ZT9 and ZT15	ZT15 and ZT21
ReverbB	<0.0001	<0.0001	<0.0001	ZT9 and ZT15	ZT9 and ZT15	ZT9 and ZT21
Cry1	<0.0001	0.0012	<0.0001	None	ZT21	ZT15 and ZT21
Cry2	<0.0001	0.3301	0.0138	ZT15 and ZT21	ZT15 and ZT21	None
Sglt1	<0.0001	<0.0001	<0.0001	ZT9	ZT9 and ZT15	ZT9 and ZT15

Table 3.2: Effect and interaction of feeding times and harvest times on clock gene and *Sglt1* expression in DF and LF rats. A two-way ANOVA was used to identify effects of feeding time and harvest time on gene expression in AL, DF and LF rats and to determine any interaction between the two variables.

Rats fed under ad libitum conditions consume the majority of their food intake during the lights off period[13, 313]. Feeding time would therefore be expected to influence gene expression patterns of both clock genes and *Sglt1*. This hypothesis was borne out by two-way ANOVA analysis of the expression levels of clock genes and *Sglt1* in AL, DF and LF rats, which showed that feeding had a significant effect on the differential expression of the majority of genes in these three groups ($p<0.001$ for all genes examined except *Clock*, Table 3.2, Figure 3.6). Harvest time also had a significant effect on gene expression for most genes with the exception of *Clock*, *Bmal1* and *Cry2* for which no effect was seen (Table 3.2, Figure 3.6) Feeding time showed a significant interaction with harvest time in this two-way ANOVA across all clock genes with the exception of *Clock*, indicating that the specific feeding regimen used influenced gene expression at the designated harvest times.

A number of clock genes examined (*Per1*, *Bmal1*, *Clock* and *Cry1*) showed no difference in expression when subjected to feeding during only the lights off phase (the DF group) compared to ad libitum feeding (AL group), as would be expected given the known nocturnal feeding behaviour of rats[13, 313] (Table 3.2, Figure 3.6A,C, D and G). In contrast differences in gene expression between DF and AL rats were noted for *Per2*, *Reverb A* and *Reverb B* and *Cry2* (Table 3.2, Figure 3.6 B, E, F and H).

Restricting feeding to the lights on period resulted in significant differences in gene expression for almost all clock genes with the exception of *Clock* and *Cry2* (compared to

DF rats, Table 3.2, Figure 3.6 C and H). Feeding during the lights on period induced increased levels of gene expression of *Bmal1*, *Clock*, *Cry1* and *Cry2* at ZT9 but suppressed levels of gene expression of *Per1*, *Per2*, *Reverb A* and *Reverb B* (Table 3.2, Figure 3.6).

Each clock gene displayed differential response to restricting feeding to either the dark phase or light phase compared to ad libitum feeding. *Per1* expression in DF and AL rats was broadly similar across the diurnal period however LF animals exhibited suppressed expression of *Per1* at ZT 9 and ZT 15 (Figure 3.6A, Table 3.2). *Per2* expression was higher at ZT 9 and ZT 15 in DF rats compared to AL or LF rats; similar to *Per1*, levels of *Per2* in LF rats were suppressed AT ZT9 and ZT 15 compared to DF or AL rats (Figure 3.6B, Table 3.2). In contrast to *Per1*, *Bmal1* expression, while similar in AL and DF animals, was increased at ZT 9 and ZT 15 in DF rats (Figure 3.6C, Table 3.2). *Clock* expression did not display significant rhythmicity in LF and DF rats, possibly due to the large variation in expression levels across rats within the same timepoints (Figure 3.6D, Table 3.2). *ReverbA* levels increased across the diurnal period in DF rats compared to AL rats (Figure 3.6E, Table 3.2) The expression of *ReverbA* decreased at ZT9 and ZT15 in LF rats compared to DF rats (Figure 3.6E, Table 3.2). Diurnal differences in *ReverbB* expression were blunted in DF rats compared to AL rats, and *ReverbB* levels suppressed at ZT9 compared to both DF and AL rats (Figure 3.6F, Table 3.2). *Cry1* expression in AL and DF rats increased between ZT3 and ZT21, but decreased between ZT9 and ZT21 in LF rats (Figure 3.6G, Table 3.2). Restricting feeding to the dark phase increased levels of *Cry2* at

ZT15 and ZT21 compared to AL rats, while restricting feeding to the lights on phase decreased *Cry2* levels at these timepoints (Figure 3.6H, Table 3.2).

Both feeding time and harvest time had a significant effect of *Sglt1* expression, and were shown on two-way ANOVA to interact to influence gene expression of *Sglt1* ($F^{6/61}$=40.78, p<0.0001, Table 3.2, Figure 3.7). Restricting feeding to only the dark phase resulted in a significantly higher level of gene expression at ZT9 compared to rats fed ad libitum (Table 3.2, Figure 3.7). In contrast, restricting feeding to the lights on phase only significantly reduced Sglt1 expression at ZT9 and ZT15 compared to AL and DF rats (Table 3.2, Figure 3.7).

Clock genes responsible for mediating diurnal rhythmicity in *Sglt1* transcription would be expected to demonstrate similar patterns of expression as *Sglt1* upon restricted feeding. I therefore examined the effect of restricted feeding on the individual clock genes and compared this to the effects on *Sglt1*. Clock genes *Per1* and *ReverbB* both displayed similar patterns of expression to *Sglt1* both ad libitum and under the two restricted-feeding regimens. As the *Sglt1* promoter does not contain binding elements for Reverbs (analysis of the *Sglt1* promoter is detailed further in Chapter 4), but does contain E-boxes which mediate the actions of the main clock gene feedback loops involving *Bmal1*, *Clock*, *Per* and *Cry* genes, *Per1* was therefore considered of particular interest. To explore this further I examined the temporal expression of PER1 protein expression in rat jejunum to compare the profiles of PER1 and *Sglt1* expression.

3.5. PER1 rhythmicity in rat jejunum occurs in antiphase to the temporal profile of *Sglt1*

AL and DL rats were culled at 6 hourly intervals (6-7 rats per group per timepoint) as described above and jejunum harvested for subsequent analysis of protein expression. Protein was extracted from jejunal mucosal scrapings of these rats and Western blotting performed as described in section 2.5. Protein expression for PER1 and SGLT1 was expressed as a ratio to the expression of the housekeeping gene β-ACTIN for the same sample. The mean and standard error of protein expression for each gene at each timepoint was calculated and is displayed graphically in Figure 3.8. A two-way ANOVA was used to identify effects of feeding time and harvest time on gene expression in DF and LF rats and to determine any interaction between the two variables; values are shown in Table 3.3.

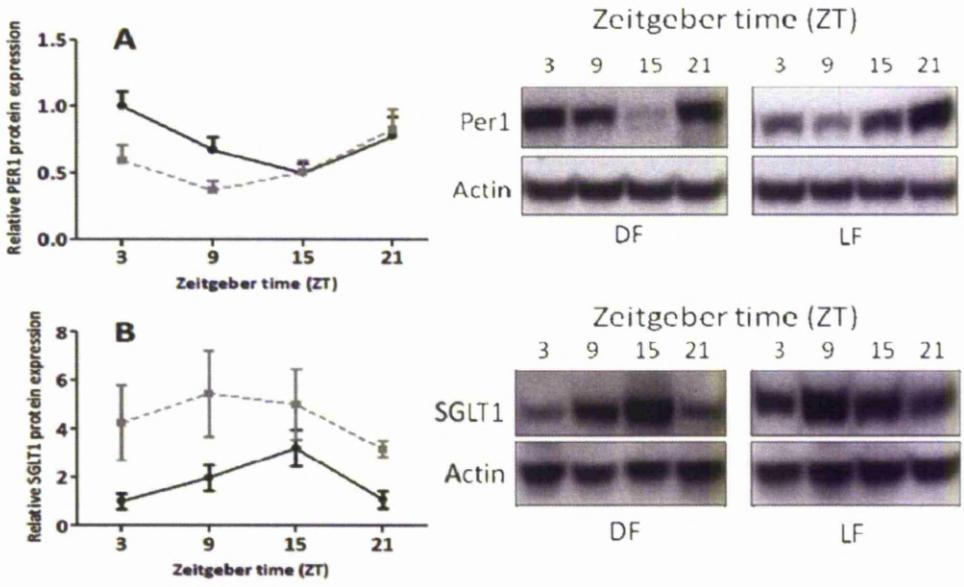

Figure 3.8: PER1 and SGLT1 protein expression in rat jejunum. Rats fed ad lib were culled at 6 hourly intervals (6-7 rats per timepoint) beginning at ZT 3 (10am) and jejunum harvested for analysis of protein expression of PER1 (**A**) and SGLT1 (**B**). Protein was extracted from jejunal mucosal scrapings and Western blotting performed. Blot images were quantified by densitometry and protein expression for each gene expressed as a ratio to the expression of the housekeeping gene β-ACTIN for the same sample. Values represent the mean and standard error for each gene at each timepoint. DF rats are represented in the graphs by black circles and LF rats by grey squares.

Gene	Effect of feeding time (p value)	Effect of harvest time (p value)	Interaction (p value)	Significant differences in gene expression at specific timepoints between DF and LF
PER1	0.0364	0.0063	0.1070	None
SGLT1	0.0009	0.5901	0.9707	None

Table 3.3: Expression of PER1 and SGLT1 in DF and LF rats. The expression of each protein was normalized to the expression of β-ACTIN for the same sample. A two-way ANOVA was used to identify effects of feeding time and harvest time on gene expression in DF and LF rats and to determine any interaction between the two variables.

PER1 protein expression was influenced by both feeding time and harvest time in DF and LF rats. PER1 levels were highest at ZT3 in DF animals but at ZT21 in LF animals, however this difference did not meet statistical significance (Figure 3.8A, Table 3.3). In addition no interaction was noted between feeding time and harvest time for PER1 on two-way ANOVA ($F^{3,42}$=2.16, p=0.107, Table 3.3). Feeding time had a significant effect on SGLT1 expression, as evidenced by higher levels of expression in LF animals than in DF animals at all timepoints, however harvest time did not have any effect on SGLT1 expression at the protein level (Figure 3.8B, Table 3.3). No interaction was demonstrated between the effects of feeding time and harvest time on SGLT1 ($F^{3,42}$=0.08, p=0.971, Figure 3.8, Table 3.3).

Given the similar phase shifts in *Per1* and *Sglt1* expression, it was proposed that PER1 might act as a transcription factor regulating *Sglt1* expression. The temporal profiles of PER1 and *Sglt1* in DF and LF rats were therefore juxtaposed and compared. The decrease in PER1 protein between ZT 3 to 15 in DF rats coincided with the increase in *Sglt1* mRNA expression between ZT 3 to 9 (Figures 3.8A and 3.7). Similarly the reduction in PER1 protein between ZT 21 to 9 in LF rats coincided with the increase in *Sglt1* mRNA expression between ZT 21 to 3 (Figures 3.8A and 3.7).

3.6. Discussion

My findings above demonstrate the presence of a robust peripheral clock in the intestine in rats, which is likely to be cued by nutrient availability. All clock genes exhibited diurnal rhythmicity with 24 hour periodicity in jejunal mucosa of AL rats (Figure 3.2, Table 3.1). *Sglt1* also displayed diurnal rhythmicity in AL rats (Figure 3.3, Table 3.1), consistent with previous findings[13, 69]. Restricting food availability to only the lights-on period shifted the peak expression of rhythmic clock genes (Figure 3.6, Table 3.2), showing that nutrient availability is a stronger Zeitgeber in the intestine than light cycle. Notably, expression patterns of both *Sglt1* mRNA and protein were also altered by restricted feeding to only the lights-on period (Figures 3.7 and 3.8B, Tables 3.2 and 3.3). These results therefore establish nutrient availability as a key Zeitgeber for the peripheral intestinal clock as well as the expression rhythm of the glucose transporter SGLT1.

Circadian rhythmicity was demonstrated for *Per1-2*, *Bmal1*, *Clock*, *ReverbA*, *ReverbB* and *Cry1-2* in this study on cosinor analysis, although no significant differences between individual timepoints could be demonstrated for *Clock* on ANOVA (Figure 3.2A-H). Previous studies have examined diurnal rhythmicity in a more limited group of clock genes in the intestines of ad libitum fed rodents[16, 311]. Froy et al[311] examined the temporal profile of *Bmal1*, *Clock*, *Per1-2* and *Cry1* in mouse jejunum while Saito et al[16] examined the expression of the same five genes in rat jejunum. Both groups showed

diurnal rhythmicity in all five genes with patterns of expression similar to those demonstrated in my results (Figure 3.2A-D and G, Table 3.1). The acrophases of *Bmal1* and *Clock* in the above mentioned studies occurred at ZT 0, similar to their peaks at ZT 23 and 21 respectively as noted in my study (Figure 3.2C and D and Table 3.1). The *Per* and *Cry* genes are known to suppress transcription of *Clock* and *Bmal1*, acting as the negative limb of the clock gene feedback loop[134, 158]. As expected therefore peak expression of the *Per* and *Cry* genes occurred in the light-dark transition period (Figures 3.2A-B and G-H, Table 3.1) in antiphase to peak expression of *Bmal1* and *Clock* in the early lights-on period (Figures 3.2C-D, Table 3.1), in keeping with findings from other groups[16, 311]. Neither of the two previous studies profiling clock genes in the intestine examined the temporal expression of *ReverbA* or *B* or *Cry2*[16, 311]. My study was the first to examine rhythmicity of these genes in jejunum and demonstrated that all three genes exhibited diurnal rhythmicity (Figures 3.2E-F and H, Table 3.1).

The temporal expression of *Per3* was not examined in my studies as previous studies[314] showed that *mPer3-/-* mice demonstrate only subtle effects on circadian rhythmicity. Loss of PER3 did not alter despite rhythmicity of core clock genes[314]. Mutant mice in this study displayed persistent rhythmicity in a 24-hour dark-dark cycle (DD); the only effect of PER3 loss noted was a shortening of the circadian period[314]. These findings were corroborated by a further study showing that similar behavioural rhythms in mPer1/mPer3 and mPer2/mPer3 double-mutant mice and mice with disruption of mPer1 or mPer2 alone[159]. Indeed it has been proposed that PER3 may in fact act as a clock output protein rather than a core clock gene[314]. This lack of

evidence for a substantial role for *Per3* in the circadian clock led me to investigate only *Per1* and *Per2* in my experiments.

The peak expression of *ReverbA* and *B* at ZT 6 and 9 respectively (Figures 3.2E-F, Table 3.1) occurred in antiphase to the peak in expression of *Bmal1* and *Clock* (Figures 3.2C-D, Table 3.1). This is consistent with the known role of REVERBA and B, which act as transcriptional suppressors of *Bmal1* expression via ROREs (retinoic acid receptor-related orphan receptor responsive element), a GGTCA consensus core motif preceded by a 6A/T rich region, on the *Bmal1* promoter[164, 309]. Another orphan nuclear receptor RORA (retinoic acid receptor-related orphan receptor alpha) competes with REVERBA and B to bind to the RORE on the *Bmal1* promoter, but in contrast to the suppressive effect of REVERBA and B[309] RORA stimulates the *Bmal1* promoter[308, 309]. In contrast to the profound rhythms in gene expression of *ReverbA* and *B* in most peripheral tissues[309, 315] *Rora* does not display circadian rhythmicity in the majority of peripheral tissues (including skeletal muscle, kidney and thymus[315] and brown adipose tissue and liver[309]) and shows only weak circadian oscillation in white adipose tissue[315]. *Rora* was therefore not examined in my studies however the expression of *Rora* in the intestine and the response to a restricted feeding schedule may be worthy of investigation in future studies.

Other studies have confirmed that circadian rhythmicity in peripheral clock gene expression is not only restricted to the jejunum but is also present at other sites along

the gastrointestinal tract. While rhythmicity of clock genes in the liver is well-described[180, 193], rhythmicity of clock genes in the stomach[182] and colon[182, 316] have only recently been characterized. Hoogerwerf et al examined the expression of *Bmal1*, *Clock*, *Per1-3* and *Cry1-2* in the stomach, proximal, mid and distal colon of ad libitum fed mice[182], but did not examine rhythmicity of clock gene expression in the small intestine. The authors showed rhythmicity of the peripheral clock throughout the length of the gastrointestinal tract examined, with acrophases broadly similar to that noted for clock genes in the jejunum in my study (Figure 3.2A-H, Table 3.1). These findings were corroborated by Sladek et al, who described similar rhythmicity in the colon[316].

Determining the relative shifts in glucose transporter and clock gene rhythms in response to restricted feeding was a major study aim. Nocturnal food restriction (DF rats) would not be expected to produce a shift in intestinal clock gene or *Sglt1* expression as only a modest amount of food is usually consumed during the day (10-20% daily intake)[13, 313]. It was therefore surprising to find that nocturnal food restriction significantly affected expression of *Per2*, *ReverbA*, *ReverbB* and *Cry2* as well as *Sglt1* (Figures 3.6B, E, F and H, 3.7 and Table 3.2). Restriction of food to the lights-off period only in DF rats effectively prevented "early phase eating" – consumption of food in the late light phase – and may have enhanced entrainment signals normally produced by hunger or hormonal responses, thereby sharpening the anticipatory intestinal gene induction and altering peak expression in DF rats. In either case, it is clear that restricting food access to 12 hours during the lights-off period led to detectable

alterations in the expression of selected clock genes and *Sglt1* (Figures 3.6A-H, 3.7 and 3.8, Table 3.2).

The majority of clock genes continued to exhibit peaks and troughs of expression in LF and DF animals despite the change in period of nutrient availability (Figures 3.6A-H, Table 3.2). Notable exceptions were *Clock* and *Cry2*, which exhibited blunted expression in DF and LF animals rhythmicity in both these genes was abolished by both LF and DF restricted feeding patterns (Figures 3.6D and H and Table 3.2). *Clock* is known to be arrhythmic in the SCN[158, 317, 318] and its rhythmicity in peripheral tissues such as colon[182, 316] and liver[319] has not been conclusively demonstrated. *Cry2* similarly lacks robust rhythmicity along the gastrointestinal tract, displaying lack of rhythmicity in the stomach and proximal colon but relatively robust rhythmicity in the mid and distal colon[182]. Overall these findings suggest weak rhythmicity in these clock genes in the gastrointestinal tract. Knockout studies to date suggest a redundant role for both these genes in maintaining rhythmicity of circadian behaviour; circadian rhythmicity persists in both *Clock -/-* mice[320] and *Cry2-/-* mice[321] but with an extended circadian period. The effects on intestinal gene expression have not been investigated and would be of interest in future studies.

After 7 days of restricting feeding to either the light or dark period, phase differences of 6-12 hours were observed in the peak expression of *Sglt1* and 6 of the 8 clock genes examined (*Per1*, *Per2*, *Bmal1*, *ReverbA* and *ReverbB* and *Cry1*, Figures 3.6A-C and E-G,

3.7 and 3.8, Table 3.2). This is similar to the phase shift of 7-12 hours and 8-12 hours observed in the colon of mice in two previous studies after a 2 day and 14 day study duration respectively of restricted feeding during the lights-on period only compared to ad libitum feeding[182, 316]. The lack of a complete 12 hour phase shift in clock gene expression between dark- and light-fed rats may reflect the influence of other factors on clock gene expression. Glucocorticoids in particular are known to exhibit circadian rhythmicity in expression and have been shown to regulate clock gene expression in other organs such as the liver[85, 322]. Of further interest, rhythmicity in clock gene expression persisted in glucocorticoid receptor null mice[85], confirming that glucocorticoids are not sole mediators of the regulation of the phase-setting of clock gene expression in peripheral tissues.

The duration of nutrient availability may have also affected the degree of phase shift. A shorter period of food availability (chow available only between ZT 2-8) was used by Saito et al[16] with an attendant full 12 hour phase shift in the expression of selected clock genes in the intestine, greater than the 1.7 hour phase shift observed in my study (Figure 3.8). Moreover, peripheral clocks have been noted to adapt to restricted feeding at different rates – for example clock genes in the liver phase shift much more quickly than clock genes in the lungs[180]. While it is possible that the small intestine would achieve a complete phase shift following a longer duration of restricted feeding (such as 2 weeks rather than the 7 days used in this study), the sufficiency of 4 days adaptation as previously reported[16], the similarity in phase shift of clock gene expression in the colon following 2 days[182] versus 14 days[316] of restricted feeding and the equal

weights between the DF and LF rats and the plateau in food intake in the LF rats (matching that expected for rats of that weight[89]) by the end of the study period in this study all suggest that the partial phase shift noted in my study was due to factors other than incomplete adaptation.

The rapid adaptation observed in liver in other studies[180] may result from more direct (i.e. local) stimulus-response pathways. Adaptation in the intestine, particularly for diurnally rhythmic functions, is indirect (as shown by isolated loops)[323] and may entail cephalic and other inputs. The apparently longer period required for adaptation by intestine vs. liver may reflect a tissue-specific feature necessary to stabilize the rhythms in intestinal functions despite moderately varying nutrient intake patterns. Linkage of phases of critical intestinal functions such as proliferation and absorption to external stimuli such as nutrient availability could serve to optimally coordinate the rhythms in DNA synthesis and peak absorption.

In this study, the difference between peak and trough SGLT1 protein expression was blunted over the diurnal period in LF rats (Figure 3.8B, Table 3.3). Previous studies from our group and others have shown that rhythmicity of SGLT1 protein expression correlates with functional rhythmicity in the form of intestinal glucose uptake[13, 69]. Rhythmicity of glucose uptake in ad libitum fed rats in these previous studies was abolished in the presence of the SGLT1-specific inhibitor phloridzin[13, 69], confirming that rhythmicity in glucose uptake was mediated entirely by SGLT1. Peak glucose uptake

at ZT 15 in ad libitum fed rats corresponded with the peak in SGLT1 protein expression at ZT 15 in the abovementioned study. Although glucose uptake was not measured in my studies, the data from these previous studies[13, 69] suggest that glucose uptake in this study would be likely to show similar diurnal rhythmicity in both AL and DF rats, which displayed rhythmicity in SGLT1 expression, but not in LF rats.

Overall SGLT1 protein expression was higher in LF rats compared to DF rats (Figure 3.8B), suggesting that regulation of SGLT1 expression may be occurring at the post-transcriptional level and is consistent with previous data from our laboratory showing that post-transcriptional events are also important in regulating intestinal SGLT1 expression[89, 323]. The increase in overall SGLT1 protein expression in LF rats may be an attempt to increase nutrient absorption to compensate for the loss of the diurnal peak in SGLT1 expression that would normally be expected to occur at times of maximal nutrient availability. In light of reports that SGLT1 expression is increased in experimental models of obesity in rodents[38] and diabetes (both in experimental models[326] and in humans[327]), it would be interesting to assess the functional consequences of this observation by comparing glucose homeostasis in light vs. dark fed rats, as well as measuring SGLT1 expression in shift workers, who are forced to eat off-schedule and have increased risk of developing glucose intolerance[328].

In AL rats, *Per1* and *ReverbB* mRNA expression peaked in phase with *Sglt1* (Figure 3.2A and F and Figure 3.3), slightly preceding *Sglt1* expression by 1-2h. Restricted feeding

produced similar patterns of expression for *Sglt1*, *Per1* and *ReverbB* (Figure 3.7 and Figure 3.6A and F and Table 3.2). The presence of 4 canonical E-boxes in the *Sglt1* promoter raises the possibility that PER1 may be involved in controlling *Sglt1* rhythmicity. If so, occurrence of the *Sglt1* mRNA nadir (Figure 3.7) when the PER1 protein level is rising (Figure 3.8A) suggests that PER1 exerts a negative influence. Lack of REVERB response elements in the *Sglt1* promoter argues against REVERBB involvement but does not preclude indirect regulation or binding to a non-canonical element. The relationship between PER1 and *Sglt1* is explored further using in vitro studies in the following chapter.

The mechanisms cuing the adaptation of clock gene rhythmicity to the shift in nutrient availability remain unknown. The SCN in the hypothalamus acts as the master pacemaker in mammals by receiving direct retinohypothalamic input and entraining circadian rhythmicity in visceral functions to the light cycle[81, 329]. SCN-lesioned rodents display loss of behavioural[330, 331], endocrine[329] and cardiovascular rhythms[81], however the effects of SCN lesions on the entrainment to nutrient availability are less profound[332]. Lesioning the SCN abolishes spontaneous circadian rhythmicity and hence disrupts the normal pattern of ad libitum feeding[333-335]; however these rodents are still able to entrain to a scheduled feeding regimen[192, 333] both in the form of meal-associated behaviour[333] as well as in phase shifting clock gene expression in the liver[192]. These studies suggest that while the SCN may play a role in mediating nutrient-associated rhythmicity, it is unlikely to be the main cue

regulating these rhythms. No studies to date have examined the effect of SCN-lesioning on clock gene expression in the intestine.

Neuronal factors may also mediate the entrainment of gene expression to nutrient availability. The vagus nerve, the main extrinsic nerve supply to the intestine, has been implicated in regulating rhythmicity in the expression of intestinal nutrient transporters which are known to display a robust 24-hour periodicity abrogated at the post-transcriptional level by vagotomy[88, 89]. Although the effects of vagotomy in clock gene expression in the small intestine have yet to be investigated, Hoogerwerf et al found no difference in the rhythmicity or acrophase of clock genes *Bmal1*, *Per1-3* and *Cry1* rhythmicity in the colon between vagotomised and control mice[182]. In the above mentioned study gene expression was measured at the transcriptional level only and hence a post-transcriptional effect of vagotomy on clock gene rhythmicity cannot be excluded.

These findings support the hypothesis that clock genes cue intestinal rhythmicity in response to nutrient availability. Clock genes are clearly important transcriptional regulators[14-16]. Clock genes and clock-controlled genes have been implicated in the regulation of other genes such as the Na^+/H^+ *exchanger Nhe3* in the kidney[14]; the oligopeptide transporter *Pept1* [16]; and the *multidrug resistance 1* (*Mdr1*) gene[15]. To date no studies have examined the role of clock genes in the regulation of SGLT1 rhythmicity and thereby the rhythmicity of glucose uptake in the intestine.

The glucose concentration generated from digestion may be a major stimulus in regulating the expression of clock and *Sglt1* genes in the intestine. In an intriguing study, glucose was shown to down-regulate *Per1* and *Per2* mRNA expression in rat-1 fibroblasts[336]. The authors hypothesized that glucose itself (which displays a modest circadian rhythm in rodents[337]) provides a Zeitgeber for peripheral clocks, acting to downregulate *Per1* and *Per2* via other transcriptional regulators. This hypothesis is consistent with decreased *Per1* mRNA levels during the period of nutrient consumption in both AL and DF rats (Figure 3.2A and 3.6A, Tables 3.1 and 3.2). Enterocytes are likely to experience abrupt increases in glucose supply and intracellular concentrations following feeding. Thus, glucose suppression of *Per* expression may be the molecular basis for resetting intestinal clocks by nutrient availability. The ability of the intestine to respond rapidly to nutrient intake patterns via the peripheral circadian clock would have great adaptive value by optimally coordinating absorptive functions with nutrient delivery.

In summary, we have shown that nutrients provide a major Zeitgeber for intestinal clock genes and that shifting the period of availability simultaneously phase shifts expression of clock genes and intestinal transporters. Further studies are required to define the molecular mechanism linking clock genes to *Sglt1* rhythmicity. The regulatory mechanisms governing diurnal rhythmicity of intestinal function may have a considerable role in obesity and diabetes and a better understanding could lead to new therapies for these worsening epidemics.

Chapter 4: PER1 modulates SGLT1 transcription in vitro independent of E-box status

4.1. Introduction

Clock genes are known to control the rhythmicity behind many circadian functions[128, 129] by regulating a large number of circadian genes[14-16]. These molecular feedback loops have themselves been shown to express circadian rhythmicity in several peripheral tissues[176-179]. In the intestine in particular clock genes have been implicated in the regulation of the diurnal rhythmicity of other intestinal transporters such as the *Pept1* gene[16] and the *Mdr1* gene[15], making clock genes candidate regulatory factors for rhythmicity of *Sglt1* expression. *Sglt1* is known to demonstrate profound diurnal rhythms in expression in the intestine, as shown in Chapter 3, however the molecular pathways regulating this rhythmicity of expression remain unclear.

The studies detailed in the previous chapter (Chapter 3) demonstrated rhythmicity of all clock genes as well as *Sglt1* in ad libitum fed rats. The similar phase shifts of 2 specific clock genes, *Per1* and *ReverbB,* with *Sglt1* under the two restricted-feeding regimens led me to consider these two genes as potential regulators of *Sglt1*. To explore this further I analysed the *SGLT1* promoter for binding sites for either of these genes. I found that this promoter does not contain binding elements for REVERBs but does contain E-boxes – binding sites for PER1 in association with the CLOCK-BMAL1 heterodimer (analysis of the *SGLT1* promoter is detailed further in section 4.5). *PER1* was therefore considered a potential candidate clock gene which might act to mediate rhythmicity in *SGLT1* expression. Subsequent examination of the rhythmicity of protein expression of PER1

showed a decrease in PER1 protein between ZT 3 to 15 in DF rats coincident with the increase in *SGLT1* mRNA expression between ZT 3 to 9 (Figures 3.9A and 3.7). This suggests a potential suppressive role for PER1 on *SGLT1* mRNA expression in enterocytes. To explore this further, I examined the effects of manipulating *PER1* expression levels on *SGLT1* transcription in vitro by using knockdown of *PER1* and attempted to decipher the specific effects of *PER1* on binding elements on the *SGLT1* promoter.

4.2. Testing the knockdown efficiency of acquired shPER1 sequences

To determine the effects of PER1 on SGLT1 in vitro, I decided to knockdown PER1 expression in Caco-2 cells. Knockdown vectors containing short-hairpin RNA sequences against *PER1* (pLKO.1-puro) were purchased from Sigma, consisting of 5 shRNA sequences designed against the *PER1* RefSeq sequence NM_002616. The pLKO.1-puro vector containing a scrambled oligonucleotide sequence (Sigma) was purchased for use as a negative control. Knockdown efficiency of each sequence was determined by measuring *PER1* mRNA expression after transient transfection of HEK293 cells with either knockdown sequences for *PER1* or the control scrambled shRNA sequence. The HEK293 cell line is human embryonic kidney derived and was used to test the knockdown efficiencies of *PER1* shRNA sequences as it has endogenous clock gene expression and was recommended by the shRNA sequence manufacturers to test shRNA knockdown efficiency due to its property of being easy to transfect. HEK293 cells were maintained as described in section 2.6.4 and transiently transfected at passages 10-12 with knockdown sequences for *PER1* or the control scrambled shRNA at 70% confluence using the transfection reagent Effectene. Cells were harvested after 48 hours for determination of *PER1* mRNA expression. RNA was extracted, reverse transcribed and subjected to qPCR. *PER1* expression was expressed relative to the expression of the housekeeping gene *β -ACTIN*. Knockdown efficiency of each of the shRNA vectors is shown in Figure 4.1 and residual expression and significance of difference compared to the control shown in Table 4.1.

All 5 sequences produced significant levels of knockdown compared to the scrambled control vector as tested by one-way ANOVA with post-hoc Tukey ($F^{5,12}$=21.63, p<0.0001, Figure 4.1, Table 4.1). ShPER1 sequences A and B showed the greatest knockdown efficiency with 0.28 and 0.29 the expression of the control respectively (Figure 4.1, Table 4.1). ShPER1 sequence C had a slightly lower knockdown efficiency with residual expression of 0.34 of the control while sequences D and E were least successful with residual expression of 0.62 and 0.57 of the control respectively (Figure 4.1, Table 4.1).

ShPER1 sequences A and B, the two constructs with the highest knockdown efficiency, were chosen for stable knockdown of *PER1* in Caco-2 cells to determine the effects of *PER1* on endogenous *SGLT1* expression in vitro and co-transfected with the *SGLT1* promoter for promoter-reporter assays in CHO cells.

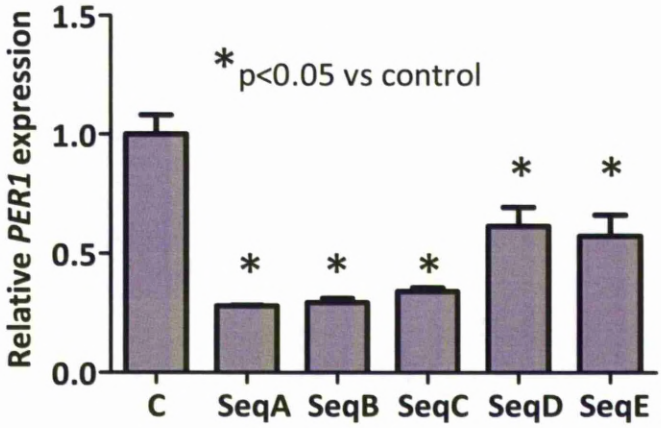

Figure 4.1: Knockdown efficiency of shPER1 vectors in HEK293 cells. Each of the five acquired sequences or the scrambled negative control was transfected transiently into HEK293 cells, which were harvested for RNA after 48 hours. *PER1* expression was quantified by qPCR and expressed relative to β *-ACTIN* expression for the same sample. One-way ANOVA with post-hoc Tukey was used to identify significant differences in *PER1* expression between cells transfected with each knockdown sequence versus controls. The experiment was carried out thrice and each sample was plated in triplicate. The graphs show the mean and standard error of the mean. Expression of *PER1* in knockdown vector-transfected cells has been expressed as a ratio to the expression in control cells, labelled C.

Sequence	Expression relative to control	p-value
SeqA	0.28	<0.0001
SeqB	0.29	<0.0001
SeqC	0.34	<0.0001
SeqD	0.62	<0.01
SeqE	0.57	<0.01
Control	1.00	

Table 4.1: Residual expression of *PER1* following knockdown in HEK293 cells. *PER1* expression was measured in HEK293 cells transiently transfected with either one of 5 knockdown sequences for *PER1* or the scrambled negative control. mRNA expression was measured by qPCR and *PER1* expression expressed relative to *β-ACTIN*. Expression of *PER1* in knockdown vector-transfected cells is shown relative to expression in control cells. Differences in expression from the control were considered significant if $p<0.05$ as calculated by one-way ANOVA with post-hoc Tukey.

4.3. Downregulation of PER1 increases *SGLT1* expression in Caco-2 cells

Caco-2 cells are human colonic carcinoma-derived cells. These cells were chosen as the cell type for assessing the effects of clock genes on endogenous *SGLT1* expression as Caco-2 cells are known to express SGLT1 upon reaching confluence, wherein they differentiate into cells with features of small intestinal epithelium[338]. Caco-2 cells at passages 10-12 at 40% confluence were transfected with ShPER1 knockdown vectors A and B using the transfection agent Effectene. At 48 hours, the transfected cells were trypsinized and re-plated at 40% confluence with 4ug/ml puromycin to allow stable selection of transfected cells. A previously performed kill-dose curve using normal untransfected Caco-2 cells plated at 40% confluence in media containing antibiotic concentrations ranging from 1ug/ml to 10ug/ml showed that 4ug/ml puromycin was sufficient to kill all untransfected cells within 5 days of plating, hence this concentration of puromycin was used for selection of stably transfected cells. Cells were monitored for the onset of confluence and harvested for RNA at 7 days post-confluence. mRNA was reverse transcribed and *PER1* and *SGLT1* expression quantified by qPCR. The housekeeping gene *β-ACTIN* was used to control for RNA loading. *PER1* mRNA and protein expression in transfected cells is shown in Figure 4.2A and B. *SGLT1* expression in transfected cells is shown in Figure 4.3. Residual expression and significance of difference compared to the control shown in Table 4.2.

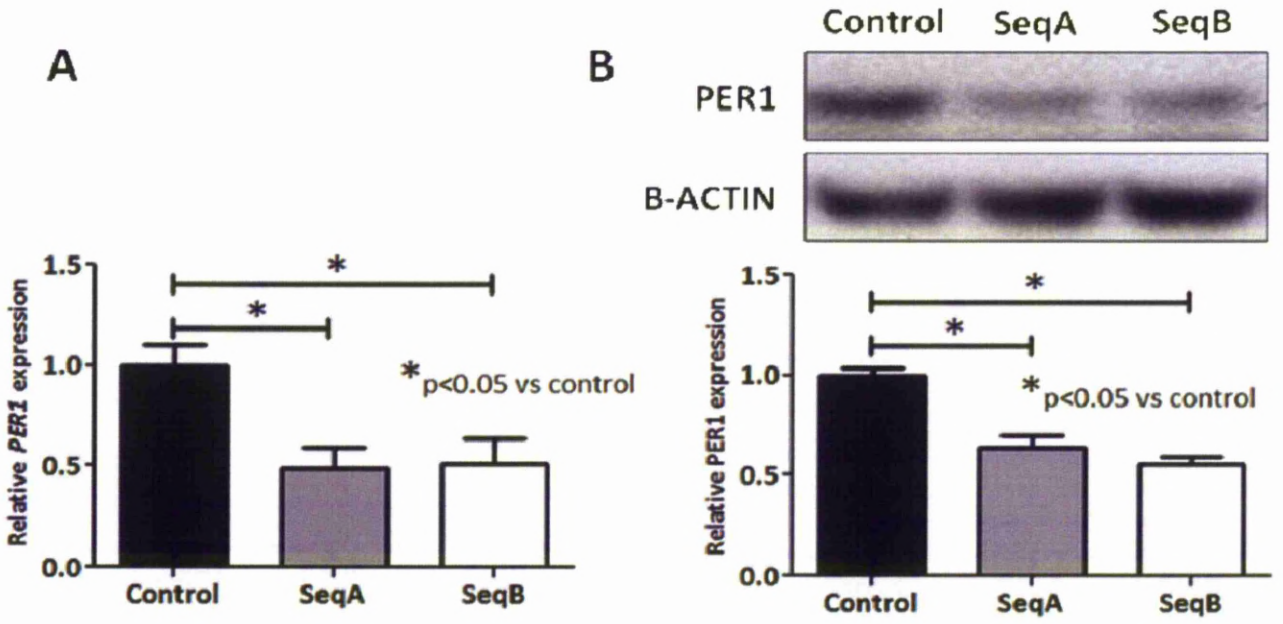

Figure 4.2: *PER1* mRNA and protein expression in Caco-2 cells following *PER1* knockdown.Caco-2 cells were stably transfected with one of two knockdown vectors for *PER1* or the scrambled sequence negative control, then harvested for RNA and protein expression 7 days after reaching confluence. **(A)** *PER1* expression was measured using qPCR and normalised to β *-ACTIN*. Samples were plated in triplicate and the experiment was performed a total of three times. **(B)** PER1 expression was measured using Western blotting and normalised to β -ACTIN. The experiment was performed a total of three times. Both graphs show mean and standard error and significant differences ($p<0.05$) between each knockdown group and the control group identified using one-way ANOVA with post-hoc Tukey.

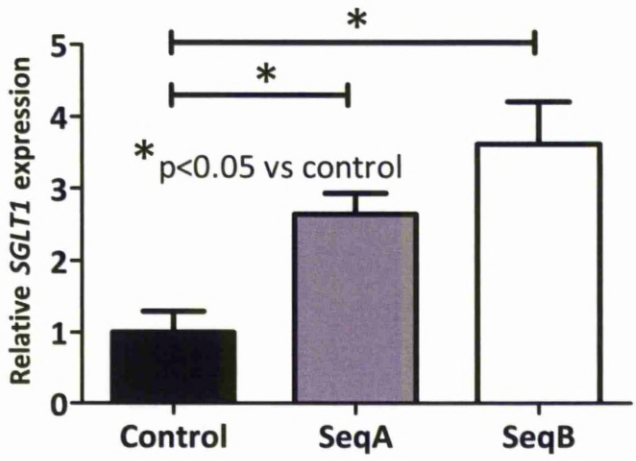

Figure 4.3: *SGLT1* mRNA expression following *PER1* knockdown in Caco-2 cells. Caco2 cells were stably transfected with knockdown vectors for *PER1* or the scrambled sequence negative control, then harvested for RNA and protein expression 7 days after reaching confluence. *SGLT1* expression was measured using qPCR and normalised to *β-ACTIN*. Samples were plated in triplicate and the experiment was performed a total of three times. The graph shows mean and standard error and significant differences ($p<0.05$) between each knockdown group and the control group were identified using one-way ANOVA with post-hoc Tukey.

Gene/ protein		Expression relative to control	p-value on ANOVA	p-value on post-hoc Tukey
PER1	shPER1 SeqA	0.49	0.0273	<0.05
	shPER1 SeqB	0.51		<0.05
PER1	shPER1 SeqA	0.64	0.0016	<0.01
	shPER1 SeqB	0.55		<0.01
SGLT1	shPER1 SeqA	2.65	0.0076	<0.05
	shPER1 SeqB	3.62		<0.01

Table 4.2: *PER1* mRNA and protein expression and *SGLT1* mRNA expression following knockdown of *PER1* in Caco-2 cells. Caco-2 cells were stably transfected with one of two knockdown vectors for *PER1* or the scrambled sequence negative control then harvested for protein and mRNA 7 days post-confluence. mRNA expression was measured by qPCR and protein by Western blotting; both were normalized to the housekeeping gene *β-ACTIN*. Expression of *PER1*, PER1 and *SGLT1* in knockdown vector-transfected cells was expressed relative to control cells and significant differences ($p<0.05$) between each knockdown cell line and the control cell lines were identified using one-way ANOVA with post-hoc Tukey.

Stable transfection of Caco-2 cells with the two shRNA knockdown vectors shPER1 SeqA and SeqB, each bearing distinct shRNA sequences to PER1, reduced *PER1* expression to 0.49 and 0.51 the level of controls (cells transfected with scrambled shRNA, $F^{2,6}=6.95$, $p=0.027$, Figure 4.2A and Table 4.2). PER1 protein expression similarly decreased in *PER1* knockdown vector-transfected cells. PER1 expression in cells transfected with

either shPER1 SeqA or shPER1 SeqB was 0.64 and 0.56 that of controls ($F^{2,6}$=3.04, p=0.0016, , Figure 4.2B, Table 4.2).

Coincident with PER1 knockdown, *SGLT1* expression in cells transfected with shPER1 SeqA or shPER1 SeqB was 2.6-fold and 3.0-fold that of controls ($F^{2,6}$=15.06, p=0.0076 on ANOVA and p<0.05 and p<0.01 vs controls respectively on post-hoc Tukey, Figure 4.3 and Table 4.2). These results indicate that PER1 acts to suppress *SGLT1* expression in enterocytes in vitro.

4.4. Downregulation of PER1 does not significantly alter expression of other clock genes

Clock genes are known to form interconnected molecular feedback loops due to their ability to stimulate or repress the expression of other clock gene family members. Altering the expression of one clock gene, in this case *PER1*, would therefore be expected to change the expression of other clock genes. To investigate this, I examined the mRNA expression of *PER2*, *BMAL1*, *CLOCK*, *REVERBA*, *REVERBB*, *CRY1* and *CRY2* in Caco-2 cells stably transfected with either shPER1 SeqA or shPER1 SeqB or the scrambled sequence negative control. mRNA expression was quantified using qPCR and expressed relative to *β-ACTIN* and shown in Figure 4.4 and Figure 4.5. The fold-changes and p-values are shown in Table 4.3.

There was no significant difference in the expression of *PER2* in either of the sequences vs the control vector ($F^{2,6}$=1.68, p=0.29 on ANOVA). *PER2* expression increased slightly in Caco-2 cells transfected with shPER1 SeqB but this was not statistically significant (1.5-fold; p>0.05 vs. control, Figure 4.4 and Table 4.3). *PER2* expression was unchanged in cells transfected with shPER1 SeqA (p>0.05 vs. control, Figure 4.4 and Table 4.3).

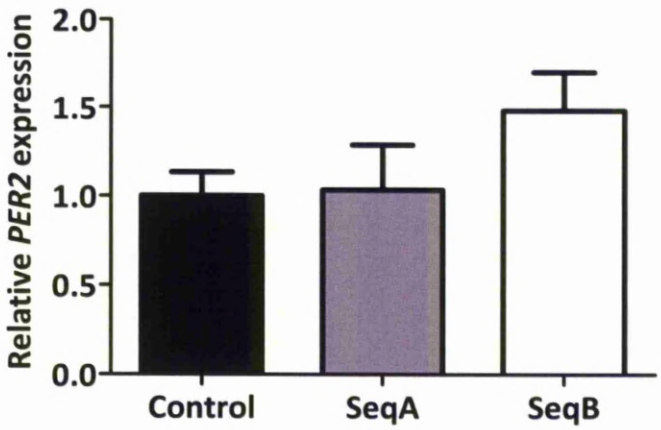

Figure 4.4: *PER2* mRNA expression following *PER1* knockdown in Caco-2 cells. Caco-2 cells were stably transfected with knockdown vectors for *PER1* or the scrambled sequence negative control, then harvested for RNA and protein expression 7 days after reaching confluence. *PER2* expression was measured using qPCR and normalised to *β-ACTIN*. Samples were plated in triplicate and the experiment was performed a total of three times. The graph shows mean and standard error. One-way ANOVA with post-hoc Tukey was used to identify significant differences between each knockdown group and the control group.

Gene		Expression relative to control	p-value on ANOVA	p-value on post-hoc Tukey
PER2	shPER1 SeqA	1.035	0.2949	>0.05
	shPER1 SeqB	1.481		>0.05
BMAL1	shPER1 SeqA	0.865	0.4811	>0.05
	shPER1 SeqB	1.067		>0.05
CLOCK	shPER1 SeqA	0.973	0.7474	>0.05
	shPER1 SeqB	1.200		>0.05
REVERBA	shPER1 SeqA	0.613	0.0535	>0.05
	shPER1 SeqB	1.117		>0.05
REVERBB	shPER1 SeqA	0.923	0.7009	>0.05
	shPER1 SeqB	1.109		>0.05
CRY1	shPER1 SeqA	1.137	0.9443	>0.05
	shPER1 SeqB	1.108		>0.05
CRY2	shPER1 SeqA	1.288	0.5386	>0.05
	shPER1 SeqB	1.462		>0.05

Table 4.3: Relative expression of clock gene mRNA expression following knockdown of *PER1* in Caco-2 cells. Caco-2 cells were stably transfected with one of two knockdown vectors for *PER1* or the scrambled sequence negative control then harvested for RNA 7 days post-confluence. mRNA expression of *PER2*, *BMAL1*, *CLOCK*, *REVERBA*, *REVERBB*, *CRY1* and *CRY2* was measured by qPCR and normalized to the housekeeping gene *β-ACTIN*. Expression of *PER2*, *BMAL1*, *CLOCK*, *REVERBA*, *REVERBB*, *CRY1* and *CRY2* in knockdown vector-transfected cells was expressed relative to the control cells and significant differences ($p<0.05$) between each knockdown cell line and the control cells were identified using one-way ANOVA with post-hoc Tukey.

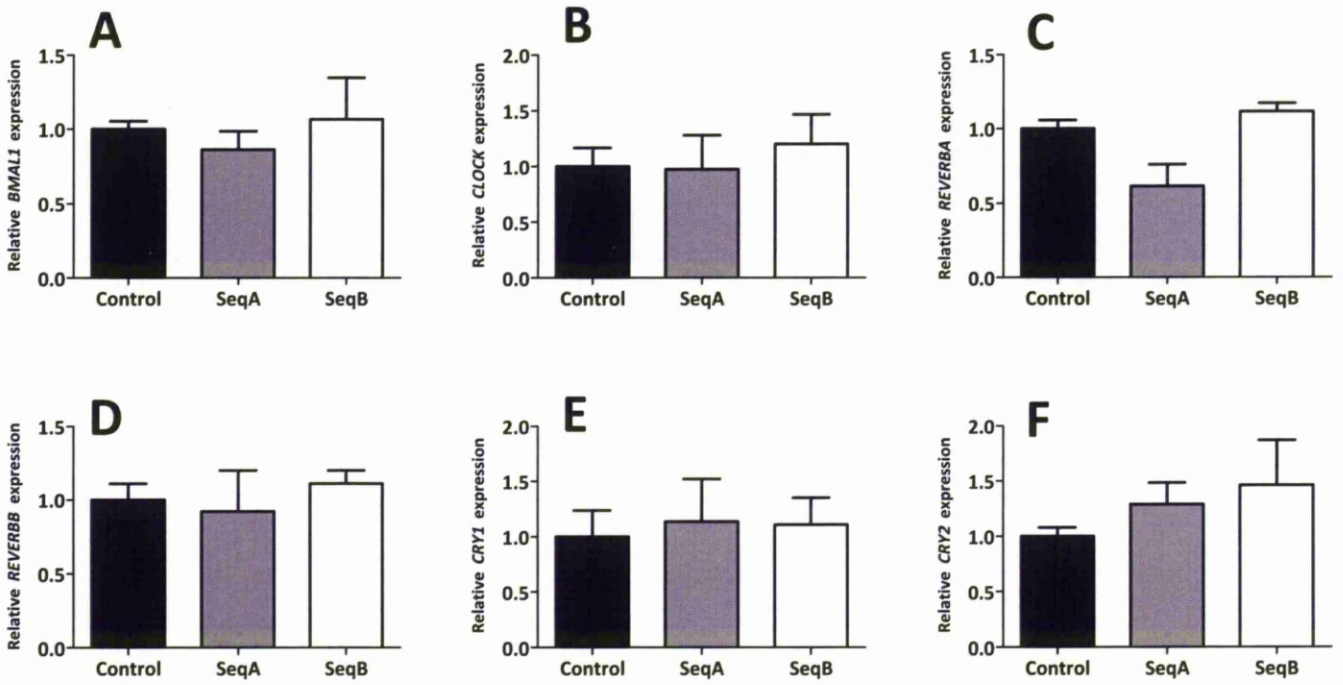

Figure 4.5: mRNA expression of *BMAL1*(A), *CLOCK*(B), *REVERBA*(C), *REVERBB*(D), *CRY1*(E) and *CRY2*(F) following *PER1* knockdown in Caco-2 cells. Caco-2 cells were stably transfected with knockdown vectors for *PER1* or the scrambled sequence negative control, then harvested for RNA and protein expression 7 days after reaching confluence. Expression of *BMAL1*, *CLOCK*, *REVERBA*, *REVERBB*, *CRY1* and *CRY2* was measured using qPCR and normalised to *β-ACTIN*. Samples were plated in triplicate and the experiment was performed a total of three times. The graph shows mean and standard error. One-way ANOVA with post-hoc Tukey was used to identify significant differences between each knockdown group and the control group.

Similarly, none of the remaining clock genes showed a significant alteration in expression following PER1 knockdown. *CRY2* showed the greatest change in expression, with levels increased to 1.3-fold and 1.5-fold in shPER1 SeqA and B respectively, however this did not meet statistical significance ($F^{2,6}$=0.725, p=0.54 on ANOVA and p>0.05 for each sequence vs control, Figure 4.5F and Table 4.3). *REVERBA* showed inconsistent changes with the two knockdown vectors, showing no change in expression with shPER1 SeqB but a decrease in expression with shPER1 SeqA (0.6-fold vs 1.1-fold difference, $F^{2,6}$=4.96, p=0.054 on ANOVA and p>0.05 for each sequence vs control on post-hoc Tukey testing, Figure 4.5C and Table 4.3). Other clock genes were only mildly altered following PER1 knockdown (0.86-1.20-fold vs. control cells, p>0.05, Figures 4.5A, B, D and E, Table 4.3).

Clock genes are known to regulate gene transcription and I therefore hypothesized that the actions of PER1 on *SGLT1* were likely to occur via the *SGLT1* promoter, possibly via E-boxes, binding sites which are known to mediate the actions of clock proteins on other genes[14, 339-341]. To investigate this I next examined the effects of PER1 on the *SGLT1* promoter in vitro and the effects of E-boxes on the *SGLT1* promoter in regulating *SGLT1* transcription.

4.5. Analysis of the *SGLT1* promoter

The sequence of the human *SGLT1* promoter, which has been previously characterized[31], was obtained from the University of California Santa Cruz (UCSC) Genome Browser, freely available at http://genome.ucsc.edu (accessed 16th April 2008). Analysis of the *SGLT1* promoter sequence showed the presence of two non-canonical E-box consensus sequences (CANNTG) within this minimal promoter at -306 and -352 relative to the transcription start site. A further two non-canonical E-box consensus sequences were identified more distally at -827 and -837 relative to the transcription start site. E-box sequences within the *SGLT1* promoter are shown in Figure 4.6.

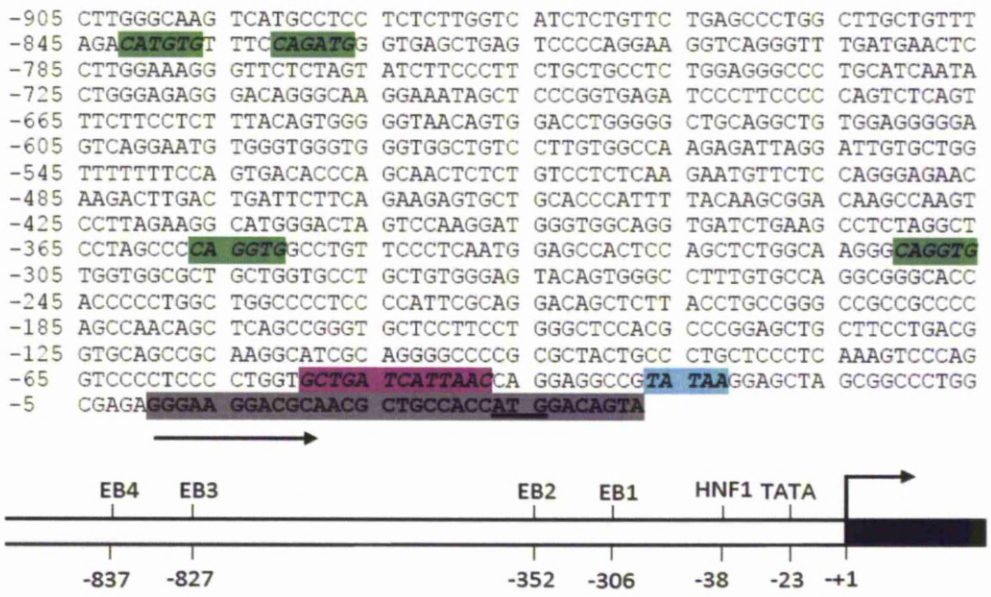

Figure 4.6: The *SGLT1* promoter sequence. The four E-box non-canonical consensus sequences (CANNTG) at -306, -352, -827 and -837 are shown in highlighted in green. Also shown are the non-canonical HNF sequence (GCTGATCATTAAC) at -50 to -38 in pink and the TATAA site at -28 to -23 in blue. The dark grey highlighting and black arrow indicate the *SGLT1* transcription start site, with the translation start site (ATG) underlined.

4.6. Creation and validation of the *SGLT1* promoter construct

The proximal 1kb of the human *SGLT1* promoter (−1000/+33, designated WT *SGLT1*-Luc)[31] was cloned by PCR from human genomic DNA using PCR conditions as described in section 2.8.3. Primers used encoded MluI and BglII restriction sites at the 5' and 3' ends respectively (listed in Table 2.11). The amplified PCR product was digested using restriction enzymes MluI and BglII and ligated into the similarly digested pGL3 basic empty vector, containing the firefly luciferase expression cassette driven by the inserted promoter and chosen for the lack of any native eukaryotic promoter or enhancer sequences. After ligation the plasmids were amplified in *E.coli* and grown on agar at 37°C overnight. Colonies were cultured in LB and plasmids extracted and sent for sequencing. To confirm a functional clone of the human *SGLT1* promoter, reporter assays were carried out using expression vectors for a known activator of the *SGLT1* promoter, HNF1α (kindly donated by Dr David B Rhoads), which binds to the HNF1 consensus sequence GCTGATCATTAAC at -50 to -37 on the *SGLT1* promoter (Figure 4.6).

Chinese Hamster Ovary (CHO) cells were chosen as the cell type to be used for all promoter-reporter assays to assess the effect of clock genes on *SGLT1* promoter activity as this cell type is easy to maintain and easily transfected. While the use of enterocytes such as Caco-2 cells might have provided a more relevant genetic background for investigation of the role of clock genes on *SGLT1*, the low efficiency of transient transfection in these cells would have made interpretation of the resulting data difficult. Furthermore the non-intestinal phenotype allows CHO cells to act as a blank canvas

facilitating manipulation of clock gene expression levels without the confounding effects of other intestinal transcription factors.

Cells at passages 10-12 were transiently transfected at 70% confluence using the transfection reagent Effectene with combinations of the wild-type *SGLT1* promoter reporter construct pGL3/WT-*SGLT1*luc) and the expression vector (pcDNA3.1 with or without *HNF1α* cDNA). Renilla luciferase was co-transfected into all wells in all experiments to normalize for transfection efficiency. Measurement of Firefly and Renilla luciferase-induced luminescence was carried out after 48 hours. Each sequence of transient transfection to measurement of luminescence was performed three times and each combination transfected in triplicate. The relative luciferase expression induced by transfection with HNF1α is shown in Figure 4.7.

Transfection with *HNF1α* induced 3.7-fold higher luciferase expression than that induced by transfection with the empty vector pcDNA (p=0.009, Figure 4.7). This increase in expression is similar to the effect of *HNF1α* noted in previous studies[31]. These findings, corroborated by sequencing which confirmed insertion of the correct sequence without mutations, indicated a functioning *SGLT1* promoter suitable for further investigation of the effects of PER1 on *SGLT1*.

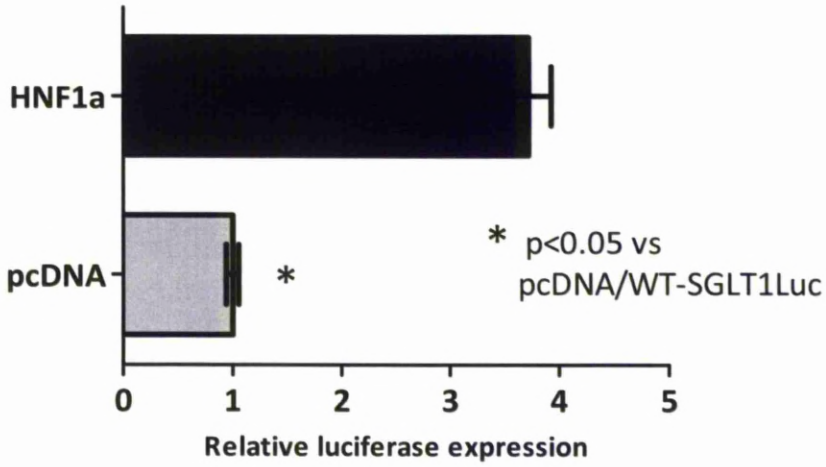

Figure 4.7: Activation of the *SGLT1* promoter by *HNF1α* in CHO cells. CHO cells were transiently transfected with the wild-type SGLT1 promoter (designated WT-SGLT1luc) and either the overexpression vector for *HNF1α* or the empty pcDNA vector. Renilla luciferase was co-transfected into each well to normalize for transfection efficiency. Each combination was plated in triplicate and the experiment performed three times. Luciferase expression induced by *HNF1α* was expressed relative to that of the pcDNA control. Graphs show the mean and standard error. Student's t-test was used to identify any significant difference between the two groups.

4.7. Creation and validation of the *PER1* overexpression construct

To assess the effect of PER1 on the *SGLT1* promoter, a *PER1* overexpression construct was created by cloning the human *PER1* sequence into the pcDNA 3.1 (+) vector, which constitutively overexpresses the insert under the control of the cytomegalovirus (CMV) promoter. Human *PER1* cDNA was amplified from Caco-2 cDNA, reverse transcribed from extracted Caco-2 mRNA. PCR amplification of *PER1* was carried out using the Platinum Taq High-Fidelity DNA polymerase using primer-encoded NheI and NotI restriction sites (cloning primers listed in Table 2.6). This DNA polymerase was used for its ability to amplify large fragments of DNA such as the 4kb *PER1* cDNA fragment with high-fidelity. Thermal cycling conditions and other details can be found in Section 2.8.1.

The PCR product and the pcDNA 3.1 vector were individually digested using restriction enzymes NotI and NheI at 37°C overnight, then ligated using T4 DNA ligase at 16°C overnight. After ligation, the plasmids were amplified by transforming E.coli, colonies grown on agar plates then amplified in LB before plasmids were extracted and sent for sequencing.

To confirm overexpression of PER1, CHO cells were transiently transfected with either the *PER1* overexpression construct or the pcDNA empty vector. Transfections were carried out in CHO cells between passages 8 and 9 at 80% confluence using the transfection agent Effectene. Cells were harvested at 48 hours for analysis of RNA and protein expression. mRNA expression was measured via qPCR and protein expression via

Western blotting. *PER1* mRNA and protein levels were expressed relative to *β-ACTIN*; results are shown in Figure 4.8A and B and Table 4.4.

Cells transfected with the overexpression vector for *PER1* had significantly higher levels of *PER1* mRNA compared to controls (222-fold the levels of controls, p=0.0033, Figure 4.8A and Table 4.4). PER1 protein levels were similarly elevated, at 185-fold the level of controls, p=0.0408, Figure 4.8B and Table 4.4), confirming successful overexpression of PER1 using this construct.

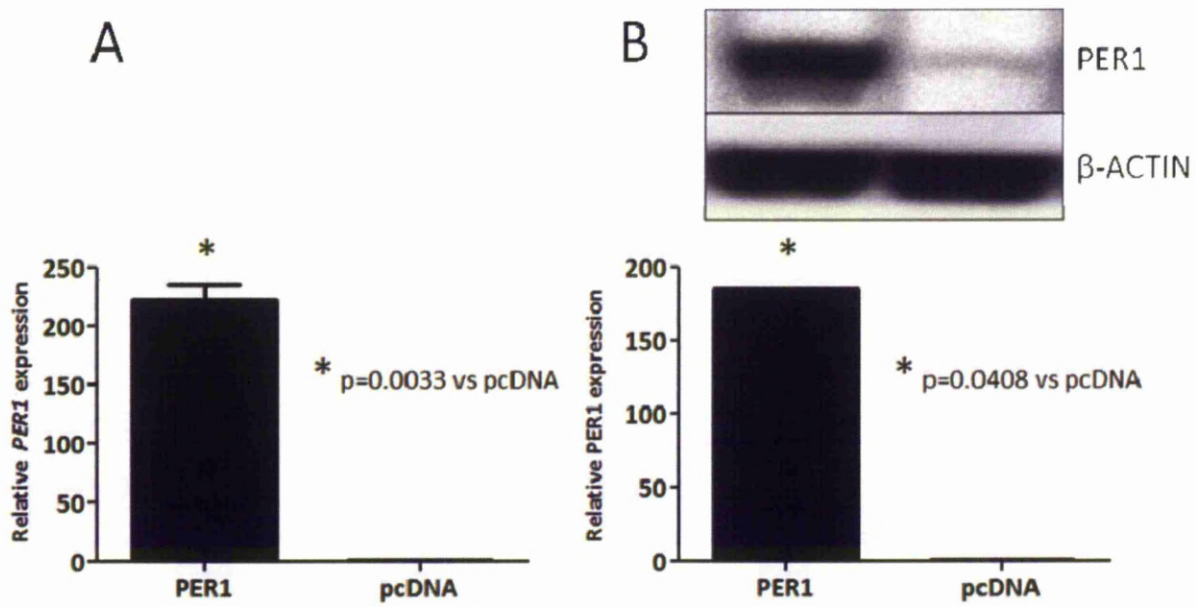

Figure 4.8: PER1 overexpression in CHO cells. CHO cells were transfected with either overexpression vectors for *PER1* or the empty pcDNA vector as a control. Cells were harvested after 48 hours and mRNA expression quantified by qPCR **(A)** and protein expression quantified by Western blotting **(B)** (a representative blot is shown). PER1 levels were expressed relative to β-ACTIN. The experiment was performed three times. PER1 expression in PER1-overexpressing cells has been expressed relative to expression in the pcDNA empty vector-transfected control cell line. Graphs show means with standard error. Student's t-test was used to identify significant differences in PER1 expression between PER1 overexpression vector-transfected cells and controls.

	Fold-change vs control	p-value
PER1	222.5	0.0033
PER1	185.2	0.0408

Table 4.4: Overexpression of *PER1* in CHO cells. CHO cells transfected with either overexpression vectors for *PER1* or the empty pcDNA vector as a control were harvested after 48 hours and mRNA expression quantified by qPCR and protein expression quantified by Western blotting. PER1 levels were expressed relative to β-ACTIN. The experiment was performed three times. PER1 levels in PER1-overexpressing cells have been expressed relative to levels in the empty vector-transfected control cell line. Student's t-test was used to identify significant differences ($p<0.05$) in PER1 expression between overexpression vector-transfected cells and controls.

4.8. PER1 represses *SGLT1* promoter activity in vitro

Reporter assays were performed in CHO cells to determine the effect of PER1 on the human *SGLT1* promoter (-1000/+33; Figure 4.6). CHO cells were transfected as described in section 2.7.1 above. The effect of PER1 overexpression on the *SGLT1* promoter was assessed in CHO cells passages 10-12 transfected at 80% confluence with combinations of the wild-type *SGLT1* promoter reporter construct pGL3/WT-*SGLT1*luc and expression vector (pcDNA3.1 with or without PER1 cDNA). Conversely, the effect of PER1 knockdown on *SGLT1* promoter activity was assessed by co-transfection of shRNA vectors shPER1 SeqA and B or the scrambled negative control with the wild-type *SGLT1* promoter pGL3/WT-*SGLT1*luc. Renilla luciferase was co-transfected into all wells in all experiments to normalize for transfection efficiency. Luminescence (firefly and Renilla) was measured after 48 hours. The results are displayed graphically in Figures 4.9A and B and Table 4.5.

PER1 overexpression did not alter *SGLT1* promoter activity from baseline (0.89-fold vs pcDNA control, p=0.24, Figure 4.9A, Table 4.5). In contrast the reduction in PER1 levels concomitant with transfection of PER1 knockdown vectors resulted in increased *SGLT1* promoter activity (1.46 and 1.47-fold that of controls with transfection of shPERSeqA and B respectively, $F^{2,6}$=6.26, p=0.0098, Figure 4.9B and Table 4.5), suggesting that PER1 suppresses the *SGLT1* promoter.

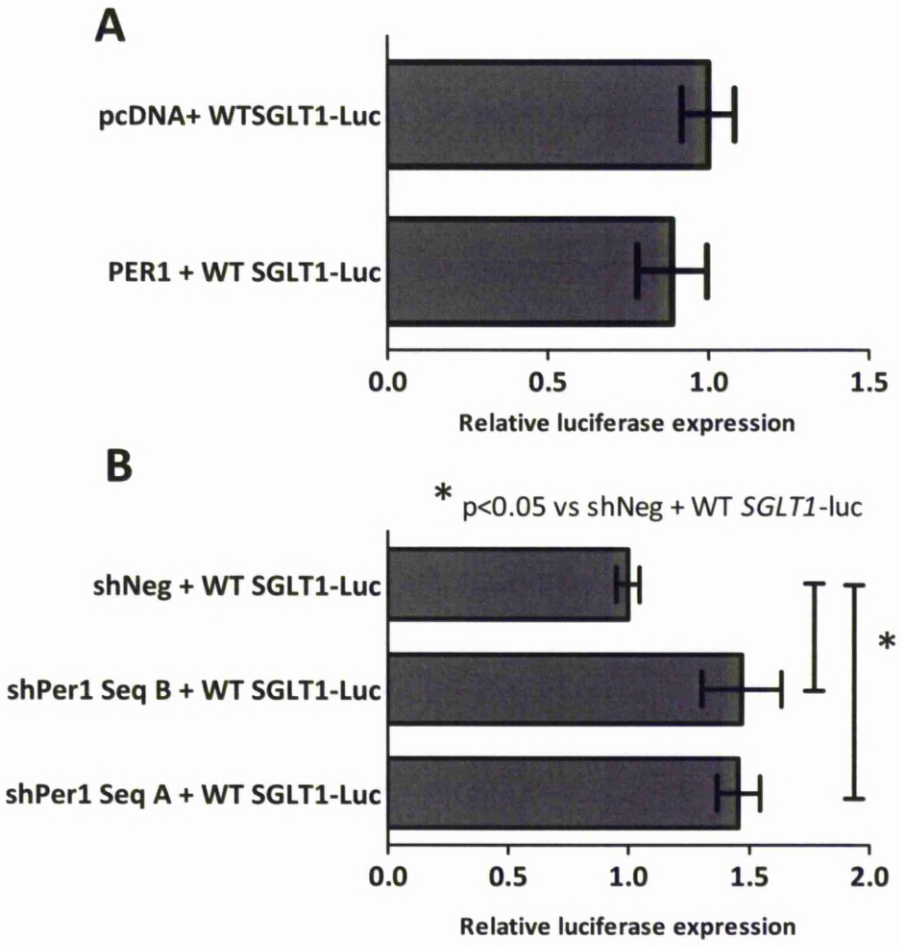

Figure 4.9: Effect of PER1 overexpression and knockdown on *SGLT1* promoter activity. **(A)** CHO cells were transfected at 80% confluence with combinations of the wild-type *SGLT1* promoter reporter construct pGL3/WT-*SGLT1*luc and expression vector (pcDNA3.1 with or without PER1 cDNA). **(B)** The effect of *PER1* knockdown on *SGLT1* promoter activity was assessed by co-transfection of shRNA vectors shPER1 SeqA and B or the scrambled negative control with the wild-type *SGLT1* promoter reporter construct pGL3/WT-*SGLT1*luc. Renilla luciferase was co-transfected into all wells in all experiments to normalize for transfection efficiency. Luminescence (firefly and Renilla) was measured after 48 hours. Graphs show mean and standard error and luminescence levels are expressed relative to the corresponding control. Student's t-test was used to compare expression between overexpression of PER1 versus control and one-way ANOVA to compare effects of knockdown of PER1 versus control

Vector combination		Fold change in promoter activity vs. control	p-value
Expression vector	**Reporter vector**		
PER1	WT-*SGLT1*luc	0.89	0.24
shPER1SeqA	WT-*SGLT1*luc	1.46	<0.05
shPER1SeqB	WT-*SGLT1*luc	1.47	<0.05

Table 4.5: Effect of PER1 overexpression and knockdown on *SGLT1* promoter activity. CHO cells were transfected at 80% confluence with combinations of the wild-type *SGLT1* promoter pGL3/WT-*SGLT1*luc reporter vector and either expression vectors (pcDNA3.1 with or without PER1 cDNA) or shRNA vectors shPER1 SeqA and B or the scrambled negative control. Renilla luciferase was co-transfected into all wells in all experiments to normalize for transfection efficiency. Luminescence (firefly and Renilla) was measured after 48 hours. Student's t-test was used to compare expression between overexpression of PER1 versus control and one-way ANOVA to compare effects of knockdown of PER1 versus control

4.9. E-boxes are negative elements in the *SGLT1* promoter

E-boxes are known to act as binding sites for clock genes and other transcription factors and thereby affect gene promoter activity and transcription. The most proximal 1kb of the *SGLT1* promoter contains 4 non-canonical E-boxes (CANNTG), potential binding sites for PER1, situated at -306/-311, -352/-357, -827/-832 and -837/-842 relative to the *SGLT1* transcription start site. To explore the role of E-boxes in mediating *SGLT1* promoter activity, mutations were introduced into each of the four present in the *SGLT1* promoter, designated EB1-EB4 starting from the most proximal. These E-box sites were mutated by conversion to NheI restriction sites (GCTAGC) and designated *SGLT1*-Luc mutEB1, mutEB2, mutEB3 and mutEB4. Site-directed mutagenesis was performed on the pGL3-*SGLT1* vector created above using the Phusion Site-directed Mutagenesis kit. Forward primers for the site-directed mutagenesis were designed to incorporate the NheI restriction site in place of the E-box sequence and including 15-20bp of the proximal and distal flanking sequences; while reverse primers did not incorporate any mutations.

To assess whether E-boxes might act cooperatively to mediate the activity of the *SGLT1* promoter, 2 or more E-box sites were mutated in combination. For this, a further set of primers was designed to incorporate combinations of E-box mutations (designated mutEB1+2, 1+3 and 1+2+3), which were created by adding a further mutation onto a mutated promoter. All constructs (single and combinatorial mutants) were sequenced to confirm successful mutation. Mutagenesis primers are listed in Table 2.11 and sequencing primers listed in Table 2.12.

I aimed to first investigate the effects of E-boxes on *SGLT1* promoter activity without exogenous transcription factors or clock genes. For this, CHO cells were transfected at 80% confluence as previously described with the empty pcDNA vector and reporter vectors bearing either the intact wild-type *SGLT1* promoter or single or multiple E-box site mutations. No overexpression vectors were used in this experiment. Renilla luciferase was co-transfected into all wells to normalize for transfection efficiency. Cells were harvested after 48 hours and both firefly and Renilla luminescence measured. Results are displayed graphically in Figure 4.10. Fold-changes are shown in Tables 4.6 and 4.7.

The effect of mutating two or more E-box sites was compared to the effect of individual mutations by a previously published method termed "interaction response"[32]. This was determined by the mean logarithm of the ratio of the effect observed with two or more mutations to the sum of effects observed with two or more single mutations (e.g., log {(EB1+2+3)/ [(EB1) + (EB2) + (EB3)]}). Interaction values from -0.1 to +0.1 were defined as additive, with values > +0.1 considered synergistic and values < -0.1 considered antagonistic.

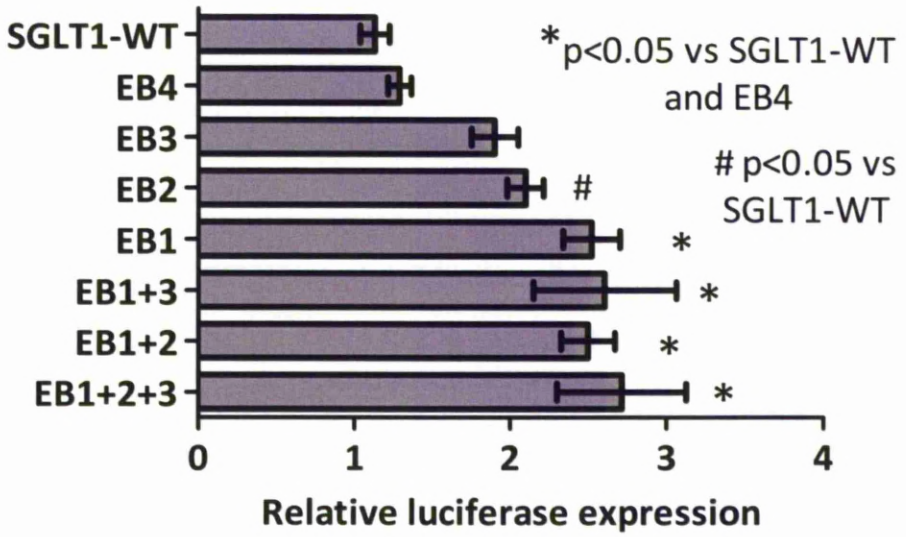

Figure 4.10: Effect of E-box mutations on *SGLT1* promoter activity in CHO cells. E-boxes at -306/-311, -352/-357, -827/-832 and -837/-842 on the *SGLT1* promoter were mutated either singly or in combination using site-directed mutagenesis to the NheI site. CHO cells were transfected with either the wild-type *SGLT1* promoter or the four E-box mutants (single or combinatorial). Renilla luciferase was used to normalize for transfection efficiency. Firefly and Renilla luciferase activity were measured after 48 hours. All experiments were performed three times. Graphs show means and standard error. One-way ANOVA with post-hoc Tukey was used to identify significant differences between luciferase expression of mutants and the wild-type promoter.

Expression vector	Single E-box mutant	Fold change vs wild-type
pcDNA	*SGLT1*-Luc mutEB1	2.23
pcDNA	*SGLT1*-Luc mutEB2	1.85
pcDNA	*SGLT1*-Luc mutEB3	1.68
pcDNA	*SGLT1*-Luc mutEB4	1.14

Table 4.6: Effect of single E-box mutations on *SGLT1* promoter activity in CHO cells. E-boxes at -306/-311, -352/-357, -827/-832 and -837/-842 on the *SGLT1* promoter were mutated using site-directed mutagenesis to the NheI site. CHO cells were transfected with either the wild-type *SGLT1* promoter or any one of the four E-box mutants. Renilla luciferase was used to normalize for transfection efficiency. Firefly and Renilla luciferase activity were measured after 48 hours. All experiments were performed three times. One-way ANOVA with post-hoc Tukey was used to identify significant differences between luciferase expression of mutants and the wild-type promoter.

Expression vector	Combinatorial mutant	Fold-change relative to wild-type promoter	Interaction response	Effect
pcDNA	*SGLT1*-Luc mutEB1+2	2.20	-0.267	Antagonistic
pcDNA	*SGLT1*-Luc mutEB1+3	2.30	-0.230	Antagonistic
pcDNA	*SGLT1*-Luc mutEB1+2+3	2.40	-0.381	Antagonistic

Table 4.7: Effect of combinatorial E-box mutations on *SGLT1* promoter activity in CHO cells. E-boxes at -306/-311, -352/-357, -827/-832 and -837/-842 on the SGLT1 promoter were mutated in combination using site-directed mutagenesis to the NheI site. CHO cells were transfected with either the wild-type SGLT1 promoter or combinatorial mutants. Renilla luciferase was used to normalize for transfection efficiency. Firefly and Renilla luciferase activity were measured after 48 hours. All experiments were performed three times. The effect of mutating two or more E-box sites was compared to the effect of individual mutations by a previously published method termed "interaction response"[32]. This was determined by the mean logarithm of the ratio of the effect observed with two or more mutations to the sum of effects observed with two or more single mutations (e.g., log {(EB1+2+3)/ [(EB1) + (EB2) + (EB3)]}). Interaction values from -0.1 to +0.1 were defined as additive, with values > +0.1 considered synergistic and values < -0.1 considered antagonistic.

Transient transfection of CHO cells with the E-box mutants revealed that promoter activity increased 2.2- and 1.9- fold with mutations in the E-boxes EB1-2, respectively ($F^{7,22}$=8.433, p<0.0001 on ANOVA and p<0.01, <0.05 and >0.05 vs. wild-type *SGLT1* promoter respectively on post-hoc Tukey, Figure 4.10, Table 4.6). Mutation of the most distal two E-boxes EB3 and EB4 had smaller effects which did not meet statistical significance (1.7 and 1.1-fold increase in promoter activity vs. wild-type *SGLT1* promoter, p>0.05, Figure 4.10, Table 4.6). These data indicate that the two proximal E-boxes have a repressive function on the *SGLT1* promoter. Mutant EB4 had a negligible effect on *SGLT1* promoter activity and hence was not included in the combinatorial mutants. Mutant EB1 had the strongest effect on the *SGLT1* promoter hence mutant EB1 was included in all combinatorial mutants.

Mutating E-boxes in combination had a slightly greater effect on *SGLT1* promoter activity than individual mutants. Mutant combination EB1+2+3, involving mutations of all three of the most proximal E-boxes, had the strongest effect on *SGLT1* promoter activity however this was not statistically significant (2.4-fold the activity of the wild-type *SGLT1* promoter, p<0.001, Figure 4.10, Table 4.7). Mutant combination EB1+3 had a smaller but significant effect on *SGLT1* promoter activity (2.3-fold the activity of the wild-type *SGLT1* promoter, p<0.01, Figure 4.10, Table 4.7). Mutant combination EB1+2 had the smallest effect on *SGLT1* promoter activity, inducing a 2.2-fold increase in luciferase activity compared to the wild-type *SGLT1* promoter, this was also statistically significant (p<0.01, Figure 4.10, Table 4.7).

Although each mutant combination led to a greater than 2-fold increase in activity over wild-type, the interaction between the individual E-boxes as determined by the interaction response was antagonistic in all cases (interaction response <-0.1). This shows that the effect of mutating these E-boxes in combination is less than the sum of effects of each individual mutant. These findings suggest that the E-boxes on the *SGLT1* promoter do not act cooperatively and that each E-box suppresses promoter activity independently.

4.10. Repression of *SGLT1* promoter activity by PER1 occurs despite mutation of E-boxes

PER1 activates target gene transcription by its interaction with other transcription factors that bind to E-boxes. To determine whether PER1 repression of the *SGLT1* promoter was mediated via E-boxes, the effect of PER1 overexpression on the mutant promoters was measured. CHO cells were transfected with the PER1 overexpression vector and either the wild-type *SGLT1* promoter or the four E-box mutants (single or combinatorial). Renilla luciferase was used to normalize for transfection efficiency. Firefly and Renilla luciferase activity were measured after 48 hours. The results are displayed graphically in Figure 4.11 and fold-changes and p-values shown in Tables 4.8 and 4.9.

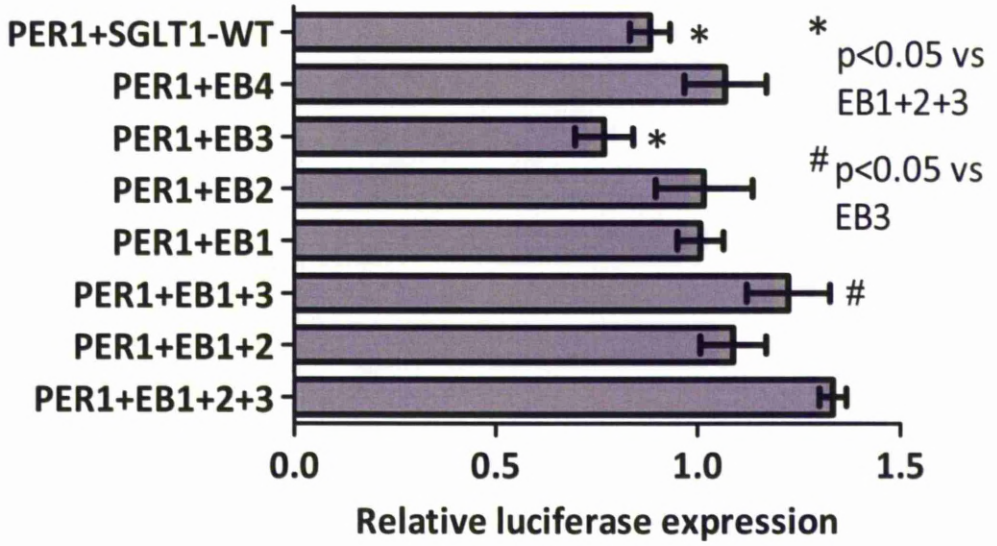

Figure 4.11: Effect of PER1 on the *SGLT1* promoter bearing E-box mutations in CHO cells. E-boxes at -306/-311, -352/-357, -827/-832 and -837/-842 on the *SGLT1* promoter were mutated either singly or in combination using site-directed mutagenesis to the NheI site. CHO cells were transfected with the PER1 overexpression vector and either the wild-type *SGLT1* promoter or the four E-box mutants (single or combinatorial). Renilla luciferase was used to normalize for transfection efficiency. Firefly and Renilla luciferase activity were measured after 48 hours. All experiments were performed three times. Graphs show mean and standard error. One-way ANOVA with post-hoc Tukey was used to identify significant differences between luciferase expression of mutants and the wild-type promoter.

Expression vector	Single E-box mutant	Fold change vs wild-type promoter
PER1	*SGLT1*-Luc mutEB1	1.14
PER1	*SGLT1*-Luc mutEB2	1.15
PER1	*SGLT1*-Luc mutEB3	0.87
PER1	*SGLT1*-Luc mutEB4	1.21

Table 4.8: Effect of PER1 on single E-box mutations in the *SGLT1* promoter in CHO cells. E-boxes at -306/-311, -352/-357, -827/-832 and -837/-842 on the *SGLT1* promoter were mutated using site-directed mutagenesis to the NheI site. CHO cells were transfected with the PER1 overexpression vector and either the wild-type *SGLT1* promoter or any one of the four E-box mutants. Renilla luciferase was used to normalize for transfection efficiency. Firefly and Renilla luciferase activity were measured after 48 hours. All experiments were performed three times. One-way ANOVA with post-hoc Tukey was used to identify significant differences between luciferase expression of mutants and the wild-type promoter.

Expression vector	Combinatorial mutant	Fold-change relative to wild-type promoter	Interaction response	Effect
PER1	*SGLT1*-Luc mutEB1+2	1.23	-0.270	Antagonistic
PER1	*SGLT1*-Luc mutEB1+3	1.38	-0.162	Antagonistic
PER1	*SGLT1*-Luc mutEB1+2+3	1.51	-0.322	Antagonistic

Table 4.9: Effect of PER1 on the *SGLT1* promoter bearing combinatorial E-box mutations in CHO cells. E-boxes at -306/-311, -352/-357, -827/-832 and -837/-842 on the *SGLT1* promoter were mutated in combination using site-directed mutagenesis to the NheI site. CHO cells were transfected with the PER1 overexpression vector and either the wild-type *SGLT1* promoter or combinatorial mutants. Renilla luciferase was used to normalize for transfection efficiency. Firefly and Renilla luciferase activity were measured after 48 hours. All experiments were performed three times.. One-way ANOVA with post-hoc Tukey was used to identify significant differences between luciferase expression of each combinatorial mutant and the wild-type promoter and single mutants. The effect of PER1 on two or more simultaneous E-box mutations was compared to the effect of PER1 on individual mutations by a previously published method termed "interaction response"[32]. This was determined by the mean logarithm of the ratio of the effect observed with two or more mutations to the sum of effects observed with two or more single mutations (e.g., log {(EB1+2+3)/ [(EB1) + (EB2) + (EB3)]}). Interaction values from -0.1 to +0.1 were defined as additive, with values > +0.1 considered synergistic and values < -0.1 considered antagonistic.

Mutation of E-boxes increased *SGLT1* promoter activity in the absence of exogenous transcription factors as shown above (Figure 4.10 and Tables 4.6 and 4.7). PER1 was shown earlier in this chapter to suppress *SGLT1* promoter activity. If E-boxes mediated this suppression, transfection of PER1 overexpression vectors would not be expected to alter the increase in *SGLT1* promoter activity induced by mutation of the E-boxes. In contrast, PER1 overexpression reduced activities of mutated promoters mutEB1, mutEB2, mutEB3 and mutEB4 such that there was no significant difference to luciferase activity of the unmutated wildtype *SGLT1* promoter on one-way ANOVA ($F^{7,24}$=4.720, p=0.0019) with post-hoc Tukey analysis (1.1-fold, 1.1-fold, 0.9-fold and 1.2-fold luciferase activity of the wildtype promoter, p>0.05, Figure 4.11, Table 4.8).

The three combination mutants (mutEB1+2, EB1+3 and EB1+2+3) were similarly inhibited by PER1 overexpression. Combinatorial mutation of the 3 proximal E-boxes in the *SGLT1* promoter resulted in increased levels of luciferase activity compared to the wildtype *SGLT1* promoter. The interaction of all three E-box mutations in the presence of PER1 was antagonistic (Table 4.9). This shows that the effect of PER1 on the *SGLT1* promoter containing E- boxes mutated in combination is less than the sum of effects of PER1 on each individual mutant.

To analyse the relationship between PER1 activity on the *SGLT1* promoter and E-box status a two-way ANOVA with post-hoc Bonferroni was performed (Figure 4.12). The analysis showed a significant interaction between PER1 activity and E-box mutation ($F^{7,46}$=5.78, p<0.0001). In addition, PER1 continued to suppress *SGLT1* promoter activity

despite single mutations of EB1-3 or combinatorial mutation of EB1+2, 1+3 or 1+2+3 ($p<0.001$ vs pcDNA, Figure 4.12), indicating that the effects of PER1 on the *SGLT1* promoter are independent of the status of E-boxes 1-3. PER1 had no effect on the *SGLT1* promoter compared to pcDNA upon mutation of EB4 ($p>0.05$, Figure 4.12), however this mutation did not appear to significantly alter *SGLT1* promoter activity on one-way ANOVA in the absence of PER1 ($p>0.05$, Figure 4.10), suggesting that the EB4 binding site does not contribute to *SGLT1* promoter activity.

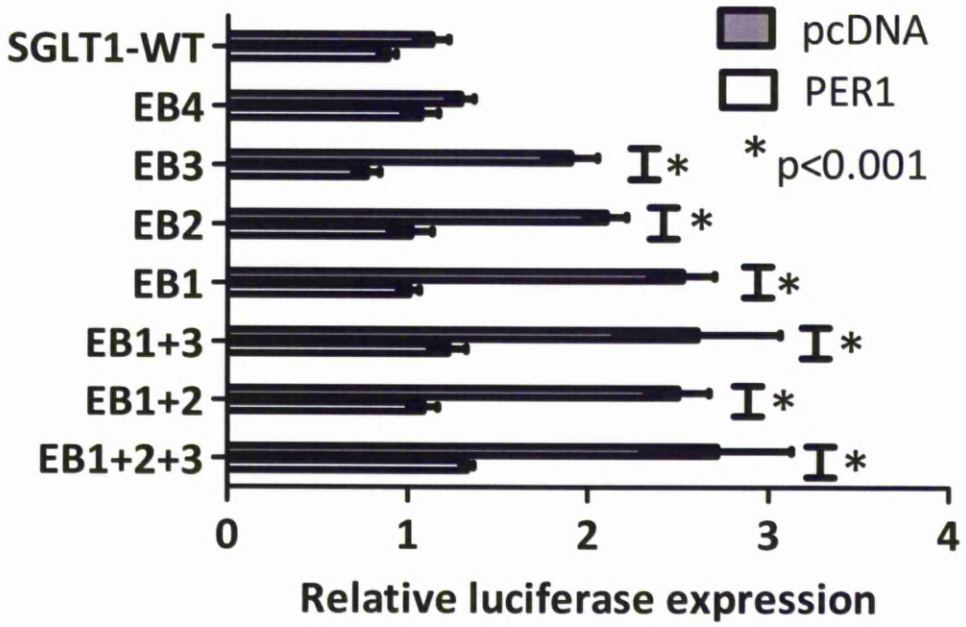

Figure 4.12: Effect of PER1 vs pcDNA on the *SGLT1* promoter bearing E-box mutations in CHO cells. The data shown in Figures 4.10 and 4.11 have been juxtaposed to allow comparison of the effects of PER1 on the wild-type and mutated *SGLT1* promoter. E-boxes at -306/-311, -352/-357, -827/-832 and -837/-842 on the *SGLT1* promoter were mutated either singly or in combination using site-directed mutagenesis to the NheI site. CHO cells were transfected with the PER1 overexpression vector and either the wild-type *SGLT1* promoter or the four E-box mutants (single or combinatorial). Renilla luciferase was used to normalize for transfection efficiency. Firefly and Renilla luciferase activity were measured after 48 hours. All experiments were performed three times. Graphs show mean and standard error. Two-way ANOVA with post-hoc Bonferroni was used to identify any interaction between the effects of PER1 and mutation of E-boxes on the *SGLT1* promoter.

4.11. Discussion

My data show for the first time an effect of clock genes on *SGLT1* in vitro. Knockdown of PER1 increased native *SGLT1* expression in Caco-2 enterocytes (Figure 4.3, Table 4.2), while promoter studies confirmed that the inhibitory activity of PER1 on *SGLT1* occurs via the proximal 1kb of the *SGLT1* promoter (Figure 4.9, Table 4.5). E-box sites exerted a suppressive effect on the *SGLT1* promoter (Figure 4.10, Table 4.6), however mutation of E-boxes had little effect on the inhibitory activity of PER1 on the *SGLT1* promoter (Figure 4.11, Table 4.8) suggesting that the actions of PER1 on *SGLT1* are independent of E-boxes EB1-3. Overall the above findings suggest that PER1 exerts an indirect suppressive effect on *SGLT1*, possibly acting via other clock-controlled genes binding to non-E-box sites on the *SGLT1* promoter.

PER1 inhibition of *SGLT1* expression was demonstrated by showing that knockdown *of PER1* in Caco-2 cells by two independent shRNAs increased *SGLT1* expression (Figure 4.3, Table 4.2). The lack of major changes in other clock genes following *PER1* knockdown (Figure 4.4, Table 4.2) suggests that the effect is mediated by PER1 itself or indirectly via a non-clock PER1 target. The absence of a significant effect of *PER1* knockdown on other clock genes noted in this study is in contrast to previous studies showing decreased expression of *Bmal1*, *Clock*, *Per2* and *Cry1* in the peripheral tissues of PER1-/- mice, indicating that PER1 regulates other clock genes at a transcriptional level in peripheral tissues[342]. In the SCN of PER1-/- mice however the effect of PER1 knockdown on other clock genes is only seen at a translational and not at a

transcriptional level[159, 343], suggesting that PER1 may play different roles in clock gene molecular feedback loops in the peripheral clock versus the SCN.

Several other alternatives may exist to explain the lack of effect of PER1 knockdown on the expression of other clock genes in Caco-2 cells (Figure 4.4, Table 4.2). One possibility is that the lack of synchronization in cultured Caco-2 cells may have dampened interactions of PER1 with other clock genes. Synchronized cells in culture (for example with a serum shock) are known to exhibit circadian oscillations in clock gene expression[84]. Synchronization of Caco-2 cells was not possible as the protocol for synchronization requires non-confluent rapidly growing cells; in contrast the expression of SGLT1 by Caco-2 cells only occurs in the confluent state upon which Caco-2 cells differentiate into a small bowel enterocytic phenotype[338]. Confluence is associated with reduced growth and proliferation rate and the attendant reduction in cell turnover and metabolism suggests that confluent cells may thus be less responsive to expression changes of clock components. Alternatively, the extent of *PER1* knockdown in this study may have been insufficient to modulate expression other clock genes. Regardless, these findings demonstrate that reducing *PER1* expression alone is sufficient to increase *SGLT1* expression in enterocytes without requiring cooperation of other clock genes (Figure 4.3, Table 4.2).

The increase in *SGLT1* promoter activity following PER1 knockdown in CHO cells (Figure 4.9B, Table 4.5) suggests that the suppressive effects of PER1 on *SGLT1* transcription as demonstrated in Caco-2 cells (Figure 4.3, Table 4.2) are mediated at least in part by

effects on the *SGLT1* promoter. Surprisingly, overexpression of PER1 did not induce a significant decrease of *SGLT1* promoter activity in CHO cells as would be expected (Figure 4.9A, Table 4.5). CHO cells are not an enterocytic cell line and the inability of PER1 overexpression to decrease *SGLT1* transcription may be due to the already low basal *SGLT1* promoter activity in these cells[31]. Promoter studies using the *SGLT1* promoter construct in an enterocytic cell line such as Caco-2 may have added some insights into the contribution of other innate intestinal transcription factors in cooperative regulation of the *SGLT1* promoter with PER1, however the low transfection efficiency of Caco-2 cells made transient transfections for promoter studies impractical. One alternative that may be suitable for future studies is the use of Caco-2 cells stably transfected with each of the promoter and expression vector combinations. The promoter studies in CHO cells carried out in this chapter nevertheless provide valuable data showing that clock genes, specifically PER1, are able to exert an effect on the *SGLT1* promoter even in the absence of other known *SGLT1* transcriptional modulators.

PER1 traditionally regulates genes by its indirect actions on canonical and non-canonical E-boxes in cooperation with other proteins [344]. I therefore next examined the *SGLT1* promoter for E-boxes. 4 non-canonical E-box consensus sequences (CANNTG) are present in the 1kb region proximal to the transcription start site (Figure 4.6). Promoter studies showed that the proximal E-boxes in this region appear to modulate *SGLT1* transcription (Figure 4.10, Table 4.6). The presence of E-box rich regions in circadian genes has been previously demonstrated[162, 345, 346]. Some clock gene family members, especially *PER* and *CRY* genes, contain E-boxes in their promoter regions[162,

345, 346] allowing the binding and transcriptional activation by CLOCK and BMAL1 which ultimately forms the positive limb of the molecular feedback loop[162]. The number and type of E-boxes (canonical vs non-canonical) and the presence of other binding sites such as RORE sites on the gene promoter are factors which have been postulated to determine the time of peak expression of rhythmic clock genes[346]. For instance the different peaks in expression of *Per1* and *Per2* in the SCN[347, 348] and in peripheral tissues [181] have been suggested to be due to the presence of multiple canonical E-box sequences in the promoter region of *PER1*[162] compared to a single non-canonical E-box sequence in the promoter region of *PER2*[345].

Other circadian genes outside the clock gene family also contain E-box regions in the promoter. A recent large-scale promoter analysis from microarray data revealed overrepresentation of E-box sequences in 167 circadian clock-controlled genes compared to randomly selected genes[349]. One example is the circadian gene peroxisome-proliferator-activated-receptor alpha (*PPAR-α*), which has been shown to contain 2 canonical E-box sequences and 4 non-canonical E-box sequences; clock genes have been shown to regulate this gene by via binding of the CLOCK-BMAL1 complex to this region [350].

The *SGLT1* promoter was found to have 4 non-canonical E-box sites (Figure 4.6). Although E-boxes are generally positive elements, mutation of 3 of the 4 E-boxes within the proximal 0.9kb of the *SGLT1* promoter, whether singly or in combination, increased *SGLT1* promoter activity (Figure 4.10, Tables 4.6 and 4.7), showing that E-boxes have a

suppressive effect on *SGLT1*. E-box mediated gene suppression, as we observed for the *SGLT1* gene, is not without precedent. E-boxes have been shown to mediate hormonal suppression of the luteinizing hormone (*LH*) promoter in vitro[351] and contribute to the regulation of the fatty acid synthase (*FAS*) promoter in vivo[352]. Of greater interest, the circadian Na^+/H^+ exchanger *NHE3* in the kidney, a transporter like SGLT1, has also been shown to bear an E-box on its promoter[14]. Binding of the CLOCK-BMAL1 complex to this E-box has been shown to activate transcriptional activity of *NHE3*, while transfection of PER2 or CRY1 was able to suppress or abolish this transactivation respectively[14]. My data showed a greater effect of the proximal E-boxes on the *SGLT1* promoter than the distal E-boxes (Figure 4.10, Table 4.6). Similar to these findings, other studies have also shown that E-boxes more distal to the transcription start site were of less functional relevance for gene transcription[339].

Individual E-box sequences were able to suppress the *SGLT1* promoter (Figure 4.10, Table 4.6); however *SGLT1* promoter activity upon mutating 2 or more E-boxes in combination was less than would have been expected from the sum of each of the individual effects (Figure 4.10, Table 4.7), suggesting that these E-boxes did not exhibit cooperative effects on regulation of *SGLT1* transcription. Cooperative activity of E-boxes has, however, been demonstrated for other genes. The two most proximal adjacent E-boxes on the rat acetylcholine receptor β (*AChRβ*) promoter have been shown to be necessary for transcriptional regulation of this gene[339]. Both of these E-boxes were shown to be necessary for stimulation of transcriptional activity of the *AChRβ* promoter; mutation of individual E-boxes did not exert any significant effect on promoter

activity[339]. Combinatorial effects of E-boxes were also noted by Lenka et al on the rat *COX VIII* gene[353] and by Oishi et al on the *PPAR-α* promoter[350]. The lack of cooperativity of E-boxes in my study may have been due to the distance of 40bp between the 2 most proximal E-boxes on the SGLT1 promoter (Figure 4.6); in contrast in previous studies cooperative E-boxes have often been immediately adjacent to each other[339]. The degree of cooperativity of E-boxes on a promoter may be a reflection of a conformational change upon binding of the transcription factor to one of the E-box sites thereby facilitating binding to the other E-box site.

The observation that PER1 continued to suppress the *SGLT1* promoter in transient assays despite its mutations of its 4 E-boxes (Figure 4.11, Table 4.8) indicates that PER1 suppression of *SGLT1* is independent of E-boxes. These findings demonstrate that PER1 and E-boxes are both able to suppress *SGLT1* promoter activity but via independent mechanisms. The lack of effect of E-box mutation on PER1 activity in my studies (Figure 4.11, Table 4.8) suggests that PER1 may regulate *SGLT1* via non-E-box binding transcription factors such as clock-controlled genes. The clock controlled gene DBP has been shown to regulate other intestinal transporters by binding not to E-boxes but to its own canonical consensus sequence of GTTACGAAAC[16]. Other clock-controlled genes such as DEC1 and DEC2 are known to bind to and suppress E-boxes in the promoters of other genes[344] and may similarly be binding to E-boxes to regulate *SGLT1* transcription. DEC1 is known to be expressed in the intestine[354]; however the expression of DEC2 and the temporal expression profile of DEC1 and DEC2 in the intestine remain unknown.

A further possibility for the indirect regulation of *SGLT1* by PER1 is the involvement of non-clock genes such as intestinal transcription factors hepatocyte nuclear factor (HNF1) α, HNF1β, GATA binding protein (GATA) factors or caudal-type homeobox protein 2 (CDX2). Rhoads et al demonstrated differential binding of the HNF1β to the rat *Sglt1* promoter, with increased levels of binding occurring during the daylight hours than the hours of darkness in the evening. In contrast HNF1α showed no circadian pattern of binding to the *Sglt1* promoter[63]. HNF1α and β, GATA factors and CDX2 all have binding sites on the *SGLT1* promoter and have previously been shown to regulate activity of the human *SGLT1* promoter [355]. PER1 may act on the *SGLT1* promoter in cooperation with one of more of these transcription factors, acting via binding sites for these factors on the *SGLT1* promoter. Further studies using EMSAs are currently ongoing in our laboratory to not only confirm binding of PER1 to the *SGLT1* promoter, but also to identify the other transcription factors which may be acting in cooperation with PER1 to regulate *SGLT1* transcription.

Other factors besides clock genes such as microphthalmia-associated transcription factor (MITF)[356], TWIST[357], upstream stimulatory factor (USF)[357] and the proto-oncogene c-myc[358] have also been shown to regulate the promoters of other genes via E-boxes. The expression profiles of these genes in the intestine have yet to be investigated.

This study revealed a suppressive role for PER1 on *SGLT1* transcription (Figure 4.3, Table 4.2). PER1 has similarly been shown to suppress other genes. WEE1, a key cell cycle regulator is downregulated by PER1 overexpression in the colon cancer HCT 116 cell line, suggesting direct circadian control of this gene by core clock components[359]. PER1 has also been shown to inhibit the transcriptional activity of the androgen receptor (*AR*) gene in the prostate via effects on the *AR* promoter[360]. Furthermore, in pancreatic and hepatocellular cancer cell lines, PER1 knockdown was shown to increase expression of the apoptosis-related proteins poly-ADP-ribose-polymerase (PARP), caspase 7 and BAX, as well as inducing apoptosis in these cells, in keeping with its known role as a tumour suppressor gene[361]. However the effects of PER1 are not always suppressive and appear likely to be gene-specific: in the same pancreatic and hepatocellular cancer cell lines in the previous study PER1 was shown to increase expression of the pro-survival protein BCL2[361].

Knockout mice have proved useful in deciphering the role of PER1 in circadian rhythmicity. Zheng et al[343] showed reduced stability and precision of circadian behavioural rhythms in mice with loss of functional PER1 expression. *mPer1-/-* and *mPer2 -/-* mice show gradual arrhythmicity in circadian behavioural patterns upon removal from the 12:12 light dark cycle and introduction into constant darkness, however the duration to onset and extent of rhythm persistence in both groups of knockout mice was variable[159]. In contrast, double mutant *mPer1-/-mPer2-/-* knockout mice had an abrupt immediate loss of rhythmicity upon transfer to constant darkness[159], leading the authors to suggest that PER1 and PER2 played similar but

redundant roles in the molecular clock. Another study showed that knockout of PER1 in mice resulted in a delayed peak in PER1 expression in peripheral tissues (kidney, heart and skeletal muscle)[362]. These findings led the authors to propose that PER1 may be specifically involved in modulation of physiological rhythmicity of the peripheral clock[362]. Although enterocyte gene expression in these knockout mice has yet to be examined, a recent study identified loss of rhythmicity of colonic motility in *mPer1-/- mPer2-/-* double knockout mice but persistent rhythmicity in individual *mPer1-/-* or *mPer2-/-* mice[363].

Knockout mice are likely to be invaluable in investigating the role of PER1 in mediating diurnal rhythmicity of *SGLT1* expression in the intestine and in deciphering the effect of selective loss of PER1 expression on the expression of other clock genes in the intestine. The in vitro data in this chapter (Figure 4.3, Table 4.2) suggest that loss of PER1 in vivo would be expected to result in increased baseline *SGLT1* expression with possible loss of circadian rhythmicity, while expression of other clock genes remained unchanged. Analysis of clock gene and *SGLT1* expression in the intestines of PER1 knockout mice would allow confirmation of this proposal.

In summary, the studies in this chapter show a suppressive role for the clock gene PER1 on *SGLT1* expression in enterocytes (Figure 4.3, Table 4.2). These effects are likely to be mediated by the *SGLT1* promoter (Figure 4.9, Table 4.5), however are independent of E-box sites, which also have a suppressive effect on the *SGLT1* promoter (Figure 4.10, Table 4.6). It seems likely that PER1 may be acting via other clock-controlled genes

binding to non-E-box sites on the *SGLT1* promoter, while E-box sites mediate the effects of other genes on *SGLT1* transcription. While the suppressive effect of PER1 on *SGLT1* is clear, the exact genes involved in the regulation of diurnal rhythmicity of *SGLT1* transcription unknown. It is hoped the ongoing research in our laboratory will allow further characterization of the molecular pathways regulating the effect of PER1 on *SGLT1*.

Chapter 5: *mir-16* exhibits diurnal rhythmicity in vivo and arrests enterocyte proliferation in vitro via suppression of cell cycle genes.

5.1. Introduction

Circadian rhythms (24-h oscillations) play a key role in the regulation of numerous physiological functions. Circadian rhythmicity of up to 10% of gene transcripts and an even greater fraction of proteins indicate the involvement of both transcriptional and translational pathways[258-260, 364, 365]. The mechanisms regulating these rhythms remain unknown, but regulation at both the transcriptional and post-transcriptional level suggests that microRNAs may have a role in this process. MicroRNAs are relatively recently discovered non-coding RNAs, which are able to silence numerous genes simultaneously. microRNAs suppress protein expression following recognition of complementary sequences on the 3'UTR of target genes by one of two mechanisms, either by inducing mRNA cleavage (which manifests as changes in mRNA levels) or inhibiting translation (manifesting as changes in protein levels)[208, 230, 231]. The presence of a specific target sequence for each microRNA on the 3'UTR of multiple genes permits simultaneous regulation of protein expression from numerous genes by a single microRNA[248, 366, 367]. Bioinformatics analysis suggests that up to 30% of mammalian gene transcripts are regulated by microRNAs, short non-coding RNAs[232-234, 248]. microRNAs have been postulated to "fine-tune" the expression of multiple targets in both insects and mammals by effecting small changes simultaneously in the expression of many genes, making these molecules candidates for coordinating the circadian rhythmicity of many genes and proteins[17, 203, 229, 261]. microRNAs have been shown to exhibit circadian rhythmicity in the liver where they regulate circadian

rhythms in several target genes[17], however the expression and rhythmicity of microRNAs in the intestine has not been investigated.

The intestine displays profound rhythmicity of morphology, resulting in peak absorptive function (e.g. for glucose) coinciding with maximal nutrient delivery to the bowel[13, 69]. The number of enterocytes per villus also exhibits a diurnal rhythmicity, with peak number occurring around the time of maximal nutrient availability[307]. Similar rhythmicity has been reported in human gastrointestinal mucosa[126, 127]. The exact pathways coordinating rhythmicity in proliferation are presently unknown.

I hypothesize that microRNAs are integral components for mediating circadian rhythms in intestinal proliferation, morphology and function. Prior to this study, the profile of microRNAs in the intestine was unknown. Identifying microRNAs that might be candidates for regulation of circadian rhythmicity therefore necessitated microRNA microarray profiling to identify the microRNAs in the intestine that exhibited circadian rhythmicity in expression. The studies in this chapter subsequently investigated the role of one of the rhythmic microRNAs, *mir-16*, in intestinal proliferation in vitro and corroborate these findings by comparing the rhythmicity of *mir-16* with rhythms of *mir-16* targets as well as rhythms of intestinal morphology and proliferation in vitro.

5.2. microRNAs exhibit diurnal rhythmicity in rat intestine

As the profile of microRNAs in the intestine was unknown, my first aim was to determine the temporal profile of microRNA expression in the jejunum. Rats were fed ad lib then 6-7 rats per timepoint were harvested at 3 hourly intervals. I extracted total RNA from mucosal scrapings of jejunum then sent the RNA to the Harvard Partners Center for Genetics and Genomics for bioanalysis and microRNA microarray hybridization. Pooled RNA from rats harvested at time ZT 0 (where ZT is hours after light onset and ZT 0 is 7am) was used as the reference sample on the arrays. 3 arrays were used per timepoint. RNA from 2 animals was used per timepoint and one sample per timepoint was run with the dye swapped to act as a biological replicate and control for any dye bias. 21 arrays were used in total. Biostatistical analysis of the microarray data was performed by Mr Jonathan Dreyfuss and Dr Peter Park from the Harvard Partners Center for Genetics and Genomics. The methods used for the microRNA microarrays and the data analyses of the arrays are described in detail in section 2.3.1. I was provided with the list of the 238 microRNAs identified to be expressed in the intestine on the microRNA microarrays and narrowed these down to the final list of microRNAs to be validated using the criteria described below.

The commercially available Exiqon microRNA microarrays used had probes for a total of 238 rat microRNAs – the total number of rat microRNAs that had been characterized at the time of the array production. All of these microRNAs were picked up on the arrays but found to be expressed to varying degrees in the intestine. The array data is stored in

the Gene Expression Omnibus (GEO) accession database under the accession number GSE20603[368]. I used a number of criteria to narrow down these microRNAs to the final number of microRNAs of interest.

The first criterion was to only consider microRNAs expressed at a reliable level in the intestine. For this I looked at the average intensity of expression of each microRNA on the arrays. The 238 microRNAs varied in intensity of expression on the microarrays, with a mean intensity of 6.7. Upon discussion with the biostatistics team (Dr Peter Park and Mr Jonathan Dreyfuss), an intensity of 8 (one standard deviation above the mean) was considered the threshold at which the expression was considered more reliable and less subject to error. 77 microRNAs had intensities of 8 and above. The 161 remaining microRNAs showing an average intensity of less than 8 were therefore not considered for further study.

The second criterion was to only consider microRNAs which exhibited a $\geq$ 2-fold difference between any two timepoints (including non-adjacent timepoints). Q-values, calculated by Mr Jonathan Dreyfuss, were used to ensure that this $\geq$ 2-fold difference was statistically significant. Of the 77 microRNAs still under consideration, 13 microRNAs exhibited a $\geq$ 2-fold difference between any two timepoints.

The third criterion was to exclude any microRNAs that did not display sequence conservation across human, mouse and rat species. microRNAs whose sequences have

been conserved across the species during evolution are more likely to be functional and biologically consequential and hence most suitable for further clinical analysis. Furthermore microRNA target specificity can be affected by a single base pair difference. microRNAs that do not display sequence conservation across human, mouse and rat species may therefore be less likely to have targets and effects conserved between rats and humans and were therefore excluded from further analysis. microRNA sequences were analysed by the use of the miRBase website, which curates the specific sequence of each microRNA across the major species[295]. Sequences of 5 of the 13 microRNAs were not conserved across human mouse and rat and hence these microRNAs were excluded from further consideration.

Overall, of 238 known rat microRNAs tested on in situ hybridization arrays, 8 microRNAs met all three criteria, i.e. exhibited $\geq$ 2-fold difference between any two timepoints, had an average intensity of $\geq$ 8 and had sequences conserved across the human, mouse and rat species. These microRNAs were *mir-16*, *mir-141*, *mir-20a*, *mir-142*, *mir-21*, *mir-503*, *mir-17* and *mir-26a*. These 8 microRNAs exhibited 2.0- to 3.4-fold difference between any two timepoints ($q<0.05$) and were subjected to further validation by qPCR.

5.2.1. *mir-16*, *mir-141* and *mir-20a* demonstrate diurnal rhythmicity on qPCR.

To validate the above 8 microRNAs, the total RNA extracted from the ad lib fed rats harvested at 3 hourly intervals as described above (6-7 rats per timepoint) was subject

to reverse transcription and qPCR using commercially available Taqman microRNA qPCR assays as described in section 2.3.2. The rat *small nucleolar RNA* gene (*snoRNA*) was used as a housekeeping gene to normalize for RNA loading. Figure 5.1a confirms that the means and spread of *mir-16* expression (taken as a representative microRNA) and of *snoRNA* expression for ZT 0 (Hours After Light Onset, where ZT 0 is 7am, taken as a representative timepoint) are similar.

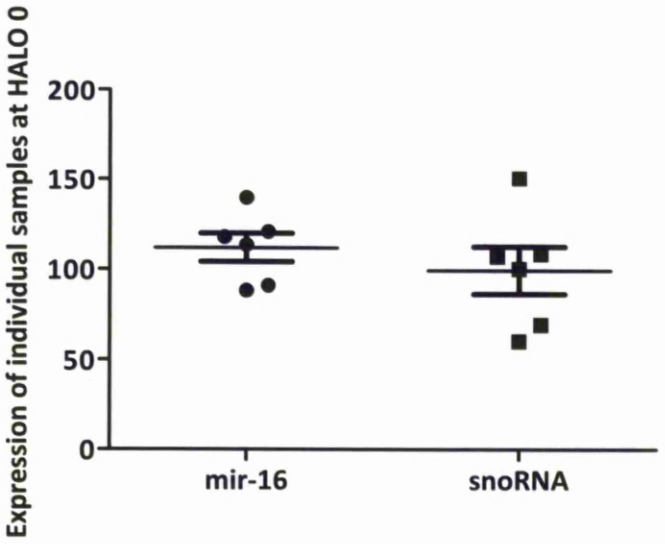

Figure 5.1: *mir-16* and *snoRNA* expression at ZT 0. RNA from the jejunum of rats (n=6) killed at ZT 0 (7am) was extracted, reverse transcribed and subjected to qPCR. Each reverse transcription and PCR was performed three times for each gene and each sample was plated in triplicate for each PCR. The mean expression of each gene for each sample at ZT 0 is shown as a circle (*mir-16*) or a square (the housekeeping gene *snoRNA*) and the mean expression and standard error of the mean for each gene per timepoint indicated.

The level of each microRNA validated was expressed as a ratio to the level of *snoRNA* in the same sample. Circadian rhythmicity of microRNA expression was determined using the Cosinor procedure, freely available from www.circadian.org, assuming a 24-h period [312]. Specifically, cross-sectional pattern analysis was performed on data arranged as if a single animal was harvested at 3-hourly intervals over 6 days. microRNAs were considered to display diurnal rhythmicity if a significant fit to a 24-hour period (as indicated by the p-value) was determined by the cosinor analysis performed by the program. For microRNAs that were shown to display diurnal rhythmicity the acrophase (time of peak expression) was determined by the program. The mean relative expression for each microRNA at each timepoint and the standard error of the mean was calculated and is displayed graphically in Figure 5.2A-C, and the significance of fit to a 24-hour period and the acrophase for each microRNA are expressed in Table 5.1. One-way ANOVA was also carried out to identify significant differences between expression levels at individual timepoints; p-values are also shown in Table 5.1

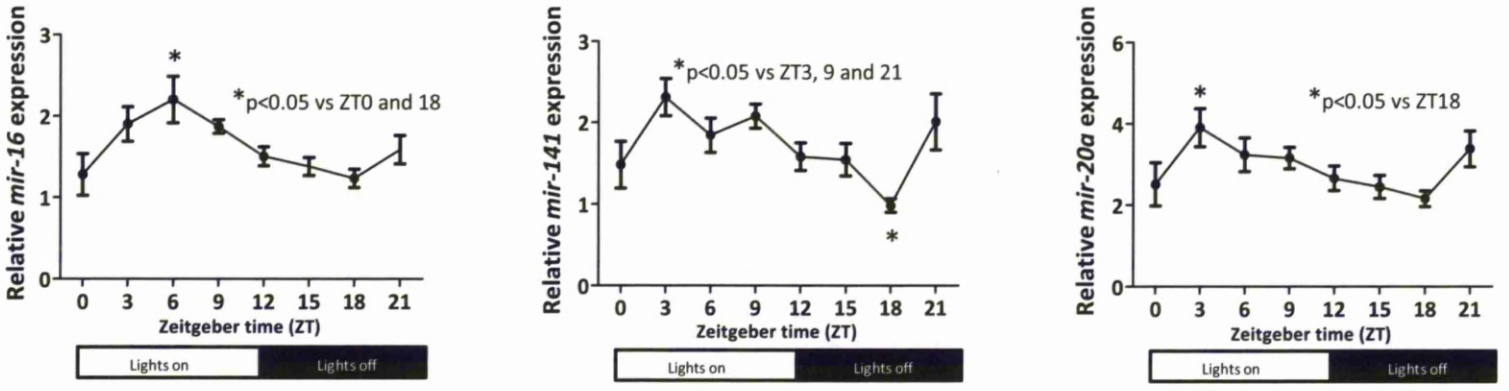

Figure 5.2: Temporal pattern of microRNAs mir-16 (A), mir-141 (B) and mir-20a (C) showing a 24-hour periodicity in rat jejunum (Fig 5.2A-C). Total RNA was extracted from the intestinal mucosa of rats (n=6-7 per time point) harvested 3 hourly beginning at ZT 0 (7am). RNA was run on microRNA microarrays and conserved microRNAs with an intensity of expression of $\geq$ 8 and showing a 2-fold or greater change between any two timepoints were validated by real-time PCR. microRNA expression was expressed relative to the expression of *snoRNA*, a housekeeping gene used to normalize for RNA loading. The reverse transcription and PCR was carried out three separate times for each gene and the mean expression for each sample from each run used to calculate an average from all three runs. The significance of fit to a 24-hour period was determined using the cosinor procedure and one-way ANOVA was used to identify significant differences between timepoints as shown in Table 5.1 as described in Table 5.1.

microRNA	Rhythmicity on qPCR			p-value on ANOVA
	p value	acrophase (ZT, h)	Fold change	
mir-16	0.001	6	1.8	0.039
mir-141	0.003	5	2.4	0.0024
mir-20a	0.019	4	1.8	0.0320
mir-142	0.071			
mir-21	0.244			
mir-503	0.300			
mir-17	0.320			
mir-26a	0.551			

Table 5.1: 24-hour periodicity of microRNAs validated by qPCR. Conserved microRNAs showing an intensity of expression of $\geq$ 8 and a 2-fold change or greater between any two timepoints on microRNA in situ hybridization microarrays were profiled by qPCR. The expression of each microRNA was normalized to the expression of the housekeeping gene *snoRNA* for the same sample. The data were arranged as if a single animal was harvested at 3-hourly intervals over 6 days and cross-sectional pattern analysis was performed with the cosinor procedure[312], freely available at www.circadian.org (accessed 23rd September 2008). This software was used to determine the significance of fit of the temporal expression of the data to a cosinor pattern with a 24-hour period. The acrophase (time of peak expression) was abstracted from the programme. A cosinor rhythm is necessary for the calculation of acrophase, hence no acrophase can be calculated for microRNAs that do not display a significant fit a cosinor rhythm.

Analysis of the expression of the 8 shortlisted microRNAs by qPCR showed that the expression of microRNAs *mir-16*, *mir-141* and *mir-20a* in rat jejunum demonstrated a significant fit to a 24-hour period (p=0.001, 0.003 and 0.019 respectively, Table 5.1) as determined by the cosinor procedure, indicating that these microRNAs display diurnal rhythmicity in the intestine of rats. Peak expression of these three microRNAs occurred between ZT 4 and 6, corresponding to the lights-on fasting period (Table 5.1, Figure 5.2A-C). The expression profiles of the remaining five shortlisted microRNAs (*mir-142*, *mir-21*, *mir-503*, *mir-17* and *mir-26a*) did not display a significant fit to a 24-hour period and hence these microRNAs were not considered to display diurnal rhythmicity in rat intestine.

Two of the three microRNAs exhibiting diurnal rhythmicity in the intestine have been reported to play a role in proliferation: *mir-20a* is pro-proliferative[22-24] and *mir-16* is anti-proliferative[18-21]. Intestinal villus height and cell number have been shown to peak in anticipation of maximal nutrient intake in previous studies[369]. Because anti-proliferative *mir-16* began to wane late in the light phase, when intestinal proliferation has been shown to increase, I selected this microRNA for further study. As the qPCR had been performed on total mucosal scrapings, which included all three fractions of crypt, villus and smooth muscle, my next aim was to determine the exact intestinal fraction which demonstrated diurnal rhythmicity in *mir-16* expression.

5.2.2. *mir-16* rhythmicity is restricted to the crypt fraction of the intestine

To compare *mir-16* expression levels in crypt, villus and smooth muscle, rats (3 per timepoint) were culled at ZT 6 and ZT 18, the respective *mir-16* peak and nadir. Fresh frozen sections were cut at 9μm thickness, stained and crypts (lower half), villi (top half) or smooth muscle isolated by laser capture microdissection. 20 crypts or villi were captured from each section and 10 sections used per animal. Smooth muscle was captured from the circumference of each section. Extracted total RNA was subjected to microRNA reverse transcription and qPCR. Purity of isolation was confirmed by measuring *PCNA* (*proliferating cell nuclear antigen*, denoting isolation of the crypt fraction), *SMA* (*smooth muscle actin*, denoting isolation of the smooth muscle fraction) and *IFABP* (*intestinal fatty acid binding protein*, denoting isolation of the differentiated cells of the villi) expression via qPCR. *mir-16* expression for each sample was expressed as a ratio to the expression of the housekeeping gene *snoRNA* for the same sample and mean relative *mir-16* expression for each fraction at each timepoint calculated. ANOVA (analysis of variance) was used to identify the presence of a significant difference in *mir-16* expression across the 3 intestinal fractions at each timepoint and post-hoc Tukey's multiple comparisons test was used to compare the relative expression of *mir-16* between individual fractions.

mir-16 expression was not significantly different across crypt, villus or smooth muscle fractions at ZT 18 (Figure 5.3; p=0.97). However, *mir-16* expression was 3.2-fold higher in crypts at ZT 6 vs. ZT 18 (Figure 5.3; p=0.003) while it was not detectably different

between these two timepoints in villi or smooth muscle. Thus, *mir-16* rhythmicity appears restricted to crypts, the proliferative compartment of the intestinal mucosa. My next aim was to determine the exact role of *mir-16* in the proliferative function of the intestine.

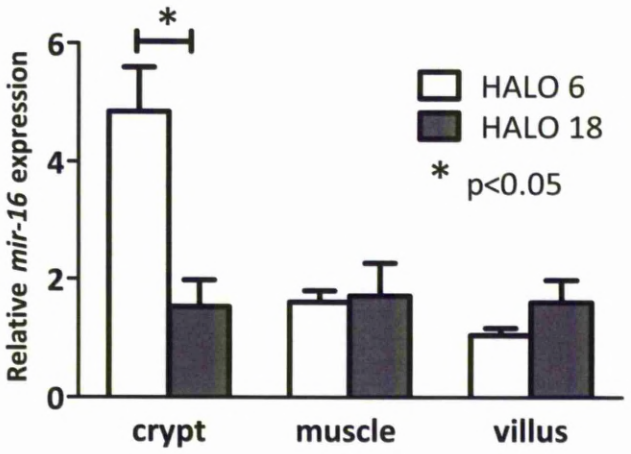

Figure 5.3: *mir-16* expression in intestinal fractions. Rats were killed at ZT 6 or and ZT 18, n= 3 per timepoint. Sections of jejunum were embedded in OCT over isopentane and dry ice, and subjected to cryosectioning. Laser capture microdissection was performed to isolate fractions of crypts, villi and smooth muscle. RNA was extracted from each section and subjected to reverse transcription and real-time PCR. *mir-16* expression was expressed relative to the expression of snoRNA. Students t-test was used to identify a significant difference in *mir-16* expression in each fraction between ZT 6 and ZT 18.

5.3. *mir-16* suppresses cell proliferation in enterocytes

Having determined that the alteration in *mir-16* expression at diurnal timepoints was confined to the crypt compartment, I decided to use crypt-derived cells to investigate the effects of *mir-16* in vivo. Although the use of a human-derived crypt cell line would have been preferable, there are no commercially available human intestinal crypt cell lines at present. Therefore the commercially available rat crypt-derived cell line IEC-6 was chosen for further investigation of *mir-16* effects on the intestine in vitro.

I decided to investigate the effects of *mir-16* overexpression in IEC-6 cells to determine the effects on proliferation, an approach that has been previously adopted by Liu et al[20] to investigate the effects of *mir-16* in hepatocytes. As microRNAs exert their effects at a post-transcriptional level, I believed that an induced decrease in target gene expression due to overexpression of *mir-16* might be more accurately and consistently measured than an increase, which may be confounded by any changes in transcription of these targets.

The effects of *mir-16* on enterocyte proliferation were assessed by tetracycline-induced overexpression of either *mir-16* or the negative control (a commercially available scrambled microRNA sequence) in IEC-6 cells. *mir-16* expression was 2.1-fold higher following overexpression vs. the negative control ($p=0.03$, Figure 5.4). Although this was a relatively small difference in expression of *mir-16*, it was comparable to the

peak/trough difference observed in *mir-16* expression on a diurnal basis. This modest difference in the level of *mir-16* expression had a profound effect on cell proliferation.

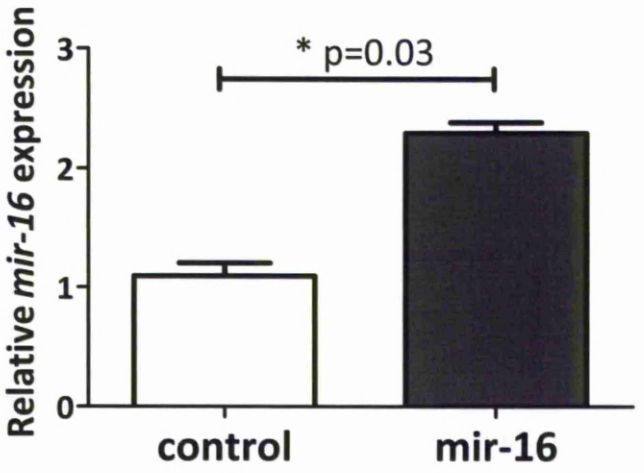

Figure 5.4: Overexpression of *mir-16* in IEC-6 cells. The *mir-16* sequence with the flanking 200bp was cloned from human genomic DNA and inserted into the pTRIPZ vector. IEC-6 cells were stably transfected with the *mir-16* overexpressing pTRIPZ vector or the scrambled control, and *mir-16* (or scrambled control) expression induced with doxycycline. Cells were harvested for RNA expression after 48 hours, and *mir-16* expression was quantified by reverse transcription and real-time PCR and normalized to the expression of the housekeeping gene *snoRNA*. Wells were plated in triplicate for the qPCR reaction and the experiment was performed a total of three separate times. Student's t-test was used to identify a significant difference in *mir-16* expression in *mir-16* overexpressing cells compared to the control.

The effects of *mir-16* on enterocyte proliferation were determined using the MTS assay and cell counting. IEC-6 cells stably overexpressing *mir-16* vs. scrambled negative control were seeded in triplicate in 96-well plates and proliferation indices measured 48 hours later using the MTS assay as per section 2.12.1. The experiment was performed a total of three separate times and the mean level of proliferation for *mir-16*

overexpressing cells and control cells calculated. Students t-test was used to identify a significant difference in proliferation between the two stable cell lines. At 48 hours after plating, the proliferation rate was decreased by 76% vs. control cells as measured by the MTS assay (4.2-fold difference; p=0.006, Figure 5.5A).

Cell growth rates were also confirmed by manual cell counting. IEC-6 cells stably overexpressing either *mir-16* or the scrambled control were seeded in triplicate in 6-well dishes and after 48 hours, were trypsinized and counted. The experiment was performed a total of three separate times and the mean cell count for *mir-16* overexpressing cells and control cells calculated. Students t-test was used to identify a significant difference in cell counts between the two stable cell lines. Cell counts were 5.2-fold higher in the control cells compared to the *mir-16* overexpressing cells (p=0.02, Figure 5.5B). Together these findings show that *mir-16* has a significant effect on the regulation of cell number. I next set out to identify the mechanism by which *mir-16* exerted this effect. Changes in cell number can be effected either by changing the level of cellular proliferation or by changing the rate of apoptosis and it was therefore necessary to determine the effects of *mir-16* on cell cycle and apoptosis in enterocytes.

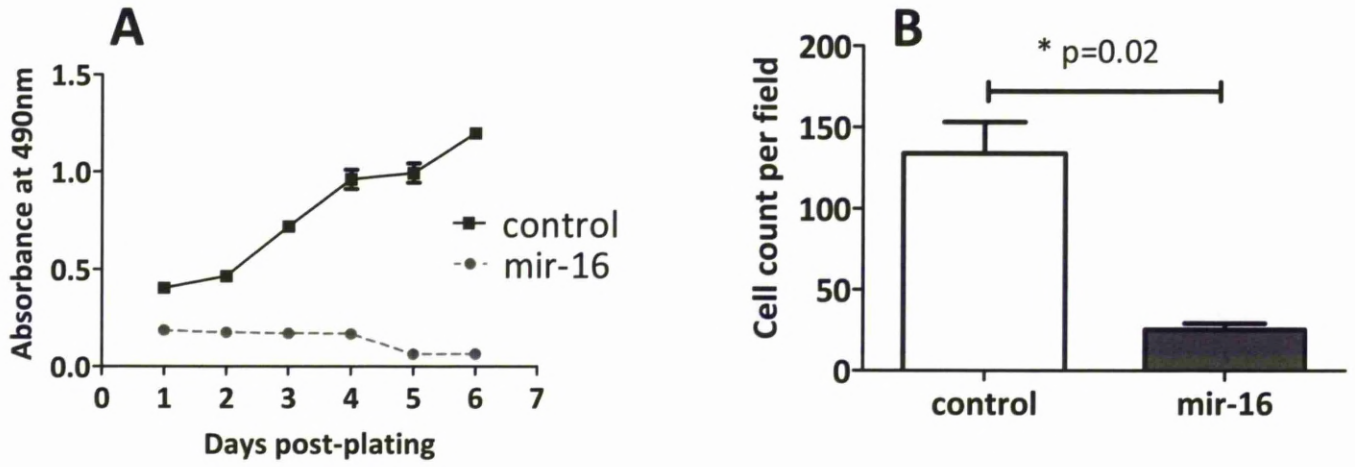

Figure 5.5: Effect of *mir-16* on IEC-6 proliferation. Proliferation and cell viability were determined using **(A)** the MTS assay and **(B)** cell counting respectively. IEC-6 cells stably overexpressing *mir-16* vs. control were seeded in triplicate in 96-well plates and proliferation indices measured 48 hours later using the MTS assay as per section 2.12.1. The experiment was performed a total of three separate times and the mean level of proliferation for *mir-16* overexpressing cells and control cells calculated. **(B)** IEC-6 cells stably overexpressing either *mir-16* or the scrambled control were seeded in triplicate in 6-well dishes then trypsinized and counted after 48 hours. The experiment was performed a total of three separate times and the mean cell count for *mir-16* overexpressing cells and control cells calculated. Students t-test was used to identify a significant difference between the two stable cell lines. Graphs show mean and standard error of the mean.

5.4. *mir-16* induces cell cycle arrest in enterocytes

To determine the mechanism by which *mir-16* exerted its anti-proliferative effects on enterocytes, I examined the effect of *mir-16* overexpression on the cell cycle of IEC-6 cells. IEC-6 cells stably overexpressing either *mir-16* or the scrambled negative control were grown in triplicate in 10cm tissue-culture treated dishes in the presence of doxycycline to induce *mir-16* (or scrambled control) expression. After 48 hours, cells were trypsinized and resuspended in 70% ethanol and incubated overnight at -20°C. The next day cells were centrifuged, the ethanol aspirated off and the cell pellet resuspended in propidium iodide. Resuspended cells were incubated for 30mins at 37°C in darkness and analyzed at 10,000 events per sample by Ashley Lansing, a technician at the Dana Farber Cancer Institute Flow Cytometry Core Facility on a BD FACScan flow cytometer (BD). The percentage of cells in each of the cell cycle stages (G1, S, G2 and M) was determined by Ashley Lansing using the software ModFit (Verity, Topsham, ME) and the results provided to me for further analysis.

Overexpression of *mir-16* led to a significantly larger fraction of cells in G1 compared to control (65% vs. 25%, p=0.001, Figure 5.6). The fraction of *mir-16* overexpressing cells was much smaller in G2 (13% vs. 31% in controls, p=0.018) and S (21% vs. 43% in controls, p=0.001), suggesting that *mir-16* overexpression was able to arrest cells in the G1 stage of the cell cycle, preventing progression to the S and G2 stages and thereby arresting proliferation.

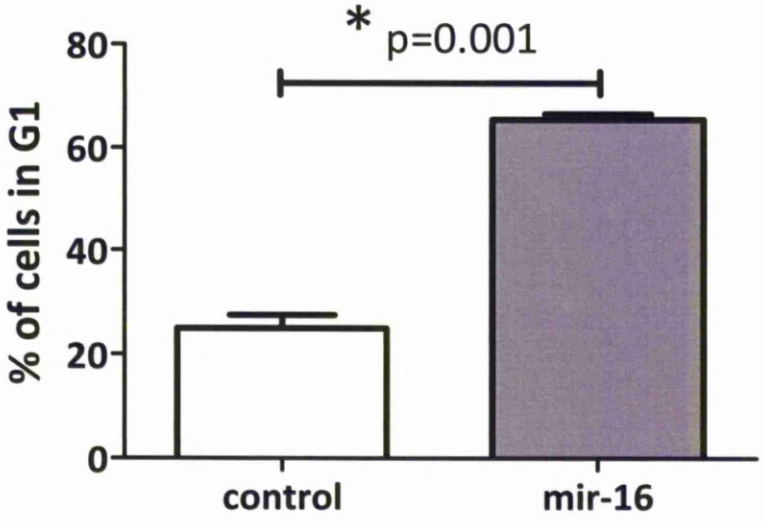

Figure 5.6: Effect of *mir-16* on G1 of the cell cycle in IEC-6 cells. IEC-6 cells stably overexpressing either mir-16 or the scrambled negative control were grown in the presence of doxycycline for 48 hours then trypsinized and resuspended in 70% ethanol and incubated overnight at -20°C. The next day cells were resuspended in propidium iodide then incubated for 30mins at 37°C in darkness. Cells were analyzed at 10,000 events per sample and the percentage of cells in each of the cell cycle stages (G1, S, G2 and M) determined using the software ModFit. The experiment was performed a total of three separate times and the mean percentage of cells in each of the cell cycle stages for *mir-16* overexpressing cells and control cells calculated. Students t-test was used to identify a significant difference in the percentage of cells in each cell cycle stage between the two stable cell lines.

Because *mir-16* has previously been shown to regulate apoptosis, I also investigated whether *mir-16* was also able to exert an effect on apoptosis in enterocytes. Apoptosis in *mir-16* overexpressing IEC-6 cells was quantified using the measurement of Annexin-V, a protein that binds to the phospholipid phosphotidylserine that translocates from the inner to the outer leaflet of the plasma membrane during apoptosis and is hence exposed in apoptotic cells. The nucleic acid stain Sytox Blue was used as a counter stain to specifically identify dead or necrotic cells which also stain Annexin-V positive. IEC-6 cells stably overexpressing either *mir-16* or the scrambled negative control were grown in 10cm tissue-culture treated dishes. After 48 hours, cells were trypsinized and counted and stained with Annexin V-FITC and Sytox Blue then analyzed at 10,000 events per sample by Miss Ashley Lansing, a technician at the Dana Farber Cancer Institute Flow Cytometry Core Facility on an LSRII flow cytometer (BD). The percentage of live, apoptotic and dead cells was determined by Ashley Lansing using the software Diva (BD) and the results provided to me for further analysis.

The average rate of apoptosis was similar in both groups of cells (3.8% in *mir-16* overexpressing cells vs. 3.3% in control cells, p=0.32, Figure 5.7), suggesting that the effect of *mir-16* on proliferation is due to the arrest of enterocytes in G1 as shown in Figure 5.6, rather than an effect on apoptosis[18, 370]. These results point to an effect of *mir-16* on the cell cycle in enterocytes, specifically genes involved in the regulation of the G1/S transition.

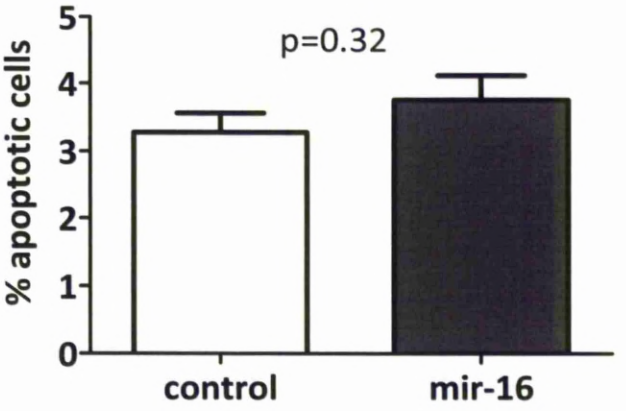

Figure 5.7: Effect of *mir-16* on apoptosis in IEC-6 cells. IEC-6 cells stably overexpressing either *mir-16* or the scrambled control were trypsinized and counted after 48 hours growth and stained with Annexin V-FITC and Sytox Blue. Cells were analyzed at 10,000 events per sample. The experiment was performed a total of three separate times and the mean percentage of live, apoptotic and dead cells calculated. The mean and standard error of the mean of the percentage of *mir-16* overexpressing and control cells exhibiting apoptosis is shown in the figure. Students t-test was used to identify a significant difference between apoptosis levels in the two stable cell lines.

5.5. *mir-16* suppresses key G1/S regulators in enterocytes

To identify specific *mir-16* targets involved in inducing G1 arrest, the 3'UTRs of G1/S regulatory genes were interrogated for the presence of *mir-16* binding sequences using the microRNA target prediction algorithm Targetscan[248, 371]. *Cyclin D1* (*Ccnd1*), *cyclin D2* (*Ccnd2*), *cyclin D3* (*Ccnd3*), *cyclin E* (*Ccne1*) and *cyclin-dependent kinase 6* (*Cdk6*) were identified as targets of *mir-16*. These are all known to regulate the G1/S transition and were therefore examined using in vitro experiments for responsiveness to *mir-16* in enterocytes. As a negative control, the effect of *mir-16* on *cyclin-dependent kinase 4 (Cdk4)*, a G1/S regulator lacking a *mir-16* target site in its mRNA 3'UTR, was also examined.

IEC-6 cells stably overexpressing *mir-16* or the scrambled control were grown in 10cm tissue-culture treated dishes and harvested after 48 hours for determination of the expression of CCND1, CCND2, CCND3, CCNE1, CDK4 and CDK6. Protein expression of these genes was measured using Western blotting using the protocol described in section 2.5. Western blot images were quantified by densitometry and protein expression for each gene expressed as a ratio to the expression of the housekeeping gene β-actin for the same sample. The experiment was performed a total of three separate times and the mean expression of CCND1, CCND2, CCND3, CCNE1, CDK4 and CDK6 in *mir-16* overexpressing cells and control cells calculated. Students t-test was used to identify a significant difference in the expression of these genes between the two stable cell lines.

Figure 5.8 shows the representative blots for each of the six genes examined along with the corresponding blot of the housekeeping gene β-ACTIN, as well as a graphical presentation of the densitometry results from these blots. Overexpression of *mir-16* significantly decreased protein levels of all five *mir-16* targets, CCND1, CCND2, CCND3, CCNE1 and CDK6, in IEC-6 cells compared to the non-silencing control (p=0.030 to 0.039, Figure 5.8A-E, Table 5.2). Interestingly the degree of suppression of protein expression was very similar across all five targets, with levels in *mir-16* overexpressing cells suppressed to 0.3-0.5 that of controls. CDK4, a cell cycle regulator that is not a predicted target of *mir-16*, did not demonstrate any change in expression following *mir-16* overexpression (p=0.223, Figure 5.8F, Table 5.2), confirming that *mir-16* did not exert any non-specific effect on cellular protein expression.

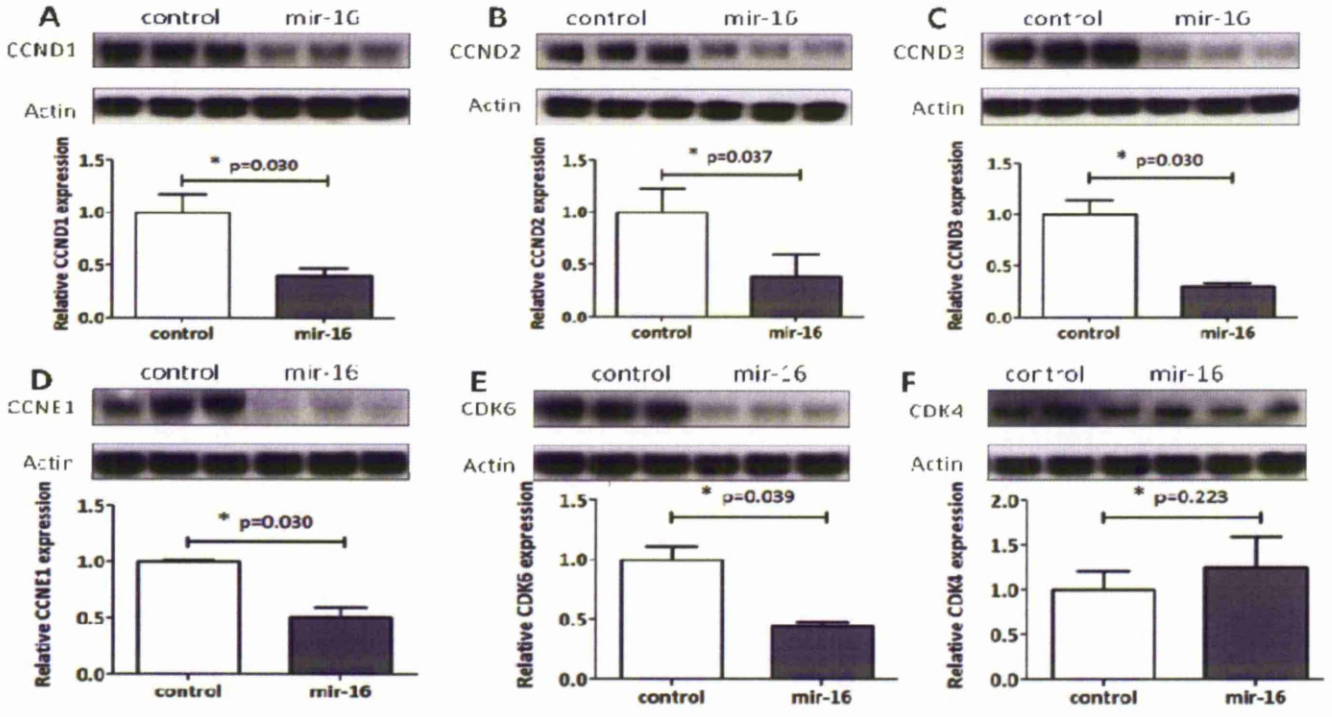

Figure 5.8: Effect of mir-16 on protein expression of G1/S regulators in IEC-6 cells. IEC-6 cells stably overexpressing *mir-16* or the scrambled control were harvested after 48 hours for determination of protein expression of CCND1 **(A)**, CCND2 **(B)**, CCND3 **(C)**, CCNE1 **(D)**, CDK4 **(E)** and CDK6 **(F)** by Western blotting. Blot images were quantified by densitometry and expressed as a ratio to β-ACTIN for each sample. The experiment was performed thrice. Mean expression and standard error of CCND1, CCND2, CCND3, CCNE1, CDK4 and CDK6 in *mir-16* overexpressing cells was calculated and is expressed in the graph as a ratio to the expression in control cells in the graph for ease of interpretation. Students t-test was used to identify a significant difference in the expression of these genes between the two stable cell lines.

Protein expression of G1/S regulators		
Target	**Fold-change vs control**	**p-value**
Ccnd1	0.4	0.030
Ccnd2	0.4	0.037
Ccnd3	0.3	0.030
Ccne1	0.5	0.030
Cdk6	0.4	0.039
Cdk4	1.2	0.223

Table 5.2: Effect of *mir-16* overexpression on G1/S regulator protein expression in IEC-6 cells. Western blot images were quantified by densitometry and protein expression for each gene expressed as a ratio to the expression of β-ACTIN for the same sample. The experiment was performed a total of three separate times and the mean expression of CCND1, CCND2, CCND3, CCNE1, CDK4 and CDK6 in *mir-16* overexpressing cells and control cells calculated. Students t-test was used to identify a significant difference in the expression of these genes between the two stable cell lines.

For measurement of mRNA expression of *Ccnd1*, *Ccnd2*, *Ccnd3*, *Ccne1*, *Cdk4* and *Cdk6,* IEC-6 cells stably overexpressing *mir-16* or the scrambled control were grown in 10cm tissue-culture treated dishes and harvested after 48 hours. RNA was extracted and reverse transcribed and qPCR performed according to protocols described in section 2.2. The expression of individual genes quantified by qPCR was expressed as a ratio to the expression of the housekeeping gene *β-actin* for the same sample.

The expression of *Ccnd2* and *Cdk6* mRNA was reduced by 75% (p=0.002) and 58% (p=0.001) respectively following *mir-16* overexpression (Table 5.3, Figure 5.9), suggesting that *mir-16* may regulate these genes via effects on mRNA cleavage. *mir-16* overexpression did not change the mRNA expression of *Ccnd1*, *Ccnd3* and *Ccne1* (p=0.660, 0.151 and 0.181 respectively, Table 5.3, Figure 5.9) despite suppression at a protein level (Figure 5.8A,C and D, Table 5.2) suggesting that these specific genes may be regulated by *mir-16* at a translational level rather than mRNA cleavage. *Cdk4,* a G1/S regulator which is not a target of *mir-16* but measured as a negative control, was unaltered at both the mRNA and protein level following *mir-16* overexpression (p=0.223 and 0.591 respectively, Tables 5.2 and 5.3) These results confirm that CDK4 is not a *mir-16* target and indicate that *mir-16* overexpression does not exert non-specific effects on cell cycle proteins.

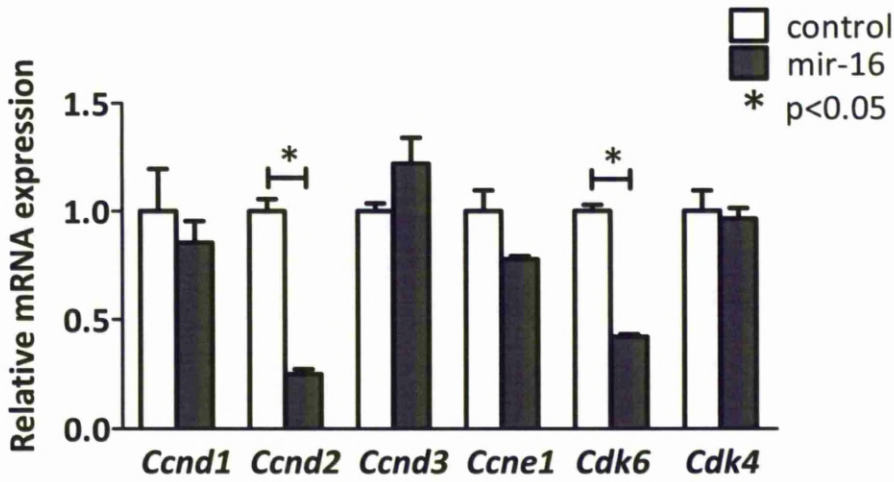

Figure 5.9: Effect of *mir-16* on the mRNA expression of G1/S regulators in IEC-6 cells. IEC-6 cells stably overexpressing *mir-16* or the scrambled control were grown in 10cm tissue-culture treated dishes and harvested after 48 hours. RNA was extracted and reverse transcribed and qPCR performed. The expression of individual genes was expressed as a ratio to the expression of the housekeeping gene *β-actin* for the same sample. Each well was plated in triplicate and the qPCR reaction performed twice for each experiment. The experiment was performed a total of three separate times and the mean expression and standard error of *Ccnd1*, *Ccnd2*, *Ccnd3*, *Ccne1*, *Cdk4* and *Cdk6* in *mir-16* overexpressing cells and control cells calculated. The expression of these genes in *mir-16* overexpressing cells has been presented as a ratio of the expression in control cells in the graph for ease of interpretation. Students t-test was used to identify a significant difference in the expression of these genes between the two stable cell lines.

mRNA expression of G1/S regulators		
Target	**Fold-change vs control**	**p-value**
Ccnd1	0.9	0.660
Ccnd2	0.2	0.002
Ccnd3	1.2	0.151
Ccne1	0.8	0.181
Cdk6	0.4	0.001
Cdk4	1.0	0.591

Table 5.3: Effect of *mir-16* overexpression G1/S regulator mRNA expression in IEC-6 cells. mRNA expression was determined by qPCR. The expression of individual genes was expressed as a ratio to the expression of the housekeeping gene *β-actin* for the same sample. The experiment was performed a total of three separate times and the mean mRNA expression of *Ccnd1*, *Ccnd2*, *Ccnd3*, *Ccne1*, *Cdk4* and *Cdk6* in *mir-16* overexpressing cells and control cells calculated. Students t-test was used to identify a significant difference in the expression of these genes between the two stable cell lines.

My data suggest that the effects of *mir-16* on G1 arrest of cell cycle progression in enterocytes may be mediated by one or more of these G1/S proteins. I therefore proposed that the rhythmic expression of *mir-16* in vivo would therefore be expected to induce rhythmicity in its target genes in vivo and sought to confirm rhythmicity of *Ccnd1*, *Ccnd2*, *Ccnd3*, *Ccne1* and *Cdk6* in the jejunum of diurnally harvested rats.

5.6. G1/S regulatory proteins targeted by *mir-16* peak in antiphase to *mir-16* expression in jejunum

Cell cycle proteins are able to regulate cellular proliferation[123-125] and may therefore be mediators of the known diurnal rhythmicity in intestinal proliferation[112, 307]. My data so far has shown that these proteins may be regulated in vitro by the diurnally rhythmic microRNA *mir-16*. Involvement of *mir-16* in the cell cycle of enterocytes in the jejunal mucosa via suppression of these proteins as suggested by the IEC-6 studies would likely be evidenced by a corresponding temporal displacement of their rhythms from that of *mir-16* in vivo. However to date the rhythms of cell cycle proteins in the small intestine have not been sufficiently characterized. I therefore examined the temporal protein expression patterns for the 5 *mir-16* targets (*Ccnd1*, *Ccnd2*, *Ccnd3*, *Ccne1,* and *Cdk6*) as well as the non-*mir-16* target *Cdk4* in the jejunum of rats harvested at 3-hourly diurnal timepoints.

To do this, rats fed ad lib were culled at 3 hourly intervals (6-7 rats per timepoint) and jejunum harvested for subsequent analysis of protein and mRNA expression. Protein was extracted from jejunal mucosal scrapings of these rats and Western blotting performed as described in section 2.5.

Circadian rhythmicity of protein expression of CCND1, CCND2, CCND3, CCNE1, CDK6 and CDK4 was determined using the Cosinor procedure assuming a 24-h period[312]. Specifically, cross-sectional pattern analysis was performed on data arranged as if a single animal was harvested at 3-hourly intervals over 6 days. The significance of fit to a 24-hour period and acrophase of rhythmic genes were determined by the programme and are expressed in Table 5.4. In addition, one-way ANOVA was used to identify significant differences in expression between timepoints.

All five *mir-16* targets (CCND1, CCND2, CCND3, CCNE1 and CDK6*)* exhibited diurnal rhythmicity at the protein level with a 24-hour period, with acrophases (expression peaks) mostly falling during the nocturnal feeding period between ZT 12 and ZT 18 ($p<0.05$, Figure 5.10 A-E; Table 5.4) and nadirs during the lights-on period between ZT 0 and 6. Peak expression of *mir-16* at ZT 6 coincided with low levels of protein expression for all five targets, providing further evidence that *mir-16* may act to suppress these proteins and contribute to their rhythmicity in vivo.

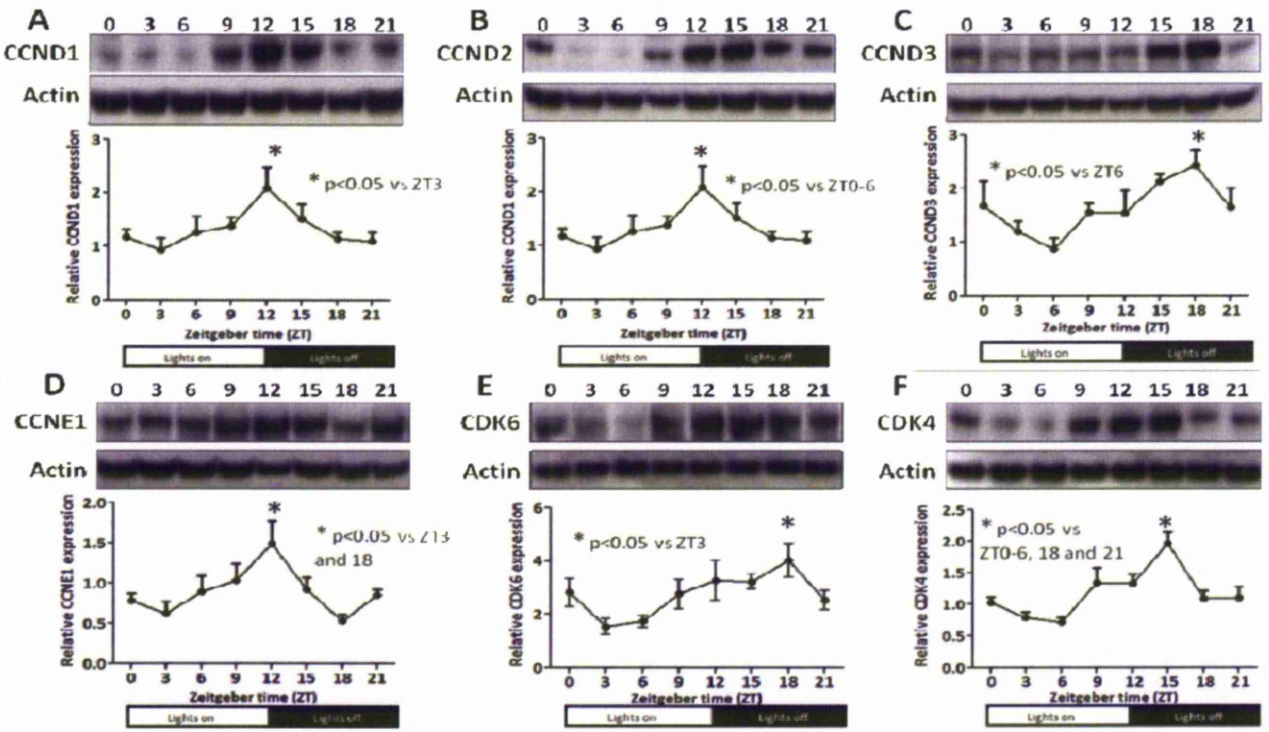

Figure 5.10: Rhythmicity of protein expression in rat jejunum. Rats fed ad lib were culled at 3 hourly intervals (6-7 rats per timepoint) beginning at ZT 0 (7am) and jejunum harvested for analysis of protein expression of *mir-16* targets CCND1 (**A**), CCND2 (**B**), CCND3 (**C**), CCNE1 (**D**), CDK6 (**E**) and the non *mir-16* target CDK4 (**F**) by Western blotting. Protein expression for each gene expressed as a ratio to the housekeeping gene β-ACTIN for the same sample. Values represent the mean and standard error for each gene at each timepoint. In addition, one-way ANOVA was used to identify significant differences in expression between timepoints.

Rhythmicity of protein expression				
Target	p value on cosinor	Acrophase (ZT, h)	Fold-change peak/trough	p value on ANOVA
CCND1	0.009	12	2.3	0.047
CCND2	0.001	14	4.4	0.009
CCND3	0.004	17	2.8	0.034
CCNE1	0.013	11	2.8	0.008
CDK6	0.004	16	2.5	0.039
CDK4	0.000	15	2.8	<0.0001

Table 5.4: Rhythms in G1/S regulator protein expression in diurnally harvested rat jejunum. Protein was extracted from jejunal mucosal scrapings and Western blotting performed. Blot images were quantified by densitometry and protein expression for each gene expressed as a ratio to the expression of the housekeeping gene β-ACTIN for the same sample. Cross-sectional pattern analysis was performed with the cosinor procedure[312], used to determine the significance of fit of the temporal expression of the data to a 24-hour cosinor pattern and to calculate the acrophase (peak expression) for each protein. One-way ANOVA was used to identify significant differences in expression between individual timepoints

I next determined whether these genes were rhythmic at the mRNA level. Total RNA was extracted from jejunal mucosal scrapings from these rats and subject to reverse transcription and qPCR as described in section 2.2. The non-circadian gene *β-actin* was used as a housekeeping gene to normalize for RNA loading. The level of each gene was expressed as a ratio to the level of *β-actin* in the same sample.

Circadian rhythmicity of mRNA expression of *Ccnd1*, *Ccnd2*, *Ccnd3*, *Ccne1*, *Cdk6* and *Cdk4* was determined using the Cosinor procedure assuming a 24-h period [312] as described above. The significance of fit to a 24-hour period and the acrophase of rhythmic genes were determined by the Cosinor programme and are expressed in Table 5.5. In addition, one-way ANOVA was used to identify significant differences in expression between timepoints.

Ccnd2 and *Ccnd3* displayed rhythmicity at the transcriptional level ($p<0.05$ on both cosinor analysis and ANOVA; Figures 5.11 B and C, Table 5.5). The temporal expression of *Ccnd1*, *Ccne1* and *Cdk6* did not fit a 24-hour period and hence did not qualify as a diurnal rhythm ($p>0.1$ on both cosinor analysis and ANOVA, Figures 5.11 A, D and E). CDK4, which demonstrated no response to *mir-16* overexpression in vitro, displayed significant rhythmicity at both the transcriptional and post-transcriptional level in vivo ($p=0.005$ and <0.001 on cosinor analysis and 0.021 and <0.0001 on ANOVA, Figures 5.11 F and 5.10 F), suggesting that other mechanisms besides *mir-16* are likely to play a role in governing diurnal rhythmicity of cell cycle proteins, as will be discussed later.

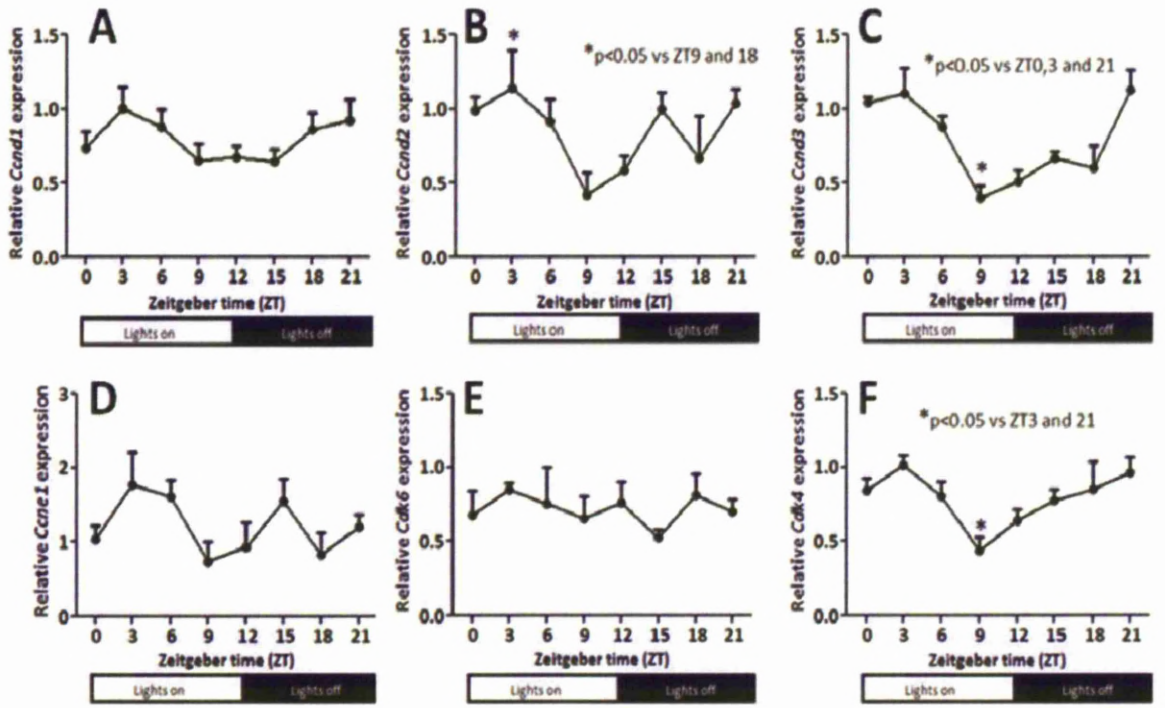

Figure 5.11: Rhythmicity of mRNA expression in rat jejunum. Rats fed ad lib were culled at 3 hourly intervals (6-7 rats per timepoint) beginning at ZT 0 (7am). mRNA was extracted from jejunal mucosal scrapings and subjected to reverse transcription and qPCR to determine the expression of of *mir-16* targets *Ccnd1* (**A**), *Ccnd2* (**B**), *Ccnd3* (**C**), *Ccne1* (**D**), *Cdk6* (**E**) and the non *mir-16* target *Cdk4* (**F**). mRNA expression for each gene was expressed as a ratio to the expression of the housekeeping gene *β-actin* for the same sample. Each well was plated in triplicate and the qPCR reaction performed twice for each experiment. The graphs show the mean and standard error for each gene at each timepoint. One-way ANOVA was used to identify significant differences in expression between individual timepoints.

Rhythmicity of mRNA expression				
Target	**p value on cosinor**	**Acrophase (ZT, h)**	**Fold-change peak/trough**	**p value on ANOVA**
Ccnd1	0.120			0.258
Ccnd2	0.039	0	2.7	0.001
Ccnd3	0.000	0	2.8	<0.0001
Ccne1	0.330			0.112
Cdk6	0.770			0.847
Cdk4	0.005	2	2.3	0.021

Table 5.5: Rhythms in G1/S regulator mRNA expression in diurnally harvested rat jejunum. RNA was extracted from jejunal mucosal scrapings and qPCR performed. mRNA expression for each gene was expressed as a ratio to the expression of the housekeeping gene *β-actin* for the same sample. The cosinor procedure[312] was used to determine the significance of fit of the temporal expression of the data to a 24-hour cosinor pattern and the acrophase (peak expression) for each gene displaying a significant 24-hour rhythm was abstracted from the program. The acrophase cannot be calculated for genes that do not display a significant fit to a 24-hour cosinor pattern. One-way ANOVA was used to identify significant differences in expression between individual timepoints.

Cell cycle proteins regulate the transitions between the various stages of the cell cycle[123-125] and thereby contribute to the proliferative activity of the cell. I therefore proposed that these rhythms in cell cycle proteins were likely to correlate with rhythms in jejunal enterocyte morphology and proliferation.

5.7. Diurnal rhythmicity in DNA synthesis and morphology in rat jejunum

To assess rhythmicity in enterocyte morphology and proliferation, rats fed ad lib were culled at 3 hourly intervals (6-7 rats per time point) and sections of jejunum harvested and fixed overnight in 10% buffered formalin. These sections were processed by technicians at the Brigham and Women's Histopathology Core Facility. For determination of cells in S-phase, sections were stained with anti-BrdU primary antibody and counterstained with haematoxylin and eosin to facilitate counting of BrdU-negative nuclei. Stained sections on microscope slides were returned to the author for analysis. I trained Miss Britta Thompson, a medical student in our laboratory, to perform measurements of crypt and villus morphology. The following crypt- villus axis parameters were measured: crypt depth, villus height, villus width (at the midpoint of the villus), crypt enterocyte width and villus enterocyte width (as measured by number of nuclei over 125 μm) and number of enterocytes per crypt. I performed the BrdU staining measurements by counting the number of BrdU-stained nuclei per crypt.

Circadian rhythmicity of DNA synthesis and morphologic parameters was determined using the Cosinor procedure assuming a 24-h period[312]. The significance of fit to a 24-hour period (as indicated by the p-value) and acrophase of rhythmicity for each parameter were determined by the program and are expressed in Table 5.6. One-way ANOVA was used to identify significant differences in expression between timepoints.

The number of cells per crypt labelled with BrdU peaked at ZT 3 (p=0.005 on cosinor analysis and 0.003 on ANOVA, Figure 5.11A). The total number of cells per crypt peaked several hours later at ZT 12 (p=0.001 on cosinor analysis and 0.014 on ANOVA, Figure 5.11B). Peak crypt depth occurred at ZT 13 on cosinor analysis and ZT15 on ANOVA (Figure 5.11C). Villus height shown significant rhythmicity on cosinor analysis with a peak at ZT14 (p=0.043) but not on ANOVA (p=0.480, Figure 5.11 D). There was no diurnal rhythmicity in cell width of villi crypts (p>0.1 on both cosinor analysis and ANOVA, Figure 5.11E and F). Similarly crypt and villus width both showed no rhythmicity over the diurnal period (p>0.05 on both cosinor analysis and ANOVA, Figure 5.11G and H). Overall these data demonstrate that cell proliferation in the crypt is the main factor contributing to the observed rhythmicity in crypt and villus morphology (Table 5.6).

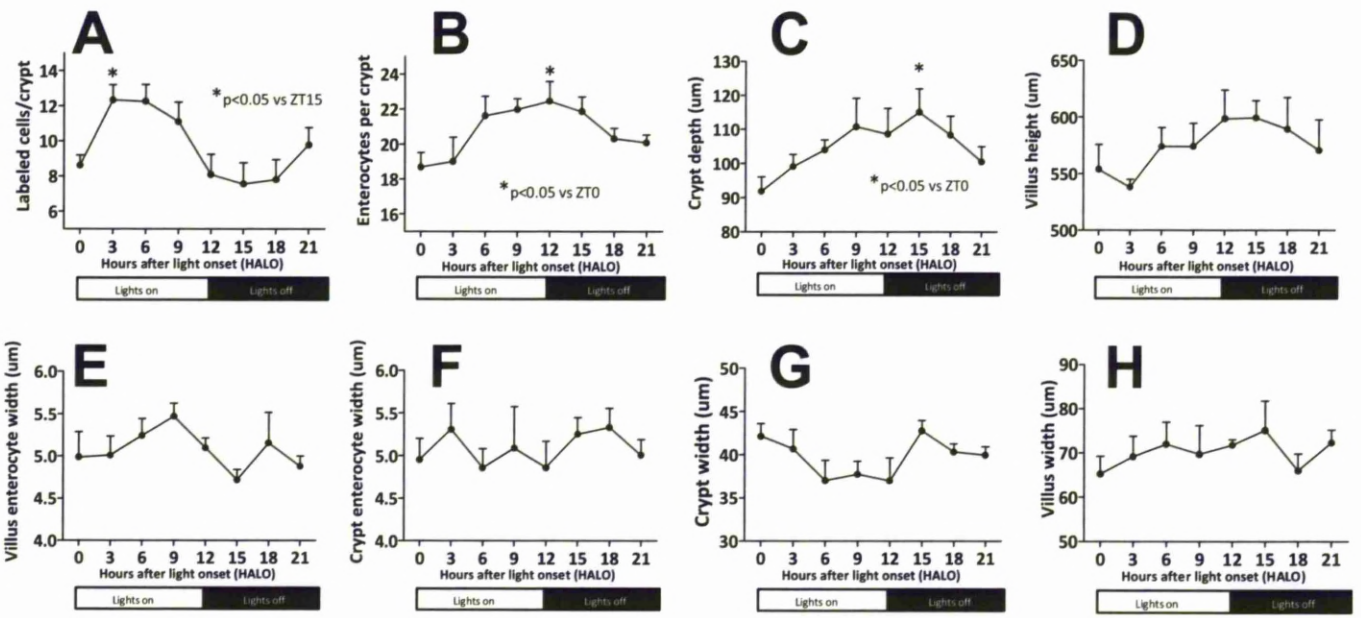

Figure 5.12: Temporal changes in intestinal DNA synthesis and morphologic parameters. Rats fed ad lib were culled at 3-hourly intervals (n=6-7 per time point) beginning at ZT 0 (7am). Sections of formalin-fixed jejunum were embedded in paraffin blocks, cut at 4μm thickness and stained with haematoxylin and eosin. For determination of cells in S-phase, sections were also stained with anti-BrdU primary antibody. DNA synthesis (as measured by the number of BrdU labelled cells per crypt, **A**), enterocyte number per crypt (**B**), crypt depth (**C**), villus height (**D**), villus enterocyte width (**E**), crypt enterocyte width (**F**), crypt width (**G**), villus width (**H**) were measured under light microscopy at 40-400x magnification. Five measurements were made per rat for each parameter. Measurements were only taken from sections displaying a single layer of enterocytes and villi with a visible central lacteal. Graphs show the mean and standard error for each timepoint. One-way ANOVA was used to identify significant differences between expression at individual timepoints.

Parameter	p value	Acrophase (ZT, h)	Fold change (peak/trough)	p value on ANOVA
BrdU	0.005	5	1.6	0.003
Enterocytes per crypt	0.001	12	1.2	0.014
Crypt depth	0.005	13	1.3	0.049
Villus height	0.043	14	1.1	0.480
Villus enterocyte width	0.217			0.408
Crypt enterocyte width	0.8			0.192
Crypt width	0.080			0.139
Villus width	0.610			0.806

Table 5.6: Rhythmicity in morphological parameters in diurnally harvested rat jejunum. The cosinor procedure[312] was used to determine the fit of the data to a cosinor curve with 24-hour periodicity and the acrophase (peak expression) for each gene displaying a significant 24-hour periodicity. The acrophase cannot be calculated for genes that do not display a significant fit to a 24-hour cosinor pattern. One-way ANOVA was used to identify significant differences between timepoints.

5.8. Discussion

Intestinal proliferation is known to exhibit a circadian rhythm, but the mechanisms underlying this have not been investigated. MicroRNAs are known to regulate proliferation in other tissues[18-24]. I hypothesized that microRNAs may therefore contribute to the regulation of circadian rhythms in intestinal proliferation. Prior to this study the temporal profile of microRNAs in the intestine and their role in the regulation of intestinal proliferation was unknown. To investigate this, I profiled microRNAs in the intestine of *ad libitum* fed rats using oligonucleotide arrays and identified a candidate microRNA that may regulate diurnal rhythmicity in intestinal proliferation from three microRNAs exhibiting diurnal rhythmicity. I further examined the effects of this microRNA on proliferation in an enterocyte cell line in vitro and identified the genes targeted by this microRNA in cultured enterocytes. Finally, I correlated rhythmicity in microRNA expression in vivo with rhythms in intestinal morphology and proliferation.

The data shown in this chapter have a number of novel key findings. Firstly, that the anti-proliferative microRNA *mir-16* is expressed in both crypt and villus enterocytes but exhibits diurnal rhythmicity only in the crypts. Secondly, that the cell cycle regulators CCND1, CCND2, CCND3, CCNE1 and CDK6 exhibit diurnal rhythmicity with a peak in expression which occurs in antiphase to *mir-16*. Thirdly, that *mir-16* has an anti-proliferative role in cultured enterocytes, as shown by its ability to inhibit proliferation and decrease the expression of genes involved in cell cycle regulation when over-

expressed in rat IEC-6 cells. My data therefore identifies *mir-16* as a potentially important microRNA in regulating diurnal rhythms in the intestine.

This study is the first to profile microRNA expression in rat jejunum as well as to establish rhythmic expression of specific microRNAs. Three microRNAs, *mir-16*, *mir-141* and *mir-20a* were found to exhibit 24-hour periodicity of expression in rat jejunum. All three microRNAs peaked at 4 to 6 hours after light onset, during the fasting period in ad libitum fed rats and reached their lowest levels of expression 18 hours after light onset during the lights off feeding period (Figure 5.2, Table 5.1). This suggests the possibility of regulation of the rhythmicity of microRNA expression by either light or nutrient availability, both factors which exhibit diurnal periodicity. Further studies dissecting the relationship between microRNAs and light and nutrient exposure, for instance with restricted feeding regimens, are necessary to adequately determine which of these factors influences microRNA rhythmicity in the intestine.

Previous studies have attempted to investigate the effect of circadian rhythmicity in microRNA expression, although not in the intestine. Circadian rhythmicity of microRNA expression has been shown by other groups to regulate cell behaviour and gene expression in tissues with known rhythmicity of function, such as the retina[203], the SCN[229] and the liver[17]. In the retina, 12 microRNAs display circadian rhythmicity, of which two – *mir-96* and *mir-182* – were shown to mediate rhythmic expression of the *Adcy6* (*adenylate cyclase type 6*) gene, which exhibited rhythmicity in antiphase to *mir-*

96 and *mir-182*[203]. Interestingly, the 1.8- to 3.2-fold amplitude changes observed in intestinal microRNAs in this study (Figure 5.2A-C) are consistent with the 1.25- to 3-fold changes observed in the retina[203, 229, 261]. Another microRNA shown to demonstrated transcriptional rhythmicity is *mir-122*; depletion of this microRNA in the liver disrupted the circadian rhythmicity of numerous transcripts regulating lipid metabolism[17, 372].

In mouse SCN, rhythmic expression of *mir-219* and *mir-132* mediates photic entrainment of circadian clock activity[229]. These microRNAs exhibited a 2-3 fold change in expression between peak and trough levels and displayed rhythmicity restricted to the SCN, with no rhythms observed in the adjacent cortex. The authors demonstrated further that these microRNAs were differentially regulated. A light pulse in the middle of the subjective night was able to reproduce the peak in expression of *mir-132*, but had no effect on *mir-219*. Inhibition of *mir-219* levels with antagomirs (microRNA inhibitors) resulted in lengthening of the circadian period as measured by wheel running activity[229]. Inhibition of *mir-132* levels with antagomirs had a different effect, producing inhibition of light-induced phase shifts in wheel running behaviour. These data suggest that *mir-219* regulates the length of the circadian period while *mir-132* acts as a negative regulator of light-induced resetting of the circadian clock. In the same study, *mir-132* or *mir-219* were each able to induce transcription of the clock gene PER1. The authors further demonstrated that co-expression of either *mir-132* or *mir-219* with known PER1 regulators CLOCK and BMAL1 resulted in a greater induction of *Per1* transcription than CLOCK and BMAL1 alone.

The above microRNAs which were found to exhibit circadian rhythmicity in other tissues were expressed in the intestine on our arrays, however none of these microRNAs met our criteria for qPCR validation from our array data and hence identification of rhythmicity of these microRNAs in the intestine was not attempted. Moreover, none of these previous studies had identified rhythmicity in *mir-16*. My data presented in this chapter is to date the first description of diurnal rhythmicity of *mir-16* expression and the first identification of a potential role for microRNAs in regulating the rhythmicity of intestinal proliferation.

Rhythmicity of *mir-16* expression was shown to be restricted to the crypts, the proliferative fraction in the intestine (Figure 5.3) and is consistent with my data showing that *mir-16* suppresses proliferation of intestinal crypt-derived cells in vitro (Figure 5.5). Of particular note, the level of *mir-16* in IEC-6 cells following *mir-16* overexpression produced a difference in expression similar to the degree of change observed on a diurnal basis in jejunum. This modest increase almost completely arrested growth in *mir-16* overexpressing IEC-6 cells (Figure 5.5) making this the first study to investigate and identify an anti-proliferative role for *mir-16* in untransformed cells and specifically in the small intestine. Previous studies have identified an anti-proliferative role for *mir-16* in other cell types[18-21, 373]. Bonci et al[373] identified a role for *mir-16* as a tumour suppressor gene in the prostate: *mir-16* is frequently downregulated in advanced prostate cancer and *mir-16* knockdown in prostate cancer cells promotes

proliferation and invasiveness. Similarly, *mir-16* expression is reduced in squamous cell carcinomas and adenocarcinomas of the lung[21] and *mir-16* overexpression in lung cancer cell lines induces cell cycle arrest[21]. Linsley et al[19] found a similar effect of *mir-16* in colorectal carcinoma cell lines (HCT116 and DLD-1 cells). All these cell types are cell lines derived from malignant tissues and hence each bears various mutations (such as the mutation of the Ras proto-oncogene in HCT 116 cells[19] and the mutation of p53 in DLD-1 cells[19]) which contribute to a pre-existing tumorigenic phenotype in these cells, making them different from untransformed cells. Previous characterization of IEC-6 has confirmed that these cells do not express any of the features of transformed cells[374] hence my data on the anti-proliferative function of *mir-16* in IEC-6 cells shows that *mir-16* serves an important physiological role in untransformed cells and may have a key regulatory role in enterocytes in vivo.

My studies do not show an effect of *mir-16* on apoptosis in IEC-6 cells (Figure 5.7). However, *mir-16* has been shown to increase apoptosis in leukaemic cell lines, gastric cancer cells and prostate cancer via downregulation of pro-survival protein BCL2 (B-cell lymphoma 2)[18, 370, 373, 375]. This apparent discrepancy between my observations and those of others may in fact be due to different properties of BCL2 pathways in the small intestine; although BCL2 is expressed in enterocytes, it may perform different functions in this tissue. Indeed, ablation of *Bcl2* in mice increases the apoptosis rate in the colon but not the small intestine[110, 111, 376].

The reduction in proliferation induced by *mir-16* overexpression in vitro was associated with suppressed expression of five key G1/S regulators—CCND1, CCND2, CCND3, CCNE1 and CDK6 (Figure 5.8, Table 5.2). In normal cell cycle progression, D-type cyclins (CCND1, CCND2 and CCND3) are synthesized during G1, in response to proliferative signals and complex with cyclin-dependent kinases (CDK4 and CDK6) [123, 124]. This results in the phosphorylation and inactivation of the retinoblastoma protein pRb. Loss of pRb function results in dissolution of complexes of pRb with members of the E2F transcription factor family and chromatin-modifying enzymes. This in turn activates cell cycle proteins vital for entering S-phase (including CCNE1 and the protein with which it forms a complex, CDK2) [123, 124]. The effects of the D cyclin/Cdk4/6 complexes is countered by INK4 CDK inhibitors, such as p16INK4a which, in conditions of cellular stress, blocks CDK4/6 activity, locking pRb in its active, antiproliferative state. The G2/M transition is regulated by levels of cyclins A and B (CCNA and CCNB) and cyclin-dependent kinase 1 (CDK1). CCNA and CCNB show progressive accumulation during the cell cycle, allowing entry into mitosis and then are abruptly degraded at the end of anaphase, resulting in exit of the cells from the stage of mitosis[125]. *mir-16* increased the proportion of cells in G1 but did not affect the G2/M transition in my studies (Figure 5.6). Similarly *mir-16* did not appear to play a role in the G2/M transition in the non-intestinal tissues studied by others[19, 21, 373] and in addition is not predicted to target either cyclins A or B or CDK1[371]. Together, this suggests that its effects on cell proliferation are specific to the G1/S stage of the cell cycle. In my studies, upregulation of *mir-16* expression suppressed expression of CCND1, CCND2, CCND3, CCNE1 and CDK6 *in vitro*, but downregulated the expression of each protein by only 50 to 70% (Figure 5.8, Table 5.2), thereby corroborating existing evidence that small changes in microRNA

expression alter cellular phenotypes by downregulating multiple components of single pathways[209, 366, 377].

Protein abundances of all five G1/S regulators presumably targeted by *mir-16* were found to exhibit diurnal rhythmicity in rat jejunum in antiphase to *mir-16* as shown in Figure 5.10 and summarized in Table 4.4. G1 proteins CCND1 and CCND2 peaked at ZT 12, at the same time as CCNE1, while the remaining D-type cyclin family member CCND3 peaked later at ZT 18 (Figure 5.10, Table 5.4). While this would appear to deviate from the traditionally described linear sequence of events in the cell cycle in which D cyclins would be expected to peak before CCNE1[123, 124], increasing evidence suggests that this linear sequence may not hold true in all tissues[122, 378, 379]. CCNE1 has been shown to substitute for deficiencies in D cyclin expression in vivo[378]. Mice deficient in all three D cyclins demonstrate normal intestinal development and normal development of all but the cardiovascular and haematopoietic system, suggesting that tissues can be divided into those dependent on or independent of D cyclin activity[379]. The simultaneous peak in both CCND1 and CCNE1 in my data is corroborated by a previous study investigating circadian expression of cyclin D1 and E in the human colon, showing a similar simultaneous peak in both cyclins[122]. To date, no studies have examined the temporal profile of cyclins in human small intestine; however as these sites undergo similar developmental and physiological processes, the pattern of cell cycle protein changes would be expected to be similar. Other studies have reported differences in the relative timing of D cyclins in various non-intestinal cell types, hence the different peaks in protein expression of cyclins D1 and D2 to that of cyclin D3 in this study (as shown in

Figure 5.10 and Table 5.4) may be a result of differential regulation and a degree of functional redundancy[380, 381]. Lack of transcriptional rhythmicity in vivo (Figure 5.11, Table 5.5) corroborated the lack of response of *Ccnd1* and *Ccne1* at an mRNA level to mir-16 overexpression in vitro. *Ccnd3* exhibited strong rhythmicity at a transcriptional level in vivo (Figure 5.11C) despite a lack of transcriptional responsiveness to *mir-16* overexpression in IEC-6 cells (Figure 5.8C) while in complete contrast, CDK6 did not display diurnal rhythmicity of transcription in vivo (Figure 5.11F) despite its transcriptional responsiveness to *mir-16* overexpression in IEC-6 cells (Figure 5.9F). The lack of significant transcriptional rhythmicity in *Ccnd1* and *Ccne1* expression (Figure 5.11) but the presence of significant rhythmicity of *Ccnd2* and *Ccnd3* expression (Figure 5.11) further highlights the possibility of differential regulation of the D cyclins in the intestine.

The acrophase of *mir-16* occurs at ZT 6, as indicated in Figure 5.2A and Table 5.1 and is coincident with the troughs in enterocyte number and crypt depth, as shown in Figure 5.12B-D. These coordinated responses point to *mir-16* as an important regulator of proliferation in jejunal crypts. This function may be essential to coordinate intestinal circadian rhythms, serving to optimally match proliferation and absorptive capacity with nutrient availability. My data showed peak S-phase to occur at ZT 3 (Figure 5.12A, Table 5.6), indicating a G1/S duration of approximately 10 to 15 hours, in agreement with previous studies showing a long G1/S and short G2/M period in the small intestine[382-384]. The degree of change in cell labelling observed at ZT 3 vs. ZT 15 (63%, Figure

5.12A) is also similar to the 30-60% increase at ZT 3 in murine jejunum reported by Scheving et al[112, 117].

My data show that *mir-16* is able to affect translation of CCND1, CCND3 and CCNE1 without affecting mRNA expression, as demonstrated in Figures 5.8 and 5.9, corroborating previous data showing microRNAs are able to suppress protein levels independent of mRNA expression[209]. This was also demonstrated by my findings in vivo; CCND1 and CCNE1 showed rhythmicity only at the protein level (Figure 5.10). This is in keeping with previous data by Reddy et al[260] showing that almost half of the proteins demonstrating circadian rhythmicity in the mouse liver lack a corresponding cycling transcript. The rhythmicity in CCND1 and CCNE1 does not appear to be initiated at the transcriptional level in rat jejunum (Figure 5.11) and my findings suggest the possibility that the rhythmic protein expression of these two genes in the jejunum in my study as noted in Figure 5.8 may be produced solely by miRNAs, whether by *mir-16* alone or in combination with others. Cell-type specificity of the rhythmicity of *mir-16* itself, such as seen in the intestinal crypts in my study (Figure 5.3), would then lead to consequent rhythmicity of target proteins.

The amplitude of change in protein and mRNA expression of each these genes in my diurnal studies is rather modest, ranging from a 2.3 to 4.4 fold diurnal change in protein expression and a 2.3 to 2.8 fold change (where present) in mRNA expression (Figures 5.10 and 5.11 respectively). Similarly the reduction in protein and mRNA expression

following microRNA overexpression was equally modest, ranging from a 2 to 3-fold reduction in protein expression compared to controls and for some genes, 2.5 to 5 fold reduction in mRNA expression compared to controls (Figures 5.8 and 5.9 respectively). These findings are in keeping with data from Baek et al[209], who demonstrated that proteins were only repressed to 0.8 fold of the levels of controls by each microRNA in vitro. mRNA expression was even less repressed, with a mean decrease in expression to 0.9 fold of the level of controls. Similar effects were demonstrated on deleting a single microRNA in vivo – target protein expression was increased by 1.2 fold and target mRNA expression by 1.1 fold[209]. In the abovementioned study each microRNA was able to repress hundreds of target genes, with consistently greater effects on protein expression compared to mRNA expression. The authors further noted that the more highly repressed proteins were more likely to exhibit repression at the transcriptional level[209]. This is in keeping with the data from my study; 3 of the 4 proteins exhibiting the greatest peak-trough fold-change in rat jejunum exhibited rhythmicity at the mRNA level as well. Such a correlation was not as clear in vitro in the effects of mir-16 on protein and mRNA expression in IEC-6 cells. Only 2 of the 5 proteins repressed at a protein level exhibited repression at the mRNA level in vitro. This discrepancy may be a reflection of the presence of additional factors in vivo that may also play a role in the regulation of rhythmicity. One example is humoral regulation of the cell cycle[128, 385, 386], for instance by corticosteroids. Cortisol has been previously described to suppress enterocyte proliferation in vivo as well as in vitro and cortisol levels are known to exhibit diurnal rhythmicity in vivo[128, 385, 386]. The superimposition of rhythmicity in cortisol expression on to the rhythmicity of mir-16 in vivo but lack of rhythmicity in cortisol in

vitro may be one cause of the discrepancy in findings between my in vivo and in vitro data.

Other factors may also be mediating this discrepancy between protein and mRNA rhythmicity in vivo. Regulation of gene expression by microRNAs is a complex process, with the potential for each to target many related or unrelated genes and for responsive genes to be regulated by multiple microRNAs. As such, *mir-16* may not be the only potential microRNA regulating diurnal rhythms in cell cycle genes. Several other microRNAs are known to affect target proteins involved in the cell cycle. Overexpression of *mir-34a* suppresses E2F1 and E2F3, members of the E2F signalling pathway, in colon cancer cell lines, arresting cell proliferation[387]. *mir-192* and *mir-215* also had a negative effect on proliferation, arresting colon cancer cells in G1[388]. In contrast, *mir-106b* and *mir-221* accelerate G1/S progression by suppressing the cyclin-dependent kinase inhibitors p21 and p27, respectively[389, 390]. As none of these microRNAs met the criteria for PCR validation (sequence conservation and a two-fold change or greater between timepoints on microarrays), they were not investigated further in my studies. There is therefore insufficient evidence to speculate as to whether these microRNAs might play a role in regulating the circadian rhythmicity in proliferation in the rat jejunum, however the possibility that they might act to regulate proliferation along with *mir-16* despite a presumed lack of rhythmicity cannot be excluded.

Factors other than microRNAs are also clearly important in cuing the intestinal proliferation rhythm. Members of the clock gene family have been shown to regulate rhythmicity of genes involved in proliferation[391-393]. For instance, *mPer2* deficient mice exhibit deregulation of the temporal expression of cell cycle genes c-*Myc, Cyclin A, Mdm-2* and *Gadd45*α[391]. Both PER and CRY have been found to indirectly regulate cyclin D1 expression in vivo[342, 393] – this is likely to occur via transcriptional regulation of the clock-controlled gene *c-myc*, which is a regulator of cyclin D1, but to date has not been found to affect expression of the other G1/S regulators examined in this study.

Although microRNAs are particularly well known for their ability to dissociate protein expression from mRNA expression, other genes may also be responsible for the regulation of post-transcriptional rhythmicity of gene expression. In this study cyclin D1 exhibited rhythmicity at the protein level but not at the transcriptional level. The protein SNIP1 has been found to play a role specifically in the post-transcriptional regulation of cyclin D1 via regulation of mRNA stability as the absence of SNIP1 destabilizes cyclin D1 mRNA and results in its premature degradation [394], making SNIP1 a potential candidate for non-microRNA mediated regulation of post-transcriptional rhythmicity. A further candidate for the post-transcriptional regulation of cell cycle gene rhythmicity is Skp1-Cdc53/Cul1-F-box (SCF) protein SCF^{hCDC4} which mediates the ubiquitination and degradation of cyclin E1[395], another *mir-16* target which, as shown in Figure 5.10 and 5.11, demonstrates post-transcriptional but not transcriptional rhythmicity on a circadian basis. To date the presence of any circadian rhythmicity in SNIP1 or SCF^{hCDC4}

expression in the intestine that might contribute to the observed post-transcriptional circadian rhythmicity of cell cycle gene expression is unknown.

Ultimately, proliferation and cell cycle rhythms may be a result of combined inputs of circadian clock components, post-transcriptional regulators, other transcription factors and rhythmic microRNAs. This potentially multifactorial regulation of circadian rhythmicity may explain, amongst the other observations described above, rhythmicity in CDK4 (Figure 5.10), a cell cycle gene shown not to be regulated by *mir-16* in vitro (Figure 5.8 and 5.9) and the lack of transcriptional rhythmicity in *Cdk6* in vivo (Figure 5.11) despite responsiveness to *mir-16* overexpression in vitro (Figure 5.8 and 5.9). Generation of knockout mice lacking *mir-16* will be invaluable in defining its functions and dissecting these regulatory pathways.

Finally, a broader implication can be drawn from these findings. The temporal expression profile of *mir-16* in vivo and its suppression of cell proliferation in vitro highlight microRNA-mediated gene silencing as another potential route for linking proliferation to nutrient availability, which cues the intestinal rhythms. Rhythmic *mir-16* expression in crypt cells could be initiated by luminal nutrients directly or via neuro-hormonal pathways. In either case, proliferation may be a key early component to expand the mucosal surface area in the anticipatory diurnal increases in absorptive capacities for glucose, peptides and other nutrients[69, 70].

In summary, the studies in this chapter show for the first time rhythmicity of microRNA expression in the intestine and anti-proliferative effects of the diurnally expressed *mir-16* in untransformed enterocytes *in vitro*. My findings here lead me to hypothesize that rhythmicity of *mir-16* in jejunum may act to mediate the rhythmicity in intestinal proliferation and coordinate the proliferative response with nutrient availability to optimize intestinal absorption and function.

Chapter 6: Conclusions

Short bowel syndrome is a clinical condition that results from the loss of a large proportion of functioning intestine[2, 396]. The absorptive capacity of the remnant intestine fails to meet the individual's nutritional needs, requiring supplementation of nutrients by the parenteral route[2, 396]. This condition therefore remains one of high morbidity and mortality[2]. Current treatments involve lifelong intravenous feeding[396] or intestinal transplantation[397], management options which are associated with significant side-effects including the risk of death. There is therefore a great need for alternative therapies for short bowel syndrome and the work from our laboratory aims to address this. To identify better management options for short bowel syndrome we chose to investigate the molecular pathways governing the important physiological phenomenon of diurnal rhythmicity in intestinal absorption, which allows upregulation of intestinal absorptive capacity to match nutrient availability.

Rhythmicity in nutrient absorption by the rat intestine occurs with a 24-hour periodicity, with peak absorption occurring at the time of maximal nutrient delivery[12]. This is facilitated by rhythmicity of intestinal proliferation and various morphological parameters such as crypt depth and enterocyte number [112, 307], thereby increasing the intestinal surface area available for absorption of vital nutrients and matching nutrient availability to absorptive capacity. Superimposed on this background of rhythms in intestinal proliferation is the specific rhythmicity of expression of selected intestinal genes; work by our group[13, 63, 69] and others[398, 399] have shown diurnal rhythmicity in the expression of specific key nutrient transporters, specifically SGLT1,

but a lack of rhythmicity in the expression of certain other genes[71]. This suggests that separate molecular pathways may mediate the rhythms in intestinal proliferation and the specific rhythmicity of individual gene expression. Analysis of the current literature suggested the possible existence of distinct regulatory mechanisms mediating the rhythmicity of intestinal absorption. microRNAs, a newly discovered class of endogenous gene silencers, have been shown to play a role in the simultaneous silencing of many genes. These molecules have been shown to regulate rhythmicity of hepatic genes[17] and mediate the proliferative response in other tissues[19, 21, 373, 387-390]. On the other hand, clock genes, circadian molecular feedback loops, have been shown to regulate the expression of individual transporters such as MDR1 and PEPT1 in the intestine[15, 16] and of NHE3 in the kidney[14]. I therefore hypothesized that rhythmicity in intestinal absorption may be a result of clock-gene mediated regulation of rhythmicity of SGLT1 expression superimposed on a background of microRNA-mediated regulation of circadian rhythmicity of intestinal proliferation.

A major aim of this thesis was to correlate rhythms in *Sglt1* expression with rhythms in clock gene expression and identify clock genes that might act as potential transcriptional regulators of *Sglt1* using in vitro studies. My studies show diurnal rhythmicity of the expression of clock genes *Clock*, *Bmal1*, *Per1*, *Per2*, *Cry1*, *Cry2*, *ReverbA* and *ReverbB* as well as *Sglt1* in the jejunum of rats harvested at diurnal timepoints (Figure 3.2, Table 3.1). The shift in the temporal expression of the clock genes (Figure 3.6, Table 3.2) as well as SGLT1 (Figure 3.7, Tables 3.2) in the jejunum of rats with nutrient availability restricted to only the lights-on period shows nutrients to be a strong cue of rhythmicity in the intestine. PER1 in particular was found to shift in phase with *Sglt1* expression in

these rats (Figure 3.11, Table 3.3). I therefore postulated that PER1 might act as a transcriptional regulator of *Sglt1* and chose PER1 for further in vitro studies to investigate this.

My subsequent studies using knockdown of PER1 in Caco-2 enterocytes showed that PER1 downregulates *SGLT1* in vitro (Figure 4.3, Table 4.2) without altering the expression of *Clock*, *Bmal1*, *Per2*, *Cry1*, *Cry2 ReverbA* or *ReverbB* (Figure 4.5, Table 4.3). Promoter studies using the human *SGLT1* promoter and PER1 overexpression vectors in the non-enterocytic CHO cell line showed that PER1 acted via the proximal 1kb of the *SGLT1* promoter (Figure 4.9, Table 4.5). E-boxes are consensus binding sites for various transcription factors including clock genes; 4 E-box sites were found on the proximal 1kb of the *SGLT1* promoter (Figure 4.6). Mutation of these E-box sites on the *SGLT1* promoter increased *SGLT1* promoter activity, suggesting that E-box sites mediated a suppressive effect on the *SGLT1* promoter (Figure 4.10, Table 4.6). Introduction of the PER1 overexpression vector suppressed *SGLT1* promoter activity despite mutation of E-boxes, indicating that the actions of PER1 on *SGLT1* are independent of E-boxes (Figure 4.11, Table 4.8) and likely to occur via other binding sites on the *SGLT1* promoter. Moreover E-boxes themselves are likely to mediate rhythmicity in SGLT1 promoter activity via other rhythmic genes such as clock-controlled genes, known to mediate rhythmicity of other intestinal genes[16]. The above findings, detailed in Chapters 3 and 4, are shown as a schematic in Figure 6.1. These new insights into the regulation of SGLT1 by clock genes suggest that manipulation of clock gene expression may facilitate modulation of SGLT1-mediated glucose absorption for the management of short bowel syndrome.

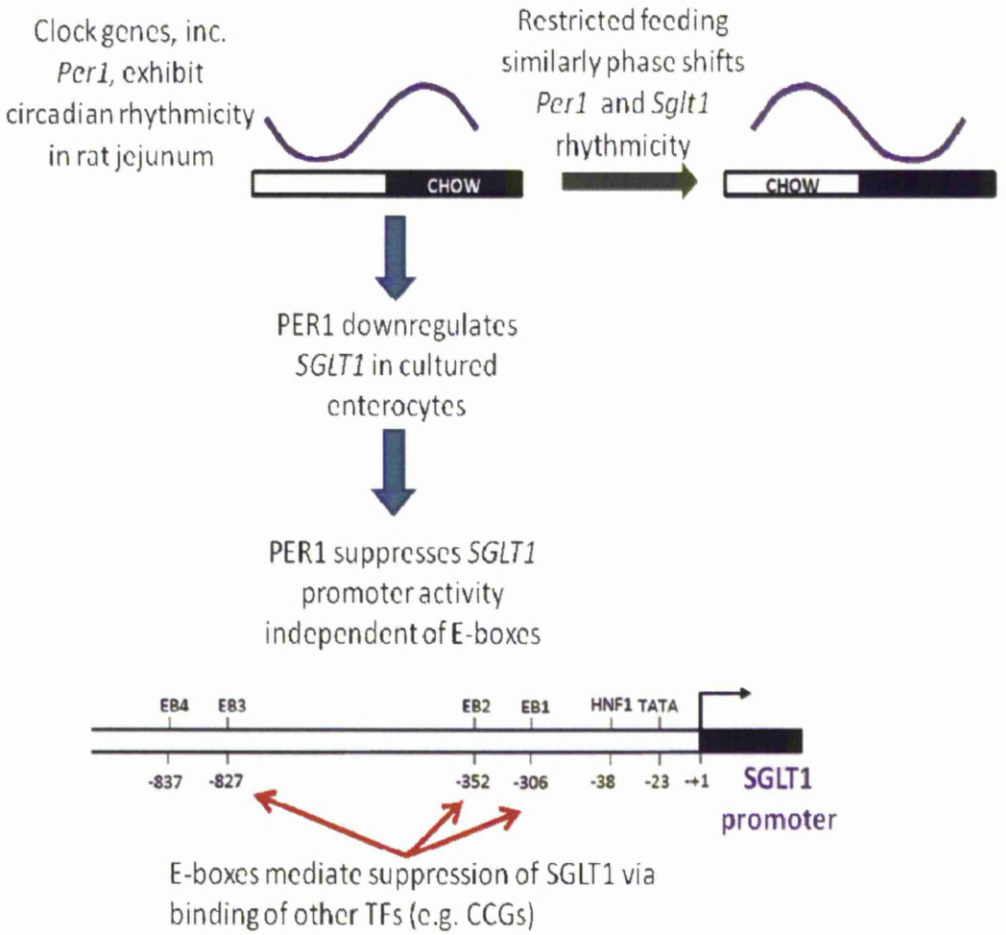

Figure 6.1: Interaction of clock genes and *SGLT1*.A schematic of my data (detailed in Chapters 3 and 4) demonstrating rhythmicity of clock gene and Sglt1 expression in vivo and suppression of SGLT1 by PER1 in vitro. TF=transcription factor, CCG=clock-controlled gene.

Another major aim of this thesis was to identify microRNAs exhibiting diurnal rhythmicity in expression in the intestine and correlate rhythmicity in microRNA expression with rhythms in morphology and proliferation in vivo. In my studies, levels of *mir-16*, *mir-20a* and *mir-141* were found to oscillate with a 24-hour periodicity in the jejunum of ad libitum fed rats (Figure 5.2, Table 5.1.), identifying for the first time

diurnal rhythmicity in intestinal microRNA expression. The decrease in expression of *mir-16* during the late light phase (Figure 5.2A, Table 5.1), coinciding with the peak in morphological parameters such as crypt depth, number of enterocytes per crypt and the proliferation marker BrDU in the intestine (Figure 5.12, Table 5.6) and in keeping with its known anti-proliferative function in other tissues[18-21], meant that *mir-16* was chosen for further investigation.

A further aim of this thesis was to subsequently determine the effects of these microRNAs on enterocyte proliferation in vitro. My proposal that *mir-16* might regulate intestinal proliferation is supported by my data showing significantly higher levels of *mir-16* in LCM-captured crypts of rats harvested at ZT 6 compared to ZT 18 (Figure 5.3), indicating diurnal rhythmicity of *mir-16* in the crypt fraction, the site of proliferation in the intestine. Loss of *mir-16* was found to suppress expression of the cell cycle regulators CCND1, CCND2, CCND3, CCNE1 and CDK6 in crypt-derived IEC-6 cells (Figure 5.8, Table 5.2), thereby inhibiting proliferation and inducing G1 arrest (Figures 5.6 and 5.5). Measurement of the temporal profile of morphological parameters in rat jejunum showed diurnal rhythmicity of crypt depth, villus height and number of enterocytes per crypt (Figure 5.10, Table 5.4), all of which oscillated in antiphase to the temporal expression of *mir-16* (Figure 5.2, Table 5.1). My data therefore identifies *mir-16* as a potentially important microRNA in regulating diurnal rhythms in intestinal proliferation. The findings of Chapter 5 are summarised in the schematic shown in Figure 6.2, highlighting microRNAs as potential targets in the modulation of intestinal proliferation and thereby the development of new treatments for short bowel syndrome.

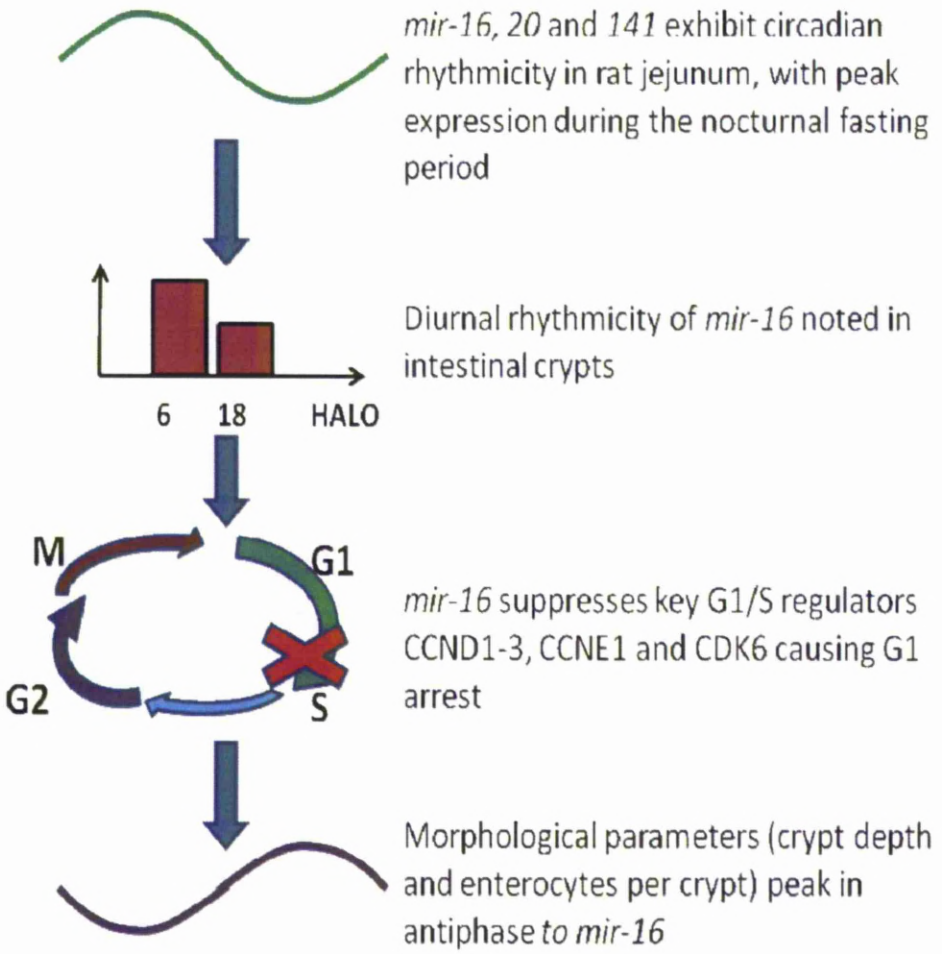

Figure 6.2: Effects of *mir-16* on intestinal proliferation. A schematic of my data (detailed in Chapter 5) highlighting the postulated role of *mir-16* in regulation of intestinal proliferation.

My findings therefore support my hypothesis that several independent molecular regulatory pathways may contribute to the known rhythmicity in intestinal absorption (Figure 6.3). MicroRNAs, such as *mir-16,* may have a role in regulating the rhythmicity in intestinal proliferation, thereby increasing intestinal surface area to match absorptive capacity to the times of peak nutrient delivery. In contrast clock genes, such as PER1,

may act on individual genes, upregulating the expression of key transporters during maximal nutrient availability to further increase the absorptive capabilities of the intestine.

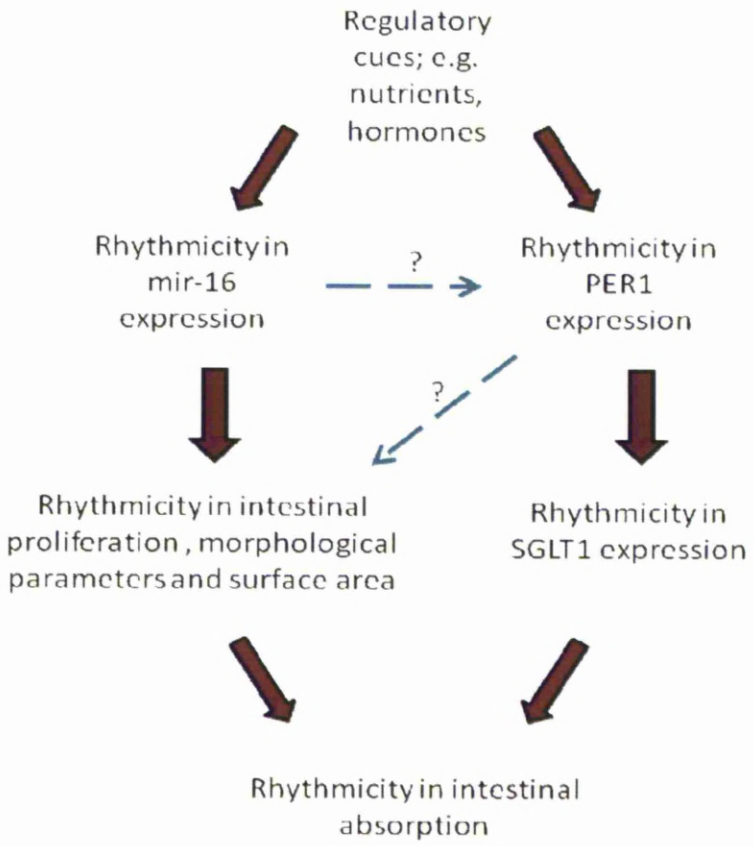

Figure 6.3: Schematic showing the proposed regulatory mechanisms contributing to the rhythmicity in intestinal absorption. The filled arrows show the regulatory pathways that have been investigated in my studies and proposed as potential regulatory mechanisms behind rhythms in intestinal absorption. The dashed arrows suggest possible alternative or additional regulatory pathways that have not been investigated in these studies.

The existence of separate molecular pathways regulating rhythmicity of intestinal proliferation and regulating rhythmicity of individual transporters may represent a

means of conservation of energy by the organism. While rhythmicity in intestinal proliferation contributes to an overall increase in absorptive capacity, regulation of individual transporters on the other hand allows additional specific upregulation of transporters required for nutrient absorption, minimizing the energy wastage that would accompany simultaneous upregulation of all transporters regardless of function. The existence of distinct regulatory pathways allows unique peaks in transporter expression, temporally distinct from the peak in global increase in absorptive capacity that would be expected to accompany the peak in morphological parameters. One example of this can be found in the rhythmicity exhibited by intestinal drug transporters, shown in previous studies from our laboratory[71]. A select number of drug transporters in the jejunum (*Mdr1*, monocarboxylate transporter *Mct1*, multidrug resistance protein *Mrp2* and breast cancer resistance protein *Bcrp*) were found to show peak expressions occurring out of sync with the time of peak morphological parameters. This difference is likely related to the role of drug transporters which control drug efflux[73, 400] rather than nutrient absorption. Clock genes have been shown to play a role in the regulation of the rhythmicity of at least one of these drug transporters, MDR1[15]. The separate regulation of the rhythmicity of these drug transporters by clock genes allows modulation of the time of peak expression and matches the time of peak expression to the more relevant parameter of peak drug metabolite concentration in the intestine.

Although the proposal that rhythmicity of intestinal proliferation is regulated by a pathway distinct and separate to that regulating rhythmicity in transporter expression is attractive, to date there are insufficient data to completely exclude overlapping roles of

each of these molecular regulatory pathways; for instance clock genes may also play a role in the regulation of intestinal proliferation and similarly microRNAs may regulate the expression of individual transporters. Deciphering the interactions of these regulatory mechanisms may allow new insights into the understanding of physiological rhythmicity of intestinal absorption and therapies targeting one or both of these pathways and may hence contribute to developing new treatments to upregulate intestinal absorption in short bowel syndrome.

While the role of clock genes in regulation of rhythmicity of intestinal proliferation has not previously been studied, recent data has identified a role for clock genes in the regulation of tumorigenesis in the small intestine and colon[401]. Downregulation of PER2 was found to increase cell proliferation in colon cancer cell lines via upregulation of cyclin D1 and β-catenin[401]. Similarly, expression of β-catenin and cyclin D1 was increased in the small intestine and colon of *Per2-/-* mice. Loss of PER2 also accelerated tumorigenesis as measured by the rate of polyp formation in the small intestine of $Apc^{Min/+}$ mice[401]. Clock genes have been found to regulate proliferation in other tissues besides the intestine; for instance the circadian clock mediates tumorigenesis in a breast cancer model in vitro[402]. Depletion of PER1 and PER2 enhanced tumour growth in implanted breast cancer cells in a circadian manner, with the greatest enhancement noted at the time of physiological peak in PER1 and PER2 expression[402]. BMAL1 has been shown to indirectly suppress expression of the cell cycle inhibitor p21 via ROR response elements on the p21 promoter[403]. Consistent with these in vitro findings, hepatocyte proliferation was impaired in *Bmal1-/-* mice[403]. *Clock* has been

shown to be pro-proliferative; cell-cycle inhibitory genes (e.g., p21, p27, Chk1, Chk2 and Atr1) were up-regulated while proproliferative genes (e.g., Jak2, ERα, Pbef, Akt1, Cdk2, cyclins D3 and E1) were down-regulated in the liver of *Clock-/-* mice, concomitant with a lack of proliferation of cultured fibroblasts from *Clock-/-* mutant mice [404]. These studies suggest that the possibility that clock genes may also contribute at least in part to the regulation of proliferation in the intestine cannot be discounted.

To determine whether microRNAs may play a role in the specific regulation of SGLT1 in addition to regulating intestinal proliferation, I analysed the 3'UTR of SGLT1 for the presence of complimentary binding sites to any of the three validated rhythmically expressed microRNAs – *mir-16*, *mir-20a* and *mir-141* - using the microRNA target prediction algorithm Targetscan, freely available at www.targetscan.org (accessed on 29th August 2008)[206]. There were no complementary sites for any of the three rhythmic microRNAs on the SGLT1 3'UTR. Furthermore there were no microRNA binding sites conserved across mammalian species for any microRNA on the 3'UTR of SGLT1. While a number of non-conserved sites were identified, these have been suggested to represent sites of reduced evolutionary significance and are considered therefore to be of reduced biological importance[405], making it less likely that microRNAs might play a role in the regulation of the rhythmicity of SGLT1.

While the data in Chapters 3-5 suggest that both clock genes and microRNAs may contribute to the regulation of rhythmicity of intestinal absorption, the relationship between intestinal clock genes and intestinal microRNAs has not been explored in my

studies. However several examples of microRNA-clock gene interactions exist in the literature[17, 229, 406, 407]. *miR-132* and *miR-219* display circadian rhythmicity in murine brain[229], with up to a 3-fold difference in microRNA levels between subjective day and night. Two other miRNAs examined in this study, *miR-16* and *miR-128a*, exhibited no significant change in expression over a diurnal cycle, suggesting that the rhythmicity noted in *miR-219* and *miR-132* expression was unique to these microRNAs and not a simple reflection of oscillation in the microRNA-processing machinery. *mir-132* or *mir-219* indirectly stimulated *Per1* promoter activity in vitro, acting synergistically with each other and with increased effect in the presence of CLOCK and BMALI[229]. Circadian rhythmicity of *mir-219* was obliterated upon genetic deletion of the clock components *Cry1* and *Cry2*, indicating that the circadian rhythmicity of these microRNAs is dependent on the molecular clock[229]. Functional experiments using wheel-running activity revealed a role for *miR-219* in modulating circadian period length, as reduction of *miR-219* levels using antisense microRNA increased period length in mice[229]. *miR-132* expression was stimulated by light and in turn was found to mediate the phase-shifting capacity of light[229]. Subsequent analysis of *miR-219* and *miR-132* targets revealed circadian oscillation of these transcripts in mouse brain. In vitro experiments showed that *miR-219* and *miR-132* acted synergistically to increase *Per1* transcription, further confirming a role for these microRNAs in modulation of the circadian clock[229].

Recently the primary transcript of *miR-122*, the most abundant microRNA in the liver, was shown to exhibit circadian rhythmicity in wild-type mice; this was lost in *ReverbA* null mice[17]. The authors further demonstrated that depletion of *miR-122* levels with

antisense oligonucleotides selectively dysregulated the expression of transcripts known to exhibit circadian rhythmicity[17].

The *mir-192/194* cluster in turn suppresses PER1-3 expression[406] in colon cancer cell lines. The known high expression of *miR-192* and *miR-194* in the liver and kidney[408, 409], tissues capable of rhythmicity in clock gene expression independent of the SCN, suggests that these microRNAs may play a role in maintaining tissue-autonomous clock gene expression. At present the pattern of expression of these microRNAs in these tissues remains unknown. In recent studies Kadener et al[407] identified a role for the Drosophila microRNA *bantam* as a regulator of the clock gene *clk*. *Bantam* is highly expressed in circadian cells in Drosophila and suppresses *clk* via evolutionarily conserved sites on the 3'UTR of the *clk* gene, which are essential for maintenance of circadian rhythmicity of *clk*. Both *bantam* and *clk* exhibited circadian rhythmicity, and overexpression of bantam delayed the circadian clock by 3 hours at both a molecular and behavioural level[407].

The relationship between *mir-16* and clock genes has yet to be explored. This is in great part due to the difficulty in accurately establishing the site of the promoter, which has been found in microRNAs to range from a few kb to up to 50kb upstream of the microRNA sequence[410], hence requiring further studies to define the *mir-16* promoter before the use of conventional promoter assays to assess the role of clock genes as transcriptional regulators of *mir-16*.

Although my data suggest a role for clock genes and microRNAs in regulating the rhythmicity of intestinal absorption, accurately identifying the contribution of each of these molecular pathways and delineating any areas of overlap of their suggested functions would require the use of knockout mice. Loss of *mir-16* in vivo would be expected to blunt the rhythmicity of intestinal proliferation, but may also reveal unexpected effects on individual intestinal transporters and on the rhythmicity of clock genes themselves. Similarly loss of PER1 in vivo would be expected to blunt rhythmicity in SGLT1 expression, but may unexpectedly reveal blunting of microRNA rhythmicity or intestinal proliferation. Both *mir-16* and PER1 are expressed ubiquitously in both rodents and humans, necessitating the creation of mice bearing intestine-specific deletion of these genes to exclude confounding effects of loss of expression in other tissues. At present such mice do not exist, hence these remain aims for future studies.

My data suggest that rhythmicity in intestinal absorption may be mediated by at least two molecular pathways, circadian clock genes and microRNAs (Figure 6.1). These studies add new insights into our understanding of the factors mediating these physiological rhythms in absorption. The interaction between the microRNA and clock-gene mediated gene regulatory pathways remains an important subject for future studies, however my findings are an essential first step in attempts to develop new therapies for conditions of insufficient absorption such as short bowel syndrome.

REFERENCES:

1 Sinnathamby C. *Last's Anatomy*: Churchill Livingstone, Elsevier 2005.

2 Buchman AL. Etiology and initial management of short bowel syndrome. *Gastroenterology* 2006;**130**:S5-S15.

3 Moore KL. *Clinically Oriented Anatomy*: Lippincott Williams and Wilkins 2009.

4 Barker N, van de Wetering M, Clevers H. The intestinal stem cell. *Genes Dev* 2008;**22**:1856-64.

5 Sancho E, Batlle E, Clevers H. Live and let die in the intestinal epithelium. *Current opinion in cell biology* 2003;**15**:763-70.

6 Hober. *Pflugers Arch* 1898;**70**.

7 Goldschmidt. *Physiol Reviews* 1921;**1**.

8 Cushny Wa. *The American journal of physiology* 1898;**1**.

9 Hewitt JA. The Metabolism of Carbohydrates. Part III: The Absorption of Glucose, Fructose and Galactose from the Small Intestine. *The Biochemical journal* 1924;**18**:161-70.

10 Crane RK. Na+ -dependent transport in the intestine and other animal tissues. *Federation proceedings* 1965;**24**:1000-6.

11 Wright EM, Martin MG, Turk E. Intestinal absorption in health and disease--sugars. *Best practice & research* 2003;**17**:943-56.

12 Fisher RB, Gardner ML. A diurnal rhythm in the absorption of glucose and water by isolated rat small intestine. *The Journal of physiology* 1976;**254**:821-5.

13 Tavakkolizadeh A, Berger UV, Shen KR, *et al.* Diurnal rhythmicity in intestinal SGLT-1 function, V(max), and mRNA expression topography. *Am J Physiol Gastrointest Liver Physiol* 2001;**280**:G209-15.

14 Rohman SM, Emoto N., Nonaka, H., Okura, R., Nishimura, M., Yagita, K., van der Horst, G.T.,, Matsuo M, Okamura, H., and Yokoyama, M. Circadian clock genes directly regulate expression of the Na(+)/H(+) exchanger NHE3 in the kidney. *Kidney International* 2005;**67**:1410-9.

15 Murakami Y, Higashi Y, Matsunaga N, *et al.* Circadian clock-controlled intestinal expression of the multidrug-resistance gene mdr1a in mice. *Gastroenterology* 2008;**135**:1636-44 e3.

16 Saito H, Terada T, Shimakura J, *et al.* Regulatory mechanism governing the diurnal rhythm of intestinal H+/peptide cotransporter 1 (PEPT1). *Am J Physiol Gastrointest Liver Physiol* 2008;**295**:G395-402.

17 Gatfield D, Le Martelot G, Vejnar CE, *et al.* Integration of microRNA miR-122 in hepatic circadian gene expression. *Genes Dev* 2009;**23**:1313-26.

18 Cimmino A, Calin GA, Fabbri M, *et al.* miR-15 and miR-16 induce apoptosis by targeting BCL2. *Proceedings of the National Academy of Sciences of the United States of America* 2005;**102**:13944-9.

19 Linsley PS, Schelter J, Burchard J, *et al.* Transcripts targeted by the microRNA-16 family cooperatively regulate cell cycle progression. *Molecular and cellular biology* 2007;**27**:2240-52.

20 Liu Q, Fu H, Sun F, *et al.* miR-16 family induces cell cycle arrest by regulating multiple cell cycle genes. *Nucleic acids research* 2008;**36**:5391-404.

21 Bandi N, Zbinden S, Gugger M, *et al.* miR-15a and miR-16 are implicated in cell cycle regulation in a Rb-dependent manner and are frequently deleted or down-regulated in non-small cell lung cancer. *Cancer research* 2009;**69**:5553-9.
22 Xiao C, Srinivasan L, Calado DP, *et al.* Lymphoproliferative disease and autoimmunity in mice with increased miR-17-92 expression in lymphocytes. *Nature immunology* 2008;**9**:405-14.
23 Ventura A, Young AG, Winslow MM, *et al.* Targeted deletion reveals essential and overlapping functions of the miR-17 through 92 family of miRNA clusters. *Cell* 2008;**132**:875-86.
24 Inomata M, Tagawa H, Guo YM, *et al.* MicroRNA-17-92 down-regulates expression of distinct targets in different B-cell lymphoma subtypes. *Blood* 2009;**113**:396-402.
25 Fisher RB. The absorption of water and of some small solute molecules from the isolated small intestine of the rat. *The Journal of physiology* 1955;**130**:655-64.
26 Newey H, Parsons BJ, Smyth DH. The site of action of phlorrhizin in inhibiting intestinal absorption of glucose. *The Journal of physiology* 1959;**148**:83-92.
27 Semenza G, Kessler M, Hosang M, *et al.* Biochemistry of the Na+, D-glucose cotransporter of the small-intestinal brush-border membrane. The state of the art in 1984. *Biochimica et biophysica acta* 1984;**779**:343-79.
28 Mircheff AK, Wright EM. Analytical isolation of plasma membranes of intestinal epithelial cells: identification of Na, K-ATPase rich membranes and the distribution of enzyme activities. *The Journal of membrane biology* 1976;**28**:309-33.
29 Loo DD, Wright EM, Zeuthen T. Water pumps. *The Journal of physiology* 2002;**542**:53-60.
30 Hirschhorn N, McCarthy BJ, Ranney B, *et al.* Ad libitum oral glucose-electrolyte therapy for acute diarrhea in Apache children. *The Journal of pediatrics* 1973;**83**:562-71.
31 Martin MG, Wang J, Solorzano-Vargas RS, *et al.* Regulation of the human Na(+)-glucose cotransporter gene, SGLT1, by HNF-1 and Sp1. *Am J Physiol Gastrointest Liver Physiol* 2000;**278**:G591-603.
32 Krasinski SD, Van Wering HM, Tannemaat MR, *et al.* Differential activation of intestinal gene promoters: functional interactions between GATA-5 and HNF-1 alpha. *Am J Physiol Gastrointest Liver Physiol* 2001;**281**:G69-84.
33 van Wering HM, Huibregtse IL, van der Zwan SM, *et al.* Physical interaction between GATA-5 and hepatocyte nuclear factor-1alpha results in synergistic activation of the human lactase-phlorizin hydrolase promoter. *The Journal of biological chemistry* 2002;**277**:27659-67.
34 Pontoglio M, Barra J, Hadchouel M, *et al.* Hepatocyte nuclear factor 1 inactivation results in hepatic dysfunction, phenylketonuria, and renal Fanconi syndrome. *Cell* 1996;**84**:575-85.
35 Dukes ID, Sreenan S, Roe MW, *et al.* Defective pancreatic beta-cell glycolytic signaling in hepatocyte nuclear factor-1alpha-deficient mice. *J Biol Chem* 1998;**273**:24457-64.
36 Yamagata K, Furuta H, Oda N, *et al.* Mutations in the hepatocyte nuclear factor-4alpha gene in maturity-onset diabetes of the young (MODY1). *Nature* 1996;**384**:458-60.
37 Veyhl M, Spangenberg J, Puschel B, *et al.* Cloning of a membrane-associated protein which modifies activity and properties of the Na(+)-D-glucose cotransporter. *J Biol Chem* 1993;**268**:25041-53.

38 Osswald C, Baumgarten K, Stumpel F, *et al.* Mice without the regulator gene Rsc1A1 exhibit increased Na+-D-glucose cotransport in small intestine and develop obesity. *Molecular and cellular biology* 2005;**25**:78-87.
39 Ikari A, Nakano M, Kawano K, *et al.* Up-regulation of sodium-dependent glucose transporter by interaction with heat shock protein 70. *J Biol Chem* 2002;**277**:33338-43.
40 Kato Y, Sugiura T, Nakadera Y, *et al.* Investigation of the role of oligopeptide transporter PEPT1 and sodium/glucose cotransporter SGLT1 in intestinal absorption of their substrates using small GTP-binding protein Rab8-null mice. *Drug metabolism and disposition: the biological fate of chemicals* 2009;**37**:602-7.
41 Wright EM, Turk E, Martin MG. Molecular basis for glucose-galactose malabsorption. *Cell biochemistry and biophysics* 2002;**36**:115-21.
42 Wright EM. I. Glucose galactose malabsorption. *The American journal of physiology* 1998;**275**:G879-82.
43 Hediger MA, Coady MJ, Ikeda TS, *et al.* Expression cloning and cDNA sequencing of the Na+/glucose co-transporter. *Nature* 1987;**330**:379-81.
44 Thorens B, Sarkar HK, Kaback HR, *et al.* Cloning and functional expression in bacteria of a novel glucose transporter present in liver, intestine, kidney, and beta-pancreatic islet cells. *Cell* 1988;**55**:281-90.
45 Cheeseman CI. GLUT2 is the transporter for fructose across the rat intestinal basolateral membrane. *Gastroenterology* 1993;**105**:1050-6.
46 Douard V, Ferraris RP. Regulation of the fructose transporter GLUT5 in health and disease. *Am J Physiol Endocrinol Metab* 2008;**295**:E227-37.
47 Adibi SA. The oligopeptide transporter (Pept-1) in human intestine: biology and function. *Gastroenterology* 1997;**113**:332-40.
48 Terada T, Inui K. Peptide transporters: structure, function, regulation and application for drug delivery. *Current drug metabolism* 2004;**5**:85-94.
49 Hu Y, Smith DE, Ma K, *et al.* Targeted disruption of peptide transporter Pept1 gene in mice significantly reduces dipeptide absorption in intestine. *Molecular pharmaceutics* 2008;**5**:1122-30.
50 Iqbal J, Hussain MM. Intestinal lipid absorption. *Am J Physiol Endocrinol Metab* 2009;**296**:E1183-94.
51 Kato T, Hayashi Y, Inoue K, *et al.* Glycerol absorption by Na+-dependent carrier-mediated transport in the closed loop of the rat small intestine. *Biological & pharmaceutical bulletin* 2005;**28**:553-5.
52 Gehring W, Rosbash M. The coevolution of blue-light photoreception and circadian rhythms. *Journal of molecular evolution* 2003;**57 Suppl 1**:S286-9.
53 Hufeland CW. Die Kunst das menschliche Leben zu verlangern. *Akademische Buchhandlung* 1797;**85**:550-1.
54 Lemmer B. Discoveries of rhythms in human biological functions: a historical review. *Chronobiology international* 2009;**26**:1019-68.
55 Struthius J. *Ars Sphymica.* Basel: Ludovici Konigs 1602.
56 Zadek J. Die Messung des Blutdrucks des Menschen mittels des Basch'schen Apparates. *Z Klin Med* 1881;**2**:509-51.
57 Aurelianus C. De morbis acutis & chronicis. Amsterdam: J.C. Amman, recensuit, emaculavit, notulasque adjecit 1722:429, 527.

58 Sydenham T. The Whole Works of the Excellent Practical Physician Dr. Thomas Sydenham. The second edition corrected from the original Latin by John Perchey. London: Richard Wellington 1697.
59 Mills JN. Human circadian rhythms. *Physiological reviews* 1966;**46**:128-71.
60 Halberg F, Barnum CP, Silber RH, *et al.* 24-Hour rhythms at several levels of integration in mice on different lighting regimens. *Proceedings of the Society for Experimental Biology and Medicine Society for Experimental Biology and Medicine (New York, NY* 1958;**97**:897-900.
61 Strubbe JH, van Dijk G. The temporal organization of ingestive behaviour and its interaction with regulation of energy balance. *Neuroscience and biobehavioral reviews* 2002;**26**:485-98.
62 de Castro JM, Kreitzman SM. A microregulatory analysis of spontaneous human feeding patterns. *Physiol Behav* 1985;**35**:329-35.
63 Rhoads DB, Rosenbaum DH, Unsal H, *et al.* Circadian periodicity of intestinal Na+/glucose cotransporter 1 mRNA levels is transcriptionally regulated. *J Biol Chem* 1998;**273**:9510-6.
64 Furuya S, Yugari Y. Daily rhythmic change of L-histidine and glucose absorptions in rat small intestine in vivo. *Biochimica et biophysica acta* 1974;**343**:558-64.
65 Furuya S, Yugari Y. Daily rhythmic change in the transport of histidine by everted sacs of rat small intestine. *Biochimica et biophysica acta* 1971;**241**:245-8.
66 Sigdestad CP, Bauman J, Lesher SW. Diurnal fluctuations in the number of cells in mitosis and DNA synthesis in the jejunum of the mouse. *Experimental cell research* 1969;**58**:159-62.
67 Saito M. Daily rhythmic changes in brush border enzymes of the small intestine and kidney in rat. *Biochimica et biophysica acta* 1972;**286**:212-5.
68 Stevenson NR, Ferrigni F, Parnicky K, *et al.* Effect of changes in feeding schedule on the diurnal rhythms and daily activity levels of intestinal brush border enzymes and transport systems. *Biochimica et biophysica acta* 1975;**406**:131-45.
69 Balakrishnan A, Stearns AT, Rounds J, *et al.* Diurnal rhythmicity in glucose uptake is mediated by temporal periodicity in the expression of the sodium-glucose cotransporter (SGLT1). *Surgery* 2008;**143**:813-8.
70 Pan X, Terada T, Irie M, *et al.* Diurnal rhythm of H+-peptide cotransporter in rat small intestine. *Am J Physiol Gastrointest Liver Physiol* 2002;**283**:G57-64.
71 Stearns AT, Balakrishnan A, Rhoads DB, *et al.* Diurnal rhythmicity in the transcription of jejunal drug transporters. *J Pharmacol Sci* 2008;**108**:144-8.
72 Drescher S, Glaeser H, Murdter T, *et al.* P-glycoprotein-mediated intestinal and biliary digoxin transport in humans. *Clinical pharmacology and therapeutics* 2003;**73**:223-31.
73 Chan LM, Lowes S, Hirst BH. The ABCs of drug transport in intestine and liver: efflux proteins limiting drug absorption and bioavailability. *Eur J Pharm Sci* 2004;**21**:25-51.
74 Boll M, Markovich D, Weber WM, *et al.* Expression cloning of a cDNA from rabbit small intestine related to proton-coupled transport of peptides, beta-lactam antibiotics and ACE-inhibitors. *Pflugers Arch* 1994;**429**:146-9.
75 Mistlberger RE. Food-anticipatory circadian rhythms: concepts and methods. *The European journal of neuroscience* 2009;**30**:1718-29.

76 Pan X, Terada T, Okuda M, *et al.* The diurnal rhythm of the intestinal transporters SGLT1 and PEPT1 is regulated by the feeding conditions in rats. *J Nutr* 2004;**134**:2211-5.
77 Stevenson NR, Sitren HS, Furuya S. Circadian rhythmicity in several small intestinal functions is independent of use of the intestine. *The American journal of physiology* 1980;**238**:G203-7.
78 Thiesen A, Wild GE, Tappenden KA, *et al.* The locally acting glucocorticosteroid budesonide enhances intestinal sugar uptake following intestinal resection in rats. *Gut* 2003;**52**:252-9.
79 Coll AP, Farooqi IS, O'Rahilly S. The hormonal control of food intake. *Cell* 2007;**129**:251-62.
80 Ducroc R, Guilmeau S, Akasbi K, *et al.* Luminal leptin induces rapid inhibition of active intestinal absorption of glucose mediated by sodium-glucose cotransporter 1. *Diabetes* 2005;**54**:348-54.
81 Moore RY, Eichler VB. Loss of a circadian adrenal corticosterone rhythm following suprachiasmatic lesions in the rat. *Brain research* 1972;**42**:201-6.
82 Le Minh N, Damiola F, Tronche F, *et al.* Glucocorticoid hormones inhibit food-induced phase-shifting of peripheral circadian oscillators. *EMBO J* 2001;**20**:7128-36.
83 Nagoshi E, Saini C, Bauer C, *et al.* Circadian gene expression in individual fibroblasts: cell-autonomous and self-sustained oscillators pass time to daughter cells. *Cell* 2004;**119**:693-705.
84 Balsalobre A, Damiola F, Schibler U. A serum shock induces circadian gene expression in mammalian tissue culture cells. *Cell* 1998;**93**:929-37.
85 Balsalobre A, Brown SA, Marcacci L, *et al.* Resetting of circadian time in peripheral tissues by glucocorticoid signaling. *Science* 2000;**289**:2344-7.
86 Rosenfeld P, Van Eekelen JA, Levine S, *et al.* Ontogeny of the type 2 glucocorticoid receptor in discrete rat brain regions: an immunocytochemical study. *Brain research* 1988;**470**:119-27.
87 Bodosi B, Gardi J, Hajdu I, *et al.* Rhythms of ghrelin, leptin, and sleep in rats: effects of the normal diurnal cycle, restricted feeding, and sleep deprivation. *American journal of physiology* 2004;**287**:R1071-9.
88 Houghton SG, Zarroug AE, Duenes JA, *et al.* The diurnal periodicity of hexose transporter mRNA and protein levels in the rat jejunum: role of vagal innervation. *Surgery* 2006;**139**:542-9.
89 Stearns AT, Balakrishnan A, Rounds J, *et al.* Capsaicin-sensitive vagal afferents modulate posttranscriptional regulation of the rat Na+/glucose cotransporter SGLT1. *Am J Physiol Gastrointest Liver Physiol* 2008;**294**:G1078-83.
90 Iqbal CW, Fatima J, Duenes J, *et al.* Expression and function of intestinal hexose transporters after small intestinal denervation. *Surgery* 2009;**146**:100-12.
91 Potten CS, Booth C, Pritchard DM. The intestinal epithelial stem cell: the mucosal governor. *International journal of experimental pathology* 1997;**78**:219-43.
92 Potten CS, Kovacs L, Hamilton E. Continuous labelling studies on mouse skin and intestine. *Cell and tissue kinetics* 1974;**7**:271-83.
93 Muncan V, Sansom OJ, Tertoolen L, *et al.* Rapid loss of intestinal crypts upon conditional deletion of the Wnt/Tcf-4 target gene c-Myc. *Molecular and cellular biology* 2006;**26**:8418-26.

94 Chandrasekaran C, Coopersmith CM, Gordon JI. Use of normal and transgenic mice to examine the relationship between terminal differentiation of intestinal epithelial cells and accumulation of their cell cycle regulators. *J Biol Chem* 1996;**271**:28414-21.
95 Pinto D, Gregorieff A, Begthel H, *et al.* Canonical Wnt signals are essential for homeostasis of the intestinal epithelium. *Genes Dev* 2003;**17**:1709-13.
96 Fre S, Huyghe M, Mourikis P, *et al.* Notch signals control the fate of immature progenitor cells in the intestine. *Nature* 2005;**435**:964-8.
97 Mayhew TM, Myklebust R, Whybrow A, *et al.* Epithelial integrity, cell death and cell loss in mammalian small intestine. *Histology and histopathology* 1999;**14**:257-67.
98 Green DR, Kroemer G. Cytoplasmic functions of the tumour suppressor p53. *Nature* 2009;**458**:1127-30.
99 Momand J, Zambetti GP, Olson DC, *et al.* The mdm-2 oncogene product forms a complex with the p53 protein and inhibits p53-mediated transactivation. *Cell* 1992;**69**:1237-45.
100 Mihara M, Erster S, Zaika A, *et al.* p53 has a direct apoptogenic role at the mitochondria. *Molecular cell* 2003;**11**:577-90.
101 Chipuk JE, Bouchier-Hayes L, Kuwana T, *et al.* PUMA couples the nuclear and cytoplasmic proapoptotic function of p53. *Science* 2005;**309**:1732-5.
102 Chipuk JE, Kuwana T, Bouchier-Hayes L, *et al.* Direct activation of Bax by p53 mediates mitochondrial membrane permeabilization and apoptosis. *Science* 2004;**303**:1010-4.
103 Hengartner MO. The biochemistry of apoptosis. *Nature* 2000;**407**:770-6.
104 Takahashi A, Alnemri ES, Lazebnik YA, *et al.* Cleavage of lamin A by Mch2 alpha but not CPP32: multiple interleukin 1 beta-converting enzyme-related proteases with distinct substrate recognition properties are active in apoptosis. *Proceedings of the National Academy of Sciences of the United States of America* 1996;**93**:8395-400.
105 Orth K, Chinnaiyan AM, Garg M, *et al.* The CED-3/ICE-like protease Mch2 is activated during apoptosis and cleaves the death substrate lamin A. *J Biol Chem* 1996;**271**:16443-6.
106 Donehower LA, Harvey M, Slagle BL, *et al.* Mice deficient for p53 are developmentally normal but susceptible to spontaneous tumours. *Nature* 1992;**356**:215-21.
107 Merritt AJ, Potten CS, Kemp CJ, *et al.* The role of p53 in spontaneous and radiation-induced apoptosis in the gastrointestinal tract of normal and p53-deficient mice. *Cancer research* 1994;**54**:614-7.
108 Knudson CM, Tung KS, Tourtellotte WG, *et al.* Bax-deficient mice with lymphoid hyperplasia and male germ cell death. *Science* 1995;**270**:96-9.
109 Pritchard DM, Potten CS, Korsmeyer SJ, *et al.* Damage-induced apoptosis in intestinal epithelia from bcl-2-null and bax-null mice: investigations of the mechanistic determinants of epithelial apoptosis in vivo. *Oncogene* 1999;**18**:7287-93.
110 Nakayama K, Nakayama K, Negishi I, *et al.* Targeted disruption of Bcl-2 alpha beta in mice: occurrence of gray hair, polycystic kidney disease, and lymphocytopenia. *Proceedings of the National Academy of Sciences of the United States of America* 1994;**91**:3700-4.
111 Nakayama K, Nakayama K, Negishi I, *et al.* Disappearance of the lymphoid system in Bcl-2 homozygous mutant chimeric mice. *Science* 1993;**261**:1584-8.

112 Scheving LE, Tsai TH, Scheving LA. Chronobiology of the intestinal tract of the mouse. *The American journal of anatomy* 1983;**168**:433-65.
113 Watson AJ, Pritchard DM. Lessons from genetically engineered animal models. VII. Apoptosis in intestinal epithelium: lessons from transgenic and knockout mice. *Am J Physiol Gastrointest Liver Physiol* 2000;**278**:G1-5.
114 Duncan AM, Ronen A, Blakey DH. Diurnal variation in the response of gamma-ray-induced apoptosis in the mouse intestinal epithelium. *Cancer letters* 1983;**21**:163-6.
115 Ijiri K, Potten CS. The circadian rhythm for the number and sensitivity of radiation-induced apoptosis in the crypts of mouse small intestine. *International journal of radiation biology* 1990;**58**:165-75.
116 Ijiri K, Potten CS. Circadian rhythms in the incidence of apoptotic cells and number of clonogenic cells in intestinal crypts after radiation using normal and reversed light conditions. *International journal of radiation biology and related studies in physics, chemistry, and medicine* 1988;**53**:717-27.
117 Scheving LE, Tsai TH, Scheving LA, *et al.* The potential of using the natural rhythmicity of cell proliferation in improving cancer chemotherapy in rodents. *Annals of the New York Academy of Sciences* 1991;**618**:182-227.
118 Burholt DR, Etzel SL, Schenken LL, *et al.* Digestive tract cell proliferation and food consumption patterns of Ha/ICR mice. *Cell and tissue kinetics* 1985;**18**:369-86.
119 Kashiwagi Y, Fujimoto K, Iwakiri R, *et al.* Loss of diurnal variation in ornithine decarboxylase and apoptosis in small intestine of Mongolian gerbils. *Journal of gastroenterology* 2000;**35**:434-40.
120 Iwakiri R, Gotoh Y, Noda T, *et al.* Programmed cell death in rat intestine: effect of feeding and fasting. *Scandinavian journal of gastroenterology* 2001;**36**:39-47.
121 Hoogerwerf WA, Sinha M, Conesa A, *et al.* Transcriptional profiling of mRNA expression in the mouse distal colon. *Gastroenterology* 2008;**135**:2019-29.
122 Griniatsos J, Michail OP, Theocharis S, *et al.* Circadian variation in expression of G1 phase cyclins D1 and E and cyclin-dependent kinase inhibitors p16 and p21 in human bowel mucosa. *World J Gastroenterol* 2006;**12**:2109-14.
123 Deshpande A, Sicinski P, Hinds PW. Cyclins and cdks in development and cancer: a perspective. *Oncogene* 2005;**24**:2909-15.
124 Murray AW. Recycling the cell cycle: cyclins revisited. *Cell* 2004;**116**:221-34.
125 Massague J. G1 cell-cycle control and cancer. *Nature* 2004;**432**:298-306.
126 Buchi KN, Moore JG, Hrushesky WJ, *et al.* Circadian rhythm of cellular proliferation in the human rectal mucosa. *Gastroenterology* 1991;**101**:410-5.
127 Marra G, Anti M, Percesepe A, *et al.* Circadian variations of epithelial cell proliferation in human rectal crypts. *Gastroenterology* 1994;**106**:982-7.
128 Richards AM, Nicholls MG, Espiner EA, *et al.* Diurnal patterns of blood pressure, heart rate and vasoactive hormones in normal man. *Clin Exp Hypertens A* 1986;**8**:153-66.
129 Selmaoui B, Touitou Y. Reproducibility of the circadian rhythms of serum cortisol and melatonin in healthy subjects: a study of three different 24-h cycles over six weeks. *Life Sci* 2003;**73**:3339-49.
130 Hastings MH. Circadian clocks. *Curr Biol* 1997;**7**:R670-2.
131 Welsh DK, Logothetis DE, Meister M, *et al.* Individual neurons dissociated from rat suprachiasmatic nucleus express independently phased circadian firing rhythms. *Neuron* 1995;**14**:697-706.

132 Schwartz WJ, Zimmerman P. Lesions of the suprachiasmatic nucleus disrupt circadian locomotor rhythms in the mouse. *Physiol Behav* 1991;**49**:1283-7.
133 Reppert SM, Perlow MJ, Ungerleider LG, *et al.* Effects of damage to the suprachiasmatic area of the anterior hypothalamus on the daily melatonin and cortisol rhythms in the rhesus monkey. *J Neurosci* 1981;**1**:1414-25.
134 Reppert SM, Weaver DR. Coordination of circadian timing in mammals. *Nature* 2002;**418**:935-41.
135 Reppert SM, Weaver DR. Molecular analysis of mammalian circadian rhythms. *Annual review of physiology* 2001;**63**:647-76.
136 Rosato E, Tauber E, Kyriacou CP. Molecular genetics of the fruit-fly circadian clock. *Eur J Hum Genet* 2006;**14**:729-38.
137 Williams JA, Sehgal A. Molecular components of the circadian system in Drosophila. *Annual review of physiology* 2001;**63**:729-55.
138 Wager-Smith K, Kay SA. Circadian rhythm genetics: from flies to mice to humans. *Nature genetics* 2000;**26**:23-7.
139 Qiu J, Hardin PE. Developmental state and the circadian clock interact to influence the timing of eclosion in Drosophila melanogaster. *Journal of biological rhythms* 1996;**11**:75-86.
140 Konopka RJ, Benzer S. Clock mutants of Drosophila melanogaster. *Proceedings of the National Academy of Sciences of the United States of America* 1971;**68**:2112-6.
141 Krishnan B, Dryer SE, Hardin PE. Circadian rhythms in olfactory responses of Drosophila melanogaster. *Nature* 1999;**400**:375-8.
142 Chen DM, Christianson JS, Sapp RJ, *et al.* Visual receptor cycle in normal and period mutant Drosophila: microspectrophotometry, electrophysiology, and ultrastructural morphometry. *Visual neuroscience* 1992;**9**:125-35.
143 McCabe C, Birley A. Oviposition in the period genotypes of Drosophila melanogaster. *Chronobiology international* 1998;**15**:119-33.
144 Benito J, Zheng H, Ng FS, *et al.* Transcriptional feedback loop regulation, function, and ontogeny in Drosophila. *Cold Spring Harbor symposia on quantitative biology* 2007;**72**:437-44.
145 Glossop NR, Lyons LC, Hardin PE. Interlocked feedback loops within the Drosophila circadian oscillator. *Science* 1999;**286**:766-8.
146 Darlington TK, Wager-Smith K, Ceriani MF, *et al.* Closing the circadian loop: CLOCK-induced transcription of its own inhibitors per and tim. *Science* 1998;**280**:1599-603.
147 Price JL, Blau J, Rothenfluh A, *et al.* double-time is a novel Drosophila clock gene that regulates PERIOD protein accumulation. *Cell* 1998;**94**:83-95.
148 Kloss B, Price JL, Saez L, *et al.* The Drosophila clock gene double-time encodes a protein closely related to human casein kinase Iepsilon. *Cell* 1998;**94**:97-107.
149 Kloss B, Rothenfluh A, Young MW, *et al.* Phosphorylation of period is influenced by cycling physical associations of double-time, period, and timeless in the Drosophila clock. *Neuron* 2001;**30**:699-706.
150 Hunter-Ensor M, Ousley A, Sehgal A. Regulation of the Drosophila protein timeless suggests a mechanism for resetting the circadian clock by light. *Cell* 1996;**84**:677-85.

151 Myers MP, Wager-Smith K, Rothenfluh-Hilfiker A, *et al.* Light-induced degradation of TIMELESS and entrainment of the Drosophila circadian clock. *Science* 1996;**271**:1736-40.
152 Zeng H, Qian Z, Myers MP, *et al.* A light-entrainment mechanism for the Drosophila circadian clock. *Nature* 1996;**380**:129-35.
153 Sun WC, Jeong EH, Jeong HJ, *et al.* Two distinct modes of PERIOD recruitment onto dCLOCK reveal a novel role for TIMELESS in circadian transcription. *J Neurosci*;**30**:14458-69.
154 Rothenfluh A, Young MW, Saez L. A TIMELESS-independent function for PERIOD proteins in the Drosophila clock. *Neuron* 2000;**26**:505-14.
155 Chang DC, Reppert SM. A novel C-terminal domain of drosophila PERIOD inhibits dCLOCK:CYCLE-mediated transcription. *Curr Biol* 2003;**13**:758-62.
156 Kume K, Zylka MJ, Sriram S, *et al.* mCRY1 and mCRY2 are essential components of the negative limb of the circadian clock feedback loop. *Cell* 1999;**98**:193-205.
157 Vitaterna MH, Selby CP, Todo T, *et al.* Differential regulation of mammalian period genes and circadian rhythmicity by cryptochromes 1 and 2. *Proceedings of the National Academy of Sciences of the United States of America* 1999;**96**:12114-9.
158 Shearman LP, Sriram S, Weaver DR, *et al.* Interacting molecular loops in the mammalian circadian clock. *Science* 2000;**288**:1013-9.
159 Bae K, Jin X, Maywood ES, *et al.* Differential functions of mPer1, mPer2, and mPer3 in the SCN circadian clock. *Neuron* 2001;**30**:525-36.
160 King DP, Zhao Y, Sangoram AM, *et al.* Positional cloning of the mouse circadian clock gene. *Cell* 1997;**89**:641-53.
161 Hogenesch JB, Gu YZ, Jain S, *et al.* The basic-helix-loop-helix-PAS orphan MOP3 forms transcriptionally active complexes with circadian and hypoxia factors. *Proceedings of the National Academy of Sciences of the United States of America* 1998;**95**:5474-9.
162 Gekakis N, Staknis D, Nguyen HB, *et al.* Role of the CLOCK protein in the mammalian circadian mechanism. *Science* 1998;**280**:1564-9.
163 Yu W, Nomura M, Ikeda M. Interactivating feedback loops within the mammalian clock: BMAL1 is negatively autoregulated and upregulated by CRY1, CRY2, and PER2. *Biochemical and biophysical research communications* 2002;**290**:933-41.
164 Preitner N, Damiola F, Lopez-Molina L, *et al.* The orphan nuclear receptor REV-ERBalpha controls circadian transcription within the positive limb of the mammalian circadian oscillator. *Cell* 2002;**110**:251-60.
165 Ueda HR, Chen W, Adachi A, *et al.* A transcription factor response element for gene expression during circadian night. *Nature* 2002;**418**:534-9.
166 Jin X, Shearman LP, Weaver DR, *et al.* A molecular mechanism regulating rhythmic output from the suprachiasmatic circadian clock. *Cell* 1999;**96**:57-68.
167 Ripperger JA, Shearman LP, Reppert SM, *et al.* CLOCK, an essential pacemaker component, controls expression of the circadian transcription factor DBP. *Genes Dev* 2000;**14**:679-89.
168 Johnson RF, Moore RY, Morin LP. Loss of entrainment and anatomical plasticity after lesions of the hamster retinohypothalamic tract. *Brain research* 1988;**460**:297-313.
169 Lucas RJ, Freedman MS, Lupi D, *et al.* Identifying the photoreceptive inputs to the mammalian circadian system using transgenic and retinally degenerate mice. *Behavioural brain research* 2001;**125**:97-102.

170 Wright KP, Jr., Czeisler CA. Absence of circadian phase resetting in response to bright light behind the knees. *Science* 2002;**297**:571.
171 Ding JM, Chen D, Weber ET, *et al.* Resetting the biological clock: mediation of nocturnal circadian shifts by glutamate and NO. *Science* 1994;**266**:1713-7.
172 Field MD, Maywood ES, O'Brien JA, *et al.* Analysis of clock proteins in mouse SCN demonstrates phylogenetic divergence of the circadian clockwork and resetting mechanisms. *Neuron* 2000;**25**:437-47.
173 Akiyama M, Kouzu Y, Takahashi S, *et al.* Inhibition of light- or glutamate-induced mPer1 expression represses the phase shifts into the mouse circadian locomotor and suprachiasmatic firing rhythms. *J Neurosci* 1999;**19**:1115-21.
174 Kuhlman SJ, Quintero JE, McMahon DG. GFP fluorescence reports Period 1 circadian gene regulation in the mammalian biological clock. *Neuroreport* 2000;**11**:1479-82.
175 Tosini G, Menaker M. Circadian rhythms in cultured mammalian retina. *Science* 1996;**272**:419-21.
176 Oishi K, Sakamoto K, Okada T, *et al.* Humoral signals mediate the circadian expression of rat period homologueue (rPer2) mRNA in peripheral tissues. *Neuroscience letters* 1998;**256**:117-9.
177 Oishi K, Sakamoto K, Okada T, *et al.* Antiphase circadian expression between BMAL1 and period homologueue mRNA in the suprachiasmatic nucleus and peripheral tissues of rats. *Biochemical and biophysical research communications* 1998;**253**:199-203.
178 Takata M, Burioka N, Ohdo S, *et al.* Daily expression of mRNAs for the mammalian Clock genes Per2 and clock in mouse suprachiasmatic nuclei and liver and human peripheral blood mononuclear cells. *Jpn J Pharmacol* 2002;**90**:263-9.
179 Sakamoto K, Oishi K, Nagase T, *et al.* Circadian expression of clock genes during ontogeny in the rat heart. *Neuroreport* 2002;**13**:1239-42.
180 Stokkan KA, Yamazaki S, Tei H, *et al.* Entrainment of the circadian clock in the liver by feeding. *Science* 2001;**291**:490-3.
181 Damiola F, Le Minh N, Preitner N, *et al.* Restricted feeding uncouples circadian oscillators in peripheral tissues from the central pacemaker in the suprachiasmatic nucleus. *Genes Dev* 2000;**14**:2950-61.
182 Hoogerwerf WA, Hellmich HL, Cornelissen G, *et al.* Clock gene expression in the murine gastrointestinal tract: endogenous rhythmicity and effects of a feeding regimen. *Gastroenterology* 2007;**133**:1250-60.
183 Zylka MJ, Shearman LP, Weaver DR, *et al.* Three period homologues in mammals: differential light responses in the suprachiasmatic circadian clock and oscillating transcripts outside of brain. *Neuron* 1998;**20**:1103-10.
184 Oishi K, Fukui H, Ishida N. Rhythmic expression of BMAL1 mRNA is altered in Clock mutant mice: differential regulation in the suprachiasmatic nucleus and peripheral tissues. *Biochemical and biophysical research communications* 2000;**268**:164-71.
185 Yamazaki S, Numano R, Abe M, *et al.* Resetting central and peripheral circadian oscillators in transgenic rats. *Science* 2000;**288**:682-5.
186 Terazono H, Mutoh T, Yamaguchi S, *et al.* Adrenergic regulation of clock gene expression in mouse liver. *Proceedings of the National Academy of Sciences of the United States of America* 2003;**100**:6795-800.

187 Kornmann B, Schaad O, Bujard H, *et al.* System-driven and oscillator-dependent circadian transcription in mice with a conditionally active liver clock. *PLoS biology* 2007;**5**:e34.
188 Lamia KA, Storch KF, Weitz CJ. Physiological significance of a peripheral tissue circadian clock. *Proceedings of the National Academy of Sciences of the United States of America* 2008;**105**:15172-7.
189 Yamamoto T, Nakahata Y, Tanaka M, *et al.* Acute physical stress elevates mouse period1 mRNA expression in mouse peripheral tissues via a glucocorticoid-responsive element. *J Biol Chem* 2005;**280**:42036-43.
190 Torra IP, Tsibulsky V, Delaunay F, *et al.* Circadian and glucocorticoid regulation of Rev-erbalpha expression in liver. *Endocrinology* 2000;**141**:3799-806.
191 Stearns AT BA, Abolmaali K, Rhoads DB, Ashley SW, Tavakkolizadeh A. Corticosteroids Phase-Shift Intestinal Clocks and Diurnal Functional Rhythms *Gastroenterology* 2009;**136**:A-96.
192 Hara R, Wan K, Wakamatsu H, *et al.* Restricted feeding entrains liver clock without participation of the suprachiasmatic nucleus. *Genes Cells* 2001;**6**:269-78.
193 Storch KF, Lipan O, Leykin I, *et al.* Extensive and divergent circadian gene expression in liver and heart. *Nature* 2002;**417**:78-83.
194 Balsalobre A, Marcacci L, Schibler U. Multiple signaling pathways elicit circadian gene expression in cultured Rat-1 fibroblasts. *Curr Biol* 2000;**10**:1291-4.
195 Akashi M, Nishida E. Involvement of the MAP kinase cascade in resetting of the mammalian circadian clock. *Genes Dev* 2000;**14**:645-9.
196 Yagita K, Okamura H. Forskolin induces circadian gene expression of rPer1, rPer2 and dbp in mammalian rat-1 fibroblasts. *FEBS letters* 2000;**465**:79-82.
197 Travnickova-Bendova Z, Cermakian N, Reppert SM, *et al.* Bimodal regulation of mPeriod promoters by CREB-dependent signaling and CLOCK/BMAL1 activity. *Proceedings of the National Academy of Sciences of the United States of America* 2002;**99**:7728-33.
198 McNamara P, Seo SB, Rudic RD, *et al.* Regulation of CLOCK and MOP4 by nuclear hormone receptors in the vasculature: a humoral mechanism to reset a peripheral clock. *Cell* 2001;**105**:877-89.
199 Nonaka H, Emoto N, Ikeda K, *et al.* Angiotensin II induces circadian gene expression of clock genes in cultured vascular smooth muscle cells. *Circulation* 2001;**104**:1746-8.
200 von Gall C, Garabette ML, Kell CA, *et al.* Rhythmic gene expression in pituitary depends on heterologous sensitization by the neurohormone melatonin. *Nature neuroscience* 2002;**5**:234-8.
201 Hastings MH, Reddy AB, Maywood ES. A clockwork web: circadian timing in brain and periphery, in health and disease. *Nat Rev Neurosci* 2003;**4**:649-61.
202 Lowrey PL, Takahashi JS. Mammalian circadian biology: elucidating genome-wide levels of temporal organization. *Annual review of genomics and human genetics* 2004;**5**:407-41.
203 Xu S, Witmer PD, Lumayag S, *et al.* MicroRNA (miRNA) transcriptome of mouse retina and identification of a sensory organ-specific miRNA cluster. *J Biol Chem* 2007;**282**:25053-66.
204 Yi R, Poy MN, Stoffel M, *et al.* A skin microRNA promotes differentiation by repressing 'stemness'. *Nature* 2008;**452**:225-9.

205 Krichevsky AM, Sonntag KC, Isacson O, *et al.* Specific microRNAs modulate embryonic stem cell-derived neurogenesis. *Stem cells (Dayton, Ohio)* 2006;**24**:857-64.
206 Lewis BP, Shih IH, Jones-Rhoades MW, *et al.* Prediction of mammalian microRNA targets. *Cell* 2003;**115**:787-98.
207 Selbach M, Schwanhausser B, Thierfelder N, *et al.* Widespread changes in protein synthesis induced by microRNAs. *Nature* 2008;**455**:58-63.
208 Lim LP, Lau NC, Garrett-Engele P, *et al.* Microarray analysis shows that some microRNAs downregulate large numbers of target mRNAs. *Nature* 2005;**433**:769-73.
209 Baek D, Villen J, Shin C, *et al.* The impact of microRNAs on protein output. *Nature* 2008;**455**:64-71.
210 Yanaihara N, Caplen N, Bowman E, *et al.* Unique microRNA molecular profiles in lung cancer diagnosis and prognosis. *Cancer cell* 2006;**9**:189-98.
211 Volinia S, Calin GA, Liu CG, *et al.* A microRNA expression signature of human solid tumors defines cancer gene targets. *Proceedings of the National Academy of Sciences of the United States of America* 2006;**103**:2257-61.
212 Calin GA, Ferracin M, Cimmino A, *et al.* A MicroRNA signature associated with prognosis and progression in chronic lymphocytic leukemia. *The New England journal of medicine* 2005;**353**:1793-801.
213 Garzon R, Volinia S, Liu CG, *et al.* MicroRNA signatures associated with cytogenetics and prognosis in acute myeloid leukemia. *Blood* 2008;**111**:3183-9.
214 Lu J, Getz G, Miska EA, *et al.* MicroRNA expression profiles classify human cancers. *Nature* 2005;**435**:834-8.
215 Lu Y, Thomson JM, Wong HY, *et al.* Transgenic over-expression of the microRNA miR-17-92 cluster promotes proliferation and inhibits differentiation of lung epithelial progenitor cells. *Developmental biology* 2007;**310**:442-53.
216 Ikeda S, Kong SW, Lu J, *et al.* Altered microRNA expression in human heart disease. *Physiological genomics* 2007;**31**:367-73.
217 Barringhaus KG, Zamore PD. MicroRNAs: regulating a change of heart. *Circulation* 2009;**119**:2217-24.
218 Esquela-Kerscher A, Slack FJ. Oncomirs - microRNAs with a role in cancer. *Nature reviews* 2006;**6**:259-69.
219 Kalluri R, Neilson EG. Epithelial-mesenchymal transition and its implications for fibrosis. *The Journal of clinical investigation* 2003;**112**:1776-84.
220 Liang M, Liu Y, Mladinov D, *et al.* MicroRNA: a new frontier in kidney and blood pressure research. *Am J Physiol Renal Physiol* 2009;**297**:F553-8.
221 Bernstein E, Kim SY, Carmell MA, *et al.* Dicer is essential for mouse development. *Nature genetics* 2003;**35**:215-7.
222 Kanellopoulou C, Muljo SA, Kung AL, *et al.* Dicer-deficient mouse embryonic stem cells are defective in differentiation and centromeric silencing. *Genes Dev* 2005;**19**:489-501.
223 Calabrese JM, Seila AC, Yeo GW, *et al.* RNA sequence analysis defines Dicer's role in mouse embryonic stem cells. *Proceedings of the National Academy of Sciences of the United States of America* 2007;**104**:18097-102.
224 Georgantas RW, 3rd, Hildreth R, Morisot S, *et al.* CD34+ hematopoietic stem-progenitor cell microRNA expression and function: a circuit diagram of differentiation control. *Proceedings of the National Academy of Sciences of the United States of America* 2007;**104**:2750-5.

225 Iorio MV, Croce CM. MicroRNAs in cancer: small molecules with a huge impact. *J Clin Oncol* 2009;**27**:5848-56.
226 Croce CM. Causes and consequences of microRNA dysregulation in cancer. *Nat Rev Genet* 2009;**10**:704-14.
227 Fineberg SK, Kosik KS, Davidson BL. MicroRNAs potentiate neural development. *Neuron* 2009;**64**:303-9.
228 Cordes KR, Srivastava D. MicroRNA regulation of cardiovascular development. *Circulation research* 2009;**104**:724-32.
229 Cheng HY, Papp JW, Varlamova O, *et al.* microRNA modulation of circadian-clock period and entrainment. *Neuron* 2007;**54**:813-29.
230 Lee RC, Feinbaum RL, Ambros V. The C. elegans heterochronic gene lin-4 encodes small RNAs with antisense complementarity to lin-14. *Cell* 1993;**75**:843-54.
231 Wightman B, Ha I, Ruvkun G. Posttranscriptional regulation of the heterochronic gene lin-14 by lin-4 mediates temporal pattern formation in C. elegans. *Cell* 1993;**75**:855-62.
232 Lagos-Quintana M, Rauhut R, Lendeckel W, *et al.* Identification of novel genes coding for small expressed RNAs. *Science* 2001;**294**:853-8.
233 Lau NC, Lim LP, Weinstein EG, *et al.* An abundant class of tiny RNAs with probable regulatory roles in Caenorhabditis elegans. *Science* 2001;**294**:858-62.
234 Lee RC, Ambros V. An extensive class of small RNAs in Caenorhabditis elegans. *Science* 2001;**294**:862-4.
235 Lee Y, Jeon K, Lee JT, *et al.* MicroRNA maturation: stepwise processing and subcellular localization. *The EMBO journal* 2002;**21**:4663-70.
236 Zeng Y, Cullen BR. Sequence requirements for micro RNA processing and function in human cells. *RNA (New York, NY* 2003;**9**:112-23.
237 Yi R, Qin Y, Macara IG, *et al.* Exportin-5 mediates the nuclear export of pre-microRNAs and short hairpin RNAs. *Genes Dev* 2003;**17**:3011-6.
238 Lund E, Guttinger S, Calado A, *et al.* Nuclear export of microRNA precursors. *Science* 2004;**303**:95-8.
239 Grishok A, Pasquinelli AE, Conte D, *et al.* Genes and mechanisms related to RNA interference regulate expression of the small temporal RNAs that control C. elegans developmental timing. *Cell* 2001;**106**:23-34.
240 Hutvagner G, McLachlan J, Pasquinelli AE, *et al.* A cellular function for the RNA-interference enzyme Dicer in the maturation of the let-7 small temporal RNA. *Science* 2001;**293**:834-8.
241 Hammond SM, Boettcher S, Caudy AA, *et al.* Argonaute2, a link between genetic and biochemical analyses of RNAi. *Science* 2001;**293**:1146-50.
242 Hutvagner G, Zamore PD. A microRNA in a multiple-turnover RNAi enzyme complex. *Science* 2002;**297**:2056-60.
243 Martinez J, Patkaniowska A, Urlaub H, *et al.* Single-stranded antisense siRNAs guide target RNA cleavage in RNAi. *Cell* 2002;**110**:563-74.
244 Aravin AA, Lagos-Quintana M, Yalcin A, *et al.* The small RNA profile during Drosophila melanogaster development. *Developmental cell* 2003;**5**:337-50.
245 Khvorova A, Reynolds A, Jayasena SD. Functional siRNAs and miRNAs exhibit strand bias. *Cell* 2003;**115**:209-16.
246 Schwarz DS, Hutvagner G, Du T, *et al.* Asymmetry in the assembly of the RNAi enzyme complex. *Cell* 2003;**115**:199-208.

247 Zeng Y, Yi R, Cullen BR. MicroRNAs and small interfering RNAs can inhibit mRNA expression by similar mechanisms. *Proceedings of the National Academy of Sciences of the United States of America* 2003;**100**:9779-84.
248 Lewis BP, Burge CB, Bartel DP. Conserved seed pairing, often flanked by adenosines, indicates that thousands of human genes are microRNA targets. *Cell* 2005;**120**:15-20.
249 Elbashir SM, Lendeckel W, Tuschl T. RNA interference is mediated by 21- and 22-nucleotide RNAs. *Genes Dev* 2001;**15**:188-200.
250 Wu L, Fan J, Belasco JG. MicroRNAs direct rapid deadenylation of mRNA. *Proceedings of the National Academy of Sciences of the United States of America* 2006;**103**:4034-9.
251 Giraldez AJ, Mishima Y, Rihel J, *et al.* Zebrafish MiR-430 promotes deadenylation and clearance of maternal mRNAs. *Science* 2006;**312**:75-9.
252 Pillai RS, Bhattacharyya SN, Artus CG, *et al.* Inhibition of translational initiation by Let-7 MicroRNA in human cells. *Science* 2005;**309**:1573-6.
253 Humphreys DT, Westman BJ, Martin DI, *et al.* MicroRNAs control translation initiation by inhibiting eukaryotic initiation factor 4E/cap and poly(A) tail function. *Proceedings of the National Academy of Sciences of the United States of America* 2005;**102**:16961-6.
254 Chendrimada TP, Finn KJ, Ji X, *et al.* MicroRNA silencing through RISC recruitment of eIF6. *Nature* 2007;**447**:823-8.
255 Petersen CP, Bordeleau ME, Pelletier J, *et al.* Short RNAs repress translation after initiation in mammalian cells. *Molecular cell* 2006;**21**:533-42.
256 Nottrott S, Simard MJ, Richter JD. Human let-7a miRNA blocks protein production on actively translating polyribosomes. *Nature structural & molecular biology* 2006;**13**:1108-14.
257 Maroney PA, Yu Y, Fisher J, *et al.* Evidence that microRNAs are associated with translating messenger RNAs in human cells. *Nature structural & molecular biology* 2006;**13**:1102-7.
258 Akhtar RA, Reddy AB, Maywood ES, *et al.* Circadian cycling of the mouse liver transcriptome, as revealed by cDNA microarray, is driven by the suprachiasmatic nucleus. *Curr Biol* 2002;**12**:540-50.
259 Panda S, Antoch MP, Miller BH, *et al.* Coordinated transcription of key pathways in the mouse by the circadian clock. *Cell* 2002;**109**:307-20.
260 Reddy AB, Karp NA, Maywood ES, *et al.* Circadian orchestration of the hepatic proteome. *Curr Biol* 2006;**16**:1107-15.
261 Yang M, Lee JE, Padgett RW, *et al.* Circadian regulation of a limited set of conserved microRNAs in Drosophila. *BMC genomics* 2008;**9**:83.
262 Bartel DP. MicroRNAs: genomics, biogenesis, mechanism, and function. *Cell* 2004;**116**:281-97.
263 Messing B, Crenn P, Beau P, *et al.* Long-term survival and parenteral nutrition dependence in adult patients with the short bowel syndrome. *Gastroenterology* 1999;**117**:1043-50.
264 Dowling RH, Booth CC. Structural and functional changes following small intestinal resection in the rat. *Clinical science* 1967;**32**:139-49.
265 Dowling RH, Booth CC. Functional compensation after small-bowel resection in man. Demonstration by direct measurement. *Lancet* 1966;**2**:146-7.

266 Weinstein LD, Shoemaker CP, Hersh T, *et al.* Enhanced intestinal absorption after small bowel resection in man. *Arch Surg* 1969;**99**:560-2.
267 Sigalet DL, Martin GR. Mechanisms underlying intestinal adaptation after massive intestinal resection in the rat. *Journal of pediatric surgery* 1998;**33**:889-92.
268 Tzakis AG, Kato T, Levi DM, *et al.* 100 multivisceral transplants at a single center. *Annals of surgery* 2005;**242**:480-90; discussion 91-3.
269 Ruiz P, Kato T, Tzakis A. Current status of transplantation of the small intestine. *Transplantation* 2007;**83**:1-6.
270 Wales PW, Christison-Lagay ER. Short bowel syndrome: epidemiology and etiology. *Seminars in pediatric surgery*;**19**:3-9.
271 Bianchi A. Experience with longitudinal intestinal lengthening and tailoring. *Eur J Pediatr Surg* 1999;**9**:256-9.
272 Wales PW, de Silva N, Langer JC, *et al.* Intermediate outcomes after serial transverse enteroplasty in children with short bowel syndrome. *Journal of pediatric surgery* 2007;**42**:1804-10.
273 Sondheimer JM, Asturias E, Cadnapaphornchai M. Infection and cholestasis in neonates with intestinal resection and long-term parenteral nutrition. *Journal of pediatric gastroenterology and nutrition* 1998;**27**:131-7.
274 Bakker H, Bozzetti F, Staun M, *et al.* Home parenteral nutrition in adults: a european multicentre survey in 1997. ESPEN-Home Artificial Nutrition Working Group. *Clinical nutrition (Edinburgh, Scotland)* 1999;**18**:135-40.
275 Sigma. CelLytic NuCLEAR Extraction Kit Technical Bulletin accessed at http://www.sigmaaldrich.com/etc/medialib/docs/Sigma/Bulletin/nxtractbul.Par.0001.File.tmp/nxtractbul.pdf on 2nd March 2010.
276 Ambion. http://www.ambion.com/techlib/prot/fm_1560.pdf, accessed on 2nd March 2010.
277 Invitrogen. http://tools.invitrogen.com/content/sfs/manuals/superscriptIIIfirststrand_pps.pdf, accessed 2nd March 2010.
278 Primer3_software. http://frodo.wi.mit.edu/primer3/ accessed on 2nd March 2010.
279 University_of_California_Santa_Cruz. http://genome.ucsc.edu/, accessed 2nd March 2010.
280 Applied_Biosystems. http://www3.appliedbiosystems.com/cms/groups/mcb_support/documents/generaldocuments/cms_041053.pdf, accessed on 2nd March 2010.
281 Applied_Biosystems. http://www3.appliedbiosystems.com/cms/groups/mcb_support/documents/generaldocuments/cms_042996.pdf, accessed 2nd March 2010.
282 Applied_Biosystems. http://www3.appliedbiosystems.com/cms/groups/mcb_support/documents/generaldocuments/cms_042167.pdf, accessed 2nd March 2010.
283 Molecular_Devices. http://www.bmbio.com/file/201737.pdf, accessed 2nd March 2010.
284 Applied_Biosystems. http://www.ambion.com/techlib/prot/fm_1931.pdf, accessed 2nd March 2010.

285 Qiagen. http://www1.qiagen.com/literature/render.aspx?id=23749, accessed 10th March 2010.
286 Sigma. http://www.sigmaaldrich.com/etc/medialib/docs/Sigma/Bulletin/bca1bul.Par.0001.File.tmp/bca1bul.pdf accessed on 5th March 2010.
287 Invitrogen. http://tools.invitrogen.com/content/sfs/manuals/surelock_man.pdf, accessed 5th March 2010.
288 Invitrogen. http://tools.invitrogen.com/content/sfs/manuals/blotmod_pro.pdf, accessed 5th March 2010.
289 GE_Healthcare. http://www.gelifesciences.com/aptrix/upp00919.nsf/Content/4DE67EABFB9A9D25C1257628001CDC12/$file/28955347AD.pdf, accessed 5th March 2010.
290 Qiagen. http://www1.qiagen.com/literature/render.aspx?id=565, 5th March 2010.
291 Qiagen. http://www1.qiagen.com/literature/render.aspx?id=380, accessed 5th March 2010.
292 Invitrogen. http://tools.invitrogen.com/content/sfs/manuals/lipofectamine2000_man.pdf, accessed 5th March 2010.
293 Invitrogen. http://tools.invitrogen.com/content/sfs/manuals/oneshottop10_chemcomp_man.pdf, accessed 10th March 2010.
294 Qiagen. http://www1.qiagen.com/literature/render.aspx?id=370, accessed 5th March 2010.
295 mirBASE. http://www.mirbase.org/, University of Manchester, accessed 2nd March 2010.
296 Invitrogen. http://tools.invitrogen.com/content/sfs/manuals/10480010.pdf, accessed 5th March 2010.
297 Open_Biosystems. http://www.openbiosystems.com/collateral/rnai/pi/pTRIPZ_Technical_Manual.pdf, accessed 5th March 2010.
298 Sigma. http://www.sigmaaldrich.com/etc/medialib/docs/Sigma/Bulletin/na0310bul.pdf, accessed 5th March 2010.
299 Qiagen. http://www1.qiagen.com/literature/render.aspx?id=103715, accessed 5th March 2010.
300 New_England_Biolabs. http://www.finnzymes.com/pdf/phusion_mutagenesis_datasheet_f541_1_3_low.pdf, accessed 10th March 2010.
301 Promega. http://www.promega.com/tbs/tm040/tm040.html, accessed 5th March 2010.
302 BD. http://researcher.nsc.gov.tw/public/woody/Data/98611333871.pdf, accessed 10th March 2010.
303 Invitrogen. http://probes.invitrogen.com/media/pis/mp34857.pdf, accessed 10th March 2010.
304 Promega. http://www.promega.com/tbs/tb245/tb245.pdf, accessed 10th March 2010.

305 Fujimoto K, Granger DN, Johnson LR, *et al.* Circadian rhythm of ornithine decarboxylase activity in small intestine of fasted rats. *Proceedings of the Society for Experimental Biology and Medicine Society for Experimental Biology and Medicine (New York, NY* 1992;**200**:409-13.
306 Furukawa Y, Cook IJ, Panagopoulos V, *et al.* Relationship between sleep patterns and human colonic motor patterns. *Gastroenterology* 1994;**107**:1372-81.
307 Scheving LE, Burns ER, Pauly JE, *et al.* Circadian variation in cell division of the mouse alimentary tract, bone marrow and corneal epithelium. *The Anatomical record* 1978;**191**:479-86.
308 Sato TK, Panda S, Miraglia LJ, *et al.* A functional genomics strategy reveals Rora as a component of the mammalian circadian clock. *Neuron* 2004;**43**:527-37.
309 Guillaumond F, Dardente H, Giguere V, *et al.* Differential control of Bmal1 circadian transcription by REV-ERB and ROR nuclear receptors. *Journal of biological rhythms* 2005;**20**:391-403.
310 Sakamoto K, Oishi K, Shiraishi M, *et al.* Two circadian oscillatory mechanisms in the mammalian retina. *Neuroreport* 2000;**11**:3995-7.
311 Froy O, Chapnik N. Circadian oscillation of innate immunity components in mouse small intestine. *Mol Immunol* 2007;**44**:1954-60.
312 Nelson W, Tong YL, Lee JK, *et al.* Methods for cosinor-rhythmometry. *Chronobiologia* 1979;**6**:305-23.
313 Ferraris RP, Yasharpour S, Lloyd KC, *et al.* Luminal glucose concentrations in the gut under normal conditions. *The American journal of physiology* 1990;**259**:G822-37.
314 Shearman LP, Jin X, Lee C, *et al.* Targeted disruption of the mPer3 gene: subtle effects on circadian clock function. *Molecular and cellular biology* 2000;**20**:6269-75.
315 Yang X, Downes M, Yu RT, *et al.* Nuclear receptor expression links the circadian clock to metabolism. *Cell* 2006;**126**:801-10.
316 Sladek M, Rybova M, Jindrakova Z, *et al.* Insight into the circadian clock within rat colonic epithelial cells. *Gastroenterology* 2007;**133**:1240-9.
317 Tei H, Okamura H, Shigeyoshi Y, *et al.* Circadian oscillation of a mammalian homologueue of the Drosophila period gene. *Nature* 1997;**389**:512-6.
318 Shearman LP, Zylka MJ, Reppert SM, *et al.* Expression of basic helix-loop-helix/PAS genes in the mouse suprachiasmatic nucleus. *Neuroscience* 1999;**89**:387-97.
319 Lee C, Etchegaray JP, Cagampang FR, *et al.* Posttranslational mechanisms regulate the mammalian circadian clock. *Cell* 2001;**107**:855-67.
320 Vitaterna MH, King DP, Chang AM, *et al.* Mutagenesis and mapping of a mouse gene, Clock, essential for circadian behavior. *Science* 1994;**264**:719-25.
321 van der Horst GT, Muijtjens M, Kobayashi K, *et al.* Mammalian Cry1 and Cry2 are essential for maintenance of circadian rhythms. *Nature* 1999;**398**:627-30.
322 Reddy AB, Maywood ES, Karp NA, *et al.* Glucocorticoid signaling synchronizes the liver circadian transcriptome. *Hepatology (Baltimore, Md* 2007;**45**:1478-88.
323 Stearns AT, Balakrishnan A, Rhoads DB, *et al.* Diurnal expression of the rat intestinal sodium-glucose cotransporter 1 (SGLT1) is independent of local luminal factors. *Surgery* 2009;**145**:294-302.
324 Harms E, Kivimae S, Young MW, *et al.* Posttranscriptional and posttranslational regulation of clock genes. *Journal of biological rhythms* 2004;**19**:361-73.
325 Gallego M, Virshup DM. Post-translational modifications regulate the ticking of the circadian clock. *Nat Rev Mol Cell Biol* 2007;**8**:139-48.

326 Dyer J, Garner A, Wood IS, *et al.* Changes in the levels of intestinal Na+/glucose co-transporter (SGLT1) in experimental diabetes. *Biochemical Society transactions* 1997;**25**:479S.
327 Dyer J, Wood IS, Palejwala A, *et al.* Expression of monosaccharide transporters in intestine of diabetic humans. *Am J Physiol Gastrointest Liver Physiol* 2002;**282**:G241-8.
328 Hampton SM, Morgan LM, Lawrence N, *et al.* Postprandial hormone and metabolic responses in simulated shift work. *The Journal of endocrinology* 1996;**151**:259-67.
329 Stephan FK, Zucker I. Circadian rhythms in drinking behavior and locomotor activity of rats are eliminated by hypothalamic lesions. *Proceedings of the National Academy of Sciences of the United States of America* 1972;**69**:1583-6.
330 Moore RY, Silver R. Suprachiasmatic nucleus organization. *Chronobiology international* 1998;**15**:475-87.
331 Silver R, Moore RY. The suprachiasmatic nucleus and circadian function: an introduction. *Chronobiology international* 1998;**15**:vii-x.
332 Warren WS, Champney TH, Cassone VM. The suprachiasmatic nucleus controls the circadian rhythm of heart rate via the sympathetic nervous system. *Physiol Behav* 1994;**55**:1091-9.
333 Stephan FK, Swann JM, Sisk CL. Anticipation of 24-hr feeding schedules in rats with lesions of the suprachiasmatic nucleus. *Behavioral and neural biology* 1979;**25**:346-63.
334 Stephan FK, Swann JM, Sisk CL. Entrainment of circadian rhythms by feeding schedules in rats with suprachiasmatic lesions. *Behavioral and neural biology* 1979;**25**:545-54.
335 Clarke JD, Coleman GJ. Persistent meal-associated rhythms in SCN-lesioned rats. *Physiol Behav* 1986;**36**:105-13.
336 Hirota T, Okano T, Kokame K, *et al.* Glucose down-regulates Per1 and Per2 mRNA levels and induces circadian gene expression in cultured Rat-1 fibroblasts. *J Biol Chem* 2002;**277**:44244-51.
337 Yamamoto H, Nagai K, Nakagawa H. Role of SCN in daily rhythms of plasma glucose, FFA, insulin and glucagon. *Chronobiology international* 1987;**4**:483-91.
338 Blais A, Bissonnette P, Berteloot A. Common characteristics for Na+-dependent sugar transport in Caco-2 cells and human fetal colon. *The Journal of membrane biology* 1987;**99**:113-25.
339 Berberich C, Durr I, Koenen M, *et al.* Two adjacent E box elements and a M-CAT box are involved in the muscle-specific regulation of the rat acetylcholine receptor beta subunit gene. *European journal of biochemistry / FEBS* 1993;**216**:395-404.
340 Resuehr D, Wildemann U, Sikes H, *et al.* E-box regulation of gonadotropin-releasing hormone (GnRH) receptor expression in immortalized gonadotrope cells. *Molecular and cellular endocrinology* 2007;**278**:36-43.
341 Leclerc GM, Boockfor FR. Pulses of prolactin promoter activity depend on a noncanonical E-box that can bind the circadian proteins CLOCK and BMAL1. *Endocrinology* 2005;**146**:2782-90.
342 Fu L, Patel MS, Bradley A, *et al.* The molecular clock mediates leptin-regulated bone formation. *Cell* 2005;**122**:803-15.
343 Zheng B, Albrecht U, Kaasik K, *et al.* Nonredundant roles of the mPer1 and mPer2 genes in the mammalian circadian clock. *Cell* 2001;**105**:683-94.

344 Nakashima A, Kawamoto T, Honda KK, *et al.* DEC1 modulates the circadian phase of clock gene expression. *Molecular and cellular biology* 2008;**28**:4080-92.
345 Yoo SH, Ko CH, Lowrey PL, *et al.* A noncanonical E-box enhancer drives mouse Period2 circadian oscillations in vivo. *Proceedings of the National Academy of Sciences of the United States of America* 2005;**102**:2608-13.
346 Fustin JM, O'Neill JS, Hastings MH, *et al.* Cry1 circadian phase in vitro: wrapped up with an E-box. *Journal of biological rhythms* 2009;**24**:16-24.
347 Albrecht U, Sun ZS, Eichele G, *et al.* A differential response of two putative mammalian circadian regulators, mper1 and mper2, to light. *Cell* 1997;**91**:1055-64.
348 Maywood ES, Mrosovsky N, Field MD, *et al.* Rapid down-regulation of mammalian period genes during behavioral resetting of the circadian clock. *Proceedings of the National Academy of Sciences of the United States of America* 1999;**96**:15211-6.
349 Bozek K, Kielbasa SM, Kramer A, *et al.* Promoter analysis of Mammalian clock controlled genes. *Genome informatics* 2007;**18**:65-74.
350 Oishi K, Shirai H, Ishida N. CLOCK is involved in the circadian transactivation of peroxisome-proliferator-activated receptor alpha (PPARalpha) in mice. *The Biochemical journal* 2005;**386**:575-81.
351 Kowase T, Walsh HE, Darling DS, *et al.* Estrogen enhances gonadotropin-releasing hormone-stimulated transcription of the luteinizing hormone subunit promoters via altered expression of stimulatory and suppressive transcription factors. *Endocrinology* 2007;**148**:6083-91.
352 Moon YS, Latasa MJ, Griffin MJ, *et al.* Suppression of fatty acid synthase promoter by polyunsaturated fatty acids. *Journal of lipid research* 2002;**43**:691-8.
353 Lenka N, Basu A, Mullick J, *et al.* The role of an E box binding basic helix loop helix protein in the cardiac muscle-specific expression of the rat cytochrome oxidase subunit VIII gene. *J Biol Chem* 1996;**271**:30281-9.
354 Shen M, Kawamoto T, Yan W, *et al.* Molecular characterization of the novel basic helix-loop-helix protein DEC1 expressed in differentiated human embryo chondrocytes. *Biochemical and biophysical research communications* 1997;**236**:294-8.
355 Balakrishnan A, Stearns AT, Rhoads DB, *et al.* Defining the transcriptional regulation of the intestinal sodium-glucose cotransporter using RNA-interference mediated gene silencing. *Surgery* 2008;**144**:168-73.
356 Esumi N, Kachi S, Campochiaro PA, *et al.* VMD2 promoter requires two proximal E-box sites for its activity in vivo and is regulated by the MITF-TFE family. *J Biol Chem* 2007;**282**:1838-50.
357 Villavicencio EH, Yoon JW, Frank DJ, *et al.* Cooperative E-box regulation of human GLI1 by TWIST and USF. *Genesis* 2002;**32**:247-58.
358 Lin CJ, Cencic R, Mills JR, *et al.* c-Myc and eIF4F are components of a feedforward loop that links transcription and translation. *Cancer research* 2008;**68**:5326-34.
359 Gery S, Komatsu N, Baldjyan L, *et al.* The circadian gene per1 plays an important role in cell growth and DNA damage control in human cancer cells. *Molecular cell* 2006;**22**:375-82.
360 Cao Q, Gery S, Dashti A, *et al.* A role for the clock gene per1 in prostate cancer. *Cancer research* 2009;**69**:7619-25.
361 Sato F, Nagata C, Liu Y, *et al.* PERIOD1 is an anti-apoptotic factor in human pancreatic and hepatic cancer cells. *Journal of biochemistry* 2009;**146**:833-8.

362 Cermakian N, Monaco L, Pando MP, *et al.* Altered behavioral rhythms and clock gene expression in mice with a targeted mutation in the Period1 gene. *The EMBO journal* 2001;**20**:3967-74.
363 Hoogerwerf WA, Shahinian VB, Cornelissen G, *et al.* Rhythmic changes in colonic motility are regulated by period genes. *Am J Physiol Gastrointest Liver Physiol*;**298**:G143-50.
364 McDonald MJ, Rosbash M. Microarray analysis and organization of circadian gene expression in Drosophila. *Cell* 2001;**107**:567-78.
365 Claridge-Chang A, Wijnen H, Naef F, *et al.* Circadian regulation of gene expression systems in the Drosophila head. *Neuron* 2001;**32**:657-71.
366 Farh KK, Grimson A, Jan C, *et al.* The widespread impact of mammalian MicroRNAs on mRNA repression and evolution. *Science* 2005;**310**:1817-21.
367 Stark A, Brennecke J, Bushati N, *et al.* Animal MicroRNAs confer robustness to gene expression and have a significant impact on 3'UTR evolution. *Cell* 2005;**123**:1133-46.
368 Balakrishnan A, Stearns AT, Park PJ, *et al.* MicroRNA mir-16 is anti-proliferative in enterocytes and exhibits diurnal rhythmicity in intestinal crypts. *Experimental cell research* 2010.
369 Stevenson NR, Day SE, Sitren H. Circadian rhythmicity in rat intestinal villus length and cell number. *International journal of chronobiology* 1979;**6**:1-12.
370 Xia L, Zhang D, Du R, *et al.* miR-15b and miR-16 modulate multidrug resistance by targeting BCL2 in human gastric cancer cells. *International journal of cancer* 2008;**123**:372-9.
371 Lewis BP, Bartel, D.P. http://www.targetscan.org, accessed 15th March 2010.
372 Krutzfeldt J, Rajewsky N, Braich R, *et al.* Silencing of microRNAs in vivo with 'antagomirs'. *Nature* 2005;**438**:685-9.
373 Bonci D, Coppola V, Musumeci M, *et al.* The miR-15a-miR-16-1 cluster controls prostate cancer by targeting multiple oncogenic activities. *Nature medicine* 2008;**14**:1271-7.
374 Quaroni A, Wands J, Trelstad RL, *et al.* Epithelioid cell cultures from rat small intestine. Characterization by morphologic and immunologic criteria. *The Journal of cell biology* 1979;**80**:248-65.
375 Guo CJ, Pan Q, Li DG, *et al.* miR-15b and miR-16 are implicated in activation of the rat hepatic stellate cell: An essential role for apoptosis. *Journal of hepatology* 2009;**50**:766-78.
376 Merritt AJ, Potten CS, Watson AJ, *et al.* Differential expression of bcl-2 in intestinal epithelia. Correlation with attenuation of apoptosis in colonic crypts and the incidence of colonic neoplasia. *J Cell Sci* 1995;**108 (Pt 6)**:2261-71.
377 Takeshita F, Patrawala L, Osaki M, *et al.* Systemic Delivery of Synthetic MicroRNA-16 Inhibits the Growth of Metastatic Prostate Tumors via Downregulation of Multiple Cell-cycle Genes. *Mol Ther* 2009.
378 Geng Y, Whoriskey W, Park MY, *et al.* Rescue of cyclin D1 deficiency by knockin cyclin E. *Cell* 1999;**97**:767-77.
379 Kozar K, Ciemerych MA, Rebel VI, *et al.* Mouse development and cell proliferation in the absence of D-cyclins. *Cell* 2004;**118**:477-91.
380 Ko TC, Sheng HM, Reisman D, *et al.* Transforming growth factor-beta 1 inhibits cyclin D1 expression in intestinal epithelial cells. *Oncogene* 1995;**10**:177-84.

381 Ko TC, Pan F, Sheng H, *et al.* Cyclin D3 is essential for intestinal epithelial cell proliferation. *World journal of surgery* 2002;**26**:812-8.
382 Lesher S. Compensatory reactions in intestinal crypt cells after 300 Roentgens of cobalt-60 gamma irradiation. *Radiat Res* 1967;**32**:510-9.
383 Cohen AM, Philips FS, Sternberg SS. Studies on the cytotoxicity of bleomycin in the small intestine of the mouse. *Cancer Res* 1972;**32**:1293-300.
384 DuBois RN, Shao J, Tsujii M, *et al.* G1 delay in cells overexpressing prostaglandin endoperoxide synthase-2. *Cancer research* 1996;**56**:733-7.
385 Buts JP, De Meyer R, Kolanowski J. Ontogeny of cell proliferation and DNA synthesis in rat colon: role of glucocorticoids. *The American journal of physiology* 1983;**244**:G469-74.
386 Quaroni A, Tian JQ, Goke M, *et al.* Glucocorticoids have pleiotropic effects on small intestinal crypt cells. *The American journal of physiology* 1999;**277**:G1027-40.
387 Tazawa H, Tsuchiya N, Izumiya M, *et al.* Tumor-suppressive miR-34a induces senescence-like growth arrest through modulation of the E2F pathway in human colon cancer cells. *Proceedings of the National Academy of Sciences of the United States of America* 2007;**104**:15472-7.
388 Braun CJ, Zhang X, Savelyeva I, *et al.* p53-Responsive micrornas 192 and 215 are capable of inducing cell cycle arrest. *Cancer research* 2008;**68**:10094-104.
389 Ivanovska I, Ball AS, Diaz RL, *et al.* MicroRNAs in the miR-106b family regulate p21/CDKN1A and promote cell cycle progression. *Mol Cell Biol* 2008;**28**:2167-74.
390 Gillies JK, Lorimer IA. Regulation of p27Kip1 by miRNA 221/222 in glioblastoma. *Cell cycle (Georgetown, Tex* 2007;**6**:2005-9.
391 Lee CC. Tumor suppression by the mammalian Period genes. *Cancer Causes Control* 2006;**17**:525-30.
392 Fu L, Pelicano H, Liu J, *et al.* The circadian gene Period2 plays an important role in tumor suppression and DNA damage response in vivo. *Cell* 2002;**111**:41-50.
393 Matsuo T, Yamaguchi S, Mitsui S, *et al.* Control mechanism of the circadian clock for timing of cell division in vivo. *Science* 2003;**302**:255-9.
394 Bracken CP, Wall SJ, Barre B, *et al.* Regulation of cyclin D1 RNA stability by SNIP1. *Cancer research* 2008;**68**:7621-8.
395 Spruck CH, Strohmaier HM. Seek and destroy: SCF ubiquitin ligases in mammalian cell cycle control. *Cell cycle (Georgetown, Tex* 2002;**1**:250-4.
396 Platell CF, Coster J, McCauley RD, *et al.* The management of patients with the short bowel syndrome. *World J Gastroenterol* 2002;**8**:13-20.
397 Beath SV. Closure and summary of Ninth International Small Bowel Transplantation Symposium. *Transplantation proceedings* 2006;**38**:1657-8.
398 Fatima J, Iqbal CW, Houghton SG, *et al.* Hexose transporter expression and function in mouse small intestine: role of diurnal rhythm. *J Gastrointest Surg* 2009;**13**:634-41.
399 Houghton SG, Iqbal CW, Duenes JA, *et al.* Coordinated, diurnal hexose transporter expression in rat small bowel: implications for small bowel resection. *Surgery* 2008;**143**:79-93.
400 Hoffmeyer S, Burk O, von Richter O, *et al.* Functional polymorphisms of the human multidrug-resistance gene: multiple sequence variations and correlation of one allele with P-glycoprotein expression and activity in vivo. *Proceedings of the National Academy of Sciences of the United States of America* 2000;**97**:3473-8.

401 Wood PA, Yang X, Taber A, *et al.* Period 2 mutation accelerates ApcMin/+ tumorigenesis. *Mol Cancer Res* 2008;**6**:1786-93.
402 Yang X, Wood PA, Ansell C, *et al.* Circadian time-dependent tumor suppressor function of period genes. *Integrative cancer therapies* 2009;**8**:309-16.
403 Grechez-Cassiau A, Rayet B, Guillaumond F, *et al.* The circadian clock component BMAL1 is a critical regulator of p21WAF1/CIP1 expression and hepatocyte proliferation. *J Biol Chem* 2008;**283**:4535-42.
404 Miller BH, McDearmon EL, Panda S, *et al.* Circadian and CLOCK-controlled regulation of the mouse transcriptome and cell proliferation. *Proceedings of the National Academy of Sciences of the United States of America* 2007;**104**:3342-7.
405 Rajewsky N. microRNA target predictions in animals. *Nature genetics* 2006;**38 Suppl**:S8-13.
406 Nagel R, Clijsters L, Agami R. The miRNA-192/194 cluster regulates the Period gene family and the circadian clock. *The FEBS journal* 2009;**276**:5447-55.
407 Kadener S, Menet JS, Sugino K, *et al.* A role for microRNAs in the Drosophila circadian clock. *Genes Dev* 2009;**23**:2179-91.
408 Sun Y, Koo S, White N, *et al.* Development of a micro-array to detect human and mouse microRNAs and characterization of expression in human organs. *Nucleic acids research* 2004;**32**:e188.
409 Tang X, Gal J, Zhuang X, *et al.* A simple array platform for microRNA analysis and its application in mouse tissues. *RNA (New York, NY* 2007;**13**:1803-22.
410 Saini HK, Enright AJ, Griffiths-Jones S. Annotation of mammalian primary microRNAs. *BMC genomics* 2008;**9**:564.

ABSTRACTS ARISING FROM THIS WORK

1. Diurnal rhythmicity of microRNA mir-16 in the intestine is regulated by global nutrient availability and peaks in antiphase to maximal intestinal function
   Balakrishnan A, Stearns AT, Rhoads DB, Ashley SW, Tavakkolizadeh A.
   Presented at the Academic Surgical Congress, Florida, 2009
   Journal of Surgical Research 2009; 151(2): 248

2. Regulation of enterocyte proliferation by diurnally rhythmic microRNA mir-16
   Balakrishnan A, Stearns AT, Rhoads DB, Ashley SW, Tavakkolizadeh A.
   Presented at the United European Gastroenterology Week/ World Congress of Gastroenterology, London, 2009
   Awarded Young Scientist Travel award

3. Coordinated phase shift of intestinal clock gene and sodium glucose cotransporter (SGLT1) rhythms with switched feeding
   Balakrishnan A, Stearns AT, Rhoads DB, Ashley SW, Tavakkolizadeh A
   Presented at Digestive Diseases Week, San Diego 2008
   Gastroenterology 2008; 134(4): A264-A265

4. Diurnal expression of circadian clock genes in the jejunum
   Balakrishnan A, Stearns A, Rhoads DB, Ashley SW, Tavakkolizadeh A
   Presented at Digestive Diseases Week, Washington 2007
   Gastroenterology 2007; 132(4): A537

The Journal of Nutrition
Nutrient Physiology, Metabolism, and Nutrient-Nutrient Interactions

Restricted Feeding Phase Shifts Clock Gene and Sodium Glucose Cotransporter 1 (SGLT1) Expression in Rats[1–4]

Anita Balakrishnan,[5,6]* Adam T. Stearns,[5,7] Stanley W. Ashley,[5] Ali Tavakkolizadeh,[5] and David B. Rhoads[8]*

[5]Department of Surgery, Brigham and Women's Hospital and Harvard Medical School, Boston, MA 02115; [6]School of Clinical Sciences, Division of Gastroenterology, University of Liverpool, Liverpool L69 3GE, United Kingdom; [7]Department of Physiology, Anatomy and Genetics, University of Oxford, Oxford OX1 2JD, United Kingdom; and [8]Pediatric Endocrine Unit, MassGeneral Hospital for Children and Harvard Medical School, Boston, MA 02114

Abstract

The intestine exhibits striking diurnal rhythmicity in glucose uptake, mediated by the sodium glucose cotransporter (SGLT1); however, regulatory pathways for these rhythms remain incompletely characterized. We hypothesized that SGLT1 rhythmicity is linked to the circadian clock. To investigate this, we examined rhythmicity of *Sglt1* and individual clock genes in rats that consumed food ad libitum (AL). We further compared phase shifts of *Sglt1* and clock genes in a second group of rats following restricted feeding to either the dark (DF) or light (LF) phase. Rats fed during the DF were pair-fed to rats fed during the LF. Jejunal mucosa was harvested across the diurnal period to generate expression profiles of *Sglt1* and clock genes *Clock*, *Bmal1* (*brain-muscle Arnt-like 1*), *ReverbA/B*, *Per* (*Period*) *1/2*, and *Cry* (*Cryptochrome*) *1/2*. All clock genes were rhythmic in AL rats ($P < 0.05$). *Sglt1* also exhibited diurnal rhythmicity, with peak expression preceding nutrient arrival ($P < 0.05$). Light-restricted feeding shifted the expression rhythms of *Sglt1* and most clock genes (*Bmal1*, *ReverbA* and *B*, *Per1*, *Per2*, and *Cry1*) compared with dark-restricted feeding ($P < 0.05$). The *Sglt1* rhythm shifted in parallel with rhythms of *Per1* and *ReverbB*. These effects of restricted feeding highlight luminal nutrients as a key Zeitgeber in the intestine, capable of simultaneously shifting the phases of transporter and clock gene expression, and suggest a role for clock genes in regulating *Sglt1* and therefore glucose uptake. Understanding the regulatory cues governing rhythms in intestinal function may allow new therapeutic options for conditions of dysregulated absorption such as diabetes and obesity. J. Nutr. 140: 908–914, 2010.

Introduction

Circadian rhythmicity in gene and protein expression has been demonstrated in numerous mammalian organs and tissues. These rhythms serve a major physiological role by matching many visceral functions to anticipated environmental demands (1). We and others have documented circadian rhythmicity in intestinal expression of digestive enzymes and transporters for both nutrients and nonnutrients (2–5). Our studies on the intestinal sodium-glucose cotransporter (SGLT1),[9] which is responsible for all active intestinal glucose uptake, demonstrate that rhythmicity in intestinal glucose uptake is conferred entirely by rhythmicity in transcription, translation, and function of SGLT1 (3). However, the molecular cues triggering rhythmicity in the *Sglt1* gene (*Slc5a1*) and protein expression remain unknown.

Previous studies have identified a set of genes, referred to as clock genes, involved in the regulation of circadian rhythms, such as hormone secretion, and autonomic functions, including body temperature and blood pressure (6,7). In mammals, the master clock resides in the suprachiasmatic nucleus (SCN) and maintains a 24-h periodicity entrained by light (8) and regulated via opposing positive and negative molecular feedback loops. Mammalian clock components include *Per1*, *Per2*, *Clock*, *Bmal1*, *ReverbA* and *B*, and *Cry1* and *Cry2*. Heterodimers of Clock and Bmal1 positively regulate *Per* and *Cry* genes via

[1] Supported by the NIH grant 5 R01 DK047326 (S.W.A.), ADA grant 7-05-RA-121 (D.B.R.), the Harvard Clinical Nutrition Research Center grant (A.T.) P30-DK040561, the Nutricia Research Foundation (A.B.), and the Berkeley Fellowship (A.T.S.).

[2] Author disclosures: A. Balakrishnan, A. T. Stearns, S. W. Ashley, A. Tavakkolizadeh, and D. B. Rhoads, no conflicts of interest.

[3] Supplemental Figures 1 and 2 and Supplemental Table 1 are available with the online posting of this paper at jn.nutrition.org.

[4] This manuscript was presented in poster form at Digestive Diseases Week 2007 and 2008, and published in abstract form only in the supplementary issue of *Gastroenterology* (less than 400 words).

* To whom correspondence should be addressed. E-mail: anita.balakrishnan@doctors.org.uk and rhoads@helix.mgh.harvard.edu.

[9] Abbreviations used: AL, ad libitum; DF, dark fed; HALO, hours after light onset; LF, light fed; SCN: suprachiasmatic nucleus.

Manuscript received October 13, 2009. Initial review completed November 6, 2009. Revision accepted February 1, 2010.
First published online March 3, 2010; doi:10.3945/jn.109.116749.

promoter E-boxes (CAnnTG). Nuclear accumulation of Per and Cry inhibits Clock/Bmal1 activity, which represses *Per* and *Cry*, thereby setting up an oscillation in their expression (9,10). Orphan nuclear receptors *ReverbA* and *ReverbB* have been identified as key regulators linking the positive and negative limbs of the circadian oscillator, with *Reverb* transcription driven by Bmal1/Clock and suppressed by Per and Cry (11,12). In addition to the central SCN circadian pacemaker, clock genes are also expressed in many peripheral tissues, including the heart, retina, lung, kidney, peripheral blood cells, and liver (13–16). While several clock genes are known to oscillate in the intestine, the temporal expression patterns of *Reverbs* have not been characterized.

While light is the predominant Zeitgeber ("time giver" or entraining cue) for the central SCN clock, peripheral clocks can be dissociated from the central clock by various stimuli, including nutrient availability and glucocorticoid exposure (11,17,18; A. T. Stearns, A. Balakrishnan, K. Abolmaali, D. B. Rhoads, S. W. Ashley, A. Tavakkolizadeh, unpublished results). Feeding in particular is a strong Zeitgeber. Restricted feeding can reset the peripheral clocks in the liver, kidney, heart, and pancreas within 1 wk with no change in phase of the SCN clock (19–21) and is a sufficiently potent Zeitgeber to reinstate rhythmicity of the liver clock in otherwise arrhythmic SCN-lesioned mice (22).

We hypothesized that rhythmic expression of SGLT1 in the rat intestine is driven by peripheral circadian clocks to link function to nutrient availability. We surmised that *Sglt1* would have a similar phase to 1 or more clock genes and that clock genes and *Sglt1* would exhibit parallel phase shifts in response to restricted feeding. Our studies show that nutrient availability acts as a major Zeitgeber in rat intestine, independent of light cycle, and simultaneously phase shifts *Sglt1* and clock gene expression. These results provide evidence for regulation of SGLT1 by the peripheral clock.

Materials and Methods

Animal studies. All animal study protocols were prospectively approved by the Harvard Medical Area Standing Committee on Rats.

Sprague-Dawley rats (50 males, 7 wk old) were purchased from Harlan World and acclimatized to a 12-h-light/-dark photoperiod for 5 d with ad libitum access to food (Picolab Rodent Diet 20, LabDiet, containing 21% protein, 9.9% fat, 4.4% fiber, and an energy value of 3.42 kcal/g) and water. Time is designated as H After Light Onset (HALO), with HALO 0 at 0700 h (lights on). In the control arm, rats received food ad libitum (designated AL) and were killed at 3-h intervals beginning at HALO 0 (n = 6–7 per time; **Supplemental Fig. 1***A*). A second group of 50 male rats were similarly acclimatized, then randomly assigned to be fed for 7 d either during only the dark phase (designated DF; HALO 12–24, Supplemental Fig. 1*B*) or light phase (designated LF; HALO 0–12, Supplemental Fig. 1C). DF rats were pair-fed to LF rats to ensure equal food intake. Rats were housed in pairs in cages. LF animals were given 100 g of food per cage at 0700. The remaining food at 1900 was weighed and subtracted from 100 g to calculate the amount consumed per pair of rats (we assumed that both rats consumed equal amounts of food). The mean daily consumption of LF rats was calculated, multiplied by 2, and provided to each pair of DF rats at 1900. No food remained in the cages of DF rats at 0700 the next day. To minimize disruption during restricted feeding, rats were weighed only 3 times (d 0, 3, and 7). On d 7, rats (n = 6–7) were killed at 6-h intervals beginning at HALO 3.

Tissue harvest. Rats were anesthetized with sodium pentobarbital (50 mg/kg, Ovation Pharmaceuticals). The small intestine from 2 cm distal to the ligament of Treitz was harvested via midline laparotomy and rinsed with ice-cold saline to remove luminal contents. The 10 cm of jejunum was divided along the antimesenteric border, mucosa scraped from the underlying muscle, snap-frozen in liquid nitrogen, and stored at −80°C for subsequent RNA or protein extraction.

RNA extraction, RT, and real-time PCR. Total RNA was extracted using the mirVana kit (Ambion). Samples were reverse transcribed simultaneously with Superscript III (Invitrogen) and oligo-dT. Real-time PCR was performed as previously described (3). mRNA levels were expressed as ratios to the stably expressed *B*-actin. All primers were ordered as custom oligonucleotides from Invitrogen (**Supplemental Table 1**), except rat *Per2*, for which mRNA expression was measured using the Taqman primer-probe and gene expression Master mix (Applied Biosystems).

Protein extraction and Western blotting. SGLT1 protein expression was measured in total lysates from jejunal mucosal scrapings as previously described (3). Diurnal Per1 protein expression in rat jejunum was measured in nuclear extracts of freshly collected mucosal scrapings (Nxtract nuclear extraction kit, Sigma). Western blotting was performed

TABLE 1 Rhythmicity, acrophase, mesor, and amplitude of clock gene and *Sglt1* mRNA expression in AL rats fed either only during DF or LF periods[1]

Gene	Group	*P*-value[2]	Acrophase[3] (HALO, hh:mm)	Mesor[4]	Amplitude,[5] %	Phase difference[6]
Per1	AL	0.0014	09:28	1.29	48	
	DF	0.0004	07:38	1.09	63	−01:50
	LF	0.0015	01:38	0.96	57	−07:50
Per2	AL	0.0008	15:59	3.02	57	
	DF	0.0460	13:29	4.51	57	−02:30
	LF	0.0470	05:32	3.22	59	−10:27
Bmal1	AL	<0.0001	23:04	0.71	100	
	DF	0.0003	21:35	0.83	100	−01:29
	LF	0.0019	12:34	1.07	78	−10:30
Clock	AL	0.0008	21:23	0.80	38	
	DF	0.5877				
	LF	0.5065				
ReverbA	AL	<0.0001	06:21	0.57	76	
	DF	0.0001	04:34	0.37	120	−01:47
	LF	0.0002	21:34	0.19	60	−08:47
ReverbB	AL	0.0003	08:34	0.81	41	
	DF	<0.0001	07:50	0.85	78	−00:44
	LF	<0.0001	01:29	0.71	67	−07:05
Cry1	AL	0.0015	20:08	1.41	17	
	DF	0.0145	17:24	1.57	30	−02:44
	LF	0.0033	08:50	1.41	33	−14:18
Cry2	AL	0.0097	18:41	1.47	36	
	DF	0.0790				
	LF	0.6250				
Sglt1	AL	<0.0001	10:44	1.60	51	
	DF	<0.0001	09:27	1.86	118	−01:17
	LF	<0.0001	02:27	1.96	88	−08:17

[1] Cosinor analysis was used to determine rhythmicity, acrophase, mesor, and amplitude of clock gene mRNA expression in AL, DF, and LF rats.
[2] The *P*-values indicate the fit of the data to a 24-h periodicity, with a *P*-value of 0.05 indicating a 5% probability that the observed 24-h periodicity occurred by chance alone.
[3] The acrophase is expressed as HALO (lights on is at 0700; hence, HALO 0 is 0700).
[4] The mesor is the rhythm-adjusted mean.
[5] The amplitude is expressed as a percentage of the mean to facilitate comparison across means.
[6] The phase difference refers to the shift in peak expression of the gene (acrophase) in DF or LF animals compared with AL animals.

as previously described (3). Nuclear or total protein extracts (75 μg) were resolved on 4–12% Bis-Tris gels, transferred to polyvinylidene-fluoride membranes, blocked, then incubated with either rabbit anti-SGLT1 (1:4000; Chemicon International) or rabbit anti-Per1 (1:200; Santa Cruz Biotechnology), respectively. Protein expression was normalized to *B*-actin (mouse anti-*B*-actin, 1:1000, Labvision).

Statistical analysis. Data are presented as means ± SE. Graphical analysis was performed using Graphpad Prism. Circadian rhythmicity was determined as described previously by cross-sectional analysis using the Cosinor procedure, freely available online, and assuming a 24-h period (4,23,24). The acrophase (time of peak expression), mesor (rhythm-adjusted mean), amplitude of rhythmicity, and significance of fit to a 24-h period (as indicated by the *P*-value) for each gene was abstracted from the program. mRNA levels are expressed as ratios to mean expression of the respective gene at HALO 3 (DF group for all restricted-fed rats). The mesor is an arbitrary value, precluding comparisons between genes. However, amplitudes are independent of scaling and can thus be compared among genes and groups. Two-tailed *t* tests were used to compare weights of DF and LF groups. The acrophases for AL rats were subtracted from the acrophases of DF and LF rats to identify phase shifts relative to AL rats. A 1-sample *t* test was used to identify a significant difference in mean phase shift of DF or LF rats from the value 0 (complete absence of phase shift relative to AL). Differences were considered significant at $P < 0.05$.

Results

Rhythmicity of gene expression in jejunum of AL rats. All clock genes examined were expressed in intestinal jejunal mucosa. Cosinor analysis confirmed previously documented rhythmicity in expression of *Clock*, *Bmal1*, *ReverbA*, *Per1*, *Per2*, and *Cry1* (**Table 1**; **Fig. 1**) and demonstrated that rhythmicity for all measured clock genes fit a 24-h periodicity ($P < 0.05$) (4,23). Periodicities of 24 h were also detected for *ReverbB*, which exhibited an acrophase (peak) 2 h later than its paralog *ReverbA*, and for *Cry2*, which exhibited an acrophase 2 h earlier than *Cry1* (Fig. 1*C*,*E*). In AL rats, amplitudes were greatest for *Bmal1*, *ReverbA*, *Per1*, and *Per2* and more modest for *Clock*, *Cry1*, and *Cry2*. Positive clock regulators *Bmal1* and *Clock* peaked at late dark phase ($P < 0.0001$; Table 1; Fig. 1*A*, *B*). In contrast, negative regulators *Per1*, *ReverbA*, and *ReverbB* peaked between HALO 6 and 10 and reached a trough at HALO 0 during peak expression of *Bmal1* and *Clock* ($P < 0.005$; Fig. 1*D*,*E*). *Per2* expression peaked at HALO 16, a 6-h lag behind *Per1* ($P < 0.005$; Fig. 1*D*). *Sglt1* mRNA exhibited robust 24-h rhythmicity as we have reported previously (3), with peak expression at HALO 11, close to that for *Per1* (HALO 9) as well as *ReverbB* (HALO 9, Table 1; Fig. 1*D–F*).

Restricted feeding phase-shifts expression rhythms of both SGLT1 and clock genes. To identify regulatory cues triggering rhythmicity in *Sglt1* and clock genes, we sought to define their responses to imposed food availability, thus separating nutrient cues from the light-dark cycle.

Food intake and body weight. Food consumption by LF rats on d 1 was 16 g (**Supplemental Fig. 2***A*), ~4 g less than the 20 g/d consumed by AL rats of similar weight (25) but had normalized by d 3. LF rats weighed less than DF rats on d 4 despite equal food intake (244 ± 1.4 g vs. 251 ± 1.4 g; Supplemental Fig. 2*B*; $P < 0.05$). This was possibly a catabolic response to the stress of restricted feeding during daytime, or a relatively slower adaptation of intestinal nutrient absorption to the change in period of peak nutrient availability. Weights had equalized by harvest.

Rhythmicity of Sglt1 and clock genes. DF rats would be expected to display rhythms similar to AL (**Fig. 2**). Although this was broadly true, we observed a consistent advance in acrophase

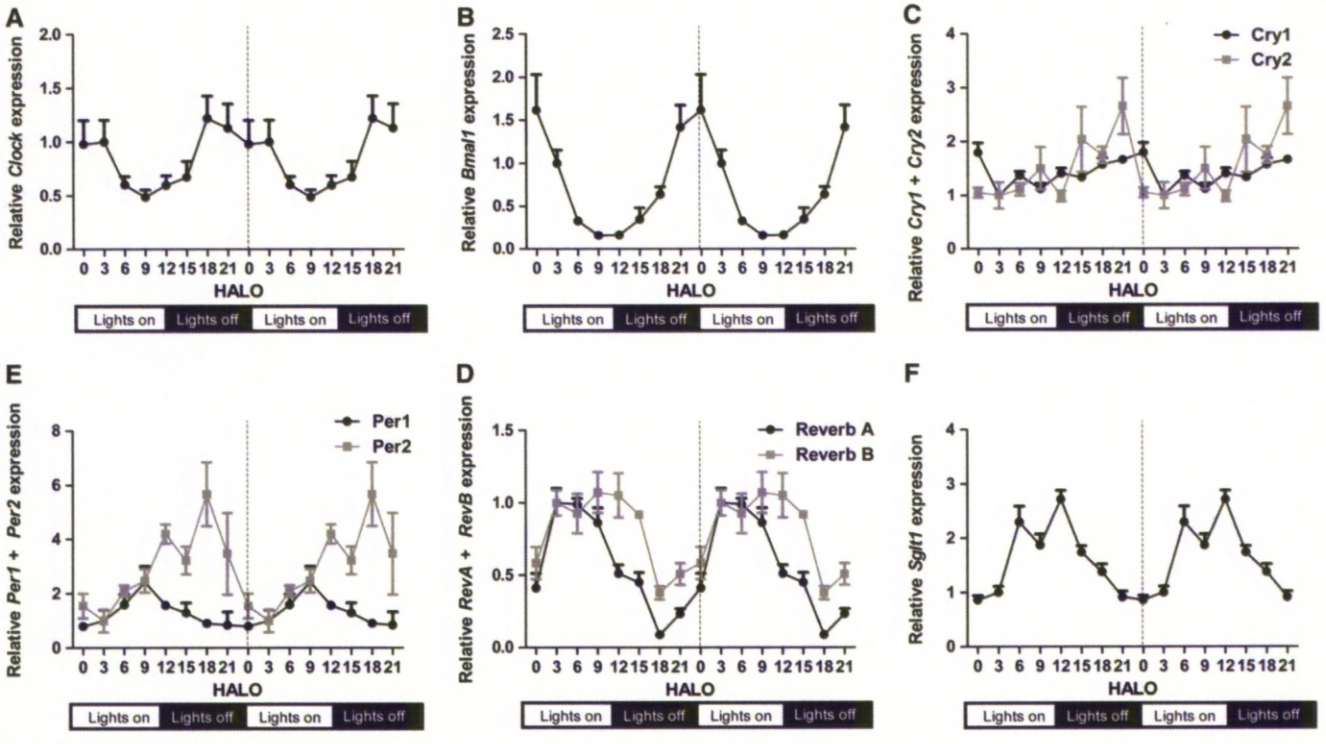

FIGURE 1 Circadian rhythmicity of *Clock* (*A*), *Bmal1* (*B*), *Cry1*/*Cry2* (*C*), *Per1*/*Per2* (*D*), *ReverbA*/*ReverbB* (*E*), and *Sglt1* (*F*) in AL rats. To facilitate comparisons of rhythmicity and amplitude, the *x*-axis was double-plotted and expression (*y*-axis) indexed to mean HALO 3 expression for each gene. Values are expressed as mean ± SEM, $n = 6$ or 7. *P*-values are shown in Table 1.

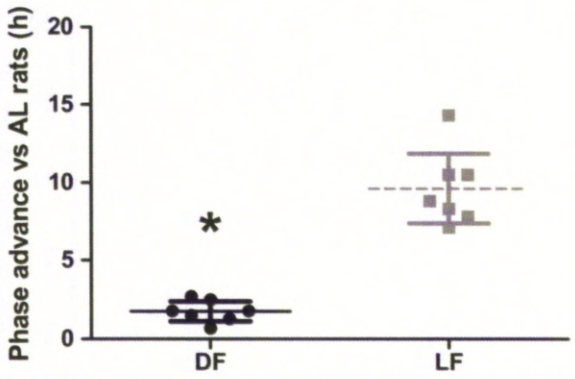

FIGURE 2 Phase difference in acrophases of clock genes and *Sglt1* in DF and LF rats relative to AL rats showing a phase advance of 1.7 and 9.6 h, respectively. Values are individual values (n = 6 or 7) and means ± 95% CI. *Different from DF, $P < 0.05$.

for most clock genes and *Sglt1* in DF compared with AL rats (mean phase advance of 1.7 h; $P = 0.0005$) (Table 1; Fig. 2). Periodicity was retained in most clock genes and *Sglt1* in LF rats, with a mean phase advance of 9.6 and 7.9 h compared with the AL and DF group, respectively ($P < 0.0001$) (Table 1; Fig. 2). In contrast, amplitudes for *Clock* and *Cry2* were lower in both restricted groups compared with AL, leading to a loss of rhythmicity (**Fig. 3***A*,*D*).

The phase of the *Sglt1* mRNA rhythm was advanced in both DF and LF rats (1 and 8 h, respectively). *Sglt1* mRNA remained rhythmic in LF rats, but with a lower peak, blunted amplitude, and a 7-h phase difference from DF rats (**Fig. 4***E*; $P < 0.05$). SGLT1 protein expression in DF rats peaked 4 h later than mRNA expression (HALO 14), 3-fold higher than the trough (**Fig. 5***A*; $P < 0.05$). SGLT1 protein expression was highest during the day in LF rats, with levels 70% higher at HALO 9 than HALO 21, but did not attain 24-h rhythmicity (Fig. 5*A*; $P = 0.24$). We also observed higher trough SGLT1 protein expression in LF than in DF rats ($P = 0.001$ at HALO 21; Fig. 5*A*).

Clock genes *Per1* and *ReverbB* both displayed similar phase shifts to *Sglt1* under the 2 restricted-feeding regimens. The concordance between SGLT1 and Per1 was also observed at the protein level in jejunal nuclear extracts (Fig. 5*A*,*B*). A 24-h periodicity was observed in both DF and LF rats, with acrophases of HALO 2 and HALO 22, respectively (Fig. 5*B*). The period of increasing Per1 protein coincided with the nadir of *Sglt1* mRNA and presumably its transcription (Figs. 4*E* and 5*B*). *ReverbA* also exhibited similar phase shifts on restricted feeding, but peak *ReverbA* expression preceded *Sglt1* expression by 4–5 h in all 3 groups.

Discussion

All clock genes exhibited robust circadian rhythmicity in jejunal mucosa of AL rats. Restricting food to the LF dissociated these

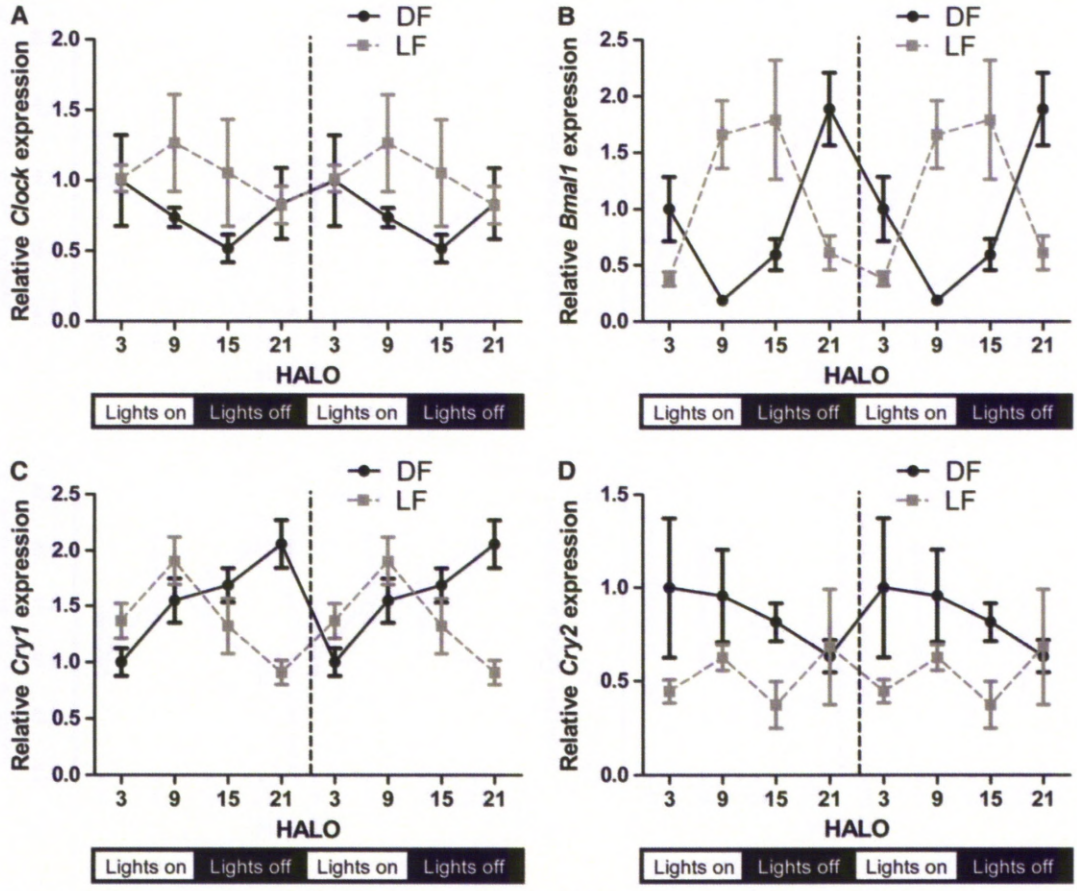

FIGURE 3 Circadian expression of *Clock* (*A*), *Bmall* (*B*), *Cry1* (*C*), and *Cry2* (*D*) in DF and LF rats. To facilitate comparisons of rhythmicity and amplitude, the *x*-axis was double-plotted and expression (*y*-axis) indexed to mean HALO 3 DF expression for each gene. Values are expressed as mean ± SEM, n = 6 or 7. *P*-values are shown in Table 1.

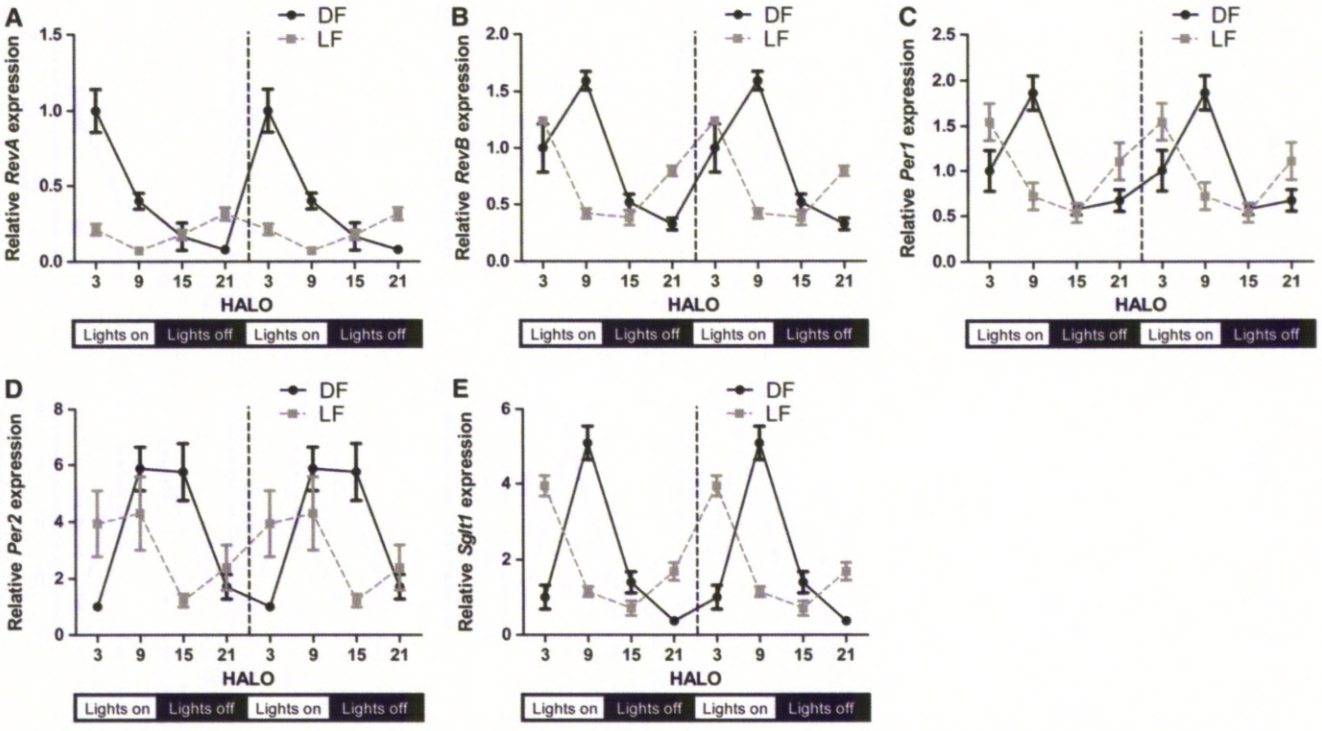

FIGURE 4 Circadian expression of *ReverbA* (*A*), *ReverbB* (*B*), *Per1* (*C*), *Per2* (*D*), and *Sglt1* (*E*) in DF and LF rats. To facilitate comparisons of rhythmicity and amplitude, the *x*-axis was double-plotted and expression (*y*-axis) indexed to mean HALO 3 DF expression for each gene. Values are expressed as mean ± SEM, $n = 6$ or 7. *P*-values are shown in Table 1.

rhythms from the light cycle. Notably, rhythmicity of both *Sglt1* mRNA and protein were shifted. Previous studies from our group and others have shown that rhythmicity of SGLT1 protein expression correlates with rhythmicity at a functional level in the intestine (2,3). These results establish nutrient availability as a key Zeitgeber for the peripheral intestinal clock(s) as well as the expression rhythm of the glucose transporter SGLT1.

Determining the relative shifts in glucose transporter and clock gene rhythms in response to restricted feeding was a major study aim. After 7 d of restricted feeding to either the light or dark period, phase differences of 6–11.5 h were observed for *Sglt1* and 5 of the 8 clock genes examined. The lack of a complete 12-h phase shift difference between dark- and light-fed rats may reflect the influence of other factors such as glucocorticoids, which can also partially phase shift gene expression (18,19; A. T. Stearns, A. Balakrishnan, K. Abolmaali, D. B. Rhoads, S. W. Ashley, A. Tavakkolizadeh, unpublished results). The duration of nutrient availability may have also affected the degree of phase shift, because a shorter period of food availability in other studies (HALO 2–8) (26) produced a greater phase shift than we observed. Moreover, peripheral clocks adapt to restricted feeding at different rates; liver shifts much more quickly than lung (19). Although it is possible that the small intestine would achieve a complete phase shift following longer restricted feeding, the sufficiency of 4-d adaptation previously reported (27), the equal weights between rats in the 2 restricted groups, and the plateau in food intake in the LF rats [matching that expected for rats of that weight (25)] all suggest that the partial phase shift was due to factors other than incomplete adaptation. We note that the rapid adaptation observed in liver may result from more direct (i.e. local) stimulus-response pathways. Adaptation in the intestine, particularly for diurnally rhythmic functions, is indirect [as shown by isolated loops (28)] and may entail cephalic and other inputs. The apparently longer period required for adaptation by intestine compared with liver may reflect a tissue-specific feature necessary to stabilize the rhythms in intestinal functions despite moderately varying nutrient intake patterns. Possibly, linkage of phases of critical intestinal functions such as proliferation and absorption to extra-luminal inputs could serve to coordinate these rhythms, thereby assuring that DNA synthesis and peak absorption do not coincide.

In AL rats, *Per1* and *ReverbB* mRNA expression peaked in phase with *Sglt1*, slightly preceding *Sglt1* expression by 1–2 h. Restricted feeding produced similar phase shifts for *Sglt1*, *Per1*, and *ReverbB*; all 3 genes were phase shifted by 1–2 h in DF rats and 7–8 h in LF rats compared with AL rats. The presence of 4 canonical E-boxes in the *Sglt1* promoter raises the possibility that the Per1 transcription factor is involved in controlling *Sglt1* rhythmicity. If so, occurrence of the *Sglt1* mRNA nadir when the Per1 protein level is rising suggests that Per1 exerts a negative influence. Lack of Reverb response elements in the *Sglt1* promoter argues against ReverbB involvement but does not preclude indirect regulation or use of a noncanonical element.

We were surprised that nocturnal food restriction advanced the phases of *Sglt1* and intestinal clock genes by 1–2 h compared with AL feeding. Although only a modest amount of food is usually consumed during the day (10–20% daily intake) (27), the restriction was apparently sufficient to shift gene expression phases. The daytime food deprivation in DF rats effectively prevented "early phase eating," consumption of food in the late LF, and may have enhanced entrainment signals normally produced by hunger or hormonal responses, thereby sharpening the anticipatory intestinal gene induction and advancing the acrophases in DF rats. In either case, it is clear that restricting food access to 12 h led to detectable alterations in intestinal rhythms.

Overall SGLT1 protein expression was higher in LF rats compared with DF rats ($P = 0.010$), despite no significant

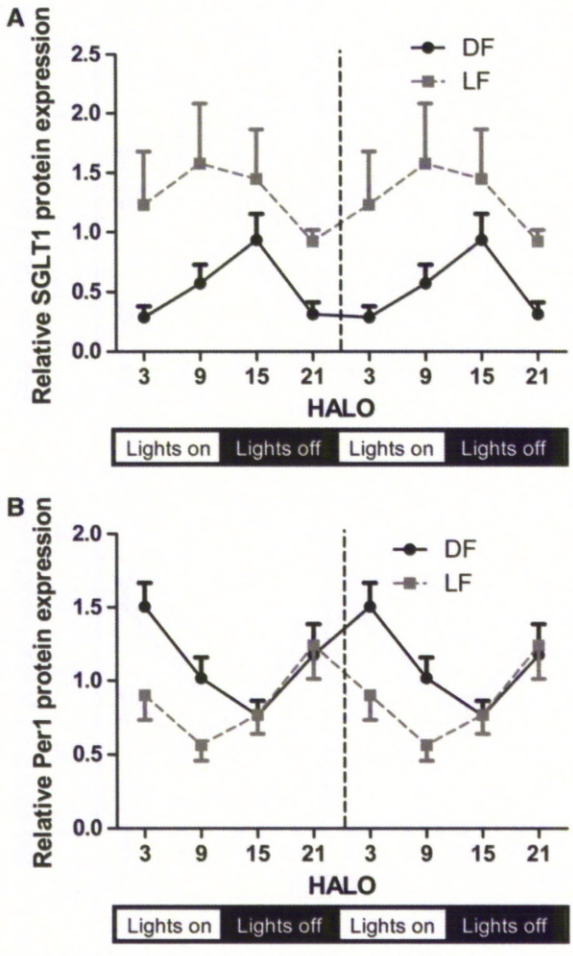

FIGURE 5 Protein expression of SGLT1 (*A*) and Per1 (*B*) in DF and LF rats. Values are expressed as mean ± SEM, $n = 6$ or 7.

difference in mRNA levels ($P = 0.946$). This result is consistent with our previous finding that post-transcriptional events are also important in regulating intestinal SGLT1 expression (28). In light of reports that SGLT1 expression is increased in obesity and diabetes (29,30), it would be interesting to assess the functional consequences of our observation by comparing glucose homeostasis in light- and dark-fed rats as well as measuring SGLT1 expression in shift workers who are forced to eat off schedule and have increased risk of developing glucose intolerance (31).

Our findings lend support to the notion that clock genes cue intestinal rhythmicity in response to nutrient availability. Clock genes are clearly important transcriptional regulators (26,32, 33). Clock and clock-controlled genes have been implicated in the regulation of other proteins such as the Na+/H+ exchanger Nhe3 in the kidney (32), the oligopeptide transporter Pept1 (26), and the multidrug resistance 1 gene (33). Pan and Hussain (34), using Clock mutant mice, presented evidence for its involvement in intestinal absorptive rhythms. Our studies add to the existing evidence implicating clock genes in absorptive rhythms and provide important information on the role of clock genes in regulating SGLT1 rhythmicity and thereby rhythmicity of glucose uptake in the intestine.

The glucose concentration generated from digestion may be a major stimulus in regulating the expression of clock and *Sglt1* genes in the intestine. In an intriguing study, glucose was shown to downregulate *Per1* and *Per2* mRNA expression in rat-1 fibroblasts (35). The authors hypothesized that glucose itself, which displays a modest circadian rhythm in rodents (36), provides a Zeitgeber for peripheral clocks, acting to downregulate *Per1* and *Per2* via other transcriptional regulators. This hypothesis is consistent with decreased *Per1* mRNA levels during the period of nutrient consumption in both AL and DF rats. Although plasma glucose levels are relatively constant, enterocytes (and probably also hepatocytes) are unique in experiencing abrupt increases in glucose supply and intracellular concentrations following feeding. Thus, glucose suppression of *Per* expression may be the molecular basis for resetting intestinal (and liver) clocks by nutrient availability. The ability of these 2 "gateway" organs to respond rapidly to nutrient intake patterns via peripheral clocks would have great adaptive value by optimally coordinating absorptive functions with nutrient delivery.

In summary, we have shown that nutrients provide a major Zeitgeber for intestinal clock genes and that shifting the period of availability simultaneously phase shifts expression of clock genes and intestinal transporters. Further studies are required to define the molecular mechanism linking clock genes to *Sglt1* rhythmicity. The regulatory mechanisms governing circadian rhythmicity of intestinal function may have a considerable role in obesity and diabetes and a better understanding could lead to new therapies for these worsening epidemics.

Acknowledgments

We thank John Young for excellent technical assistance and Jan Rounds for invaluable managerial assistance. A.B., S.W.A., A.T., and D.B.R. designed the studies; A.B. and A.T.S. conducted the research; A.B. analyzed the data; A.B., A.T., and D.B.R. wrote the paper; and A.B. and D.B.R. had primary responsibility for final content. All authors read and approved the final manuscript.

Literature Cited

1. Dunlap JC. Molecular bases for circadian clocks. Cell. 1999;96:271–90.
2. Tavakkolizadeh A, Berger UV, Shen KR, Levitsky LL, Zinner MJ, Hediger MA, Ashley SW, Whang EE, Rhoads DB. Diurnal rhythmicity in intestinal SGLT-1 function, V(max), and mRNA expression topography. Am J Physiol Gastrointest Liver Physiol. 2001;280:G209–15.
3. Balakrishnan A, Stearns AT, Rounds J, Irani J, Giuffrida M, Rhoads DB, Ashley SW, Tavakkolizadeh A. Diurnal rhythmicity in glucose uptake is mediated by temporal periodicity in the expression of the sodium-glucose cotransporter (SGLT1). Surgery. 2008;143:813–8.
4. Stearns AT, Balakrishnan A, Rhoads DB, Ashley SW, Tavakkolizadeh A. Diurnal rhythmicity in the transcription of jejunal drug transporters. J Pharmacol Sci. 2008;108:144–8.
5. Pan X, Terada T, Irie M, Saito H, Inui K. Diurnal rhythm of H+-peptide cotransporter in rat small intestine. Am J Physiol Gastrointest Liver Physiol. 2002;283:G57–64.
6. Richards AM, Nicholls MG, Espiner EA, Ikram H, Cullens M, Hinton D. Diurnal patterns of blood pressure, heart rate and vasoactive hormones in normal man. Clin Exp Hypertens A. 1986;8:153–66.
7. Selmaoui B, Touitou Y. Reproducibility of the circadian rhythms of serum cortisol and melatonin in healthy subjects: a study of three different 24-h cycles over six weeks. Life Sci. 2003;73:3339–49.
8. Hastings MH. Circadian clocks. Curr Biol. 1997;7:R670–2.
9. Panda S, Hogenesch JB. It's all in the timing: many clocks, many outputs. J Biol Rhythms. 2004;19:374–87.
10. Reppert SM, Weaver DR. Coordination of circadian timing in mammals. Nature. 2002;418:935–41.
11. Torra IP, Tsibulsky V, Delaunay F, Saladin R, Laudet V, Fruchart JC, Kosykh V, Staels B. Circadian and glucocorticoid regulation of Rev-erbalpha expression in liver. Endocrinology. 2000;141:3799–806.
12. Preitner N, Damiola F, Lopez-Molina L, Zakany J, Duboule D, Albrecht U, Schibler U. The orphan nuclear receptor REV-ERBalpha controls

circadian transcription within the positive limb of the mammalian circadian oscillator. Cell. 2002;110:251–60.
13. Oishi K, Sakamoto K, Okada T, Nagase T, Ishida N. Humoral signals mediate the circadian expression of rat period homologue (rPer2) mRNA in peripheral tissues. Neurosci Lett. 1998;256:117–9.
14. Oishi K, Sakamoto K, Okada T, Nagase T, Ishida N. Antiphase circadian expression between BMAL1 and period homologue mRNA in the suprachiasmatic nucleus and peripheral tissues of rats. Biochem Biophys Res Commun. 1998;253:199–203.
15. Takata M, Burioka N, Ohdo S, Takane H, Terazono H, Miyata M, Sako T, Suyama H, Fukuoka Y, et al. Daily expression of mRNAs for the mammalian Clock genes Per2 and clock in mouse suprachiasmatic nuclei and liver and human peripheral blood mononuclear cells. Jpn J Pharmacol. 2002;90:263–9.
16. Sakamoto K, Oishi K, Nagase T, Miyazaki K, Ishida N. Circadian expression of clock genes during ontogeny in the rat heart. Neuroreport. 2002;13:1239–42.
17. Yamamoto T, Nakahata Y, Tanaka M, Yoshida M, Soma H, Shinohara K, Yasuda A, Mamine T, Takumi T. Acute physical stress elevates mouse period1 mRNA expression in mouse peripheral tissues via a glucocorticoid-responsive element. J Biol Chem. 2005;280:42036–43.
18. Balsalobre A, Brown SA, Marcacci L, Tronche F, Kellendonk C, Reichardt HM, Schutz G, Schibler U. Resetting of circadian time in peripheral tissues by glucocorticoid signaling. Science. 2000;289:2344–7.
19. Stokkan KA, Yamazaki S, Tei H, Sakaki Y, Menaker M. Entrainment of the circadian clock in the liver by feeding. Science. 2001;291:490–3.
20. Damiola F, Le Minh N, Preitner N, Kornmann B, Fleury-Olela F, Schibler U. Restricted feeding uncouples circadian oscillators in peripheral tissues from the central pacemaker in the suprachiasmatic nucleus. Genes Dev. 2000;14:2950–61.
21. Storch KF, Lipan O, Leykin I, Viswanathan N, Davis FC, Wong WH, Weitz CJ. Extensive and divergent circadian gene expression in liver and heart. Nature. 2002;417:78–83.
22. Hara R, Wan K, Wakamatsu H, Aida R, Moriya T, Akiyama M, Shibata S. Restricted feeding entrains liver clock without participation of the suprachiasmatic nucleus. Genes Cells. 2001;6:269–78.
23. Nelson W, Tong YL, Lee JK, Halberg F. Methods for cosinor-rhythmometry. Chronobiologia. 1979;6:305–23.
24. Circadian Rhythm Laboratory. University of South Carolina. [cited 2010 Feb 16]. Available from: http://www.circadian.org.
25. Stearns AT, Balakrishnan A, Rounds J, Rhoads DB, Ashley SW, Tavakkolizadeh A. Capsaicin-sensitive vagal afferents modulate post-transcriptional regulation of the rat Na+/glucose cotransporter SGLT1. Am J Physiol Gastrointest Liver Physiol. 2008;294:G1078–83.
26. Saito H, Terada T, Shimakura J, Katsura T, Inui K. Regulatory mechanism governing the diurnal rhythm of intestinal H+/peptide cotransporter 1 (PEPT1). Am J Physiol Gastrointest Liver Physiol. 2008;295:G395–402.
27. Pan X, Terada T, Okuda M, Inui K. The diurnal rhythm of the intestinal transporters SGLT1 and PEPT1 is regulated by the feeding conditions in rats. J Nutr. 2004;134:2211–5.
28. Stearns AT, Balakrishnan A, Rhoads DB, Ashley SW, Tavakkolizadeh A. Diurnal expression of the rat intestinal sodium-glucose cotransporter 1 (SGLT1) is independent of local luminal factors. Surgery. 2009;145:294–302.
29. Dyer J, Wood IS, Palejwala A, Ellis A, Shirazi-Beechey SP. Expression of monosaccharide transporters in intestine of diabetic humans. Am J Physiol Gastrointest Liver Physiol. 2002;282:G241–8.
30. Osswald C, Baumgarten K, Stumpel F, Gorboulev V, Akimjanova M, Knobeloch KP, Horak I, Kluge R, Joost HG, Koepsell H. Mice without the regulator gene Rsc1A1 exhibit increased Na+-D-glucose cotransport in small intestine and develop obesity. Mol Cell Biol. 2005;25:78–87.
31. Hampton SM, Morgan LM, Lawrence N, Anastasiadou T, Norris F, Deacon S, Ribeiro D, Arendt J. Postprandial hormone and metabolic responses in simulated shift work. J Endocrinol. 1996;151:259–67.
32. Saifur Rohman M, Emoto N, Nonaka H, Okura R, Nishimura M, Yagita K, van der Horst GT, Matsuo M, Okamura H, Yokoyama M. Circadian clock genes directly regulate expression of the Na(+)/H(+) exchanger NHE3 in the kidney. Kidney Int. 2005;67:1410–9.
33. Murakami Y, Higashi Y, Matsunaga N, Koyanagi S, Ohdo S. Circadian clock-controlled intestinal expression of the multidrug-resistance gene mdr1a in mice. Gastroenterology. 2008;135:1636–44 e3.
34. Pan X, Hussain MM. Clock is important for food and circadian regulation of macronutrient absorption in mice. J Lipid Research. 2009;50:1800–13.
35. Hirota T, Okano T, Kokame K, Shirotani-Ikejima H, Miyata T, Fukada Y. Glucose down-regulates Per1 and Per2 mRNA levels and induces circadian gene expression in cultured Rat-1 fibroblasts. J Biol Chem. 2002;277:44244–51.
36. Yamamoto H, Nagai K, Nakagawa H. Role of SCN in daily rhythms of plasma glucose, FFA, insulin and glucagon. Chronobiol Int. 1987;4:483–91.

ARTICLE IN PRESS

YEXCR-08538; No. of pages: 10; 4C:

EXPERIMENTAL CELL RESEARCH XX (2010) XXX–XXX

available at www.sciencedirect.com

ScienceDirect

www.elsevier.com/locate/yexcr

ELSEVIER

Research Article

MicroRNA *mir-16* is anti-proliferative in enterocytes and exhibits diurnal rhythmicity in intestinal crypts

Anita Balakrishnan[a,b,c,*], *Adam T. Stearns*[a,b,d], *Peter J. Park*[e,f], *Jonathan M. Dreyfuss*[e], *Stanley W. Ashley*[a,b], *David B. Rhoads*[b,g], *Ali Tavakkolizadeh*[a,b,*]

[a] *Department of Surgery, Brigham and Women's Hospital, Boston, MA 02115, USA*
[b] *Department of Surgery, Harvard Medical School, Boston, MA 02115, USA*
[c] *School of Clinical Sciences, Division of Gastroenterology, University of Liverpool, Liverpool L69 3GE, UK*
[d] *Department of Physiology, Anatomy and Genetics, University of Oxford, Oxford OX1 2JD, UK*
[e] *Department of Medicine, Brigham and Women's Hospital, Boston, MA 02115, USA*
[f] *Harvard Medical School, Center for Biomedical Informatics, Boston, MA 02115, USA*
[g] *Pediatric Endocrine Unit, MassGeneral Hospital for Children, Boston, MA 02114, USA*

ARTICLE INFORMATION

Article Chronology:
Received 3 June 2010
Revised version received 4 July 2010
Accepted 6 July 2010

Keywords:
MicroRNA
Diurnal
Proliferation
Enterocyte

ABSTRACT

Background and aims: The intestine exhibits profound diurnal rhythms in function and morphology, in part due to changes in enterocyte proliferation. The regulatory mechanisms behind these rhythms remain largely unknown. We hypothesized that microRNAs are involved in mediating these rhythms, and studied the role of microRNAs specifically in modulating intestinal proliferation.

Methods: Diurnal rhythmicity of microRNAs in rat jejunum was analyzed by microarrays and validated by qPCR. Temporal expression of diurnally rhythmic *mir-16* was further quantified in intestinal crypts, villi, and smooth muscle using laser capture microdissection and qPCR. Morphological changes in rat jejunum were assessed by histology and proliferation by immunostaining for bromodeoxyuridine. In IEC-6 cells stably overexpressing *mir-16*, proliferation was assessed by cell counting and MTS assay, cell cycle progression and apoptosis by flow cytometry, and cell cycle gene expression by qPCR and immunoblotting.

Results: *mir-16* peaked 6 hours after light onset (HALO 6) with diurnal changes restricted to crypts. Crypt depth and villus height peaked at HALO 13–14 in antiphase to *mir-16*. Overexpression of *mir-16* in IEC-6 cells suppressed specific G1/S regulators (cyclins D1–3, cyclin E1 and cyclin-dependent kinase 6) and produced G1 arrest. Protein expression of these genes exhibited diurnal rhythmicity in rat jejunum, peaking between HALO 11 and 17 in antiphase to *mir-16*.

Conclusions: This is the first report of circadian rhythmicity of specific microRNAs in rat jejunum. Our data provide a link between anti-proliferative *mir-16* and the intestinal proliferation rhythm and point to *mir-16* as an important regulator of proliferation in jejunal crypts. This function may be essential to match proliferation and absorptive capacity with nutrient availability.

* *Corresponding authors.* Anita Balakrishnan can be contacted at Thorn 1503, Brigham and Women's Hospital, 20 Shattuck Street, Boston, MA 02115, USA. Fax: +1 617 732 8305. Ali Tavakkolizadeh can be contacted at, Department of Surgery, Brigham and Women's Hospital, 75, Francis Street, Boston, MA 02115, USA. Fax: +1 617 732 8305.

E-mail addresses: anita.balakrishnan@doctors.org.uk (A. Balakrishnan), atavakkoli@partners.org (A. Tavakkolizadeh).

Abbreviations: Adcy6, adenylate cyclase type 6; BCL2, B-cell lymphoma 2; BrdU, 5-bromo-2-deoxyuridine; Ccnd1, cyclin D1; Ccnd2, cyclin D2; Ccnd3, cyclin D3; Ccne1, cyclin E1; Cdk4, cyclin-dependent kinase 4; Cdk6, cyclin-dependent kinase 6; HALO, hours after light onset; 3′UTR, 3′ untranslated region

0014-4827/$ – see front matter © 2010 Published by Elsevier Inc.
doi:10.1016/j.yexcr.2010.07.007

Please cite this article as: Anita Balakrishnan, et al., MicroRNA *mir-16* is anti-proliferative in enterocytes and exhibits diurnal rhythmicity in intestinal crypts, Exp Cell Res (2010), doi:10.1016/j.yexcr.2010.07.007

Introduction

Circadian rhythms (24-h oscillations) play a key role in the regulation of numerous physiological functions. Circadian rhythmicity of up to 10% of gene transcripts and an even greater fraction of proteins indicate the involvement of both transcriptional and translational pathways [1–5]. Regulation at both the transcriptional and post-transcriptional levels suggests a role for microRNAs in this process. MicroRNAs are non-coding RNAs able to silence numerous genes simultaneously. Bioinformatics analysis suggests that up to 30% of mammalian gene transcripts are regulated by microRNAs, short non-coding RNAs [6–9]. microRNAs suppress protein expression following recognition of complementary sequences on the 3′UTR (untranslated region) of target genes, either by inducing mRNA cleavage (which manifests as changes in mRNA levels) or inhibiting translation (manifesting as changes in protein levels) [10–12]. The presence of the target sequence for each microRNA on multiple genes permits simultaneous regulation of protein expression from numerous genes by a single microRNA [6,13,14]. The postulated role of microRNAs in "fine-tuning" gene expression suggests that they also contribute to coordinating the circadian rhythmicity of many genes and proteins [15–18].

The intestine displays profound rhythmicity of morphology, resulting in peak absorptive function (e.g. for glucose) coinciding with maximal nutrient delivery to the bowel [19,20]. The number of enterocytes per villus also exhibits a diurnal rhythmicity, with an increase about the time of maximal nutrient availability [21]. Similar rhythmicity has been reported in human gastrointestinal mucosa [22,23]. The exact pathways coordinating rhythmicity in proliferation are presently unknown.

We hypothesize that microRNAs are integral components for mediating circadian rhythms in intestinal proliferation, morphology, and function. To investigate this, we profiled microRNAs in the intestine of *ad libitum* fed rats using oligonucleotide arrays. The anti-proliferative microRNA mir-16 was expressed in both crypt and villus enterocytes but exhibited circadian rhythmicity only in the crypts. The cell cycle regulators Ccnd1, Ccnd2, Ccnd3, Ccne1, and Cdk6 also exhibited circadian rhythmicity but in antiphase to *mir-16*. An anti-proliferative role for *mir-16* was supported by its ability to inhibit proliferation and decrease expression of genes involved in cell cycle regulation when overexpressed in rat IEC-6 cells. These studies point to *mir-16* as a potentially important microRNA in regulating circadian rhythms in the intestine.

Methods

Animal studies

All animal study protocols were prospectively approved by the Harvard Medical Area Standing Committee on Animals.

Sprague–Dawley rats (50 males, 7 weeks old) were purchased from Harlan World (Indianapolis, IN) and acclimatized to a 12:12-h light: dark photoperiod for 5 days with *ad libitum* access to food and water. Time is designated as *h*ours *a*fter *l*ight *o*nset (HALO), with HALO 0 at 7 am (lights on). Rats were injected with BrdU (5-bromo-2-deoxyuridine, 50 mg/kg; Sigma, St Louis, MO) 1 h before harvest to label DNA as an index of S-phase. Rats were killed at 3-h intervals over 24 h (n = 6–7 per time) and jejunum harvested for microRNA microarrays, RNA and protein determination, and morphological analysis (harvest protocol detailed in Supplementary Material).

Microarrays and validation by real-time PCR

Total RNA from jejunum was extracted using the mirVana kit (Ambion; Austin, TX) and profiled on in situ hybridization arrays (Exiqon, Woburn, MA) against a reference sample consisting of RNA pooled from HALO 0 rats. Dye swaps were incorporated in the arrays to correct for any dye bias. Data were subjected to Lowess normalization and log transformed.

Expression profiles of selected microRNAs were confirmed by real-time PCR. Specific microRNAs were selected from total extracted RNA by reverse transcription using the stem–loop hybridization based microRNA reverse transcription kit and microRNA-specific primers (Taqman microRNA reverse transcription kit and Taqman microRNA assays, Applied Biosystems, Foster City, CA). microRNA expression was quantified in triplicate using the Taqman microRNA PCR primers and Taqman gene expression mastermix (Applied Biosystems). Reverse transcription and PCR were performed simultaneously on all samples to minimize differences introduced by variable reaction efficiency.

mir-16 overexpression vector

The human *mir-16* gene was amplified from human genomic DNA by PCR and inserted into the MluI/ClaI sites of the tetracycline-inducible TRIPZ shRNAmir expression vector (Open Biosystems, Huntsville, AL) using restriction sites incorporated into the primers (Supplementary Table 1). A non-silencing TRIPZ inducible shRNAmir vector was used as a control (Open Biosystems). Vectors were sequenced to ensure fidelity of the microRNA sequence and insertion. Details of cell transfection are available in Supplementary Material.

Proliferation and cell counting

IEC-6 cells were seeded in 96-well plates at a density of 1000 cells per well in triplicate. Proliferation indices were measured 48 h later using the CellTiter96 Aqueous One Solution Cell Proliferation Assay (MTS assay, Promega, Madison, WI). Cell growth rates were confirmed by cell counting in trypsinized, 48-h cultures seeded in triplicate at 10^4 cells/ml in 6-well dishes. All experiments were performed thrice.

Cell cycle changes and apoptosis

For cell cycle analysis, trypsinized cells were counted and fixed overnight in 70% ethanol at −20 °C. Fixed cells were collected by centrifugation at 1200 rpm for 10 min at 4 °C, suspended in propidium iodide (BD Biosciences, San Jose, CA) for 30 min at 37 °C in darkness, and analyzed by flow cytometry (BD FACScan, BD, Franklin Lakes, NJ). Data were analyzed by ModFit (Verity, Topsham, ME). To determine apoptosis and viability, trypsinized cells were counted and stained with Annexin V-FITC (BD) and Sytox Blue (Invitrogen), respectively, and analyzed by flow cytometry (10,000 events per sample). Data were analyzed using Diva (BD).

Please cite this article as: Anita Balakrishnan, et al., MicroRNA *mir-16* is anti-proliferative in enterocytes and exhibits diurnal rhythmicity in intestinal crypts, Exp Cell Res (2010), doi:10.1016/j.yexcr.2010.07.007

RNA extraction, mRNA reverse transcription and real-time PCR

mRNA levels of *Ccnd1*, *Ccnd2*, *Ccnd3*, *Ccne1*, *Cdk4* and *Cdk6* were quantified by real-time PCR as previously described [24] (detailed in Supplementary Material) and expressed relative to *B*-actin. All genes had Cts within the same range, between Ct 22 and 27. Primers were custom-ordered from Invitrogen (Supplementary Table 2), with the exception of *Ccnd1* mRNA which was measured using the Taqman primer–probe and gene expression Master Mix (Applied Biosystems).

Protein extraction and Western blotting

Protein expression of Ccnd1, Ccnd2, Ccnd3, Ccne1, Cdk4 and Cdk6 was measured in total lysates from jejunal mucosal scrapings or IEC-6 cell lysates as previously described, and detailed in Supplementary Material [19].

Analysis of morphologic parameters and BrdU labeling

Sections of jejunum were fixed overnight in 10% formalin, then orientated and embedded in paraffin blocks, cut at 7 μm thickness, mounted and stained with haematoxylin and eosin. Crypt depth, villus height, villus width, crypt enterocyte width, villus enterocyte width, and number of enterocytes per crypt were measured by a blinded observer under light microscopy (Olympus BX50; Center Valley, PA) at 100× or 400× magnification. Only samples displaying a single layer of enterocytes and villi with a visible central lacteal were included in the analysis (5–10 measurements per rat). For measurement of rhythmicity of proliferation, blocks of jejunum were cut at 7 μm and sections incubated with anti-BrdU primary antibody (Sigma), biotinylated secondary antibody, and visualized using the avidin–biotin–peroxidase complex method with diaminobenzidine tetrahydrochloride as the chromogen. Sections were counterstained with haematoxylin and eosin to facilitate counting of BrdU-negative nuclei.

Laser capture microdissection

Sections of jejunum from rats killed at HALO 6 and HALO 18, the respective circadian peak and trough of *mir-16* expression, were embedded in OCT compound over dry ice and isopentane. Sections (9 μm) were cut from the fresh frozen specimens and stained with Histogene staining solution (Molecular Devices, Sunnyvale, CA). Crypts (all cells in the lower half), villi (all cells in the top half), or smooth muscle was isolated by laser capture microdissection (Veritas Microdissection System, Molecular Devices). Total RNA was extracted from each section (RNAqueous RNA extraction kit, Ambion, Austin, TX) and subjected to microRNA reverse transcription and real-time PCR as described above for quantification of mir-16 expression in each fraction.

Statistical analysis

Data are presented as means ± SE. Graphical analysis was performed using GraphPad Prism (San Diego, CA). microRNAs exhibiting a 2-fold or greater difference between any two timepoints were selected for further analysis, and a false discovery rate (q-value) of <0.05 was considered significant. Circadian rhythmicity of microRNAs, gene and protein expression and morphological changes in rat tissue was determined by cross-sectional analysis and assuming a 24-h period as described previously, using the cosinor procedure which is freely available online [25–27]. The acrophase (time of peak expression), mesor (rhythm-adjusted mean), amplitude of rhythmicity, and significance of fit to a 24-h period (as indicated by $p<0.05$) for each gene were abstracted from the program. ANOVA (analysis of variance) with post-hoc Tukey's multiple comparisons test was used to identify significant differences across the 3 intestinal fractions at each timepoint. T-tests were used to compare the effects of *mir-16* overexpression with control cells in the *in vitro* experiments.

Results

microRNAs exhibit diurnal rhythmicity in rat intestine

Of 238 microRNAs tested on in situ hybridization arrays, 13 microRNAs exhibited ≥2-fold difference between peak and trough values (range 2.0- to 3.4-fold; $q<0.05$), 8 of which are conserved among human, mouse and rat and were therefore selected for further evaluation. Real-time PCR (qPCR) confirmed circadian rhythmicity for *mir-16*, *mir-20a* and *mir-141* as determined by the cosinor procedure, with a 24-hour periodicity. Peak expression of these three microRNAs occurred between HALO 4 and 6, corresponding to the lights-on fasting period (Supplementary Table 3, Figs. 1A–C). Two of these are reportedly involved in proliferation: *mir-20a* is pro-proliferative and *mir-16* is anti-proliferative [28–34]. Intestinal villus height and cell number have been shown to peak in anticipation of maximal nutrient intake in previous studies [35]. Because anti-proliferative *mir-16* began to wane late in the light phase, when intestinal proliferation has been shown to increase, we selected this microRNA for further study and designed experiments to ascertain its role in the rhythm of intestinal proliferation.

To compare *mir-16* expression levels in crypt, villus and smooth muscle, these cell types were isolated by laser capture microdissection at HALO 6 and 18, the respective *mir-16* peak and nadir. At HALO 18, expression was not significantly different across all three cell types (Fig. 1D; $p=0.97$). However, *mir-16* expression was 3.2-fold higher in crypts at HALO 6 vs. HALO 18 (Fig. 1D; $p=0.003$) while it was not detectably different in villi or smooth muscle. Thus, *mir-16* rhythmicity appears restricted to crypts, the proliferative compartment of the intestinal mucosa.

mir-16 suppresses proliferation in enterocytes by inducing G1 arrest

To determine the effect of *mir-16* on enterocyte proliferation, *mir-16* was overexpressed in rat IEC-6 cells, a cell line derived from intestinal crypts. Stable transfection of IEC-6 cells with the *mir-16* expression vector led to a 2.1-fold increase in *mir-16* expression vs. the control ($p=0.03$, Fig. 2A). This modest difference, comparable to the peak/trough difference observed in *mir-16* expression on a diurnal basis, had a profound effect on cell proliferation. At 48 h after plating, the proliferation rate was decreased 76% vs. control cells as measured by the MTS assay (4.2-fold difference; $p=0.006$, Fig. 2B) and by 80% as measured by cell counts (5.2-fold difference; $p=0.02$, Fig. 2C). Overexpression of *mir-16* also led a significantly larger fraction of cells in G1 compared to control as revealed by flow cytometry (65% vs. 24%, $p<0.001$, Fig. 2D). This result

Please cite this article as: Anita Balakrishnan, et al., MicroRNA *mir-16* is anti-proliferative in enterocytes and exhibits diurnal rhythmicity in intestinal crypts, Exp Cell Res (2010), doi:10.1016/j.yexcr.2010.07.007

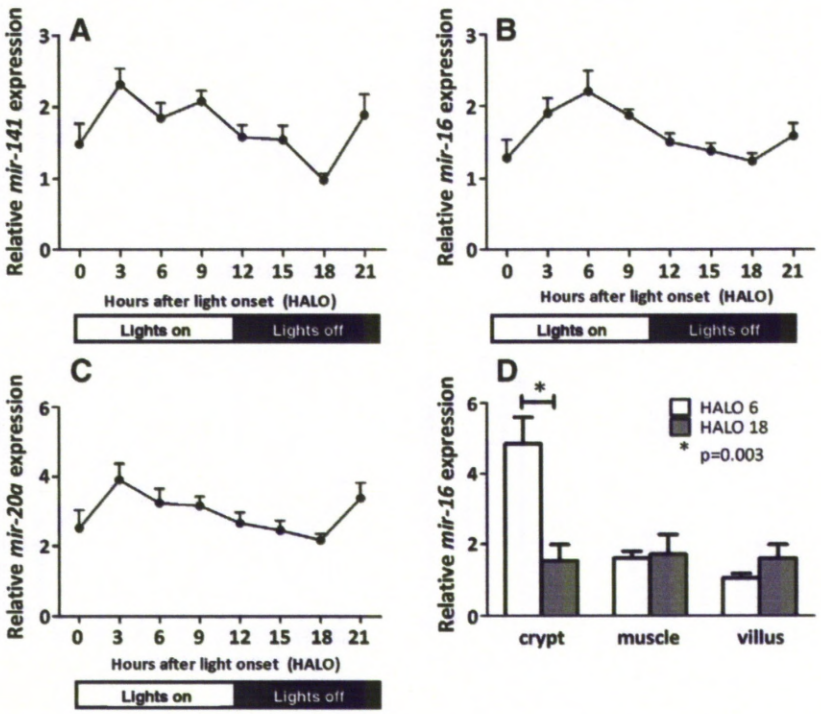

Fig. 1 – Temporal pattern of microRNAs showing a 2-fold or greater change between any two timepoints (A–C). Total RNA was extracted from the intestinal mucosa of rats harvested at the indicated times, run on microRNA microarrays and microRNAs showing a 2-fold or greater change between any two timepoints validated by real-time PCR. *mir-16* expression in enterocyte fractions (D). Laser capture microdissection and real-time PCR were used to determine *mir-16* expression in fractions of crypt, villus and smooth muscle in cryofixed sections of jejunum.

indicates that proliferation was curbed by arresting enterocytes in G1 rather than the reported effect of *mir-16* on apoptosis [31,36]. The lack of increase in apoptosis in IEC-6 cells overexpressing *mir-16* ($p=0.63$, Fig. 2E) substantiates this conclusion. These results point to an effect of *mir-16* on the cell cycle in enterocytes, specifically regulators of the G1/S transition.

mir-16 suppresses key G1/S regulators in enterocytes

To identify specific *mir-16* targets involved in reducing proliferation in enterocytes, the microRNA target prediction algorithm Targetscan was interrogated for the presence of *mir-16* binding sequences in the 3′UTRs of G1/S regulatory genes [37]. Potential *mir-16* targets in both rat and human included *cyclin D1* (*Ccnd1*), *cyclin D2* (*Ccnd2*), *cyclin D3* (*Ccnd3*), *cyclin E* (*Ccne1*) and *cyclin-dependent kinase 6* (*Cdk6*). These are all known to regulate the G1/S transition and were therefore examined for responsiveness to *mir-16*. *Cyclin-dependent kinase 4 (Cdk4)*, a G1 regulator lacking a *mir-16* target site in its mRNA 3′UTR, was included as a negative control.

Overexpression of *mir-16* significantly decreased protein levels of Ccnd1, Ccnd2, Ccnd3, Ccne1 and Cdk6 in IEC-6 cells compared to the non-silencing control (levels 0.3–0.5 that of controls, $p<0.05$, Table 1, Supplementary Fig. 1). *mir-16* appeared to affect translation of *Ccnd1*, *Ccnd3* and *Ccne1* rather than mRNA cleavage because mRNA levels did not change detectably ($p=0.660$, 0.151 and 0.181 respectively, Table 1). In contrast, reduction of *Ccnd2* and *Cdk6* mRNAs by 75% ($p=0.002$) and 58% ($p=0.001$), respectively (Table 1) indicated that *mir-16* overexpression primarily affected transcription and/or mRNA stability of these regulators. Our data point to one or more of these G1/S proteins as *mir-16*-regulated mediators on cell cycle progression. As expected, neither Cdk4 mRNA ($p=0.591$) or protein ($p=0.223$) levels were altered detectably by *mir-16* overexpression (Table 1). These results confirm that Cdk4 is not a *mir-16* target and indicate that *mir-16* overexpression does not exert non-specific effects on cell cycle proteins.

G1/S regulatory proteins targeted by mir-16 peak in antiphase to mir-16 expression in jejunum

Diurnal rhythmicity in intestinal proliferation is likely to be mediated by an underlying diurnal rhythmicity in cell cycle proteins [21,38]. Moreover, involvement of *mir-16* in the jejunal mucosa cell cycle via suppression of these proteins as suggested by the IEC-6 studies would likely be evidenced by a corresponding displacement of their rhythms from *mir-16*. To these ends, we examined the temporal protein expression patterns for the 5 *mir-16* targets as well as Cdk4 in jejunum. All six proteins exhibited diurnal rhythmicity with a 24-hour period, with acrophases (expression peaks) falling between HALO 11 and HALO 17 ($p<0.05$, Figs. 3A–E; Table 2, Supplementary Fig. 2) and nadirs between HALO 3 and 6. These temporal patterns would be expected for targets suppressed by *mir-16* with its peak expression at HALO 6. *Ccnd2*, *Ccnd3* and *Cdk4* displayed rhythmicity at the transcriptional level ($p=0.011$, 0.00018, and 0.00015,

Please cite this article as: Anita Balakrishnan, et al., MicroRNA *mir-16* is anti-proliferative in enterocytes and exhibits diurnal rhythmicity in intestinal crypts, Exp Cell Res (2010), doi:10.1016/j.yexcr.2010.07.007

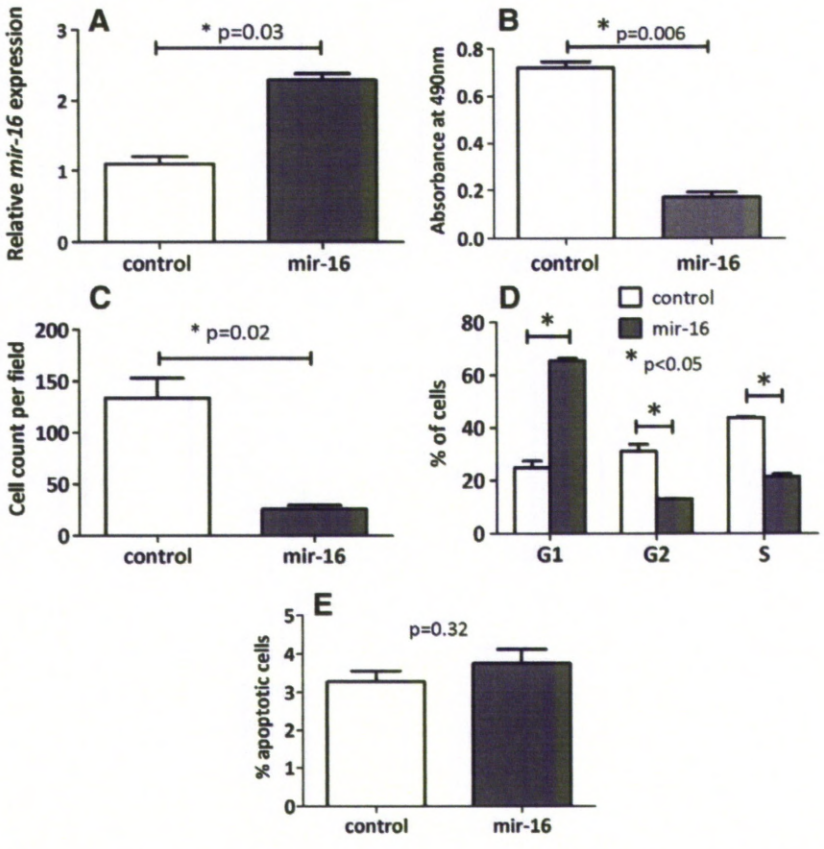

Fig. 2 – Effects of *mir-16* on enterocyte phenotype *in vitro*. *mir-16* (or a scrambled control) was stably overexpressed in IEC-6 cells as described in Methods. All assays were performed 48 h after plating. *mir-16* expression was quantified by real-time PCR following RNA extraction and reverse transcription (A). Proliferation and cell viability were determined using the MTS assay and cell counting respectively (B and C). For analysis of cell cycle, cells were fixed in 70% ethanol and stained with propidium iodide and subjected to flow cytometry as described in Methods (D). For determination of apoptosis, cells were stained with Annexin V-FITC and Sytox Blue and analyzed by flow cytometry (E).

respectively; Figs. 4B–C, Table 2). *Ccnd1* and *Ccne1* mRNAs exhibited temporal changes but these did not qualify as significant circadian rhythms, in keeping with the lack of response at an mRNA level with mir-16 overexpression *in vitro*. In contrast, *Cdk6* did not display diurnal rhythmicity of transcription *in vivo* ($p = 0.77$, Fig. 4F) despite its transcriptional responsiveness to *mir-16* overexpression in IEC-6 cells.

Table 1 – Expression of *mir-16* target protein and mRNA following overexpression of *mir-16* in IEC-6 cells. Levels have been normalized to that in control cells. Our data demonstrate regulation of targets *Ccnd2* and *Cdk6* at the transcriptional level *in vitro*, and *Ccnd1*, *Ccnd2* and *Ccne1* at the post-transcriptional level. *Cdk4* is not a predicted target of *mir-16* and correspondingly did not demonstrate alteration in expression following *mir-16* overexpression. All predicted *mir-16* targets were suppressed at the protein level.

Protein expression of G1/S regulators			mRNA expression of G1/S regulators		
Target	Fold-change vs. control	p-value	Target	Fold-change vs. control	p-value
Ccnd1	0.4	0.030	*Ccnd1*	0.9	0.660
Ccnd2	0.4	0.037	*Ccnd2*	0.2	0.002
Ccnd3	0.3	0.030	*Ccnd3*	1.2	0.151
Ccne1	0.5	0.030	*Ccne1*	0.8	0.181
Cdk6	0.4	0.039	*Cdk6*	0.4	0.001
Cdk4	1.2	0.223	*Cdk4*	1.0	0.591

Diurnal rhythmicity in DNA synthesis and morphology in rat jejunum

To define the relationship of proliferation to the cyclin expression rhythm, we assessed the temporal patterns of DNA synthesis (S-phase) and crypt–villus morphology. The number of cells in S-phase, as measured by BrdU labeling, peaked at HALO 5 ($p < 0.001$, Supplementary Fig. 3A). Crypt cell number peaked several hours later at HALO 12 ($p = 0.001$, Supplementary Fig. 3B), followed by crypt depth and villus height at HALO 13 and HALO 14, respectively ($p = 0.005$ and 0.043, Supplementary Figs. 3C and D). Enterocyte number per 100 μm of villus increased modestly in anticipation of nutrient arrival but significant rhythmicity was not achieved ($p = 0.099$, Supplementary Fig. 3E). Cell width exhibited circadian rhythmicity in crypts with a peak at HALO 15 ($p = 0.033$, Supplementary Fig. 3F) but not in villi ($p = 0.217$). Overall these data demonstrate that a combination of cell proliferation and hypertrophy produced the observed changes in crypt and villus morphology (Table 3).

Please cite this article as: Anita Balakrishnan, et al., MicroRNA *mir-16* is anti-proliferative in enterocytes and exhibits diurnal rhythmicity in intestinal crypts, Exp Cell Res (2010), doi:10.1016/j.yexcr.2010.07.007

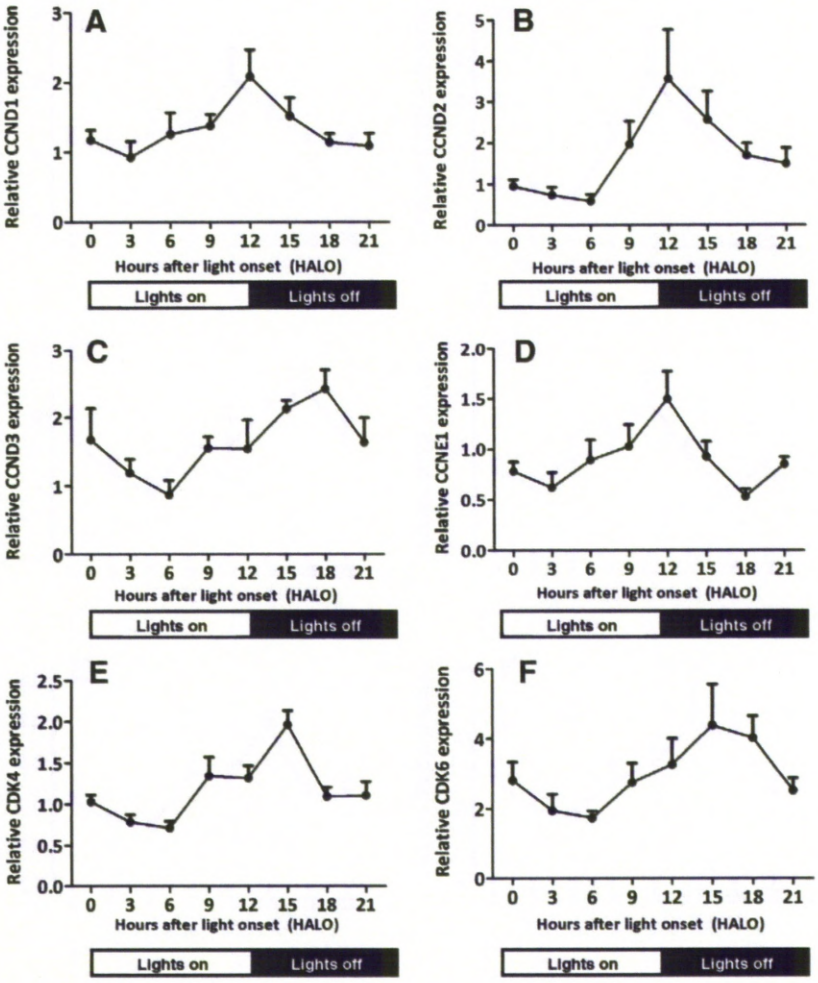

Fig. 3 – Temporal pattern of cell cycle protein expression in rat intestine. Whole-cell protein lysates of rat intestinal mucosa, harvested at the indicated times, were analyzed by immunoblotting. Diurnal amplitudes and p-values are summarised in Table 2.

Discussion

This study is the first to profile microRNA expression in rat jejunum as well as to establish rhythmic expression of specific microRNAs. In particular, our data supports a role for the anti-proliferative microRNA *mir-16* in the intestinal proliferation rhythm. In support of this, we have shown that *mir-16* expression peaks at HALO 6, coincident with the troughs in villus height and in crypt depth and cell number. *mir-16* rhythmicity was also restricted to intestinal crypts, the primary site of proliferation. The anti-proliferative effect of mir16 was confirmed *in vitro*, where *mir-16* inhibited proliferation of IEC-6 enterocytes, and suppressed expression of 5 key G1/S regulators—Ccnd1, Ccnd2, Ccnd3, Ccne1 and Cdk6. Finally, protein abundances of all five G1/S regulators presumably targeted by *mir-16* as well as the non-target Cdk4

Table 2 – Expression of cell cycle G1/S regulator protein and mRNA expression at diurnal timepoints in rat jejunum. The cosinor procedure was used to determine the fit of the data to a cosinor curve with 24-hour periodicity. Our data demonstrate circadian rhythmicity of *Ccnd2*, *Ccnd3* and *Cdk4* at the transcriptional level *in vivo*, and Ccnd1, Ccne1 and Cdk6 at the post-transcriptional level.

Rhythmicity of protein expression				Rhythmicity of mRNA expression			
Target	p-value	Acrophase (HALO, h)	Fold-change peak/trough	Target	p-value	Acrophase (HALO, h)	Fold-change peak/trough
Ccnd1	0.009	12	2.3	*Ccnd1*	0.120		
Ccnd2	0.001	14	4.4	*Ccnd2*	0.011	0	2.7
Ccnd3	0.004	17	2.8	*Ccnd3*	0.000	0	2.8
Ccne1	0.013	11	2.8	*Ccne1*	0.330		
Cdk4	0.000	15	2.8	*Cdk4*	0.005	2	2.3
Cdk6	0.004	16	2.5	*Cdk6*	0.770		

Please cite this article as: Anita Balakrishnan, et al., MicroRNA *mir-16* is anti-proliferative in enterocytes and exhibits diurnal rhythmicity in intestinal crypts, Exp Cell Res (2010), doi:10.1016/j.yexcr.2010.07.007

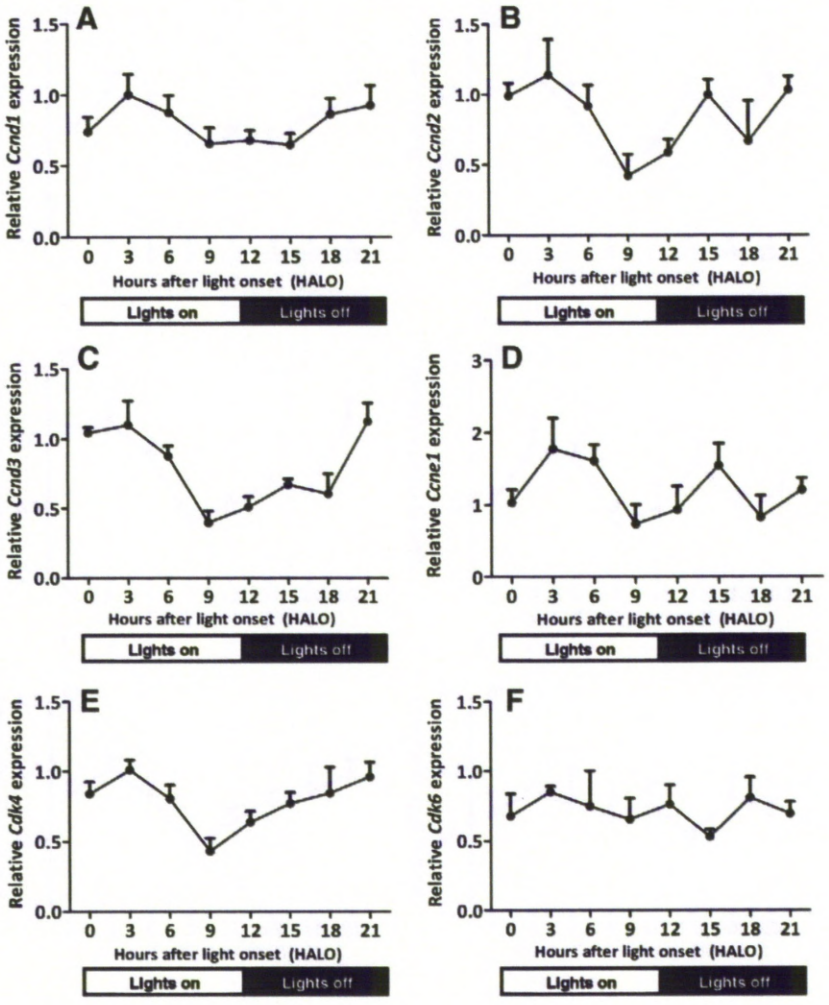

Fig. 4 – Temporal pattern of mRNA levels for cell cycle genes in rat intestine. Total RNA was extracted from rat intestinal mucosa, harvested at the indicated times and was analyzed by real-time PCR. Diurnal amplitudes and p-values are summarised in Table 2.

exhibit diurnal rhythmicity in rat jejunum in antiphase to *mir-16*. These coordinated responses point to *mir-16* as an important regulator of proliferation in jejunal crypts. This function may be essential to coordinate intestinal circadian rhythms, serving to optimally match proliferation and absorptive capacity with nutrient availability.

Table 3 – Diurnal rhythmicity in morphological parameters and BrdU labeling in rat jejunum. The cosinor procedure was used to determine the fit of the data to a cosinor curve with 24-hour periodicity. BrdU labeling, indicative of cell cycle S-phase, peaks at HALO 5, followed by peaks in crypt depth and villus height after 8 to 9 h. Rhythmicity in numbers of enterocytes per crypt suggests that increases in cell numbers contribute to this rhythmicity in crypt–villus morphology.

Parameter	p-value	Acrophase (HALO, h)	Fold-change (peak/trough)
BrdU	0.005	5	1.6
Crypt depth	0.005	13	1.3
Villus height	0.043	14	1.1
Enterocytes per crypt	0.001	12	1.2
Villus width	0.610		
Crypt width	0.080		

Circadian rhythmicity of microRNA expression has been shown to regulate cell behavior and gene expression. In the suprachiasmatic nucleus, rhythmic expression of *mir-219* and *mir-132* mediate photic entrainment of circadian clock activity [16]. Similarly, depletion of *mir-122* in liver disrupted the circadian rhythmicity of numerous transcripts regulating metabolism [18,39]. In the retina, 12 microRNAs display circadian rhythmicity of which two – *mir-96* and *mir-182* – were shown to mediate rhythmic expression of the *Adcy6* (adenylate cyclase type 6) gene [17]. Here we highlight another potential role for microRNAs as regulators of intestinal circadian rhythms. Interestingly, the 1.8- to 3.2-fold amplitude changes we observed in intestinal microRNAs are consistent with the 1.25- to 3-fold-changes observed in the retina [15–17]. Three microRNAs, *mir-16*, *mir-20a* and *mir-141* were shown to exhibit circadian rhythmicity in this study, however the limited amount of tissue obtained from laser capture microdissection restricted us to the examination of only *mir-16* expression at HALO 6 and 18. Further studies are necessary to

Please cite this article as: Anita Balakrishnan, et al., MicroRNA *mir-16* is anti-proliferative in enterocytes and exhibits diurnal rhythmicity in intestinal crypts, Exp Cell Res (2010), doi:10.1016/j.yexcr.2010.07.007

determine the rhythmicity of the remaining microRNAs in the individual intestinal fractions at circadian timepoints, particularly for mir-20a which is known to have a pro-proliferative function and may therefore contribute to the regulation of rhythmicity of intestinal proliferation.

Several observations from our studies merit further discussion. First, a modest increase of *mir-16* in IEC-6 cells, similar to the diurnal change in jejunum, almost completely arrested growth in these cells. *mir-16* has been suggested to act as a tumour suppressor gene in prostate: *mir16* is frequently downregulated in advanced prostate cancer and *mir16* knockdown in prostate cancer cells promotes proliferation and invasiveness [40]. Similarly, *mir-16* expression is reduced in squamous cell carcinomas and adenocarcinomas of the lung, and *mir-16* overexpression in lung cancer cell lines induces cell cycle arrest [34]. Our findings reveal that the anti-proliferative function of *mir-16* serves an important physiological role in normal tissues. We note that, in contrast to its lack of effect on IEC-6 cell apoptosis, *mir-16* was shown to increase apoptosis in leukaemic cell lines, gastric cancer cells and prostate cancer via downregulation of pro-survival protein BCL2 (B-cell lymphoma 2) [31,36,40,41]. This apparent discrepancy in our observations, may in fact be due to different properties of BCL2 pathways in the small intestine; while Bcl2 is expressed in enterocytes, it may perform different functions in this tissue. Indeed, ablation of Bcl2 in mice increases the apoptosis rate in the colon but not the small intestine [42,43].

Second, in IEC-6 enterocytes *mir-16* suppressed levels of several cell cycle proteins involved in the G1/S transition concomitantly with G1 arrest. In normal cell cycle progression, D-type cyclins (Ccnd1, Ccnd2 and Ccnd3) complex with cyclin-dependent kinases (Cdk4 and Cdk6) during G1 to phosphorylate and thereby inactivate the retinoblastoma protein pRb, in turn activating cell cycle proteins (including Ccne1 and its complex Cdk2) vital for entering S-phase [44,45]. Upregulation of *mir-16* expression suppressed expression of Ccnd1, Ccnd2, Ccnd3, Ccne1 and Cdk6 *in vitro*, thereby corroborating existing evidence that small changes in microRNA expression alter cellular phenotypes by downregulating multiple components of single pathways [13,46,47]. *In vivo*, we found that G1 proteins Ccnd1 and Ccnd2 peaked at HALO 12, while the remaining D-type cyclin family member Ccnd3 peaked later at HALO 17. These findings are consistent with reported differences in the relative timing of D cyclins in various cell types, as well as differential regulation and a degree of functional redundancy [48,49]. We were unable to definitively corroborate rhythms of mir-16 in the crypt with rhythms of cell cycle proteins in the crypt due to the small amount of tissue obtained from laser capture microdissection, however previous studies have demonstrated that in the intestine the D-type cyclins and cyclin-dependent kinases are most strongly expressed in intestinal crypts [50]. Our study showed peak S-phase at HALO 5, indicating a G1/S duration of approximately 12 to 17 h, in agreement with previous studies showing a long G1/S and short G2/M period in the small intestine [51–53]. The 63% change in cell labeling we observed at HALO 6 vs. HALO 15 is also similar to the 30–60% increase at HALO 3 in murine jejunum reported by Scheving et al. [38,54]. The rhythmicity in proliferation translated to rhythmicity in morphological parameters in the jejunum. The large number of crypts and villi across the length of the intestine suggests that these small changes are likely to result in a large change in absorptive surface area over the diurnal period. Examination of these morphological parameters in the terminal ileum and corroboration of these measurements with mir-16 expression in the ileum may reveal new insights into the regulation of mir-16.

Our data show that mir-16 is able to affect translation of Ccnd1, Ccnd3 and Ccne1 without affecting mRNA expression, corroborating previous data showing microRNAs are able to suppress protein levels independent of mRNA expression [46]. This was also demonstrated by our data *in vivo*; Ccnd1 and Ccne1 showed rhythmicity only at the protein level. This is in keeping with previous data showing that almost half of the proteins demonstrating circadian rhythmicity in the mouse liver lack a corresponding cycling transcript [5]. Together with our findings this suggests the possibility that the rhythmic protein expression in jejunum in our study may be produced solely by miRNAs, whether by *mir-16* alone or in combination with others. Cell-type specificity of *mir-16* rhythmicity, such as seen in the intestinal crypts in our study, would then lead to consequent rhythmicity of target proteins. Cell cycle proteins are known to have a relatively short half-life [55], which is likely to facilitate regulation of these proteins by rhythmicity in microRNA expression and allow increased responsiveness to other stimuli that may accelerate or arrest the cell cycle.

Regulation of gene expression by microRNAs is a complex process, with the potential for each to target many related or unrelated genes and for responsive genes to be regulated by multiple microRNAs. In the case of the cell cycle, microRNAs *let-7a*, *mir-34a*, *mir-192* and *mir-215* have been shown, like *mir-16*, to arrest cells in G1, while *mir-106b* and *mir-221* accelerate G1/S progression by suppressing the cyclin-dependent kinase inhibitors p21 and p27, respectively [56–61]. Factors other than microRNAs are also clearly important in cuing the intestinal proliferation rhythm. For instance, clock gene Period 2 (Per2) regulates proliferation in peripheral tissues via cell cycle genes c-*Myc*, *Cyclin A*, *Mdm-2* and *Gadd45*α, as well as the *mir-16* target *Ccnd1* [62]. Ultimately, proliferation rhythms likely result from combined inputs of circadian clock components, other transcription factors and rhythmic microRNAs. The ability of non-microRNA transcriptional regulators such as clock genes to regulate rhythmicity of proliferation may explain rhythmicity in Cdk4, a cell cycle gene not regulated by *mir-16*, and the lack of transcriptional rhythmicity in *Cdk6 in vivo* despite responsiveness to *mir-16* overexpression *in vitro*. Generation of knockout mice lacking *mir-16* will be invaluable in defining its functions and dissecting these regulatory pathways.

Finally, a broader implication can be drawn from our study. The behavior of *mir-16* reveals another potential route for linking proliferation to nutrient availability, which cues the intestinal rhythms. Rhythmic *mir-16* expression in crypt cells could be initiated by luminal nutrients directly or via neuro-hormonal pathways. In either case, proliferation may be a key early component to expand the mucosal surface area in the anticipatory diurnal increases in absorptive capacities for glucose, peptides, and other nutrients [19,63].

In summary, we show for the first time rhythmicity of microRNA expression in the intestine, and anti-proliferative effects of the diurnally expressed *mir-16* in untransformed enterocytes *in vitro*. We hypothesize that rhythmicity of *mir-16* in jejunum may act to mediate the rhythmicity in intestinal proliferation and coordinate the proliferative response with nutrient availability to optimize intestinal absorption and function.

Please cite this article as: Anita Balakrishnan, et al., MicroRNA *mir-16* is anti-proliferative in enterocytes and exhibits diurnal rhythmicity in intestinal crypts, Exp Cell Res (2010), doi:10.1016/j.yexcr.2010.07.007

Acknowledgments

The authors gratefully acknowledge the excellent technical assistance of Jan Rounds and Roger Lis in the experimental procedures.

Appendix A. Supplementary data

Supplementary data associated with this article can be found, in the online version, at doi: 10.1016/j.yexcr.2010.07.007.

REFERENCES

[1] M.J. McDonald, M. Rosbash, Microarray analysis and organization of circadian gene expression in *Drosophila*, Cell 107 (2001) 567–578.
[2] R.A. Akhtar, A.B. Reddy, E.S. Maywood, J.D. Clayton, V.M. King, A.G. Smith, T.W. Gant, M.H. Hastings, C.P. Kyriacou, Circadian cycling of the mouse liver transcriptome, as revealed by cDNA microarray, is driven by the suprachiasmatic nucleus, Curr. Biol. 12 (2002) 540–550.
[3] A. Claridge-Chang, H. Wijnen, F. Naef, C. Boothroyd, N. Rajewsky, M.W. Young, Circadian regulation of gene expression systems in the *Drosophila* head, Neuron 32 (2001) 657–671.
[4] S. Panda, M.P. Antoch, B.H. Miller, A.I. Su, A.B. Schook, M. Straume, P.G. Schultz, S.A. Kay, J.S. Takahashi, J.B. Hogenesch, Coordinated transcription of key pathways in the mouse by the circadian clock, Cell 109 (2002) 307–320.
[5] A.B. Reddy, N.A. Karp, E.S. Maywood, E.A. Sage, M. Deery, J.S. O'Neill, G.K. Wong, J. Chesham, M. Odell, K.S. Lilley, C.P. Kyriacou, M.H. Hastings, Circadian orchestration of the hepatic proteome, Curr. Biol. 16 (2006) 1107–1115.
[6] B.P. Lewis, C.B. Burge, D.P. Bartel, Conserved seed pairing, often flanked by adenosines, indicates that thousands of human genes are microRNA targets, Cell 120 (2005) 15–20.
[7] M. Lagos-Quintana, R. Rauhut, W. Lendeckel, T. Tuschl, Identification of novel genes coding for small expressed RNAs, Science 294 (2001) 853–858.
[8] N.C. Lau, L.P. Lim, E.G. Weinstein, D.P. Bartel, An abundant class of tiny RNAs with probable regulatory roles in *Caenorhabditis elegans*, Science 294 (2001) 858–862.
[9] R.C. Lee, V. Ambros, An extensive class of small RNAs in *Caenorhabditis elegans*, Science 294 (2001) 862–864.
[10] R.C. Lee, R.L. Feinbaum, V. Ambros, The *C. elegans* heterochronic gene lin-4 encodes small RNAs with antisense complementarity to lin-14, Cell 75 (1993) 843–854.
[11] B. Wightman, I. Ha, G. Ruvkun, Posttranscriptional regulation of the heterochronic gene lin-14 by lin-4 mediates temporal pattern formation in *C. elegans*, Cell 75 (1993) 855–862.
[12] L.P. Lim, N.C. Lau, P. Garrett-Engele, A. Grimson, J.M. Schelter, J. Castle, D.P. Bartel, P.S. Linsley, J.M. Johnson, Microarray analysis shows that some microRNAs downregulate large numbers of target mRNAs, Nature 433 (2005) 769–773.
[13] K.K. Farh, A. Grimson, C. Jan, B.P. Lewis, W.K. Johnston, L.P. Lim, C.B. Burge, D.P. Bartel, The widespread impact of mammalian MicroRNAs on mRNA repression and evolution, Science 310 (2005) 1817–1821.
[14] A. Stark, J. Brennecke, N. Bushati, R.B. Russell, S.M. Cohen, Animal microRNAs confer robustness to gene expression and have a significant impact on 3′UTR evolution, Cell 123 (2005) 1133–1146.
[15] M. Yang, J.E. Lee, R.W. Padgett, I. Edery, Circadian regulation of a limited set of conserved microRNAs in *Drosophila*, BMC Genomics 9 (2008) 83.
[16] H.Y. Cheng, J.W. Papp, O. Varlamova, H. Dziema, B. Russell, J.P. Curfman, T. Nakazawa, K. Shimizu, H. Okamura, S. Impey, K. Obrietan, microRNA modulation of circadian-clock period and entrainment, Neuron 54 (2007) 813–829.
[17] S. Xu, P.D. Witmer, S. Lumayag, B. Kovacs, D. Valle, MicroRNA (miRNA) transcriptome of mouse retina and identification of a sensory organ-specific miRNA cluster, J. Biol. Chem. 282 (2007) 25053–25066.
[18] D. Gatfield, G. Le Martelot, C.E. Vejnar, D. Gerlach, O. Schaad, F. Fleury-Olela, A.L. Ruskeepaa, M. Oresic, C.C. Esau, E.M. Zdobnov, U. Schibler, Integration of microRNA miR-122 in hepatic circadian gene expression, Genes Dev. 23 (2009) 1313–1326.
[19] A. Balakrishnan, A.T. Stearns, J. Rounds, J. Irani, M. Giuffrida, D.B. Rhoads, S.W. Ashley, A. Tavakkolizadeh, Diurnal rhythmicity in glucose uptake is mediated by temporal periodicity in the expression of the sodium–glucose cotransporter (SGLT1), Surgery 143 (2008) 813–818.
[20] A. Tavakkolizadeh, U.V. Berger, K.R. Shen, L.L. Levitsky, M.J. Zinner, M.A. Hediger, S.W. Ashley, E.E. Whang, D.B. Rhoads, Diurnal rhythmicity in intestinal SGLT-1 function, V(max), and mRNA expression topography, Am. J. Physiol. Gastrointest. Liver Physiol. 280 (2001) G209–G215.
[21] L.E. Scheving, E.R. Burns, J.E. Pauly, T.H. Tsai, Circadian variation in cell division of the mouse alimentary tract, bone marrow and corneal epithelium, Anat. Rec. 191 (1978) 479–486.
[22] G. Marra, M. Anti, A. Percesepe, F. Armelao, R. Ficarelli, C. Coco, A. Rinelli, F.M. Vecchio, E. D'Arcangelo, Circadian variations of epithelial cell proliferation in human rectal crypts, Gastroenterology 106 (1994) 982–987.
[23] K.N. Buchi, J.G. Moore, W.J. Hrushesky, R.B. Sothern, N.H. Rubin, Circadian rhythm of cellular proliferation in the human rectal mucosa, Gastroenterology 101 (1991) 410–415.
[24] A. Balakrishnan, A.T. Stearns, D.B. Rhoads, S.W. Ashley, A. Tavakkolizadeh, Defining the transcriptional regulation of the intestinal sodium–glucose cotransporter using RNA-interference mediated gene silencing, Surgery 144 (2008) 168–173.
[25] A.T. Stearns, A. Balakrishnan, D.B. Rhoads, S.W. Ashley, A. Tavakkolizadeh, Diurnal rhythmicity in the transcription of jejunal drug transporters, J. Pharmacol. Sci. 108 (2008) 144–148.
[26] W. Nelson, Y.L. Tong, J.K. Lee, F. Halberg, Methods for cosinor-rhythmometry, Chronobiologia 6 (1979) 305–323.
[27] http://www.circadian.org.
[28] C. Xiao, L. Srinivasan, D.P. Calado, H.C. Patterson, B. Zhang, J. Wang, J. M. Henderson, J.L. Kutok, K. Rajewsky, Lymphoproliferative disease and autoimmunity in mice with increased miR-17–92 expression in lymphocytes, Nat. Immunol. 9 (2008) 405–414.
[29] A. Ventura, A.G. Young, M.M. Winslow, L. Lintault, A. Meissner, S.J. Erkeland, J. Newman, R.T. Bronson, D. Crowley, J.R. Stone, R. Jaenisch, P.A. Sharp, T. Jacks, Targeted deletion reveals essential and overlapping functions of the miR-17 through 92 family of miRNA clusters, Cell 132 (2008) 875–886.
[30] M. Inomata, H. Tagawa, Y.M. Guo, Y. Kameoka, N. Takahashi, K. Sawada, MicroRNA-17–92 down-regulates expression of distinct targets in different B-cell lymphoma subtypes, Blood 113 (2009) 396–402.
[31] A. Cimmino, G.A. Calin, M. Fabbri, M.V. Iorio, M. Ferracin, M. Shimizu, S.E. Wojcik, R.I. Aqeilan, S. Zupo, M. Dono, L. Rassenti, H. Alder, S. Volinia, C.G. Liu, T.J. Kipps, M. Negrini, C.M. Croce, miR-15 and miR-16 induce apoptosis by targeting BCL2, Proc. Natl Acad. Sci. USA 102 (2005) 13944–13949.
[32] P.S. Linsley, J. Schelter, J. Burchard, M. Kibukawa, M.M. Martin, S.R. Bartz, J.M. Johnson, J.M. Cummins, C.K. Raymond, H. Dai, N. Chau, M. Cleary, A.L. Jackson, M. Carleton, L. Lim, Transcripts targeted by the microRNA-16 family cooperatively regulate cell cycle progression, Mol. Cell. Biol. 27 (2007) 2240–2252.
[33] Q. Liu, H. Fu, F. Sun, H. Zhang, Y. Tie, J. Zhu, R. Xing, Z. Sun, X. Zheng, miR-16 family induces cell cycle arrest by regulating multiple cell cycle genes, Nucleic Acids Res. 36 (2008) 5391–5404.
[34] N. Bandi, S. Zbinden, M. Gugger, M. Arnold, V. Kocher, L. Hasan, A. Kappeler, T. Brunner, E. Vassella, miR-15a and miR-16 are

Please cite this article as: Anita Balakrishnan, et al., MicroRNA *mir-16* is anti-proliferative in enterocytes and exhibits diurnal rhythmicity in intestinal crypts, Exp Cell Res (2010), doi:10.1016/j.yexcr.2010.07.007

implicated in cell cycle regulation in a Rb-dependent manner and are frequently deleted or down-regulated in non-small cell lung cancer, Cancer Res. 69 (2009) 5553–5559.
[35] N.R. Stevenson, S.E. Day, H. Sitren, Circadian rhythmicity in rat intestinal villus length and cell number, Int. J. Chronobiol. 6 (1979) 1–12.
[36] L. Xia, D. Zhang, R. Du, Y. Pan, L. Zhao, S. Sun, L. Hong, J. Liu, D. Fan, miR-15b and miR-16 modulate multidrug resistance by targeting BCL2 in human gastric cancer cells, Int. J. Cancer 123 (2008) 372–379.
[37] http://www.targetscan.org.
[38] L.E. Scheving, T.H. Tsai, L.A. Scheving, Chronobiology of the intestinal tract of the mouse, Am. J. Anat. 168 (1983) 433–465.
[39] J. Krutzfeldt, N. Rajewsky, R. Braich, K.G. Rajeev, T. Tuschl, M. Manoharan, M. Stoffel, Silencing of microRNAs in vivo with 'antagomirs', Nature 438 (2005) 685–689.
[40] D. Bonci, V. Coppola, M. Musumeci, A. Addario, R. Giuffrida, L. Memeo, L. D'Urso, A. Pagliuca, M. Biffoni, C. Labbaye, M. Bartucci, G. Muto, C. Peschle, R. De Maria, The miR-15a–miR-16-1 cluster controls prostate cancer by targeting multiple oncogenic activities, Nat. Med. 14 (2008) 1271–1277.
[41] C.J. Guo, Q. Pan, D.G. Li, H. Sun, B.W. Liu, miR-15b and miR-16 are implicated in activation of the rat hepatic stellate cell: an essential role for apoptosis, J. Hepatol. 50 (2009) 766–778.
[42] K. Nakayama, K. Nakayama, I. Negishi, K. Kuida, H. Sawa, D.Y. Loh, Targeted disruption of Bcl-2 alpha beta in mice: occurrence of gray hair, polycystic kidney disease, and lymphocytopenia, Proc. Natl Acad. Sci. USA 91 (1994) 3700–3704.
[43] K. Nakayama, K. Nakayama, I. Negishi, K. Kuida, Y. Shinkai, M.C. Louie, L.E. Fields, P.J. Lucas, V. Stewart, F.W. Alt, et al., Disappearance of the lymphoid system in Bcl-2 homozygous mutant chimeric mice, Science 261 (1993) 1584–1588.
[44] A. Deshpande, P. Sicinski, P.W. Hinds, Cyclins and cdks in development and cancer: a perspective, Oncogene 24 (2005) 2909–2915.
[45] A.W. Murray, Recycling the cell cycle: cyclins revisited, Cell 116 (2004) 221–234.
[46] D. Baek, J. Villen, C. Shin, F.D. Camargo, S.P. Gygi, D.P. Bartel, The impact of microRNAs on protein output, Nature 455 (2008) 64–71.
[47] F. Takeshita, L. Patrawala, M. Osaki, R.U. Takahashi, Y. Yamamoto, N. Kosaka, M. Kawamata, K. Kelnar, A.G. Bader, D. Brown, T. Ochiya, Systemic delivery of synthetic microRNA-16 inhibits the growth of metastatic prostate tumors via downregulation of multiple cell-cycle genes, Mol. Ther. 18 (1) (2010) 181–187.
[48] T.C. Ko, H.M. Sheng, D. Reisman, E.A. Thompson, R.D. Beauchamp, Transforming growth factor-beta 1 inhibits cyclin D1 expression in intestinal epithelial cells, Oncogene 10 (1995) 177–184.
[49] T.C. Ko, F. Pan, H. Sheng, D.B. Brown, E.A. Thompson, R.D. Beauchamp, Cyclin D3 is essential for intestinal epithelial cell proliferation, World J. Surg. 26 (2002) 812–818.
[50] J. Guo, S. Longshore, R. Nair, B.W. Warner, Retinoblastoma protein (pRb), but not p107 or p130, is required for maintenance of enterocyte quiescence and differentiation in small intestine, J. Biol. Chem. 284 (2009) 134–140.
[51] S. Lesher, Compensatory reactions in intestinal crypt cells after 300 Roentgens of cobalt-60 gamma irradiation, Radiat. Res. 32 (1967) 510–519.
[52] A.M. Cohen, F.S. Philips, S.S. Sternberg, Studies on the cytotoxicity of bleomycin in the small intestine of the mouse, Cancer Res. 32 (1972) 1293–1300.
[53] R.N. DuBois, J. Shao, M. Tsujii, H. Sheng, R.D. Beauchamp, G1 delay in cells overexpressing prostaglandin endoperoxide synthase-2, Cancer Res. 56 (1996) 733–737.
[54] L.E. Scheving, T.H. Tsai, L.A. Scheving, R.J. Feuers, The potential of using the natural rhythmicity of cell proliferation in improving cancer chemotherapy in rodents, Ann. NY Acad. Sci. 618 (1991) 182–227.
[55] Y. Guo, D.W. Stacey, M. Hitomi, Post-transcriptional regulation of cyclin D1 expression during G2 phase, Oncogene 21 (2002) 7545–7556.
[56] C.D. Johnson, A. Esquela-Kerscher, G. Stefani, M. Byrom, K. Kelnar, D. Ovcharenko, M. Wilson, X. Wang, J. Shelton, J. Shingara, L. Chin, D. Brown, F.J. Slack, The let-7 microRNA represses cell proliferation pathways in human cells, Cancer Res. 67 (2007) 7713–7722.
[57] H. Tazawa, N. Tsuchiya, M. Izumiya, H. Nakagama, Tumor-suppressive miR-34a induces senescence-like growth arrest through modulation of the E2F pathway in human colon cancer cells, Proc. Natl Acad. Sci. USA 104 (2007) 15472–15477.
[58] C.J. Braun, X. Zhang, I. Savelyeva, S. Wolff, U.M. Moll, T. Schepeler, T.F. Orntoft, C.L. Andersen, M. Dobbelstein, p53-Responsive microRNAs 192 and 215 are capable of inducing cell cycle arrest, Cancer Res. 68 (2008) 10094–10104.
[59] S.A. Georges, M.C. Biery, S.Y. Kim, J.M. Schelter, J. Guo, A.N. Chang, A.L. Jackson, M.O. Carleton, P.S. Linsley, M.A. Cleary, B.N. Chau, Coordinated regulation of cell cycle transcripts by p53-Inducible microRNAs, miR-192 and miR-215, Cancer Res. 68 (2008) 10105–10112.
[60] I. Ivanovska, A.S. Ball, R.L. Diaz, J.F. Magnus, M. Kibukawa, J.M. Schelter, S.V. Kobayashi, L. Lim, J. Burchard, A.L. Jackson, P.S. Linsley, M.A. Cleary, MicroRNAs in the miR-106b family regulate p21/CDKN1A and promote cell cycle progression, Mol. Cell. Biol. 28 (2008) 2167–2174.
[61] J.K. Gillies, I.A. Lorimer, Regulation of p27Kip1 by miRNA 221/222 in glioblastoma, Cell Cycle 6 (2007) 2005–2009 Georgetown, Tex 6.
[62] C.C. Lee, Tumor suppression by the mammalian Period genes, Cancer Causes Control 17 (2006) 525–530.
[63] X. Pan, T. Terada, M. Irie, H. Saito, K. Inui, Diurnal rhythm of H+-peptide cotransporter in rat small intestine, Am. J. Physiol. Gastrointest. Liver Physiol. 283 (2002) G57–G64.

Please cite this article as: Anita Balakrishnan, et al., MicroRNA *mir-16* is anti-proliferative in enterocytes and exhibits diurnal rhythmicity in intestinal crypts, Exp Cell Res (2010), doi:10.1016/j.yexcr.2010.07.007